Forming Analysis of Natural Fibre Composites

Wentian Wang

December 2015

A thesis submitted for the degree of Doctor of Philosophy

of the Australian National University

Declaration

This thesis is an account of research undertaken between February 2012 and December 2015 at The Research School of Engineering, College of Engineering and Computer Science, Australian National University, Canberra, Australia.

Except where acknowledged in the customary manner, the material presented in this thesis is, to the best of my knowledge, original and has not been submitted in whole or part for a degree in any university.

Publications

Journal Publications:

1. W. Wang, A. Lowe, S. Kalyanasundaram. "Study on continuous flax fibre reinforced polypropylene composite in stamp forming process." *Advanced Composites Letters*, vol. 22, pp. 86-89, 2013.

2. W. Wang, S. Venkatesan, A. Sexton, S. Kalyanasundaram. “Stamp Forming of Polypropylene based Polymer-Metal Laminates: The Effect of Process Parameters on Spring Back.” *Advanced Materials Research* vol. 875-877, pp 423-427, 2014.

3. W. Wang, A. Lowe, S. Kalyanasundaram. "Effect of Chemical Treatments on Flax Fibre Reinforced Polypropylene Composites on Tensile and Dome Forming Behaviour." *International Journal of Molecular Sciences*, vol. 16, pp. 6202-6216, 2015.

4. W. Wang, A. Lowe, S. Davey, N. A. Zanjani, S. Kalyanasundaram. "Establishing a new Forming Limint Curve for a flax fibre reinforced polypropylene composite through stretch forming experiments." *Composite Part A: Applied Science and Manufacturing*, vol. 77, pp. 114-123, 2015.

5. Nima A. Zanjani, W. Wang, S. Kalyanasundaram. “The effect of fibre orientation on the formability and failure behaviour of a woven self-reinforced composite during stamp forming.” *ASME – Journal of Manufacturing Science and Engineering*, 2015. doi:10.1115/1.4030894

6. W. Wang, A. Lowe, S. Kalyanasundaram. “Investigating the forming limits of a flax fibre reinforced polypropylene composite in different conditions of the water treatment.” *International Journal of Advanced Manufacturing Technology*, vol. 87, pp. 103-113, 2016

Conference Publications:

1. W. Wang, S. Venkatesan, A. Sexton, S. Kalyanasundaram. “Stamp forming of polypropylene based polymer-Metal laminates: The effect of process parameters on spring back.” *International Conference on Advanced Material and Manufacturing Science (ICAMMS), Beijing, China, December 2012.*

2. W. Wang, S. Kalyanasundaram. “Dome forming study on polypropylene aluminium laminate.” *International Conference on Mechanical Engineering and Material Science (MEMS), Shanghai, China, December 2012.*

3. W. Wang, S. Kalyanasundaram. “Forming analysis of chopped flax fibre reinforced polypropylene composites.” *European Conference on Composite Materials, Seville, Spain, June 2014.*

4. W. Wang, A. Lowe, S. Kalyanasundaram. “Non-linear quasi-isotropic material modelling of chopped flax fibre reinforced polypropylene composites in stamp forming.” *8^{th} Australasian Congress on Applied Mechanics (ACAM 8), Melbourne, Australia, November 2014.*

5. W. Wang, A. Lowe, S. Kalyanasundaram. “Effect of weave structure on flax fibres reinforced polypropylene composites in stamp forming.” *8^{th} Australasian Congress on Applied Mechanics (ACAM 8), Melbourne, Australia, November 2014.*

Awards

1. Awarded with the 2nd place for Postgraduate Student Best Paper Award, *8th Australasian Congress on Applied Mechanics (ACAM 8), Melbourne, Australia, November 2014.*

Acknowledgements

I would like to thank A/Prof. Shankar Kalyanasundaram, my supervisor in chief, for the opportunity to be a part of this great research. I would also like to thank my advisers Dr. Adrian Lowe for his support during my PhD studies.

This project would not have been successful without the advice, support and knowledge provided by Anthony Sexton, Sebastian Davey, and Nima Akhavan Zanjani. I am forever indebted to them for helping me with the equipment and software and for their patience with my questions from the beginning.

Thank you to my colleagues Jae Nam and Davood Rahiminejad for their discussions, support and help in overcoming problems that we have encountered in this research project.

I would also like to thank my cosines (Yunke Yu and Gang Zhang) who shared a great childhood with me. Their support was, is and will always be my best motivation and determination for pursuing success.

I can never thank my father (Yi Wang) and mother (Lihui Wen) enough for their support, without which I never would have achieved so much in my life. My biggest thanks are to my wife Yili Wang. She is the reason I could put all of myself into this challenging research project. Her support, encouragement, and love during my PhD studies, especially in those difficult moments, became the true motivation for me to carry on. It is the best present from the life that our daughter will join our family shortly, and she will be attending my graduation ceremony with the whole family. It will definitely be the memory of the life for sharing this great moment with my princess.

Abstract

Weight reduction can significantly contribute to reducing Green House Gas (GHG) emissions from vehicles. In addition to the significant increase in the demand on transportation due to the increase in global population, there is an urgent need to reduce the weight of vehicles to increase their fuel efficiency and therefore to reduce global GHG emissions. Driven by ecological and economic interests, there has been an increasing use of plant based material systems in various applications over the past decade. Currently, one of the main challenges in using these material systems for use in automotive components is to understand the forming behaviour of this class of material systems.

This work is designed to answer two key questions regarding the forming of natural fibre composites. The first one is when does failure initiate in this class of material systems, and what is the most effective measure for predicting it? To answer this question, hourglass samples with varying sample widths are stretched and then formed through the stamping press machine. The ARAMIS™ system beneath the press machine provides displacement and strain deformation which could be used to determine the failure behaviour of the composites. This study proposes a new FLC for woven composites, which is more effectively in predicting the failure behaviour of the natural fibre composite than the conventional method as it can successfully eliminate the path dependency effect. This innovative failure criterion has been proven to be more effective than the existing failure criterion through FEA simulations. The second question that the current work tries to answer is how to improve the formability of natural fibre composites. The approach here is to perform dome forming tests in different treatment conditions, namely preheating, water treatment, and tailored blanks.

Abstract

It is found that, among all treatment, the water treatment works the best, and is more effective than the conventional treatment of preheating. Woven composite with a tailored shape becomes much more formable due to its woven nature of fibre reinforcement, while such improvement is insignificant in nonwoven composites. This study lays a foundation for rapid forming of this class of material system, and will in turn lead to possible weight savings in future vehicles.

Nomenclature

C.A	Cloudy Ammonia
CNFC	Chopped natural fibre composite
DSC	Differential Scanning Calorimetry
E	Modulus
FEA	Finite Element Analysis
FLC	Forming Limit Curve
FLD	Forming Limit Diagram
FML	Fibre Metal Laminate
FTIR	Fourier Transform Infrared spectroscopy
GHG	Green-House Gas
M.A	Maleic acid
NFC	Natural fibre composite
PEEK	Polyether ether ketone
PLA	Polylactic acid
PML	Polymer metal laminate
PPS	Polyphenylene Sulphide
R	Radius
T	Temperature
TG	Thermogravimetry
t	time
TGA	Thermogravimetric Analysis

V	Volume
ρ	density
λ	Lame's Constant
β	Strain Ratio
σ	Stress
ε_1	Major Strain
ε_2	Minor Strain
ε_X	Strain along the X direction
ε_Y	Strain along the Y direction
$\Delta\varepsilon_X$	Incremental Strain along the X direction
$\Delta\varepsilon_Y$	Incremental Strain along the Y direction
ε_{Fibre}	Amount of strain acting on the fibres

Table of Contents

List of Figures

List of Tables

Introduction

1.1 Motivation

Today, there is an urgent need to reduce the weight of vehicles to improve fuel efficiency, thereby reducing global greenhouse gas (GHG) emissions. Natural fibres such as flax, hemp, jute, sisal, kenaf, bamboo, and ramie have been investigated as reinforcements for fibre reinforced polymer composites, some of which seem to have the potential of being used in automobiles [1-5]. Natural fibres are mainly made of cellulose, hemicellulose, lignin, pectin and a small amount of extractives [6-8], and they can offer attractive properties such as low density, low price and ease of processing [6]. In addition, the biodegradability of natural fibres allows them to be recycled and probably reused at the end-of-life. The global natural fibre composite market reached $2.1 billion in 2010 with a 15% compound annual growth rate between 2006 and 2010. The size of this market is expected to reach $3.8 billion by 2016 as a result of the rising price of petroleum based products, and more importantly, strong government support for use of eco-friendly materials [9]. For instance, the European Union and some Asian countries require that, by 2015, 85% of a vehicle must be reused or recycled [10]. An extensive amount of research has been conducted to realise strategies and technological challenges for mass production automobile by using lightweight composites [11-14]. One of the many challenges in the widespread use of advanced lightweight material systems in vehicle manufacturing is a suitable manufacturing technique. The stamp forming technique is one process that has been successfully used in rapid forming of different material systems [15-17]. ***The current study investigates the forming behaviour of natural fibre composites, with a particular focus on the challenges encountered during rapid forming processes.***

1.2 Research objectives

This thesis is designed to answer two key questions regarding the forming of natural fibre composites. The first question is when does the failure occur in this class of material system, which can also be translated to what is the most effective measure for predicting the onset of its failure behaviour. Materials are considered to have failed when surface fractures begin to appear. The first phenomenon is investigated through stretch forming tests on hourglass samples that have a range of sectional widths. Experimental data is used to help determine the limiting strain condition in each deformation mode varying from biaxial-stretch to pure shear.

The second question is how to improve the formability of natural fibre composites, or what is the most effective treatment for improving the formability of this class of material system. Three different treatments - preheating, water treatment, and tailored blanks are applied to two flax fibre reinforced polypropylene composites (with different fibre reinforcement natures) in dome forming tests, and the effect of these treatments are compared. Based on strain deformation provided by the ARAMIS™ system, reasons for the difference in effectiveness are determined.

1.3 Thesis Structure

In the following Chapter (Chapter 2), an overview of the properties of natural fibres and their reinforced composites is given, together with literature review of the forming behaviour of this class of material system. The aim of the review is to provide, for laminates as well as pre-consolidated materials, a brief understanding of the forming processes used for processing natural fibre composites. Chapter 3 describes the methods used for processing flax fibre reinforced polypropylene composites, and gives details of how the forming experiments conducted in this study were done. A strain measurement

system, the ARAMIS system, is used study the forming behaviour of composite materials. Chapters 4, 5, and 6 give detailed observations of the forming tests performed on the two natural fibre composites used. FEA simulations are also developed to obtain the information which cannot be observed during forming as well as to examine the effectiveness of failure criteria proposed in this study. The aim of these three Chapters is to provide answers to the two key questions set out in Section 1.2. Finally, conclusions and recommendations for future work are presented in Chapter 7.

Literature Review

2.1 Introduction

This Chapter presents an overview of background knowledge related to forming of composite materials, both in experiments and in FEA simulations. The properties of fibres and their reinforced composites are studied. The methods that have been used in forming composite materials are reviewed, with a particular interest in the failure behaviour of composite materials. Finally, the procedure of developing FEA simulations is described in detail.

2.2 Fibre reinforced composites

Most materials can be categorised into one of the following four classes: metal, ceramic, polymer and composite. Composite materials are made of two or more different materials, and usually consist of fibres to carry the load and a matrix to transfer the load between the fibres. Therefore, the fibres usually have high strength and stiffness, whereas the matrix has a higher elongation to failure. Based on the type of polymer used to create the matrix, fibre reinforced composites can be classified into two different categories of thermoset and thermoplastic. Common matrices for thermoset materials include vinylester, epoxies, polyesters and so on, whereas thermoplastic materials usually have matrices such as Polypropylene (PP), Poly-ether-ether-ketone (PEEK), and Polyphenyle Sulphide (PPS) [18].

Thermoset composites use chemical cross-linking of low weight monomers and a prepolymer to form a high weight polymer network, resulting in a very low viscosity liquid. Thermoset matrices are typically liquid or malleable prior to curing, during

which thermoset resin is heated to melting and then recrystallizes which occurs through the cross-link of the molecular chain. Due to the nature of the cross-linking of the polymer molecules in thermosets, the polymer cannot convert back to a liquid form after the initial cure, meaning that thermoset composites must be cured in their final configuration in a mold [12]. This irreversible process is usually achieved through the application of temperature through heating or UV light radiation, or pressure or a combination of both. This process can also be carried out through a catalyst or agent. The advantages of thermoset composites include very low creep, stress relaxation, increased bond strengths between the fibres and matrices, maintaining the mechanical characteristics at high temperatures, and exhibiting good chemical resistance [18, 19].

In contrast, thermoplastic composites are typically solid and liquefy when heated above their melting temperatures, and then re-solidify when the temperature drops below the re-crystallization temperature. Thermoplastic composites have many advantages over thermoset, including high temperature damage tolerance, high fracture resistance, low manufacture cost, high recyclability, infinite shelf life, ease of material handling, better toughness, and large strain to failure [18, 19]. Due to the difference in the nature of thermoplastic and thermoset, the manufacturing procedures of composites can be illustrated from the Figure 2.1. Thermoset composites require heating such that the matrices can flow. Because of the matrix cures into a fixed cross-linked solid, the curing process limits the time available for material processing and adding new features [20]. The extended forming time of thermoset composites compared to thermoplastic composites is one of the major reasons of the increased use of thermoplastic composites, especially in industries where there is a need of mass production to meet market demand.

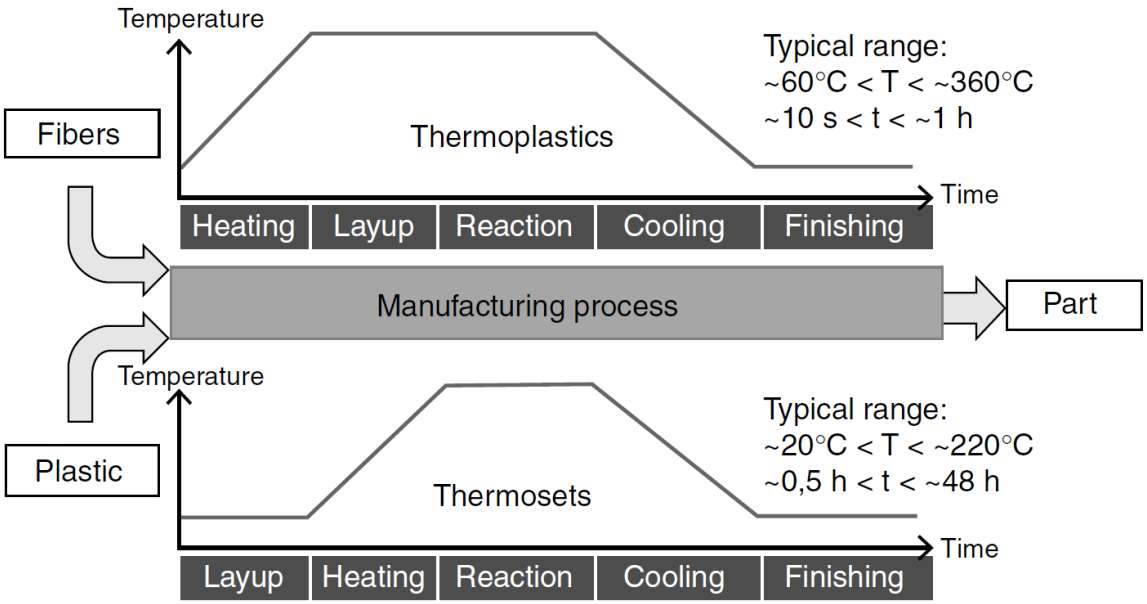

Figure 2.1: Composite manufacturing process [20].

2.2.1 Natural fibres

Driven by ecological and economic interests, natural fibres are gaining increasing acceptance worldwide. In automotive applications of North America alone, it is found that 3.07 million tons of CO_2 emissions and 1.19 million m^3 of crude oil could be saved by substituting 50% of synthetic fibres with natural fibres or their composites [15]. Natural fibres can be divided into different categories based on their origin, as shown in Figure 2.2. Animal fibres, usually from hair, silk or wool are composed of proteins [16]. Natural fibres can also be extracted from several parts of plants, and these fibres, especially bast fibres, have been considered as reinforcements for polymeric composites over animal fibres in numerous applications due to their improved mechanical properties [17]. The plants which produce natural fibres can be categorised into primary plants and secondary plants based on whether the fibres are produced as a major product or as a by-product [8].

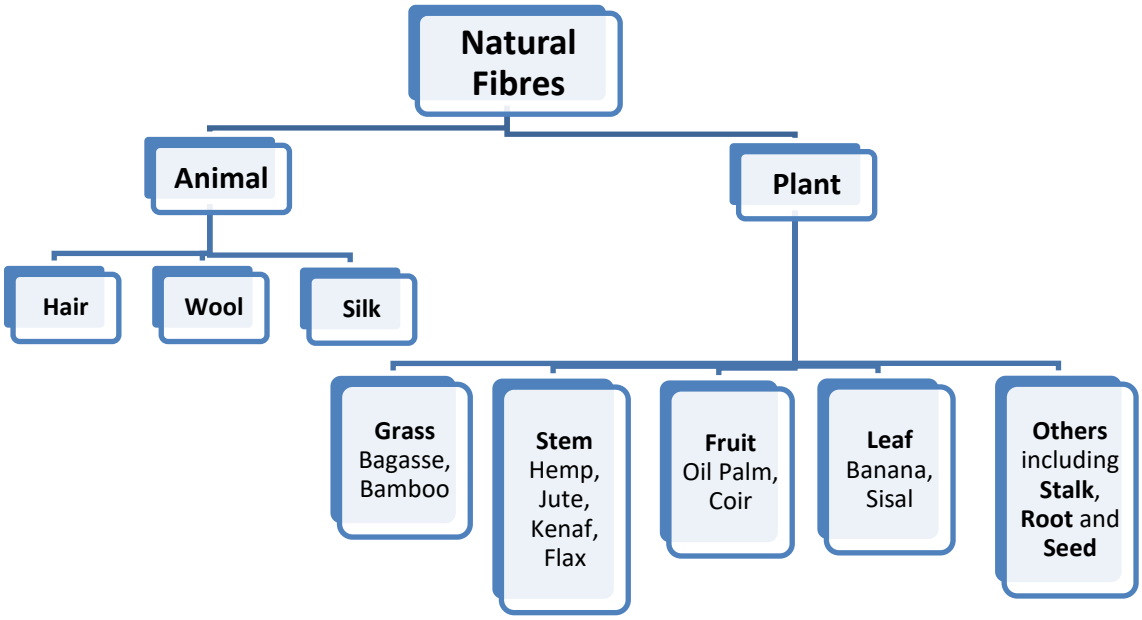

Figure 2.2: Subdivisions of natural fibres based on their origin, from [16].

Natural fibres derived from plants have a complex layer structure with one primary layer along with three secondary cell walls [17], as shown in Figure 2.3. Cellulose, hemicelluloses, and lignin are major components in each cell wall, where microfibrils (made of cellulose molecules) act as fibres that are embedded in a matrix which consists of lignin and hemicelluloses [16]. Each of these components can affect the properties of lignocellulosics fibres, as summarised in Table 2.1. With knowledge of the chemical composition of natural fibres, their degradation characterisation can therefore be predicted. Unlike synthetic fibres, natural fibres have a hollow structure due to the presence of a lumen [21].

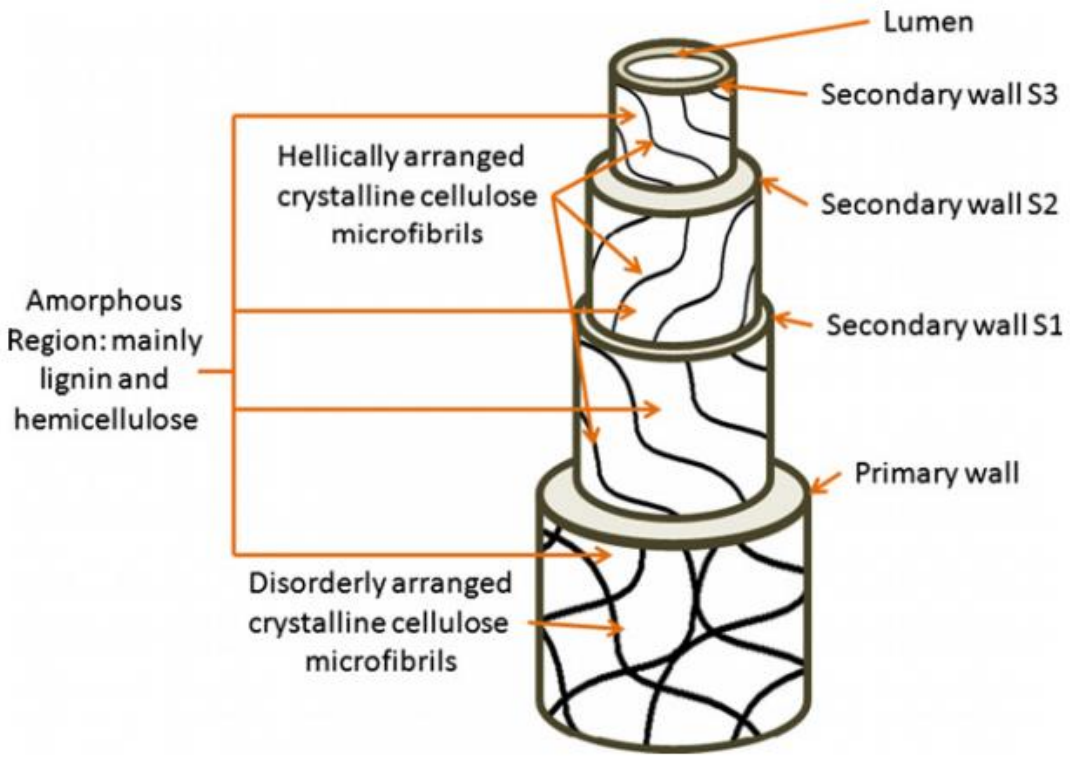

Figure 2.3: Structure of a typical biofibre [16].

Properties	**Components**
Strength	Cellulose [16, 22, 23]
Thermal degradation	Hemicellulose [23]
Biodegradation	Hemicellulose [22, 23]
Moisture absorption	Hemicellulose [22, 23]
Fibre degradation	Hemicellulose and lignin [21, 24]

Table 2.1: Cell wall polymers responsible for the properties of lignocellulosics fibres

The properties of fibres lack consistency and have a high level of variability. Intrinsically, major structural differences such as density, length and diameter result in differences in physical properties [8]. The properties of fibres can also be affected by changes in the environments of growth including the location, moisture level, and time to harvest [25]. For instance, a higher degree of voids is found in plant fibres harvested in wet habitats [22]. This can result in variations in mechanical properties of the fibres

as well as a higher saturation level when the fibre undergoes a moisture absorption process [22, 25].

Each component that comes from natural fibres is compostable, meaning the application of natural fibres makes energy saving possible. Beside biodegradation the recyclability of natural fibres could extend their useful lives, minimizing raw material consumption, and storing carbon for a longer period of time. This could in turn leads to a reduction in global impact on environment. Le Duigou *et al.* [26] studied the recycling capacity of flax/PLLA (poly(L-lactide)) bio-composites with a fibre weight fraction of 20% and 30%. Mechanical properties of composites were evaluated at beginning of the test and right after each of repeated injection process. The property retention observed in the experiment indicates the promising recyclability of this class of material systems. Furthermore, Bourmaud *et al.* [27, 28] have shown that composites of Polypropylene and vegetal fibres are recyclable following the European directive of using/recycling of at least 95% of a worn vehicle weight by 2015. This finding agrees with the conclusions from Srebrenkoska *et al.* [29, 30]. It was found that recycling of rice hulls or kenaf fibres reinforced polypropylene composites is promising due to their properties remain largely unchanged after the recycling process. It is also noted that PLA-based composites are more sensitive to processing cycles than PP-based composites.

2.2.2 Natural fibre reinforced polymer composites

Compared to thermoset polymers, thermoplastic polymers have several advantages, and the one most relevant to rapid forming is their ability to be reshaped [31]. Recyclability is another major advantage of thermoplastic over thermoset [24]. Polypropylene (PP) is a good choice for the matrix of natural fibre reinforcements due to its low cost, low

processing temperature (to facilitate the low thermal stability of natural fibres), and strong hydrophobic character (which protects the hydrophilic natural fibres) [25].

Many attempts have been made to study the shortcomings of natural fibres, efforts directed to maximise their applications in a range of industries. In general, there are two major issues associated with natural fibre composites: low thermal resistance as well as moisture absorption. Due to their inherently low elongation-to-failure, natural fibre composites usually require additional treatments before forming into parts having a high level of complexity. In auto parts manufacturing, the poor thermal resistance of natural fibre composites is a critical barrier for widespread use because the conventional treatment, preheating, is often not applicable to this class of material system. Thermogravimetric analysis (TGA) has been frequently used to study the thermal stability of natural fibres. In a typical situation, the fibre suffers a slow weight drop when it is subjected to heat, followed by a sharp drop over a narrow range of temperatures and finally returns back to the stable state as reactants are exhausted [17]. Due to similar characteristics, natural fibres usually share a similar TGA curve in which almost 60% of the thermal decomposition takes place between 215˚C and 300˚C [32]. It has been reported that lignin starts degrading at lower temperatures compared to the other major constituents of natural fibres, cellulose and hemicellulose [33]. A better thermal resistance can therefore be anticipated in natural fibres with low lignin content, such as flax fibres [34], or in those natural fibres in which the lignin has been removed by chemical treatments [33]. The thermal degradation of natural fibres is therefore an important issue associated with manufacturing natural fibres reinforced composites, especially since preheating is traditionally used to improve the formability of composites during rapid forming.

The variations in structure as well as properties of natural fibres result in variation in the performance of natural fibre reinforced composites when they are subjected to moisture absorption processes. Athijayamani *et al.* [35] studied the performance of a roselle/sisal fibre reinforced polyester hybrid composite when subjected to moisture ingression process, and the maximum weight gain reported was 4%. A significantly higher saturation level was observed by Wang *et al.* [36] for rice hulls/low density polyethylene composites which reached a stable weight gain of 17% after being immersed in distilled water for approximately 100 minutes.

Reduced mechanical properties of sisal/polypropylene composites have been observed in tensile tests as a result of increased water uptake, time of immersion, and fibre loading [37], and the driving mechanisms behind these variations was determined as the weakening of the fibre/matrix interface. Le Duigou *et al.* [38] investigated a flax fibre reinforced PLA composite with 20% fibre loading, and the composite, when saturated, exhibited an almost halved strength, and significantly reduced stiffness, but a doubled elongation-to-failure (compared to the untreated condition). This research also showed that variations in elongation-to-failure were temporary, while those in strength and stiffness were permanent. Through SEM examination of fractured surfaces, the changes in mechanical behaviour of the composite were explained by fibre plasticization as well as increased ductility of the PLA matrix. Similar observations have also been reported on a sisal fibre reinforced polypropylene composite [39].

Variations in mechanical properties are reported when natural fibres are exposed to different chemical solutions. Methacanon *et al.* [22] investigated variations in the tensile properties of water hyacinth, reed, roselle and sisal fibres caused by moisture absorption processes. A considerable increase in tensile strength was reported in all fibre yarns, and

the study attributed these observations to a higher amount and better orientation of crystalline cellulose in fibres. Extra extensions and elongations were also found in wet yarns compared to dry equivalents as the absorbed water behaved like a lubricant so that one fibre could slide over another. Goda *et al.* [40] determined the effect of alkylation on the tensile properties of ramie fibres, where the fibres were alkali-treated with a 15% NaOH solution. A 4-18% improvement in tensile strength accompanied with a reduction in stiffness was noticed in the treated fibres. A significant increase in ductility was also observed so that the treated fibres exhibited a more than doubled elongation-to-failure. Such improvements in properties were considered to be a result of changes in the morphological and chemical structure of the fibres. These observations contradict those obtained by Ray *et al.* [41] in which an increased modulus and a reduced elongation-to-failure were noticed when jute fibres were subjected to an alkaline treatment (a 5% NaOH solution at 30˚C).

Cellulosic fibres are incompatible with hydrophobic polymers due to their hydrophilic nature, which usually results in poor interfacial adhesion between two materials and hence leads to voids within the composite. It is therefore not surprising that natural fibre polymeric composites are also sensitive to moisture, and the corresponding damage can be accelerated at high temperatures [17]. As stated in Table 2.1, hemicellulose is the fibre component which is responsible for moisture absorption. A higher moisture absorption level is therefore expected for those natural fibres that have a higher content of hemicellulose. Biological activities such as fungal growth can contribute to biodegradation of composites after they have been exposed to moisture for a long period of time [42]. The hydrophilic nature of natural fibres makes their polymeric composites more prone to absorb moisture compared to polymers. An increased rate of moisture absorption was reported when the volume fraction of natural fibres increases [17]. Apart

from natural fibres, moisture exposure can also alter the interfacial conditions between different constituents of the composite. Under such circumstances, intermolecular hydrogen bonds are established between the water molecules and the cellulosic fibres, causing reduced adhesion between the fibre and the matrix [17]. A weakened fibre/matrix interface is also attributed to the fact that cellulosic fibres tend to swell when the composite absorbs solutions [43].

Moisture absorption of natural fibre composites enables the introduction of chemical treatments. Xu *et al.* [44] modified a kenaf fibre surface with a silane coupling agent to enhance adhesion between the fibres and the polystyrene matrix. A condensation reaction between alkoxysilane and the hydroxyl groups of the kenaf fibres took place, resulting in a higher storage modulus and hence an improved interaction between different constituents. A similar observation of an improved storage modulus of natural fibre composites after silane treatment was found in abaca fibre reinforced polyester composites [45].

Unlike other chemical treatments which only modify fibre surfaces, maleic acid (M.A) also modifies the polymer matrix, and lead to better bonding between the fibres and the matrix. Consequently, maleic acid can achieve better adhesion between two constituent materials compared to other treatments. Kiekens and Velde [46] treated dew-retted hackled long flax with propyltrimethoxysilane, phenylisocyanate and maleic acid anhydride modified polypropylene, and the highest increase in interfacial strength was observed in the maleic acid treated composite. This work also showed that when a flax/polypropylene composite is treated with maleic acid, chemical entanglements form within the maleic anhydride/polypropylene copolymer and that this physical link improves load transfer between the fibres.

2.3 Composite forming

Composite Materials have shown great potential to be applied in auto-parts manufacturing, and their ability to be reshaped after melting during initial consolidation makes this class of material system recyclable after at the end of its life cycle. However the current manufacturing procedure for this class of material systems is labour-intensive, complex, and expensive[47, 48]. Therefore, one of the challenges for widespread usage of advanced lightweight material systems in vehicle manufacturing is a suitable manufacturing technique. The stamp forming technique has been successfully used in rapid forming of metal alloys, and more recently extended to forming of composites and FML structures [12, 47-51]. In stamp forming tests, the material is formed into the desired shape by being pressed between a blank-holder and a die. Depending on whether the edge of the specimen is allowed to move or not, stamp forming can be divided into draw forming and stretch forming. In the former forming technique, the sample edge is allowed to move towards the die centre during forming, with the amount of edge movement being closely related to blank-holder force. The drawing behaviour of the material can effectively reduce surface strain deformation, helping achieve a larger forming depth, which is crucial in forming highly complex products. However, wrinkling can also be a undesired by-product of extensive drawing behaviour.

Recently, studies have been conducted on forming composite fabrics. A spray of resin is usually required to keep the formed shape after removing it from the tools. Lee *et al.* [52] investigated the effect of blank-holder force on the stamp forming behaviour of a non-crimp fabric. Square samples of 350 mm x 350 mm were used in stamp forming tests, and the fabrics were cut such that the tows were aligned at 0°/90° (named CS-N) as well as at 45°/-45° (named CS-D) to the edge of the square. During stamp forming tests, a

dead weight was placed on the annular blank-holder before the punch moved down to a depth of 75 mm. After forming, an unsaturated polyester resin was sprayed on to harden the formed structure which was then maintained for 30 minutes before being removed from the mold. It was an advantage to reduce the area in shear deformable area in symmetric shear deformation, and therefore CS-D was a more preferable configuration compared to CS-N. In addition, a processing path with few or even no wrinkles could be found by optimizating the blank-holder forces.

In work conducted by Ouagne *et al.* [53], flax fibre fabrics with different architectures were formed into a complex tetrahedron. The significance of this shape was that it contained several geometrical sharp corners required by many automotive parts. The fabrics were formed through a tetrahedral punch with a base side of 265 mm, a base height of 20 mm and a total height of 128 mm. A resin spray was applied to the sample surface after forming so that the part could be removed from the tools while keeping its final structure. By comparing different fabric architectures, experimental observations suggested that the buckling effect can be reduced by choosing specific reinforcement architectures. Cao *et al.* [54] conducted an extensive review on characterising the mechanical behaviour of woven fabrics that comprised yarns with continuous commingled glass and polypropylene fibres. This study suggested that, in trellis frame tests and bias extension tests, composite materials were largely deformed by intra-ply shearing as the fibres in the weft and warp directions moved over each other. It was found that locking began to occur at approximately 45°, beyond which tows began to exert a compressive force on each other. When this compression force reached a maximum, wrinkling and out-of-plane buckling began to occur and the formed part was considered failure.

In addition to composite fabrics, the forming behaviour of pre-consolidated composite also becomes of great interest to researchers. Hou [55] performed draw forming tests on a pre-consolidated unidirectional glass fibre reinforced polypropylene composite. The prepreg was consolidated by firstly placing a mold filled with 8 layers in a press which was heated to 180°C. After a pre-heating period of 15 minutes, a pressure of 1.5 MPa was applied to the mold for 5 minutes, after which it was cooled to room temperature under pressure. The composite was heated above the melting temperature of polypropylene before forming by the cold metal tool. Most fibre buckling was observed at an angle of 45° to the fibre direction, and the centre of the composite experienced the most thickness reduction, while zero reduction in the flange region.

Hwang and Hwang [31] also conducted high temperature forming experiments, although unlike most other studies where the whole composite was heated prior to forming, the specimen was locally heated. This method saved the energy usually wasted while transferring the sample from the heat chamber to the stamping press machine. Unidirectional carbon fibre/nylon (6 layers) composites were formed at different heated ranges, working temperature, and holding time, and the quality of the formed parts were evaluated macroscopically for part angle and microscopically for delamination and fibre buckling. Experimental observations indicated that, although wrinkling was still observed at the flange region, the locally heated part was comparable to the wholly heated part in terms of maximum load as well as final angle.

Hou [55] studied the forming behaviour of glass fibre reinforced polyetherimide (PEI) through stamp forming tests where the composite was heated to a maximum of 120°C prior to the forming operation. It was concluded that a proper temperature and blank holder force was crucial to good quality in the formed parts. This finding was agreeable

with another research work which analysed the stamp forming of preconsolidated sheets of unidirectional glass fibre reinforced polypropylene composites under various experimental parameters such as forming speed and forming temperature [56]. This study created a novel rod-bed model to form complex three-dimensional parts. This study found that high preheat temperature was essential for good formability due to intra-ply shear deformation at high forming temperatures. It was also noted that the out-of-plane fibre wrinkling was eliminated at a forming temperature of 180°C. Sadighi *et al.* [57] investigated the effects of laminate stacking sequence on the forming of glass fibre reinforced polypropylene composite at elevated temperatures. It was concluded that the flange regions in the composite changed with different laminate stacking combinations. There was a significant reduction in the drawing behaviour along the 45°/-45° stacking scheme while the 0°/90° stacking sequence exhibited significant draw. No obvious change was observed in the wrinkling behaviour of the composites with varying stacking combinations.

Stamp forming tests are usually performed on consolidated composites [58], like the studies mentioned above, and these require a separate consolidation process prior to forming. This means that the voids within the material could be eliminated before molding, but at a higher cost. An alternative is therefore to perform consolidation and forming in a single process, which offers potential for cost reduction. For instance, Trudel-Boucher *et al.* [59] transferred and then formed E-glass reinforced polypropylene fabrics immediately after reaching a temperature of 200°C in a natural conventional oven. There were four separate stages during the forming process including closing the mold, applying pressure, holding the pressure and finally opening the mold. Composites made from un-consolidated fabrics were compared with pre-consolidated composites, and showed comparable flexural properties at low fabric

densities, but lower flexural strength at high fabric densities. This result suggests stamp forming process using this class of material system is promising.

Wakeman *et al.* [60] formed a glass fibre reinforced polypropylene composite through a similar method where the material was heated in an oven before forming and consolidated with a cold tool. The optimum compression parameters were identified when the reductions in cycle time were given higher priorities over the pressures and times required for minimum porosity. This work also pointed out that the transfer time between oven and press must be minimised to prevent the material from cooling too much. On average, the transfer time was approximately 30 seconds. By putting the oven next to the press machine, Cabrera *et al.* [61] managed to transfer the mold with a heated all-polypropylene laminate inside in approximately 3 seconds with a negligible drop in temperature.

Stretch forming tests, on the other hand, require that the sample edge is completely fixed during forming. This forming technique has been widely applied to metals [62-67], and recently to Fibre-Metal Laminates (FML) [19, 68-70] Polymer-Metal Laminate (PML) [71, 72], and composites [47, 73]. Due to the restricted drawing behaviour of materials during forming, materials would experience higher surface strains and much less wrinkling at the cost of surface fracture at smaller forming depths.

One of the main drivers of conducting stretch forming experiments is to establish the forming limits of the materials at different deformation modes. To achieve this, a number of designs on experimental geometries have been proposed for stretch forming tests. Nakazima *et al.* [74] proposed a rectangular specimen with varying middle section widths. When the width of rectangular a specimen was increased, the sample

experienced increased lateral restriction during forming, which prevents the sample from being drawn into the die cavity. This would also result in a forming mode closer to biaxial stretch. It is argued that failure would initiate at regions other than pole when applying rectangular specimens, and hence incapable of obtaining the forming limit of the desired forming mode. To ensure that failure initiates at the centre of a composite specimen (the point of interest for the purpose of FLD), Raghavan [75] proposed a new design of sample geometry where a radius was cut from each edge of a rectangular sample. However, this design was, sometimes difficult, to obtain a deformation mode of pure shear. Zanjani et al. [73] found that in stretch forming tests, the deformation mode of pure shear can be obtained at the pole of small rectangular specimens, with the fibres oriented 45°/-45° to the stretching axis. This allowed one to construct the complete FLC from stretch forming tests.

Sexton *et al*. [68] investigated room temperature formability of a fibre metal laminate system comprised of aluminium and a self-reinforcing polypropylene composite. A real-time three-dimensional photogrammetric measuring system was used to acquire surface strain evolution during forming. This work studied the meridian strain distribution of the FML, and the comparison of it to that of aluminium suggested that FML structure can indeed have superior formability than monolithic metallic alloys. Zanjani and Kalyanasundaram [47] compared the forming behaviour of glass-fibre reinforced polypropylene composites (GRPP) and self-reinforced polypropylene composites (SRPP). In the stretch forming tests conducted in this work, the specimens were cut into a circular shape with varying widths to determine the effect of aspect ratio. The induced strain deformation was measured from a pair of high speed, high resolution CCD cameras by using a Digit Image Correlation (DIC) technique. Three points at the pole, at some distance from the pole in the longitudinal direction, and at some distance from the

pole in the 45° to the fibre direction were selected to analyse the strain evolution of two composites. It was concluded that GRPP composites exhibit significantly higher formability under shear deformation than SRPP composites. In addition, the combination of sample's width and boundary conditions applied is a determinant factor on the formability of woven composites.

2.4 Failure behaviour and failure criteria for composite materials

2.4.1 Failure behaviour

The failure behaviour of fibre reinforced composites is strongly dependent on the material structural organization. The damage initiation and development in the material is controlled by the properties of matrix, fibre-matrix interface and material structural organization [76].

Gorbatikh and Lomov [76] described the typical sequence of damage in the situation where a composite was loaded in the longitudinal direction with an increased tensile load. The first damage typically appears in the form of transverse cracks which usually initiate inside the yarns with the highest local fibre volume fraction or at yarn boundaries, depending on the textile architectures. Transverse cracks would propagate along the yarn direction, and the number of cracks is increased until saturation is reached when loading is further increased. Once transverse cracks are well developed, they further propagate as local delaminations. The onset and propagation of delamination depend on the interlaminar fracture toughness of the composite. When the transverse strength of longitudinal yarns is exceeded by the local stresses, splitting would initiate. Finally, massive breakage of fibres in the longitudinal yarns begins. It is noted that the strain at which it happens is usually below the ultimate strain of fibres due to inefficient stress transfer caused by fibre crimp and developed delaminations.

Matrix cracks is also a typical mechanism observed in textile composites, and the onset of which usually starts as micro-debonding at fibre-matrix interface [76]. De Greef *et al.* [77] observed quasi-elliptical shape yarn cross-sections in a carbon-epoxy twill composite. Fibre interface debonds appeared firstly on yarn boundaries, and later inside yarns which then grew into transverse cracks. A similar situation was also found in a carbon-epoxy 3D woven orthogonal non-crimp composite by Bogdanovich *et al*. [78]. However, in natural fibre reinforced composites which have a low transverse stiffness, the initiation of matrix cracks can be delayed until later stages of loading [76]. Kersani *et al.* [79] found that the onset of matrix cracks starts just before the entire woven flax-epoxy composite fails or never appear at all.

Traditionally composite materials were manufactured using thermoset matrices, and an extensive number of studies have been carried out to investigate the failure behaviour of this class of material systems. The research conducted by Roundi *et al.* [80] examined the fatigue behaviour of glass/epoxy composite materials subjected to cyclic tensile tests under different stress ratios and the stacking sequence ($[0_2/90_2]_s$; $[90_2/0_2]_s$; $[0_3/90]_s$; $[90_3/0]_s$). All experiments were performed at room temperature through a tensile machine equipped with 100 kN loading cell, according to the standard test method ASTM D3039/D3039 M. The displacement rate was 1 mm/min with a frequency of 10 Hz. Specimens were tested under various maximum stress levels, and the applied stress ratio (the ratio between the minimum and maximum applied stress) varied between 0.1 and 0.5. Experimental results showed that it is more adequate to use the $[0_3/90]_s$ fibre orientations to achieve the maximum fatigue life. The fatigue strength of the composite was found to increase with stress ratio values for all fibre orientations. Fatigue life, however, decreases significantly with decreasing stress ratios.

Ma *et al.* [81] studied on-axis tensile tests of unidirectional carbon fibre reinforced epoxy laminates. Two typical fracture modes of splitting and the step-like mode were observed in the composite, while all 0° laminates showed the step-like fracture mode in tensile tests. To further investigated the fracture process of the laminate, step-by-step tensile tests were carried out, which stopped at strains of 0.2%, 0.8% and 1.3%. Based on observation of fracture surface vertical to the fibre direction under SEM, no delamination occurred and only few large-scale cracks could be observed, suggesting the dominating failure mode of cohesive failure. It was also found in the work that most of the cracks propagated along the thickness direction in the unidirectional carbon fibre reinforced epoxy composite. Similar findings were obtained by Mayen *et al.* [82] where the fracture mechanisms of a carbon fibre/epoxy laminate [+75/0/-75]s under uniaxial loading tests. In this work, transversal crack propagation was found as the dominating failure mechanism as fibres kept a significant amount of epoxy resin on the surface.

Unlike most studies that focused on the overall performance of thermoset composite, Wang *et al.* [83] examined the effect of different surface treatment of reinforcing fibres on fibre-matrix adhesion of a carbon/epoxy composite. The Polyacrylonitrile based AKSAca A-42 carbon fibres with a bulk density of 1.78g/cm^3 were treated with a mixture of H2SO4 and HNO (3:1 in volume) for a treatment time of varying from 15 mins to 60 mins with an increment of 15 mins. Adhesion strength at the interface between carbon fibres and epoxy resins was measured in a microbond test. Failure samples from the microbond test were then examined with field emission SEM to verify the location and mode of the failure. There was a clear evidence that interfacial separation, caused by poor adhesion, was the main failure mode of the composite. It was also found that both interfacial shear strength and fracture toughness of the interface were improved after an optimum 15-30 mins of surface treatment, and these properties

started to decline when treatment duration was prolonged beyond 30 mins.

Thermoplastic composites have higher fracture toughness and higher strain to failure compared to thermoset composites, leading to different failure behaviour seen from experiments. Venkatesan [18] studied the forming behaviour of two different composites through draw forming tests. The first one was a glass fibre reinforced polypropylene composite (Twintex), and the second was a self-reinforced polypropylene composite (Curv). Both were pre-consolidated before forming. Circular blanks with a diameter of 180 mm were formed into a hemispherical dome structure. Three different experimental parameters, including blank-holder force ranging from 2 kN to 14 kN, feed rate ranging from 20 mm/s to 60 mm/s were selected in this study. By examining the formed parts, no matrix cracking, delamination, fibre breakage, or fibre pull-out was observed. However, wrinkling at the flange region was observed frequently on both composites that were formed at low blank-holder forces. Increasing the blank-holder force can effectively reduce the amount of wrinkling, thereby improving the quality of the formed structure. The similar observation was also obtained in other researches [84]. All-PP composites were stretched to failure in tensile tests, and examination on the fracture section revealed that the failure is characterised by fibre breakage leading to matrix damage. Although considerable thinning is noticed, no failure is initiated in the matrix. Similar finding was also obtained by Romhany *et al.* [85]. Twintex exhibited a different forming behaviour compared to Curv due to significantly higher stiffness of the glass fibres compared to the polypropylene fibres. A detailed examination on the failure behaviour of Twintex was outside the scope of this study, however fibre breakages are seen when samples were stretched to failure in tensile tests.

Davey *et al.* [86] performed stamp forming tests on a carbon fibre reinforced PEEK composite. Circular discs of samples were formed into a dome structure through a 300 kN double-action mechanical press machine, and the test was not ceased until the initiation of failure in the specimen. It was found that the failure was observed in the carbon fibres, primarily due to the significantly lower failure strain of carbon fibres compared to that of the polypropylene matrix. Asumani *et al.* [87] studied the failure behaviour of kenaf fibre reinforced polypropylene composites with kenaf fibres prepared with alkaline treatment, or a combination of alkaline treatment and three-aminopropyltriethoxysilane treatment. SEM examination on the failure surface of the composite (with a fibre content of 30% and treated with 6% NaOH before silane) indicates that the fracture is characterized by fibre breakage.

2.4.2 Failure criteria

An extensive number of research have been carried out to determine the conditions beyond which failure initiates in composite materials. A number of failure criteria have been established upon mathematical models built by authors with strong understandings on the failure behaviour of composites. These failure criteria, including non-interactive and interpolation criteria, have been applied to fibre reinforced composites for predicting on their failure behaviour. Among all, the Maximum Strain and the Maximum Stress are two of the simplest.

The Maximum Stress failure criteria can be expressed as [88]:

$$\boldsymbol{X_C < \sigma_{11} < X_T,\ \ Y_C < \sigma_{22} < Y_T,\ \ Z_C < \sigma_{33} < Z_T,}$$

$$\boldsymbol{|\tau_{23}| < Q,\ \ |\tau_{13}| < R,\ \ |\tau_{12}| < S} \qquad (2.1)$$

where X_T, Y_T, and Z_T are the tensile material normal strengths; X_C, Y_C, and Z_C are the compressive material normal strengths (and have negative values); and Q, R and S are

the material shear strengths. The composite material is considered failed when one of the criteria above is met.

The Maximum Strain failure criteria can be expressed as [88]:

$$\boldsymbol{X_{\varepsilon C} < \varepsilon_{11} < X_{\varepsilon T},\ Y_{\varepsilon C} < \varepsilon_{22} < Y_{\varepsilon T},\ Z_{\varepsilon C} < \varepsilon_{33} < Z_{\varepsilon T},}$$

$$\boldsymbol{|\tau_{23}| < Q_{\varepsilon},\ |\tau_{13}| < R_{\varepsilon},\ |\tau_{12}| < S_{\varepsilon}} \quad (2.2)$$

where $X_{\varepsilon T}$, $Y_{\varepsilon T}$, and $Z_{\varepsilon T}$ are the tensile material normal failure strains; $X_{\varepsilon C}$, $Y_{\varepsilon C,}$ and $Z_{\varepsilon C}$ are the compressive material normal failure strains (and have negative values); and Q_{ε}, R_{ε} and S_{ε} are the material shear failure strains. The composite material is considered to have failed when one of the criteria above is met.

The Tsai-Hill failure criterion considers interactions between the failure modes which are ignored in both the Maximum Stress theory and the Maximum Strain theory. The full multi-axial Tsai-Hill failure surface can be written as [88]:

$$\left(\frac{\boldsymbol{\sigma_{11}}}{\mathbf{X}}\right)^2 + \left(\frac{\boldsymbol{\sigma_{22}}}{\mathbf{Y}}\right)^2 + \left(\frac{\boldsymbol{\sigma_{33}}}{\mathbf{Z}}\right)^2 + \left(\frac{\boldsymbol{\tau_{23}}}{\mathbf{Q}}\right)^2 + \left(\frac{\boldsymbol{\tau_{13}}}{\mathbf{R}}\right)^2 + \left(\frac{\boldsymbol{\tau_{12}}}{\mathbf{S}}\right)^2$$

$$-\boldsymbol{\sigma_{11}}\times\boldsymbol{\sigma_{22}}\times\left(\frac{\mathbf{1}}{\mathbf{X^2}} + \frac{\mathbf{1}}{\mathbf{Y^2}} - \frac{\mathbf{1}}{\mathbf{Z^2}}\right) - \boldsymbol{\sigma_{11}}\times\boldsymbol{\sigma_{33}}\times\left(\frac{\mathbf{1}}{\mathbf{X^2}} - \frac{\mathbf{1}}{\mathbf{Y^2}} + \frac{\mathbf{1}}{\mathbf{Z^2}}\right)$$

$$-\boldsymbol{\sigma_{22}}\times\boldsymbol{\sigma_{33}}\times\left(\frac{\mathbf{1}}{\mathbf{X^2}} + \frac{\mathbf{1}}{\mathbf{Y^2}} + \frac{\mathbf{1}}{\mathbf{Z^2}}\right) = \mathbf{1} \quad (2.3)$$

where in order to incorporate different tensile and compressive strengths:

$$\mathbf{X} = \begin{cases} \mathbf{X_T} & \boldsymbol{\sigma_{11}} \geq \mathbf{0} \\ \mathbf{X_C} & \boldsymbol{\sigma_{11}} \leq \mathbf{0}, \end{cases} \quad \mathbf{Y} = \begin{cases} \mathbf{Y_T} & \boldsymbol{\sigma_{22}} \geq \mathbf{0} \\ \mathbf{Y_C} & \boldsymbol{\sigma_{22}} \leq \mathbf{0}, \end{cases} \quad \mathbf{Z} = \begin{cases} \mathbf{Z_T} & \boldsymbol{\sigma_{33}} \geq \mathbf{0} \\ \mathbf{Z_C} & \boldsymbol{\sigma_{33}} \leq \mathbf{0} \end{cases} \quad (2.4)$$

Based on the Maximum Strain failure criteria, Hart-Smith [89, 90] applied modifications using a micromechanical approach and suggested a truncated failure envelope in biaxial tension as well as biaxial compression, as shown in Figure 2.4. The truncated Maximum Strain failure model predicts a more conservative failure envelope in in-plane shear where the reduction in strength is approximately 60%. The interactions

between the fibres in the warp and weft direction are important for pre-consolidated woven composites, resulting in inaccuracies if non-interactive failure criteria are applied to this class of material system.

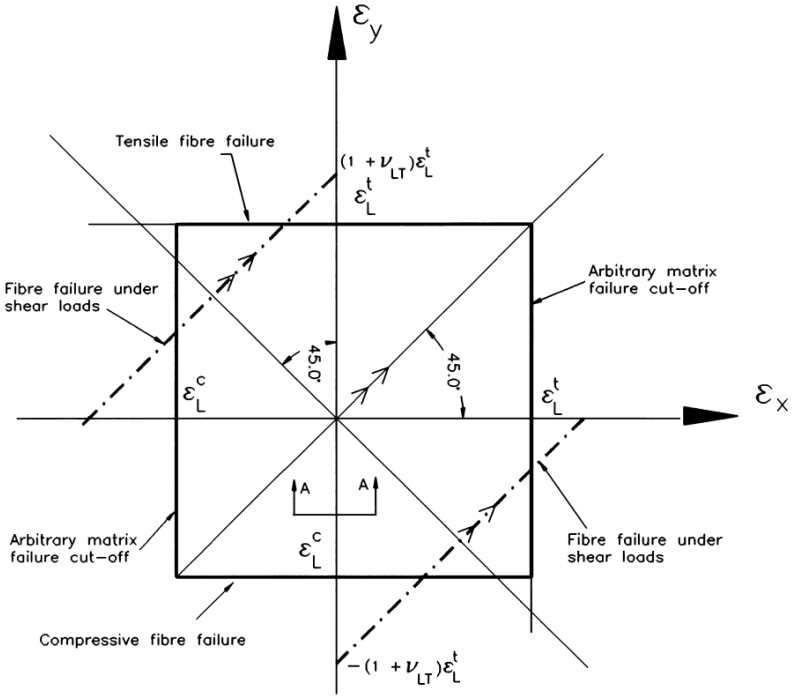

Figure 2.4: Failure envelope for 90° unidirectional laminae [90].

Tsai and Wu [91] developed tensor polynomial failure criteria, but the proposed mathematical function cannot distinguish between fibre fracture, matrix cracks or interface breakage [92]. Rotem [93] proposed a stress-based failure criterion which separates fibre failure and matrix failure of fibre-composite materials. The first version of this failure criterion was proposed in 1973 [94], and then modified in 1975 [95] and again in 1981 [96]. There are three assumption of the criterion: Firstly, the failure of fibre-composite material laminate will occur only in fibre or matrix. Secondly, the laminate is formed under the conditions that only in-plane stresses are effective, and no interlaminar stresses which may result in failure. The last assumption is that matrix material is softer and weaker than the fibres. Based on these assumptions, the criterion predicts fibre failure and matrix failure, separately.

Fibre failure criterion:

$$\boldsymbol{\sigma_A \geq S_{A+}} \tag{2.5}$$

$$\boldsymbol{\sigma_A \geq S_{A-}} \tag{2.6}$$

Where *S* is the composite lamina strength, the index A denotes the axial direction, + indicates tensile strength and − indicates compressive strength.

Matrix failure criterion:

$$\left(\frac{\boldsymbol{E_m(\varepsilon_A)\varepsilon_A}}{\boldsymbol{\pm S_m}}\right)^{\mathbf{2}} + \left(\frac{\boldsymbol{\sigma_T}}{\boldsymbol{\pm S_T}}\right)^{\mathbf{2}} + \left(\frac{\boldsymbol{\sigma_{AT}}}{\boldsymbol{S_{AT}}}\right)^{\mathbf{2}} \geq \mathbf{1} \tag{2.7}$$

Where the subscript m index stands for the matrix material, T is for transverse directions (to the fibres), and AT is for shear in a plane axis that is transverse to the fibre direction. The first term expresses the relative shear strength, and the second term is the relative normal stress in the transverse direction. The third term is for the axial stress in the matrix, which is smaller than the other and usually neglected.

The predictions of this failure criterion were then compared with some experimental results of laminate materials [97]. A large discrepancy was noted in some cases due to the huge scatter in the experimental results, the arbitrary selection of some tests, and material properties. In some experimental cases, the failure of materials is due to a failure mode of buckling and hence not covered by this criterion.

A similar stress-based failure criterion, namely Grant-Sanders method, was developed at British Aerospace Defence [98], and this failure criterion could predict failure mode as well as failure location. Unlike Rotem's failure criterion which distinguishes between fibre failure and matrix failure, this failure criterion is separated as initial failure and final failure. The final failure means that the laminate is either incapable of taking further load or fibre breakages occurred. The initial failure is a non-catastrophic event

following which the failed piles gradually shed load, and it is induced in transverse tension and compression. In some cases, final failure is predicted prior to initial failure and when this happens, the initial and final failure envelope coincide.

Initial failure:

Transverse tension/compression:

$$\boldsymbol{\sigma_2 \geq F_{2t}} \tag{2.8}$$

$$\boldsymbol{\sigma_2 \leq F_{2c}} \tag{2.9}$$

Where σ_2 is transverse shear, F_{2t} is allowable transverse tensile stress, and F_{2c} is allowable transverse compressive stress.

Combined shear and transverse tension:

$$\boldsymbol{(\frac{\sigma_2}{F_{2t}})^2 + (\frac{\tau_{12}}{F_{12}})^2 \geq 1} \tag{2.10}$$

Where τ_{12} is shear stress, and F_{12} is allowable shear stress.

Final failure:

Longitudinal tension/compression

$$\boldsymbol{\sigma_1 \geq F_{1t}} \tag{2.11}$$

$$\boldsymbol{\sigma_1 \leq F_{1c}} \tag{2.12}$$

Where σ_1 is longitudinal stress (along the fibre direction)

In-plane shear:

$$\boldsymbol{|\tau_{12}| \geq F_{12}} \tag{2.13}$$

Combined longitudinal compression and shear:

$$\boldsymbol{\frac{\sigma_1}{H_{1c}} + \frac{|\tau_{12}|}{H_{12}} \geq 1} \tag{2.14}$$

Where H_{1c} and H_{12} are parameters for shear-compression, and these two parameters may be the same as F_{1c} and F_{12} respectively, but are not necessarily so, depending on what is known about the material performance.

Delamination:

$$\boldsymbol{\tau_{12} \times t_e \geq w_{cr}} \tag{2.15}$$

Where t_e is effective ply thickness, and w_{cr} is delamination criterion

Instead of defining the failure criterion in the space of stress or strain, energy based failure models have also been developed. It is argued that the stress or strain based theories are quite reasonable for materials showing a linear stress/strain behaviour, whereas energy based criteria would be more approachable for materials exhibiting a non-linear behaviour [99]. The first model was developed by Sandhu [100], which was built from independent strain energy parameters in the longitudinal, transverse and shear directions. A restatement of this model was presented in the work conducted by Wolfe and Butalia [99], where the theory has been extended to include a variety of ply-unloading mechanism as well as to apply stress or strain loading of composite laminates.

It is important to note that most theoretical failure models are derived from unidirectional lamina or laminates made from unidirectional lamina layers. These failure criteria do not account for weave structures, whereas the behaviour of woven composites is highly affected by interactions between their different constituents. In addition, most failure criteria stated in the review were built based on fibre reinforced thermoset composites, and thermoplastic composites are much more ductile than thermoset [101]. This difference in failure behaviour would also influence the applicability of failure criteria, such that in the literature fibre breakage is prevalently

seen as the dominating failure mechanism for thermoplastic composites whereas there are many cases where the failure of thermoset composites is initiated with fibre/matrix interface. Lastly, theoretical failure models are developed for homogenized composites, whereas natural fibre reinforced composites usually exhibit a high level of porosity [102]. The geometric unevenness and material non-uniformity caused by this may also affect the application of these theoretical failure criteria.

Failure criteria of composites have also been constructed through experimental observations. A forming limit diagram (FLD), which consists of major strains and minor strains, can be established in stretch forming tests based on surface principal strains as expressed in Equation 2.16. The FLD can provide information on deformation modes, identified by the strain ratios of surface points, as computed by the Equation 2.17.

$$\boldsymbol{\varepsilon_{1,2}} = \frac{\boldsymbol{\varepsilon_x + \varepsilon_y}}{\boldsymbol{2}} \pm \sqrt{\left(\frac{\boldsymbol{\varepsilon_x - \varepsilon_y}}{\boldsymbol{2}}\right)^{\boldsymbol{2}} + \left(\frac{\boldsymbol{\gamma_{xy}}}{\boldsymbol{2}}\right)^{\boldsymbol{2}}} \tag{2.16}$$

$$\boldsymbol{\beta} = \frac{\boldsymbol{\varepsilon_2}}{\boldsymbol{\varepsilon_1}} \tag{2.17}$$

where ε_1 and ε_2 are principal major and minor strains, β is strain ratio.

Deformation mode	**Strain ratio**
Balanced-biaxial stretch	1
Plane strain	0
Uniaxial tension	-0.5
Pure shear	-1

Table 2.2: Summary of deformation modes and corresponding strain ratio for sheet metals

The importance of FLD is that it allows one to construct the forming limits for different deformation modes. The line that connects limiting strains at each deformation is named a Forming Limit Curve (FLC). Based on the FLC, the forming window of materials can therefore be obtained, and used to predict failure for production parts. FLC was designed for metal forming, and a number of studies have shown that FLCs can

successfully predict the failure associated with monolithic metal alloys [103, 104]. The potential of using FLC to predict failure in other classes of material systems has been investigated. Inspired from metal forming procedures, Zanjani *et al.* [73] proposed a FLC for a pre-consolidated woven self-reinforced polypropylene composite through experimental outcomes in stretch forming tests. A rectangular sample geometry with the width varying from 12.5 to 200 mm was used, and specimens were cut in such a way that the fibres were oriented at 0°/90° as well as at 45°/-45° to the stretching axis. A real-time strain measurement system, named the ARAMIS system™, was used in his study to monitor surface motion and to compute strain deformation. This provided principal strains of every surface point, which were then used to construct the FLD of this class of material system. Figure 2.5 shows the FLC based on limiting principal strains observed in experiments. The constructed FLC was path-dependent such that the failure occurs at a point when its deformation path and instantaneous strain state satisfies the failure criterion, meaning the path of strain evolution is as important as principal strains at a single stage.

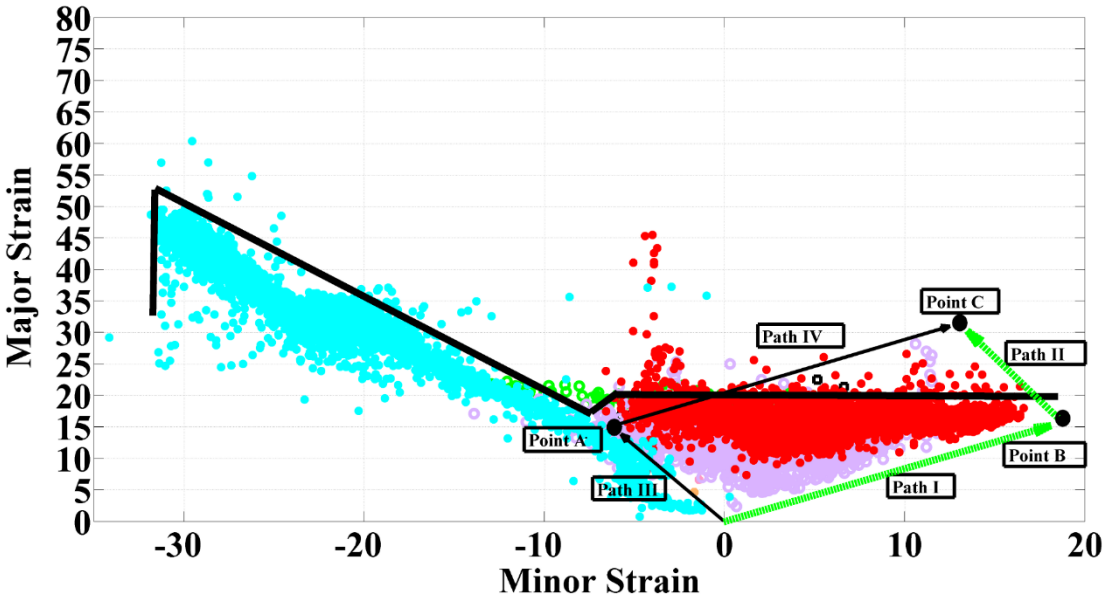

Figure 2.5: The path-dependent FLC constructed by Zanjani *et al.* [73].

Sexton [19] investigated a fibre metal laminate based self-reinforcing polypropylene composite in stretch forming tests. Samples had a self-reinforced polypropylene composite core sandwich structure between two pieces of 5005 H34 aluminum layers. Hourglass samples with widths from 25 to 200 mm were formed into hemispherical domes using a stamping press machine. Prior or to forming, a tightening torque was applied to each of six M12 bolts to fix the specimen between the blank-holder and the lock-ring, preventing the edge of the composite from being drawn into the die cavity. It was found that the failure behaviour of the fibre-metal laminate structure was more complex than just considering principal strains, as the failed data point of one specimen could lie in the unfailed region of another specimen. High shear strain deformation was the reason that an unfailed point can withstand a higher major strain than a failed point. Under shear deformation, fibres did not experience the highest strain, and the polypropylene matrix could withstand higher strain deformation than the fibres. To overcome this, a three-dimensional FLD was proposed, as shown in Figure 2.6. This three-dimensional FLD considers principal angle as a key parameter in addition to principal strains.

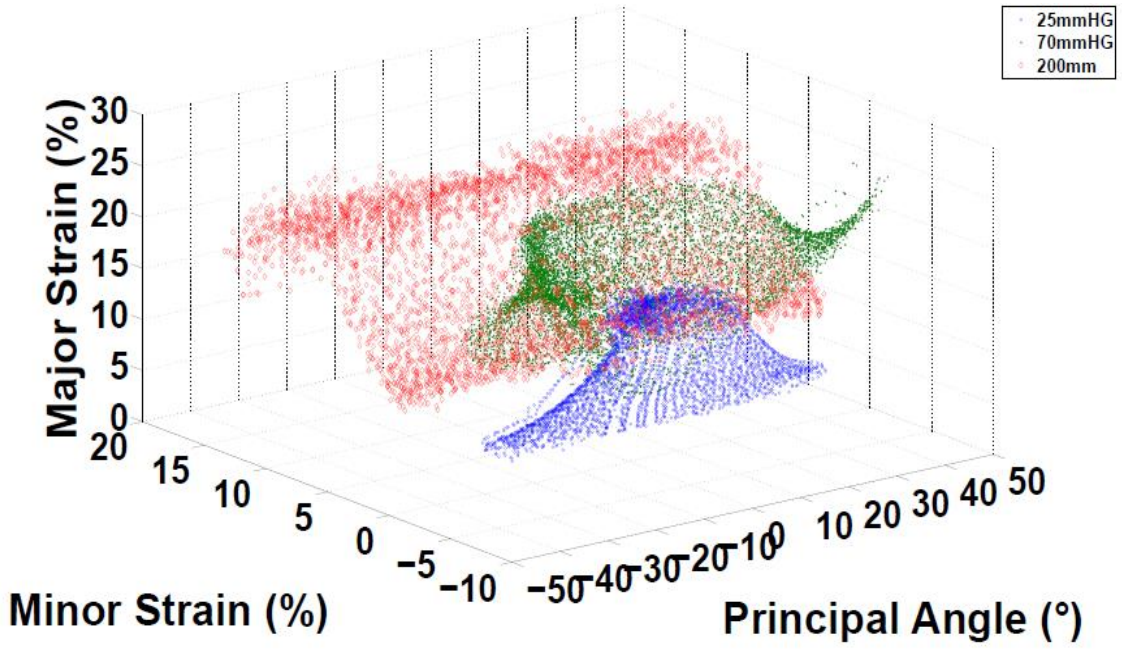

Figure 2.6: The three-dimensional FLD proposed by Sexton [19].

Studies have shown that there are certain disadvantages of expressing forming limits of materials in terms of strains [105, 106], and a major one of them is strain path dependency. In order to overcome this shortcoming, forming limit curves have been developed in the stress space [107-109]. This idea was firstly proposed by Arrieux *et al.* [110] in 1982, and this method seemed to be independent of the strain path changes. This method was then promoted as a proper solution when analysing the formability of material in multi-stage forming processes. Levy and Van Tyne [107] developed a method to calculate a stress-based forming limit curve. Under the application of the Keeler-Brazier equation, the effective stress in plane strain was proved to be a function of thickness of the sheet and the instability/damage parameter which was calculated from a uniaxial tensile test. The stress-based FLC was proved to be applicable to conventional high strength steels, and the use of this method could provide a practical approach to predict failure behaviour in sheet metal forming with complex strain paths. Panich *et al.* [108] conducted experimental and numerical analysis of Forming Limit Stress Diagram for two advanced high strength steel sheets (DP780 and TRIP780). The

stress-based forming limit curve was experimentally determined by means of the Nakazima forming tests which were performed based on the international standard ISO 120004-2 on a 600 kN Erichsen sheet metal testing machine. Analytical calculations of FLSD were carried out based on a combination of Marciniak-Kuczinsky (M-K) model, the Swift hardening law, and the Yid20000-2d yield criterion. There was a slight underestimation of the experimental FLD under uniaxial tension load. From the hole expansion test conducted in the work, it was verified that the conventional strain-based FLD was insufficient for predicting material failure, whereas the stress-based FLD could more precisely describe the forming limits of both high strength steels. However, it was also found that the accuracy of the stress-based FLD depended strongly on the yield function and hardening law used in the calculations. Although stress-based forming limit curve seemed to be valid for predicting the failure behaviour of the metals, the application of this method to composite forming is still questionable. Apart from the dependency on the selection of yield functions, as stated above, the application of stress measurement in practice could be less convenient and accurate than strain measurement.

Several issues have also been noticed when applying FLC to material systems other than metal alloys. Firstly, it has been mentioned that, due to strain path dependency effect, surface principal strains at a single stage are not enough to predict failure [19, 73]. An additional variable other than principal strains, or a new FLC with different parameters might be needed, and the accuracy of the FLC with three variables has not been verified yet in the literature. Secondly, it still remains questionable whether the FLC is more effective than theoretical failure criteria such as the Maximum Strain failure criteria. Thirdly, although an extensive amount of research has been conducted in constructing FLCs from stretch forming tests, few has applied the FLC to predict failure

in other forming practices, for instance draw forming tests. All of these issues need to be addressed properly before applying the FLC in the mass production process.

In summary, additional research effort is required to find theoretically valid and practical failure criteria for pre-consolidated woven natural fibre composites, and this forms an essential part of this research work.

2.5 Finite element analysis

In engineering design, numerical simulation is an essential tool that can reduce the trial and error part of product development [111-114]. In addition, simulating the forming behaviour of a material using Finite Element Models can provide information which cannot be gained experimentally. For the rapid forming simulations conducted in this work, two formulations can be used: implicit and explicit. In implicit procedure, the state at t+Δt is determined based on information at time t+Δt, whereas it is based on information at time t in explicit procedure [115].

2.5.1 Implicit method

Under the consideration of quasi-static problem, The implicit method can be expressed in terms of Equations 2.18 – 2.24 [116]. Firstly, the discretised equilibrium Equation for the finite element model is:

$$\mathbf{P^N - I^N = M^{NM}\ddot{\mu}^M} \tag{2.18}$$

where P^N is the external force vector; I^N is the internal force vector; M^{NM} is the mass matrix; and $\ddot{\mu}^M$ is the acceleration vector.

The internal forces are given by:

$$\mathbf{I^N = \int \beta^N : \sigma \, dV} \tag{2.19}$$

Where V is the current volume of the model, $\sigma(x)$ is the stress at a point currently located at position x, $\beta^N(x)$ is the strain rate-displacement rate transformation defined from the interpolation assumption in the element.

In static equilibrium, the d'Alembert forces are almost constant with time, implying the following expression.

$$\mathbf{M^{MN}\ddot{\mu}^{M} \approx 0} \tag{2.20}$$

ABAQUS/Standard uses Newton's method to solve for static equilibrium. By applying the Taylor's series expansion, an estimated solution at iteration (i) and $u_{(i)}^N$ can be obtained:

$$\mathbf{P^N - I^N + \left(\frac{\partial P^N}{u^M} - \frac{\partial I^N}{u^M}\right) C^M + \cdots = 0} \tag{2.21}$$

Therefore,

$$\mathbf{K^{NM} \times C^M = P^N - I^N} \tag{2.22}$$

$$\mathbf{K^{NM} = \frac{\partial P^N}{u^M} - \frac{\partial I^N}{u^M}} \tag{2.23}$$

where K^{NM} is the system's tangent stiffness, or Jacobian matrix.

The incremental displacement can also be updated as:

$$\mathbf{\Delta u^N_{(i+1)} = \Delta u^N_i + C^N_i} \tag{2.24}$$

where $\Delta u_{(i+1)}^N$ is the incremental displacement at the increment of i+1; Δu_i^N is the incremental displacement at the increment of i; C^N is the correlation to the solution at the degree of freedom N at the increment of i.

2.5.2 Explicit method

The explicit method was originally developed to solve dynamic problems involving deformable bodies [115]. ABAQUS/Explicit method solves for a state of dynamic equilibrium at the current time increment (t).

$$\mathbf{P^N - I^N|_t = M^{NM}\ddot{\mu}^M|_t} \tag{2.25}$$

Therefore:

$$\mathbf{\ddot{\mu}^M|_t = [M^{NM}]^{-1}\times(P^N - I^N)|_t} \tag{2.26}$$

By applying central difference integration rule, the velocities and displacements can, in turn, be updated.

$$\mathbf{\dot{u}^N|_{t+\frac{\Delta t}{2}} = \dot{u}^N|_{t-\frac{\Delta t}{2}} + \left(\frac{\Delta t|_{t+\Delta t}+\Delta t|_t}{2}\right)\ddot{\mu}^N|_t} \tag{2.27}$$

$$\mathbf{u^N|_{t+\Delta t} = u^N|_t + \Delta t|_{t+\Delta t}\dot{u}^N|_{t+\Delta t}} \tag{2.28}$$

The central integration rule is only conditionally stable, and the solution can diverge rapidly if the time increment is too large. An estimate of stable time increment is given by:

$$\boldsymbol{\Delta t = \min\left(\frac{L^e}{C^d}\right)} \tag{2.29}$$

where L^e is a characteristic element length and C^d is the dilatational weave speed of the material. For linear elastic material:

$$\mathbf{C^d = \sqrt{\frac{\lambda+2\mu}{\rho}}} \tag{2.30}$$

Where λ and μ are Lame's constants and ρ is the material density.

In sheet forming which is a quasi-static process, contact conditions are of great importance. The implicit procedure has to iterate to satisfy all boundary conditions and the time increment needs to be reduced if contact conditions are not satisfied. However, in the explicit procedure, no iterations are required to enforce contact conditions, and the time increment is irrelevant to the number of contact points as well as the contact conditions. In terms of the computational cost, there is a linear relationship between the size of the model and the solution for the explicit procedure. For the implicit procedure, the solution time is proportional to the square of the wavefront size in the global stiffness matrix, which could be very expensive in computational cost when running

large size models or 3D simulations [115]. Therefore, the implicit procedure offers a lower solution cost at small model size, and less solution cost-effective at large model size.

2.5.3 Shell formulation

Compared to solid elements, shell elements can provide good accuracy with considerable savings in computational costs when modelling blanks in rapid forming simulations [12]. ABAQUS/Standard offers a shell element called S4 or S4R where R stands for reduced integration. The geometric descriptions of shell elements are presented in Equations 2.31-2.41 [117].

The position of a material point in the shell is defined as:

$$\mathbf{x}(\mathbf{S_i}) = \bar{\mathbf{x}}(\mathbf{S_\alpha}) + \overline{\mathbf{f_{33}}}(\mathbf{S_\alpha})\mathbf{t_3}(\mathbf{S_\alpha})\mathbf{S_3} \tag{2.31}$$

Where the subscript i and other Romans in the Equations below range from 1 to 3; α and other lower Greek subscripts in the Equations below represent the quantities in the reference surface of the shell range from 1 to 2; t_3 is the normal to the reference surface of the shell.

The gradient of the position can therefore be represented as:

$$\frac{\partial \mathbf{X}}{\partial \mathbf{S_\beta}} = \frac{\partial \bar{\mathbf{X}}}{\partial \mathbf{S_\beta}} + \overline{\mathbf{f_{33}}}\frac{\partial \mathbf{t_3}}{\partial \mathbf{S_\beta}}\mathbf{S_3}, \quad \frac{\partial \mathbf{X}}{\partial \mathbf{S_3}} = \overline{\mathbf{f_{33}}}\mathbf{t_3} \tag{2.32}$$

Where we have neglected derivative of $\overline{f_{33}}$ with respect to S_β, and the thickness increase factor $\overline{f_{33}}$ is assumed to be independent of S3.

In the deformation state, the local, orthonormal shell directions t_i can be defined as follow:

$$\mathbf{t_i}\times\mathbf{t_j} = \boldsymbol{\delta_{ij}},\ \ \mathbf{t_i t_i} = \mathbf{I} \tag{2.33}$$

Where δ_{ij} is the Kronecker delta and I is the identity tensor of rank 2.

$$\mathbf{f_{\alpha\beta}} = \mathbf{t_\alpha}\frac{\partial \mathbf{X}}{\partial \mathbf{S_\beta}} = \overline{\mathbf{f_{\alpha\beta}}} + \mathbf{B_{\alpha\beta}S_3} \tag{2.34}$$

The reference surface deformation gradient and the reference normal gradient can therefore be expressed as:

$$\overline{\mathbf{f_{\alpha\beta}}} = \mathbf{t_\alpha}\frac{\partial \mathbf{X}}{\partial \mathbf{S_\beta}}\,|_{\mathbf{S_3=0}} = \mathbf{t_\alpha}\frac{\partial \bar{\mathbf{X}}}{\partial \mathbf{S_\beta}} \tag{2.35}$$

$$\mathbf{B_{\alpha\beta}} = \mathbf{t_\alpha}\frac{\partial \mathbf{t_3}}{\partial \mathbf{S_\beta}} \tag{2.36}$$

In the original (reference) configuration, the position is denoted by X (the reference surface by $\bar{X}$) and the direction vectors are denoted by T_i. Therefore Equation 2.31 can be transformed to the following equation.

$$\mathbf{x}(\mathbf{S_i}) = \bar{\mathbf{x}}(\mathbf{S_\alpha}) + \mathbf{T_3}(\mathbf{S_\alpha})\mathbf{S_3} \tag{2.37}$$

The gradient of the position, and the in-plane components of the gradient can be written as:

$$\frac{\partial \mathbf{X}}{\partial \mathbf{S_\beta}} = \frac{\partial \bar{\mathbf{X}}}{\partial \mathbf{S_\beta}} + \frac{\partial \mathbf{T_3}}{\partial \mathbf{S_\beta}}\mathbf{S_3},\ \ \frac{\partial \mathbf{X}}{\partial \mathbf{S_3}} = \mathbf{T_3} \tag{2.38}$$

$$\mathbf{f}^{\circ}_{\boldsymbol{\alpha\beta}} = \mathbf{T_\alpha}\frac{\partial \mathbf{X}}{\partial \mathbf{S_\beta}} = \boldsymbol{\delta_{\alpha\beta}} + \mathbf{B}^{\circ}_{\boldsymbol{\alpha\beta}}\mathbf{S_3} \tag{2.39}$$

It is assumed that the in-plane direction vectors follow from the surface coordinates, and the original reference surface normal gradient is therefore determined.

$$\mathbf{T_\beta} = \frac{\partial \mathbf{X}}{\partial \mathbf{S_\beta}}\,|_{\mathbf{S_3=0}} = \frac{\partial \bar{\mathbf{X}}}{\partial \mathbf{S_\beta}} \tag{2.40}$$

$$\mathbf{B}^{\circ}_{\boldsymbol{\alpha\beta}} = \mathbf{T_\alpha}\frac{\partial \mathbf{T_3}}{\partial \mathbf{S_\beta}} \tag{2.41}$$

It is noted that the original reference surface normal gradient from interpolation of the nodal normal with the shape functions in the FEA formulation.

2.5.4 FEA simulations of composite forming

Typically, in composite forming there are two modelling methods: micro- and macro-level methods [18]. A micro-mechanical simulation models the individual fibres and the matrix in each layer of the laminate structure, and this method can generate accurate results, but at a high computational cost. In macro-mechanical modelling, the composite material is considered a homogeneous structure. In either method, the way the material is modelled is of great importance to the accuracy of the model. Boisse *et al.* [118] developed a FEA simulation of woven fabrics forming where fibres and matrix were modelled individually. The mechanical behaviour of the material in tension was determined through bi-axial stretching tests, where different strain ratios ranging from 0 to 2 were used. It was found that the behaviour of the material was non-linear and the non-linearity zone was increased with decreasing the strain ratio value. In addition to using the biaxial stretching tests, picture-frame tests were also applied to obtain the in-plane shear behaviour of the composite. By incorporating these mechanical properties, the process of deep drawing of a square box was simulated and then compared in two different ways: tension only as well as tension plus shear. The numerical simulations suggested that the rotation angles were reduced when shear stiffness was taken into account, which was closer to reality.

Vanclooster *et al.* [119] undertook forming experiments of glass fibre reinforced polypropylene fabrics to validate commercial simulations. During experiments, a local shear profile of the formed shape was obtained in sequential steps. A reference pattern was sprayed to the surface of a pre-consolidated woven fabric, and based on the way the pattern varied the shear angle of the deformed sheet could be obtained through a DIC (Digital Image Correlation) technique. Similar to Boisse's work, two approaches were compared. The first was the kinematic approach that only considered un-resisted in-

plane shear as the deformation mechanism, and this failed to predict fibre re-orientation during forming. The second approach adopted a more refined mechanical simulation where both the shear and tensile behaviour of the fabric were taken into account. A 'biphase' model with a thermo-visco-elastic matrix and elastic fibres was used in this simulation. The total stress was given by the sum of three components from: the elastic properties based on in-plane shear behaviour of the fabric; the matrix material through a Maxwell model; and the behaviour of the reinforcement in the fibre directions. All three components were uncoupled. This method gave a reasonably good prediction of fibre reorientation, and deviations between experiments and simulations could be explained by the 'over-simplified' material model and the lack of coupling between the tensile and shear behaviour. Based on the findings observed by Boisse *et al.* [118] and Vanclooster *et al.* [119] both the tensile and shear behaviour of the composite fabric should be taken into account to ensure an accurate numerical simulation. Lee *et al.* [120] analysed the biaxial stretch forming behaviour of glass-fibre reinforced thermoplastic composite with a random fibre orientation under various forming parameters such as punch speed, temperature, and fibre volume fraction. This study found that the difference between experimental and numerical simulation was due to the inability of the material model to incorporate the effect of strain rate on the mechanical responses of the material.

Built-in material models are usually available in commercial FEA software. However, a user-defined material routine has been used to model more complicated material behaviour [121]. Sexton [19] modelled a glass-fibre reinforced polypropylene composite through a user-defined material routine, and the flow chart of the material model is shown in Figure 2.7. Due to the non-linearity nature of material stiffness in both the fibre and shear directions, the coefficients in the stiffness matrix were expressed as functions of strains.

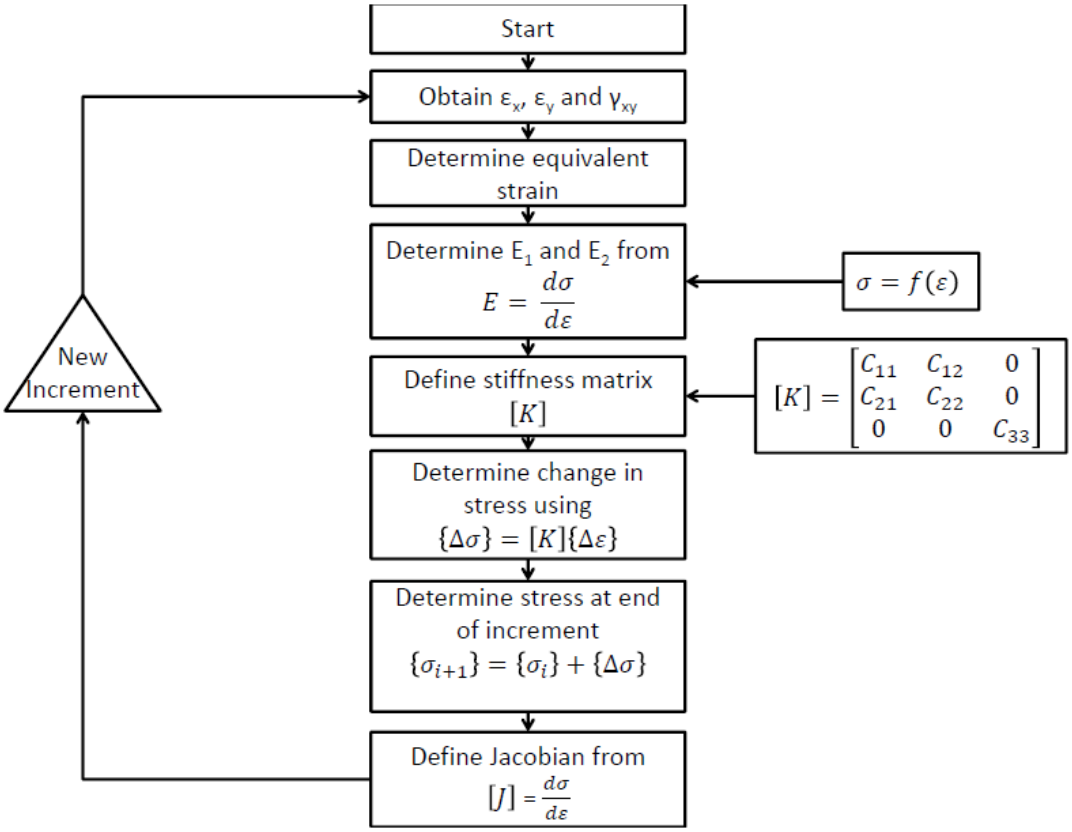

Figure 2.7: Flow chart of the material model [19].

It was found that the stress-strain behaviour of the composite material fitted the following expressions:

$$\boldsymbol{\sigma = Ae^{B\varepsilon} + Ce^{D\varepsilon}} \tag{2.42}$$

$$\boldsymbol{\sigma = Y\varepsilon + H} \tag{2.43}$$

where σ is stress; ε is strain; and A, B, C, D, Y and H are coefficients.

Equation 2.42 was used when the absolute value of strain was less than 2%, otherwise the stress-strain relation was described by Equation 2.43. To help predict the forming behaviour at different temperatures, the stress-strain relations at elevated temperatures were expressed by these two equations using curve-fitting software so that all coefficients could be expressed as a function of temperature.

As well as a suitable material model, contact conditions are another essential component of FEA models. When a circular sample is formed into a hemispherical dome structure with its edge being clamped, the tension in the sheet increases with the punch displacement. If there is no friction between the composite and the tool, the greatest strain will be at the pole, which is where failure will occur. Under high friction conditions, the pole of the specimen stops deforming beyond a certain punch depth, and the maximum strain deformation appears some distance from the pole where failure by splitting is expected [122]. Because at small forming depths the maximum strain deformation spreads from the pole to nearby regions, a less lubricated contact conditions result in lower strain profile along the diameter of the specimen [19]. In some applications, a very high friction value was defined when the contact layers were assumed not able to slide against each other [50].

Previous studies have shown that the steady state friction coefficient between the thermoplastic composite and the tools can vary from 0.05 at high temperatures, low sliding speeds, and high pressures to 0.5 at low temperatures, high sliding speeds, and low pressures [123]. Much higher friction values were not uncommon. Harrison *et al.* [124] examined the effect of the coefficient of friction in press forming of a 0°/90° cross-ply thermoplastic composite at elevated temperatures. The first simulation used an artificially high value of coefficient of friction, 5.0, to account for the rapid cooling, freezing and reduction in mobility of the thermoplastic matrix composite during forming. A more realistic value of 0.3 was used in a second simulation. It was found that the localised shear zones were suppressed by a high coefficient of friction, and a higher material stiffness promoted shear localisation when the amount of friction was more realistic.

An essential application of numerical simulation is to provide information which cannot be observed experimentally. Davey *et al.* [86] developed FEA models in ABAQUS/Standard to simulate the forming behaviour of a pre-consolidated carbon fibre reinforced polyether ether ketone (PEEK) composite in draw forming tests. In the FEA simulation, a linear orthotropic material model, based on mechanical properties obtained from experiments and the literature, was assigned to the composite material. For dome forming tests, a real-time strain measurement system was used to monitor surface motion. However, the flange region of the composite was blocked by the tool, making it impossible to observe the forming behaviour of this region. Flow behaviour was observed from the FEA simulations, where much larger displacements were experienced in the fibre directions compared to at 45° to them. This was primarily due to much higher stiffness to carbon fibres compared to the PEEK matrix.

2.6 Summary

This Chapter has summarised the literature regarding the structure of natural fibre composites, and surveyed possible treatments that can help this class of material system achieve better formability. It has also reviewed composite forming and how to simulate forming experiments using FEA modelling. While an extensive amount of research has been done on the forming of composite materials, there are still two unanswered questions in the field, and this work was designed to answer them.

The first question is, how to form this class of material system? Untreated natural fibres usually cannot withstand a high level of extension, and poor formability is therefore expected when the composite is formed without receiving any additional treatment. In addition, preheating, which is the traditional method of improving the forming behaviour of composite materials, may not be applicable because of possible thermal

degradation of natural fibres at low temperatures. Even if this treatment works, are there any other treatments (either physical or chemical) that might be more? The current work also investigates the effect of the weave structure by comparing two different natural fibre composites which have the same constituent material, similar fibre fraction and thickness, but different weave structure.

The second question is that, what is the best measure of predicting the failure of the composite? Most failure models stated in the literature review were developed for finished composites subjected to uniaxial loading but not for damage during forming. More importantly these criteria do not account the weave structures in which interactions between the fibres and the matrix are important. Also, according to the literature, the conventional FLC may not be applicable to composite materials. Additional research effort is therefore needed to obtain valid failure criteria for woven composite materials.

Materials and Methodology

3.1 Introduction

Natural fibre composites are processed using different treatments prior to forming, and this section gives details of treatments. Tensile tests are performed on Instron™ 4505 testing machine at a constant loading rate of 5 mm/s. Both dome forming and stretch forming tests are conducted through a stamping press machine. An ARAMIS™ strain measurement system is used to monitor surface motion, and to calculate strain deformation. This Chapter presents the composite materials used in the current work, followed by an overview of different treatments applied to natural fibre composites and finally the setup of all experiments performed including uniaxial loading, stretch forming, and dome forming Tests.

3.2 Materials

The forming behaviour of two classes of flax fibre reinforced polypropylene (pp) composites, as shown in Figure 3.1, were analysed. Firstly, a chopped natural fibre composite was used: it was a pre-consolidated chopped flax fibre reinforced polypropylene composite, FibriBoard™, was manufactured by EcoTechnilin, UK. The second material was a continuous natural fibre composite: it was a continuous flax fibre reinforced polypropylene fabric, Biotex™, manufactured by Composites Evolution, UK and then consolidated by the Xiafei factory located in Jiayong Junctions, Dongguan, Guangdong, China. In the consolidation process, two pieces of 200×200 mm 1 mm thick fabrics were stacked on top of each other and placed in a closed steel mold with an inner height of 1 mm. The mold together with fabrics were then inserted into a heat press machine and heated to 190°C which exceeded the melting temperature of the

polypropylene. A pressure of 10bar was then applied to the mold for 3 minutes to ensure the thickness of the consolidated composite was no more than 1 mm. Consolidated composites were then cooled to room temperature before removal. The chopped natural fibre composite (CNFC) had a random distribution of short flax fibres whereas the fibre bundles in the continuous natural fibre composite (NFC) were woven in a 2 × 2 twill structure. Both composites have the same constituent material, a similar fibre weight fraction (50%) and the same thickness (1 mm). It was noted that both composites appeared to possess a higher than expected level of surface porosity, and this porosity seemed to continue through the thickness of the sample. It was assumed that this porosity was caused by the evolution of gaseous products during the hot consolidation process – a common issue with natural fibre composites.

(a) (b)

Figure 3.1: The pre-consolidated composites. (a) NFC; (b) CNFC.

3.3 Treatment methods

The natural fibre composite materials studied in this study exhibit low extensibility, as per observations in uniaxial loading tests described in Chapter 4. The inherently small elongation-to-failure of flax fibres largely prevents the natural fibre composites from being stretched a great extent. Therefore, additional treatments on consolidated

composites become necessary for improving the formability for this class of material system. In this work, three different types of treatments were selected and their effects on the forming behaviour of natural fibre composites were studied. These treatments were: preheating, chemical treatment, and tailored blanks.

3.3.1 Preheating

Preheating has been conventionally used in improving the formability of materials in rapid forming processes. This treatment was applied to the composites in both tensile tests and draw forming tests, using a heat chamber and heat press machine as shown in Figure 3.2. For the tensile tests performed at high temperatures, samples were preheated through a heat chamber before testing. The temperature inside the heat chamber could rise nonlinearly up to 340 ˚C at an average rate of 12 ˚C/min (the heating rate was much faster at low temperatures). The highest temperature at which the composites were tensile tested was 160 ˚C. For dome forming tests, a hydraulic heat press consisting of two heating plates and a manual cylinder controller was used to heat the samples. The heat press was able to heat samples safely up to 250 ˚C with a maximum pressure of 60 bar. The heat press was placed near the stamping press to minimise the temperature drop during sample transfer. Samples were preheated to 15 ˚C above the forming temperature to compensate for the drop in temperature which occurred during transfer of the samples from the heat press to the stamping machine and waiting for the punch to move down. The required adjustment was verified by temperature observations during the experimental process.

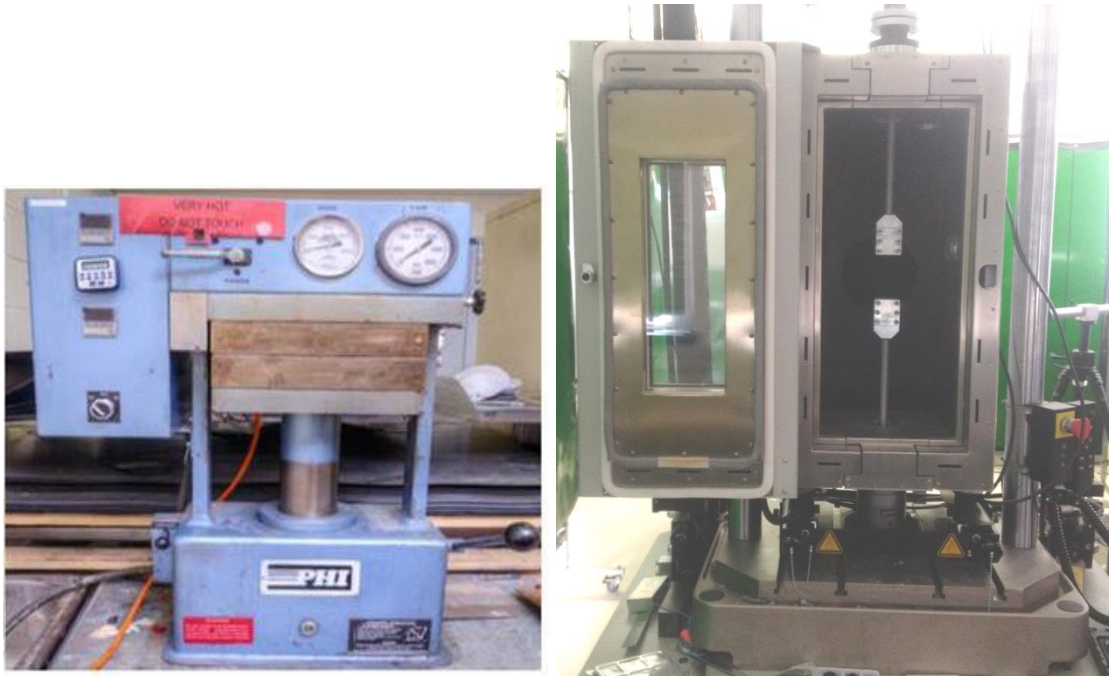

(a) (b)

Figure 3.2: The equipment used for the preheating treatment. (a) heat press; (b) heat chamber.

The thermal degradation of the composite was identified in this study. To determine the mechanisms behind degradation, Fourier Transform Infrared Spectroscopy (FTIR), Thermogravimetry (TG) mass, and Differential Scanning Calorimetry (DSC) examinations were conducted. FTIR and TG have been proved valuable tools to clarify different steps during fibre decompositions [11, 125], which is essential to determine the causes of the fibre thermal degradation observed in the current study. DSC tests have been run frequently to determine the heat flow behaviour of materials over the range of working temperatures [11, 12]. It is noted that composite materials were heated from room temperature to 200 ˚C in both TG mass and DSC examinations.

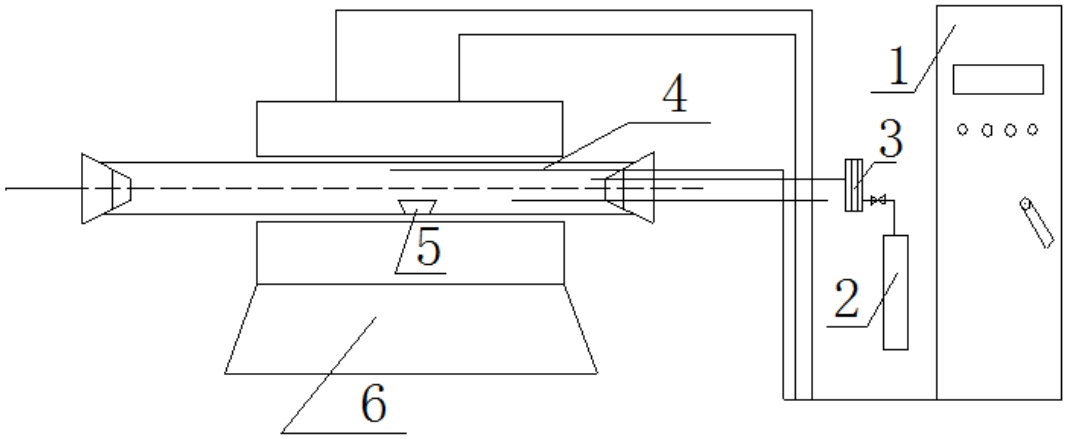

Figure 3.3: Schematic of the equipment used for preparing FTIR specimens. 1: temperature controller; 2: nitrogen-gas bottle; 3: rotameter; 4: thermocouple; 5: stainless-steel boat; 6: horizontal electric furnace.

To prepare the samples for FTIR examination, the composites were preheated to the desired temperatures and then cooled to room temperature surrounded by nitrogen gas, a procedure which prevented oxidization and ensured that the chemical composition remain unchanged. This process was done using the equipment shown in Figure 3.3. The temperature controller was set to 25 ˚C, 120 ˚C and 150 ˚C, respectively, and the temperature increased at an average rate of 20 ˚C/min. All samples were cut into a 4 mm by 10 mm rectangle using a mechanical scissors. The tube was filled with nitrogen gas and the samples were placed the stainless-steel boat at the middle of the horizontal tube. The nitrogen prevented oxidation of the materials during testing, and it usually took 15 to 20 minutes for nitrogen to fully occupy the tube. The temperature controller was turned off when the desired temperature was reached, after which the entire system cooled naturally to room temperature, and the boat was then taken from the tube. The samples that collected from the stainless boat were then subjected to FTIR tests.

3.3.2 Chemical treatments

It is an important part of the scope to investigate whether there are other treatments, in additional to the conventional method (preheating), which can effectively improve the formability of natural fibre composites, and equally important to determine whether these treatments are more effective than preheating. Chemical treatments are being seen as effective methods to modify natural fibre based composites to improve their formability. Distilled water, a 0.5 M Sodium Hydroxide solution (NaOH), a 12%wt M.A. solution and a Cloudy Ammonia (C.A.) solution with 20 g/L of ammonia were selected to determine the effect of chemical treatments on the physical and tensile properties of the samples. To determine the saturation characteristics in each solution at ambient temperature, samples were placed in plastic containers filled with chemical solutions up to a depth of 35 mm. A circular hole was drilled in the middle of the lid and sealed with a piece of flexible parafilm to create a gas bleeding mechanism and ensure safe testing conditions. The variations in sample weights were recorded accordingly during solution uptake, and subsequent moisture egress from saturation. A precision weighing balance, an A&D GX-400 milligram scale, was used to weigh samples. This balance system can measure weights ranging from 0.02 g to 410 g with precision of 0.001 g and error of 0.01 g. The balance was calibrated prior to each use, and was re-zeroed before measuring the weight of each sample (which was lightly mopped to remove surface moisture).

Three sample conditions were trialled: untreated, saturated, and dried. Untreated samples were cut from the as-received material with no chemical treatment; saturated testing was performed on samples that had reached a consistent weight gain; and dried testing was performed on samples that had been saturated, and then subsequently dried. Variations in tensile properties were observed between different conditions, and the

mechanism behind these changes was investigated using Scanning Electron Microscope (SEM) examinations on fractured surfaces. All samples were lightly platinum coated before SEM examinations using a Hitachi 4300 Field Emission Electron Microscope. Water treatment was applied to composites in all forming practices conducted in this study, including dome forming tests and stretch forming tests. During these tests, the composites were formed in untreated, water-treated and redried conditions, respectively.

3.3.3 Tailored blanks

Unlike the preheating and chemical treatments which alter the material properties, the application of tailored blanks could help the composites achieve better formability by using particular sample geometries. Tailored blanks called for specific sample shapes in which areas were cut out along fibre directions from sample edges. In dome forming tests, the tailored shape introduces unbalanced restriction on material flow (less restriction along fibre directions). Compared to a fully circular sample, blanks tailored in this way experienced less restriction in the longitudinal and transverse directions, resulting in less strain deformation on the flax fibres. The amount of strain deformation acting on the flax fibres is a key factor in composite failure, as the fibres possess a significantly lower elongation-to-failure compared to that of the polypropylene matrix. Figure 3.4 shows experimental geometries of the tailored blanks. By varying the inner radius of the tailored blank, R65, R75, and R85 specimens (the number indicates that the inner radius in mm) are used in experiments.

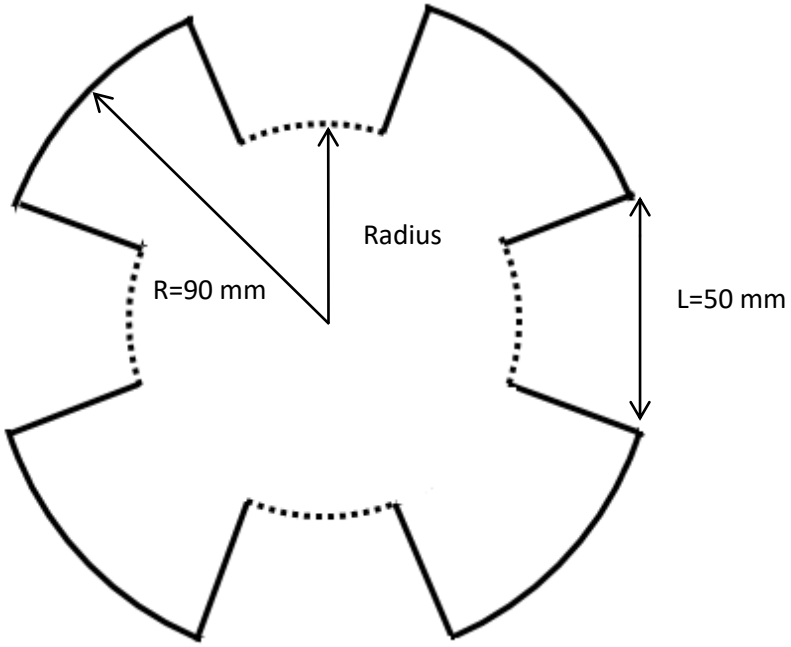

Figure 3.4: Experimental geometries of the tailored blanks.

3.4 Experimental setup

3.4.1 Tensile Tests

A number of forming tests were performed in this work. Tensile tests were performed firstly to determine the mechanical behaviour of composite materials in different temperatures or conditions of chemical treatments. The information obtained from uniaxial loading tests provides mechanical responses of this class of material systems in simple forming conditions, which can be used in analysing the behaviour of samples in more complicated experiments such as dome forming and stretch forming tests. Tensile tests were conducted to both CNFC and NFC in different conditions/treatments. All tests were conducted using an Instron™ 4505 testing frame, as shown in Figure 3.5. Specimens were tested at a rate of 5 mm/min, with failure being defined as when the applied load had dropped to 60% of its original value. Rectangular test specimens of 15 mm by 150 mm were produced, and the actual testing area was 15 mm by 100 mm. In order to obtain tensile properties along the fibre direction and off-fibre direction, NFC

samples were cut such that fibres were oriented at 0˚/90˚ as well as at 45˚/-45˚ to the sample axis. During experiments, surface displacements are captured by the ARAMIS™ system which then computes surface strains.

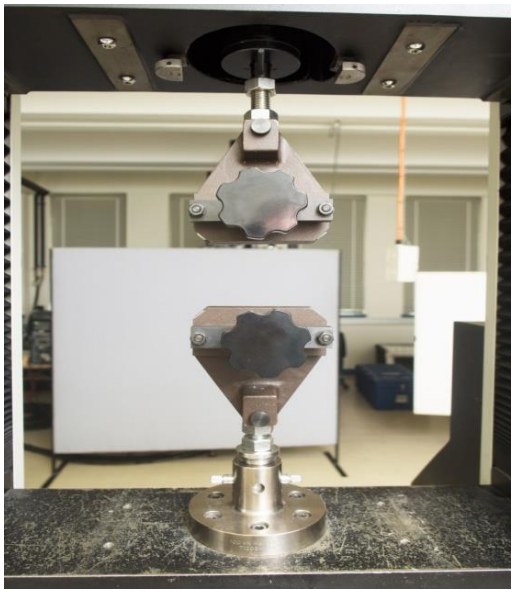

Figure 3.5: The Instron™ 4505 testing frame used in the tensile tests.

3.4.2 Stretch forming

Stretch forming experiments had been developed to investigate the failure of monolithic metal alloys, and this technique had also been successfully applied to woven composites. The current work uses stretch forming technique to determine the failure behaviour of natural fibre composites in different deforming modes. A custom-designed press was used to conduct stretch forming tests. This press machine consists of a 30-ton H-frame, a 100 mm diameter hemispherical punch, and an open die of 105 mm diameter. The stamp press was controlled through a hydraulic feed controller. A 150 kN compression load cell and a 250 mm linear potentiometer were installed to record punch force and measure displacement, respectively. Process parameters like blank-holder force (BHF), feed rate and holding time could be set up through a computer connected to the stamp press. The blank-holder force could be set to any value between 0 to 14 kN. The fastest and slowest feed rate were 40 mm/s, and 10 mm/s, respectively. The open die design of

the stamping press facilitated the application of optical strain measurements, which were made using the ARAMIS™ system. This system applies three-dimensional photogrammetry technologies to record, and to compute surface displacement and strain deformation based on photographic images captured by its two charge-coupled device (CCD) cameras. Displacement was then computed from these images using an area-based matching algorithm where two-dimensional displacements can be correlated to three-dimensional point distribution at each stage (and hence to compute strains). The ARAMIS system was placed beneath the stamping press to monitor the surface motion of the composite during dome forming and stretch forming, as shown in Figure 3.6. The specifications of the ARAMIS™ system is summarised in Table 3.1.

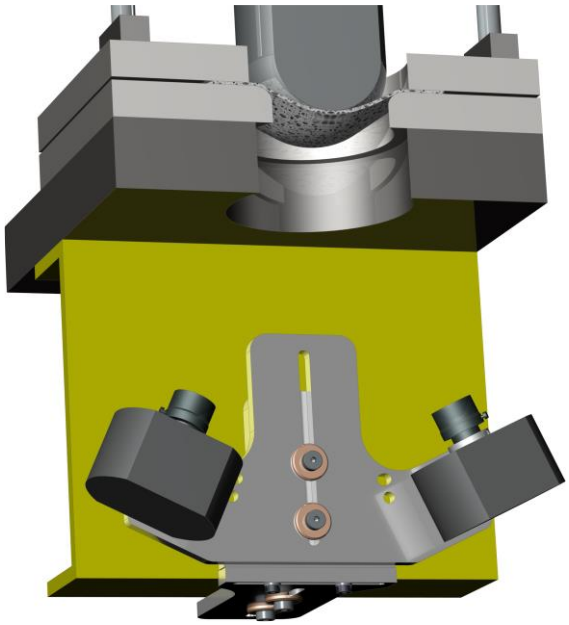

Figure 3.6: Integration of the ARAMIS™ system with the stamping press.

Parameter	**Specifications**
Measuring volume (mm)	10 × 8 to 5000 × 4150
Camera resolution (pixels)	2448 × 2050
Maximum frame rate (Hz)	15
Shutter time (s)	0.0001 to 2
Strain accuracy (%)	Less than 0.02
Strain range (%)	0.02 to >100

Table 3.1: Specifications of the ARAMIS™ system

For instance, there are usually around 30 images taken for the entire stretch forming test (including images for pre-stretch), and in each image there is a full-field strain contour consist of more than 3000 pixel/data point. For these data points, a list of metrics including major strains and minor strains are available for usage. To obtain ideal conditions for ARAMIS™ strain measurements, sample surfaces were painted with black stochastic dots on top of a white background. After painting, samples had a high level of colour contrast, were sufficient light, but not too reflective. It needs to be emphasised that the composites in this study possessed a high level of surface porosity, a property seemed to extent through the sample thickness. As a result, paint usually soaked right through the samples, making this class of material system very difficult to paint. In practice, experience suggested that an extremely light white spray helped the ARAMIS™ system recognise sample surfaces. For those experiments conducted after water treatment, saturated composites were painted quickly and then tested at maximum moisture level. Inevitably, paint at flange areas that were squeezed by the tools (the blank-holder and the die) would peel off as a result of surface moisture.

Stretch forming was an important tool in determining the failure limits of natural fibre composites at different forming modes. Figure 3.7 shows that each of hourglass geometry can represent a typical forming mode. By increasing the width of an hourglass specimen, a composite experienced increased lateral restriction during forming. This prevented the sample from drawing into the die cavity and resulted in a forming mode closer to biaxial stretch (a strain ratio close to 1), as shown in Figure 3.7.

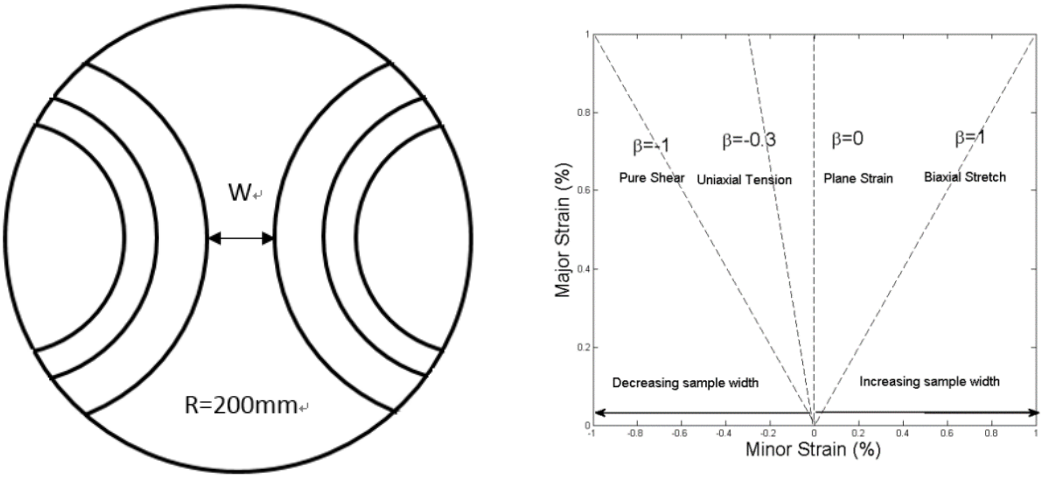

(a) (b)

Figure 3.7: Hourglass geometries (a); and the effect of sample width on the forming mode of the sample (b).

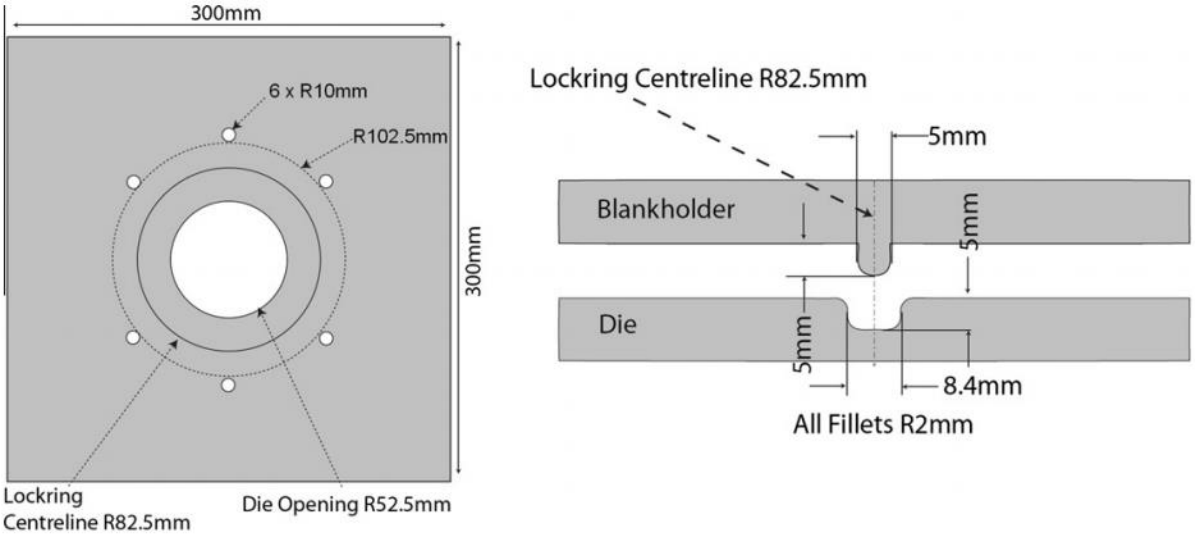

Figure 3.8 Schematic of the lock-ring used in stretch forming tests.

In material forming, the forming mode experienced by samples can be determined from the strain ratio between minor strain and major strain as illustrated in Equation 2.2. Seven experimental geometries, including one full circle specimen, three 0°/90° (fibre direction) specimens with varying widths, and three 45°/-45° (off-fibre direction) equivalent specimens, were used to obtain the failure limits of the composite in all

forming modes, ranging from biaxial stretch to pure shear. Table 3.3 summarises all forming parameters and their levels applied in stretch forming tests for NFC materials. For instance, WF25 stands for the 25 mm water-treated specimen with the flax fibres oriented 0°/90° to the stretching axis (along fibre directions). It is noted that the parameter of fibre orientation is not applicable to CNFC material system as chopped flax fibres are randomly distributed. The polypropylene matrix has a much larger elongation-to-failure compared to the flax fibres, and therefore it is anticipated that the composite can form to a greater depth when the flax fibres are oriented 45°/-45° (in off-fibre direction) than in the 0°/90° to the longitudinal direction. More importantly, 45°/-45° specimens with small sample width can exhibit a major forming mode of pure shear which cannot be obtained from 0°/90° specimens. Figure 3.8 shows the design of the lock-ring used in stretch forming tests. A 15 kN.m tightening torque was applied to six M12 bolts to fix the specimen between the blank-holder and the lock-ring prior to forming, which prevented the edge of the composite from drawing into the die cavity. A forming rate of 20 mm/s was chosen for all specimens. No premature failure or edge movement was identified during forming, which enabled the specimen to exhibit the desired forming mode influenced only by specimen's width and the fibre orientation. Since stretch forming tests are conducted using the stamping press, the ARAMIS™ system was also placed beneath the machine.

Parameters	**Variables/levels**
Treatment	Untreated (U), Water-treated (W), Redried (R)
Fibre orientation	Fibre direction (F), Off-fibre direction (O)
Sample width (mm)	25, 70, 100, 200

Table 3.2: Parameters and corresponding levels used in stretch forming experiment

3.4.3 Dome forming tests

Samples would experience a combination of drawing and stretching in all directions during dome forming test. Due to the difference in stiffness between the flax fibres and the polypropylene matrix, during forming the woven composite tends to be drawn into the die cavity along fibre directions. In general, low blank-holder forces were usually not large enough to fully restrict material flow, and the specimen tends to be stretched rather than drawn when material flow is restricted at high BHFs. Similar to stretch forming tests, all dome forming tests were performed through the custom-designed press, beneath which the ARAMIS™ system was placed to provide displacement and strain deformation during forming. In dome forming tests, a single circular geometry with a diameter of 180 mm was used, and all samples were formed at a constant punch rate of 20 mm/s. It is an important part of the thesis to compare the forming behaviour of natural fibre composites under different treatments. The treatments given to the composites and their parameters were summarised in Table 3.3.

Treatments	Variables/levels
Preheating (°C)	23, 60, 100, 110, 120, 130, 140, 150, 160
Water treatment	Water-treated (W), Untreated (U), Redried (R)
Tailored blanks (mm)	90, 85, 75, 65

Table 3.3: The treatments and their levels applied in dome forming tests

3.5 Summary

Two natural fibre composites with the same constituent material, similar fibre weight fraction (50%), same cross-sectional thickness (1 mm) but different weave structures were studied. This section has described the details of the various forming practices studied, including tensile, dome forming, and stretch forming. Via stretch forming tests, in which samples varying widths (or fibre orientation for NFCs) were formed, the failure envelope of each composite could be obtained. In dome forming tests, the major

forming mechanisms were more complicated, since the sample edge was not fixed and the composite could be drawn into the die cavity. The effect of different treatments was also able to be investigated by analysing the behaviour of composites under different conditions. The ARAMIS™ system was used for all tests to provide data on strain deformation of sample surfaces, which is of great importance for constructing failure envelopes as well as determining the forming behaviour of each sort of composite.

Characterisation of Mechanical Properties

4.1 Introduction

In tensile tests samples are stretched at a constant rate of 5 mm/s until failure for both NFC and CNFC. As mentioned previously, NFC stands for natural fibre composite and refers to the continuous flax/pp composites manufactured by Composites Evolution in UK. CNFC (Chopped natural fibre composites) refers to the chopped flax/pp composite manufactured by EcoTechnilin, UK. Both material systems are stretched at different temperatures ranging from room temperature to 160 ˚C, or in different conditions of chemical treatment including water, NaOH, C.A and M.A. The understanding on mechanical properties can aid analysis under the complicated forming situations presented in Chapters 5 and 6. The variations in mechanical responses of this class of material system could help compare the effectiveness of different treatments, and a particular focus is paid to changes in stiffness and elongation-to-failure as they are key to the forming behaviour of composites in rapid forming. A significant drop in formability is observed when the both composite materials are uniaxial loaded at temperatures higher than 140 ˚C, and the mechanism behind this observation is determined from the observations in FTIR, TG mass and DSC examinations. This section shows that the chemical treatments have the potential to outperform preheating in improving the formability of natural fibre composites. The causes of change in mechanical responses in chemical treatments are also determined through SEM examinations on the fractured surfaces.

4.2 Preheating treatments

4.2.1 Effect of temperature on tensile properties

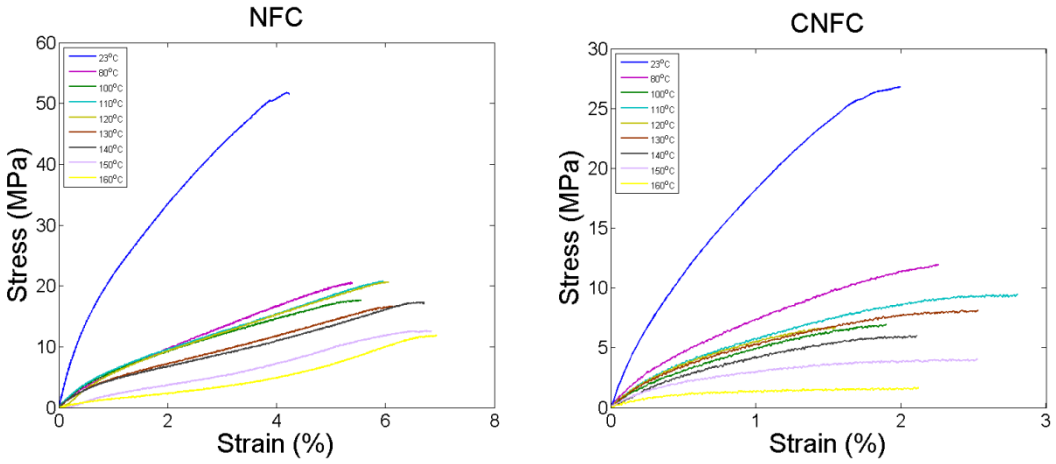

(a) (b)

Figure 4.1: High temperature tensile behaviour of natural fibre composites. (a) NFC; (b) CNFC.

In order to understand the mechanical responses of both composites at elevated temperatures, tensile tests are performed at temperatures between room temperature and 160 ˚C through an Instron™ testing frame which included a heat chamber. Heating natural fibre composites to any temperatures above 160 ˚C results in composite delamination, and is therefore avoided. Figure 4.1 shows that as temperature increases both composites exhibit improved elongation-to-failure as well as reduced stiffness. At room temperature, not much stress transfer between the flax fibres occurs, resulting in fibre breakage at small strains. At higher temperatures, the polypropylene matrix starts to soften, which helps transfer stress within the composite and in turn leads to an increased elongation-to-failure. It is essential to note that preheating can increase the limiting strains of NFC by 59%, and CNFC 40%. At higher temperature, the composite becomes soft and this leads to reduction in stiffness.

4.2.2 Mechanisms behind thermal degradation

When either composite material system is formed at higher temperatures, a significantly reduced formability is observed as described in Section 6.2, a property attributable to the thermal degradation of natural fibre composites. In order to determine the cause of this thermal degradation, FTIR, TG mass and DSC examinations were conducted. In the FTIR examination both composites were analysed at 23 ˚C, 120 ˚C, and 150 ˚C; in both TG mass and DSC examinations they were heated from room temperature to 200 ˚C. Given that the woven structure has an insignificant effect on thermal degradation, all examinations were conducted on NFCs only.

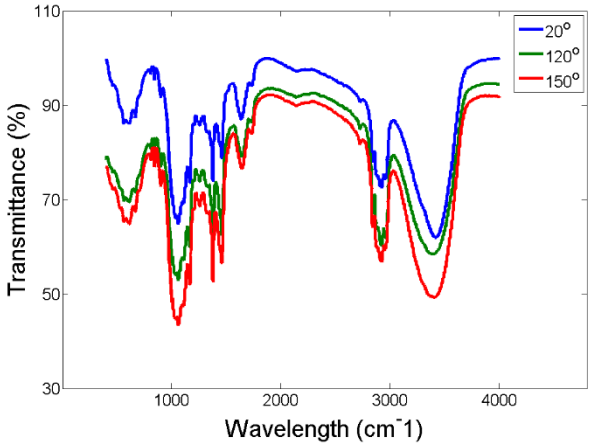

Figure 4.2: FTIR curves of the NFC at 23 ˚C, 120 ˚C and 150 ˚C.

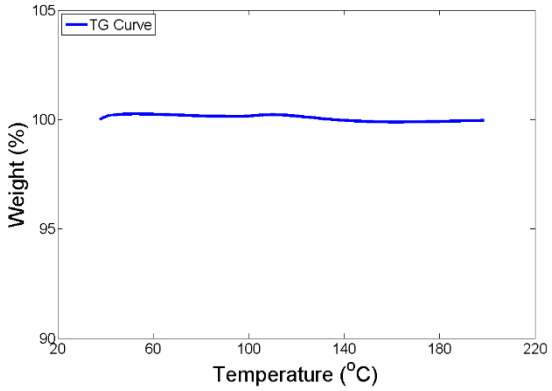

Figure 4.3: TG mass curve of flax/pp composite.

Examination of the FTIR curves shown in Figure 4.2 illustrates that there are no additional or missing peaks, suggesting that no chemical groups form or original chemical groups disappear when the natural fibre composite is heated from room temperature to 150 ˚C. Chemical change is therefore probably not the dominant mechanism for thermal degradation. This is confirmed by the TG mass curve, as shown in Figure 4.3, that there is an insignificant change in the TG mass of the composite when it is heated from ambient temperature to 200 ˚C, suggesting an insignificant amount of weight change due to decomposition. A DSC examination was conducted to investigate the flow behaviour of the composite during thermal degradation, and Figure 4.4 shows that the composite melts between 155 ˚C and 170 ˚C. Thermal degradation temperatures observed in the composite closely coincide with its melting point. When the composite melts, it exhibits a greater molecular mobility and shows a decrease in material properties, which leads to thermal degradation [126]. Based on the information provided by the supplier, the flax fibres used in the composite degrade at approximately 170 ˚C over a sustained heating period and degrade very quickly beyond 200 ˚C. According to the literature, polypropylene melts between 150 ˚C and 170 ˚C [127] which is close to the thermal degradation temperature. Therefore, the major mechanism behind thermal degradation observed in natural fibre composites must be physical changes (melting) of the polypropylene matrix.

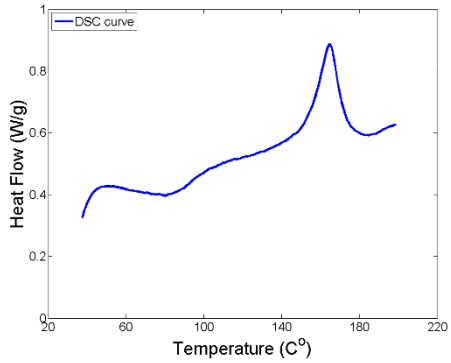

Figure 4.4: Differential Scanning Calorimetry (DSC) curves of the flax reinforced polypropylene composite.

4.3 Chemical treatments

Distilled water, a 0.5M Sodium Hydroxide solution (NaOH), a 12%wt% M.A solution and a Cloudy Ammonia (C.A.) solution with 20g/l of ammonia were selected to determine the effect of chemical treatments on the physical and mechanical properties of NFC and CNFC materials. Rectangular specimens of 15 mm × 150 mm were produced to test composite behaviour during moisture ingress and moisture egress processes, as well as for tensile tests on strength, stiffness, and elongation-to-failure. For the NFC samples, the samples were cut so that fibres were oriented at 0 ˚/90 ˚ to the sample axis. Selected failed samples were then prepared for SEM examination using a Hitachi 4300 Field Emission Electron Microscope. All samples were lightly platinum coated.

4.3.1 Composites behaviour during moisture ingress and egress

Figures 4.5 and 4.6 show the moisture ingress (to saturation) and moisture egress (subsequently dried) curves for the NFC and CNFC. Samples were rectangular dimensions 15 × 150 mm. Solution uptake is defined as the gain in weight of the specimen as a ratio of its original weight (Δm(t) in %), and is defined through the following expression. During the moisture egression process, the weight of the specimen is reduced to approximately its original weight (100% solution uptake).

$$\Delta \boldsymbol{m}(\boldsymbol{t}) = \frac{\boldsymbol{W_t - W_o}}{\boldsymbol{W_o}} * \mathbf{100}\% \tag{4.1}$$

where W_o is the original weight of the specimen and W_t is the weight of the specimen at time t. The samples were weighed after removal from the liquid reservoirs and immediate shaking to remove surface moisture. No surface moisture was detected during this weighing process and the samples were returned to the reservoirs once a stable weight reading had been recorded. Five repeats were used for each treatment in this study.

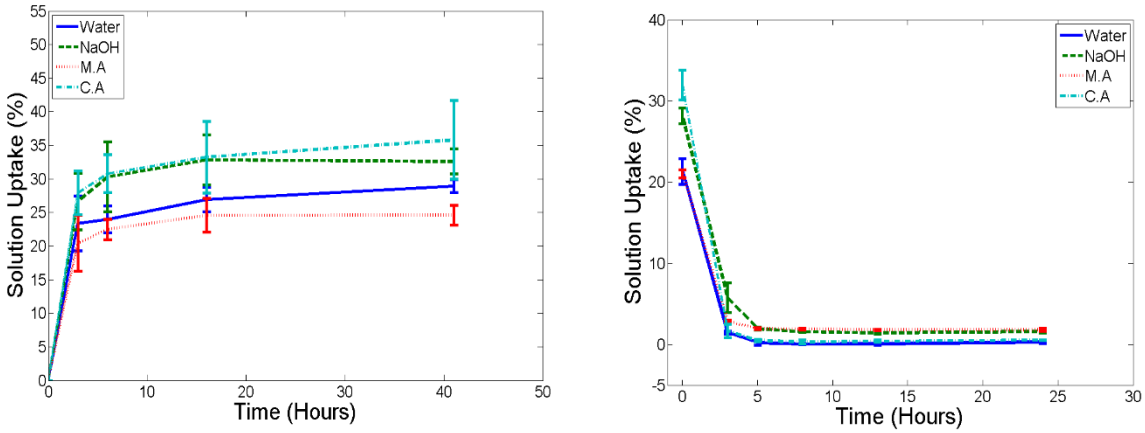

(a) (b)

Figure 4.5: The rate of solution uptake, and subsequent moisture egress from saturation for the NFC rectangular samples, (a) Moisture ingression process; (b) Moisture egression process.

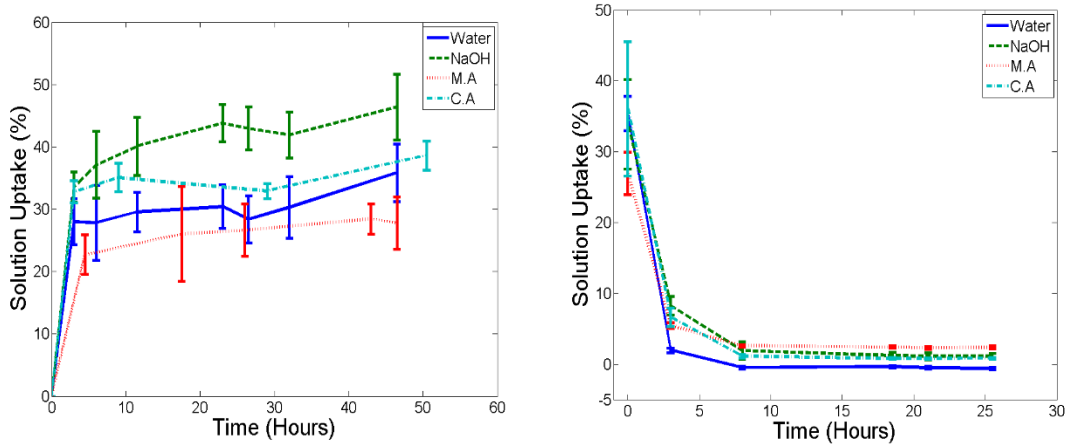

(a) (b)

Figure 4.6: The rate of solution uptake, and subsequent moisture egress from saturation for the CNFC rectangular samples, (a) Moisture ingression process; (b) Moisture egression process.

The samples all reach the maximum amount of chemical solution uptake in a similar, short amount of time, which is much quicker than in other systems, such as those reported by Wang *et al.* [36], who showed that a HDPE/rice husk composites system

(with volume fraction ranging from 40 to 60% and dimensions of 12cm × 12cm × 2.4 cm) reached saturation after over 270 hours of immersion in water. One reason for this fast saturation time is likely to be the high porosity observed in these samples. The M.A. solution has the highest solution density and both composites have the lowest amount of solution uptake in M.A. treatment compared to other treatments. No gaseous by-products were observed in any system.

A small amount of residual weight remained in dried samples treated with NaOH and M.A. This is not surprising given that both of these solutions were mixed from dry chemical powders and so would most likely remain in the sample after water has been dried off. In addition, it was noted that the dye used to colour the fibres in the CNFC samples (mostly blue and red) had been removed during the saturation process but this was thought not to affect the weight change measurements or to contribute to any chemical reaction.

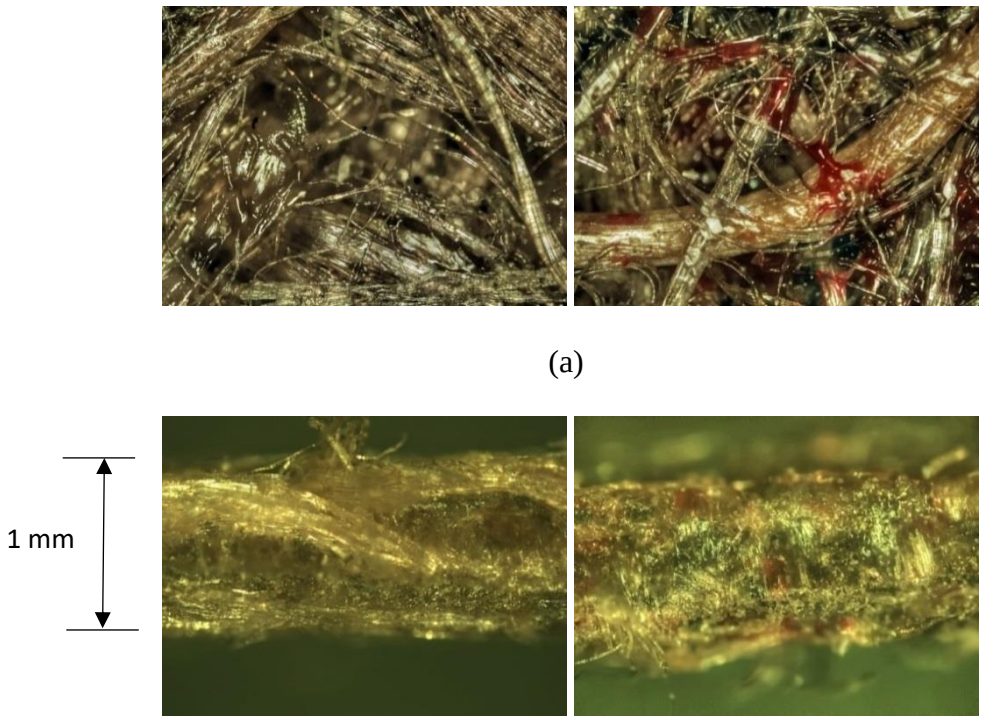

(a)

(b)

Figure 4.7: Optical micrographs of NFC composite (left) and the CNFC composite (right). The top images are of the composite surface while the bottom images are of the central cross-section.

Figure 4.7 illustrates that both composite material systems have significant porosity issues throughout the sample thickness, suggesting consolidation issues such as gaseous emission during the manufacturing process. Previous research (e.g. [128]) has demonstrated that synthetic fibre composites can attain porosity levels of less than 1% if processed accurately. Such low values are not yet possible in natural fibre/thermoplastic composites, as no processing technology can compensate for the very low wettability properties seen in these materials, which can also lead to poor interfacial quality [102]. The current study estimates that porosity levels in excess of 25% occur, with the higher values seen in the NFC materials. This may be the reason for the smaller saturation levels seen in the NFC sample set as air bubbles may prevent moisture from progressing to the fibre/matrix interface, which is probably where most of the moisture probably

resides. Indeed, since polypropylene is hydrophobic, only the flax fibre and the flax-polypropylene interface can absorb the solutions. Because of this, it is reasonable to assume that the fibre/matrix interface (and the fibres themselves) will exhibit chemical and physical changes (permanent or not) which will affect mechanical properties such as tensile behaviour and formability. Similar findings have been obtained by previous studies [43, 129].

4.3.2 Variations of the mechanical properties

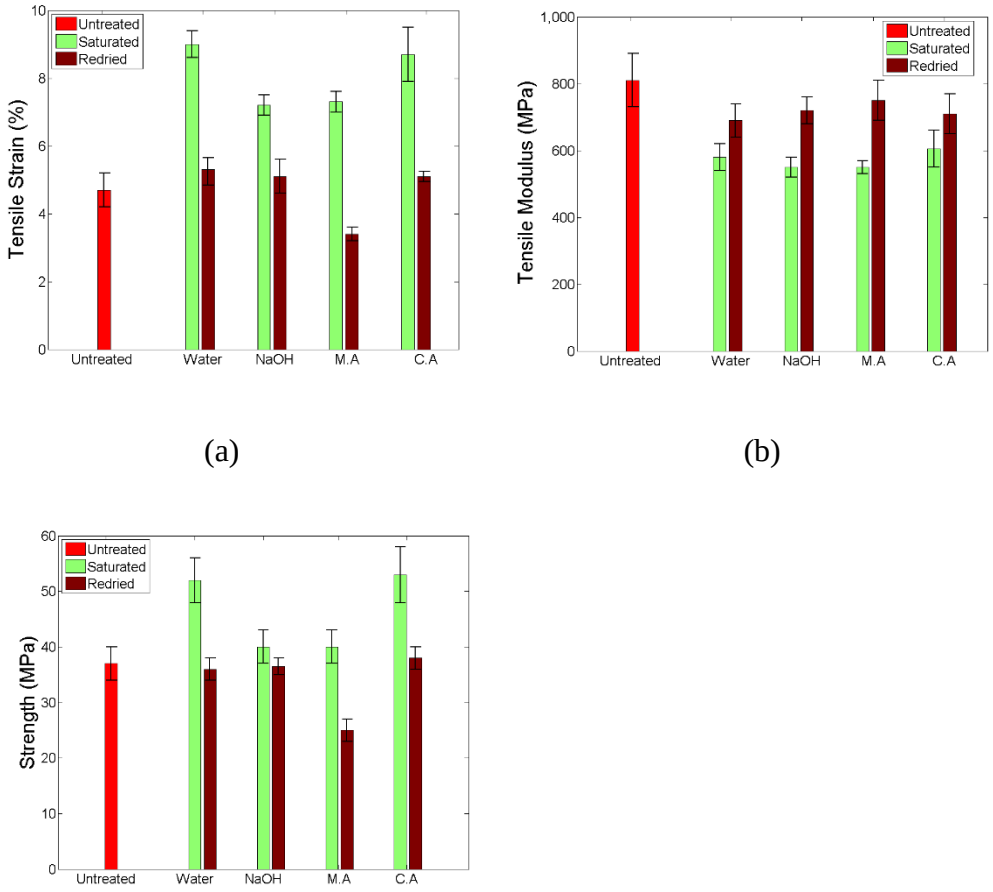

Figure 4.8: Variations in mechanical properties of the NFC under different chemical treatments obtained through tensile tests, (a) tensile strain; (b) tensile modulus; and (c) strength.

Figure 4.8 shows how the mechanical properties of NFC samples vary with treatment. Tensile stiffness is permanently reduced by the saturation/drying process, whereas elongation-to-fracture is increased significantly when saturated, but largely returns to pre-soaked values when dried suggesting a non-permanent effect. Strength, however, doesn't seem to be statistically affected by the saturation/drying process, although the maleic anhydride-treated samples may have statistically weakened.

In the NFC samples, the fibres are in the form of a 2 × 2 twill structure. Therefore, it is expected that in the NFC samples, the fibres are more restricted in their possible movement during tensile testing and will only elongate in the weave directions. In woven composites, the failure mechanisms are fibre-dominated and so if any change happens within the cellulosic fibres during soaking, they would be more apparent in the NFC samples.

Overall, the water and C.A solution treated samples appear to be identical and give significant improvements in strength and elongation-to-failure when saturated. These properties return to pre-treated levels when dried, indicating no permanent effect. The apparent increase in strength when saturated could be due to the softening of the fibres (and interfacial region), allowing for the weave structure to deform prior to fracture, as the warp and weft morphologies effectively realign. This study suggests that the chemical changes that cause these property variations are strongest in solutions that do not contain relatively bulky solute substances (maleic anhydride or sodium hydroxide). Given that such solutions have more difficulty permeating the material compared to pure water or ammonia (and thus completely hydrolysing the interfacial region), this is not surprising. Also, plasticization of flax fibres is a known phenomenon as explained in

[130] using pure water and ammonia treatments – which are often used as plasticizers for wood.

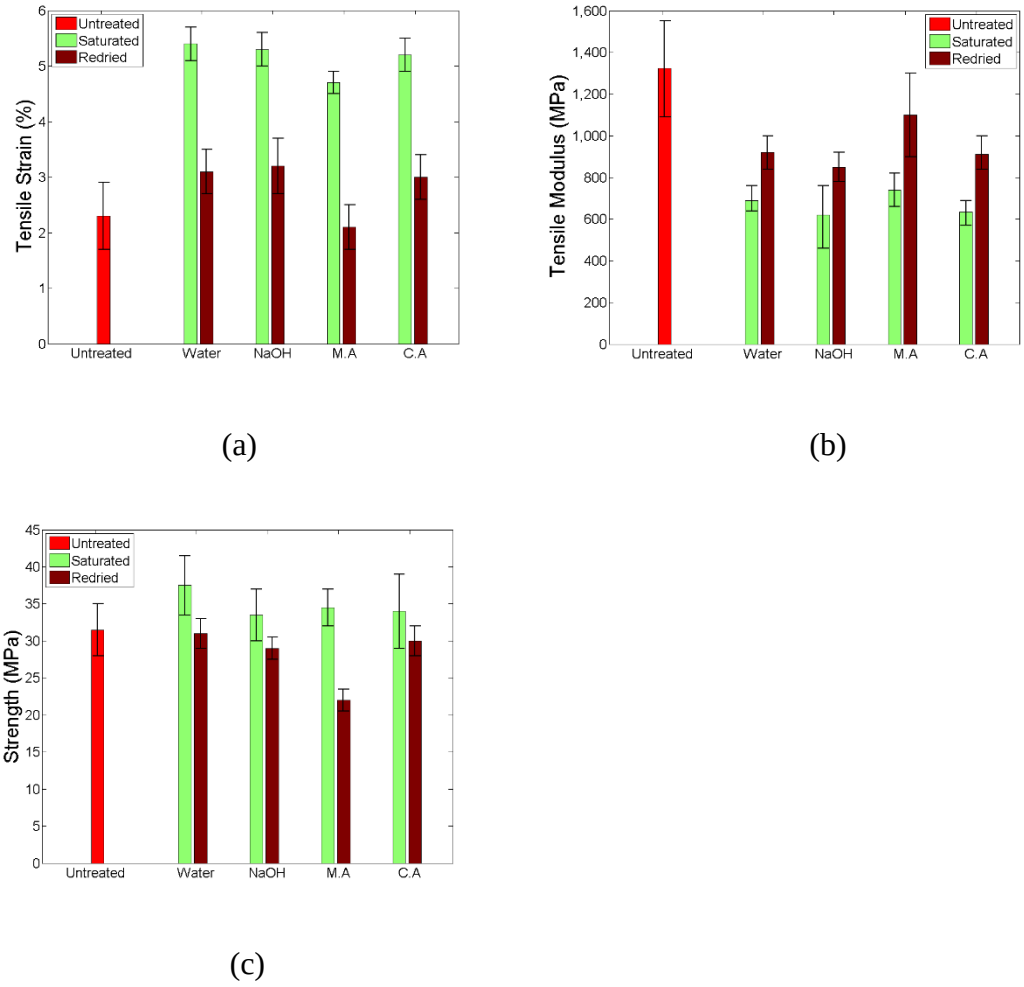

Figure 4.9: Tensile property data for CNFC samples under various aqueous treatments showing (a) tensile strain; (b) tensile modulus; and (c) strength.

The corresponding mechanical responses seen in the CNFC material are detailed in Figure 4.9. Compared to the NFC sample set, there are some differences in mechanical properties. Firstly, the magnitude of the irreversible change in stiffness seems much larger severe in the CNFC materials, particularly when redried. Secondly, the strength values seem to decrease when soaked in pure water or cloudy ammonia solution and return back to original values when redried. It is also noted that, as with the previous

sample set, the maleic anhydride-treated material appears to be permanently stronger than the others.

The stiffness results suggest that the fibre/matrix interface has been permanently altered. There is a small amount of stiffness recovery when redried, but the reduction effect is largely permanent. When the samples are saturated, all treatments significantly increase elongation properties while decreasing the stiffness response, suggesting that formability has been improved without loss of strength. Given that both elongation and strength show minimal variation in the two dry conditions, a process that can form the materials whilst wet would be very advantageous, especially in designs where stiffness response is of secondary importance. According to Van de Velde and Kiekens [131], treatment with maleic anhydride should improve the interfacial strength between fibre and matrix. However, this effect is not evident in this study, probably because the aqueous and saturated nature of the treatment does not allow for the chemical to form the correct chemical bonds with the constituents. Such treatments are often invoked using dry conditions such as adding anhydride powder to the liquid polymer, or soaking the fibres in an anhydride solution which is then subsequently dried prior to mixing with the polymer.

Figure 4.10 shows SEM images of CNFC fracture surfaces from samples tested under different conditions. For the untreated and dried specimens, the fractured flax fibre bundles are coated with polypropylene matrix and flax fibres bundles cannot be easily differentiated from the polypropylene matrix. This is a statistically consistent observation suggesting a relatively strong interface between the flax fibre and the polypropylene matrix [132]. Clean fibre surfaces are seen in the saturated sample, that is, there appears to be no post-fractured resin regions adhered to the fibre surface, and this

is indicative of a much weaker fibre-matrix interface when hydrolysed. It has been reported [43] that when solutions are absorbed by the fibre/matrix interface, the cellulosic fibres tend to swell which favours fibre debonding and weakens the fibre/matrix interface leading to tensile property variations. This would appear to be the case for the current study, as the interfacial properties (stiffness and elongation) are significantly changed when wet. In addition, the strength of the materials appears remain largely independent of the saturation and redrying process and no significant changes to fibre fracture morphology was detected during the fractographic study. Therefore, if the cellulosic fibres swell during the saturation process, they remain chemically unchanged, whilst initiating changes at the interfacial region. On drying, the fibre-matrix integrity seems to return, but there is a permanent reduction in composite stiffness. This could suggest the presence of an interphase region which remains permanently weakened from the saturation process. Thus when dried, the samples retain strength (no fibre changes observed), and regain their interfacial characteristics (as per the SEM observations) whilst maintaining a reduced stiffness through mechanical weakness in the interphase region, which may be pre-existing, or may have formed as a result of the saturation process. Mishra and Sain [133] documented a similar finding that the stiffness of natural fibre composite did not fully recover after drying the samples, and this permanent damage to the fibre was attributed to the interfacial degradation and structure breakdown of the cell wall in natural fibres. A possible exception to these trends is the maleic anhydride-treated material, where strength seems to be permanently reduced once the samples are dried. This could be due to chemical ingress of the anhydride solution into the cellulosic fibres which when dried, cause chemical changes that permanently weaken the fibres, although this was not detected during fractographic examination.

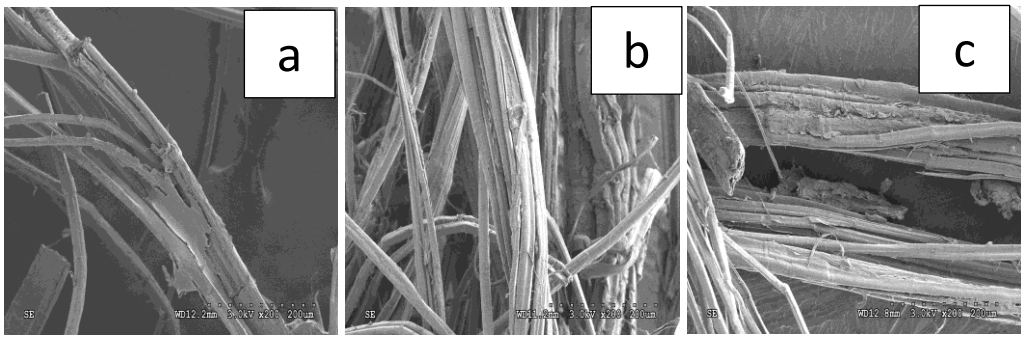

Figure 4.10: Electron microscope images of CNFC reinforced PP composites showing (a) untreated; (b) saturated; and (c) redried samples that have been fractured under simple tensile testing.

Overall, given the nature of the reinforcement fibre fracture mechanisms will tend to be more dominant in the woven twill (NFC) samples than in the random fibre (CNFC) samples and so the changes observed in the NFC samples could be due to some fibre plasticization effect that is most evident in pure water and ammonia treatments, and this effect may dominate over the interphase and interface-based mechanisms seen in the CNFC samples. It is likely therefore, that both mechanisms exist in both material systems, with one clearly dominating the other. From Figures 4.8 and 4.10, it is clear that, given the significant increase in elongation-to-failure values, the formability of the water and ammonia-soaked natural fibre composites should radically differ from dry equivalents, and this should be apparent in comparative forming experiments. The corresponding increase in strength would be important in structure strength design, but this could be less important in displacement control forming tests performed in this study. The relative decrease in stiffness in the NFC samples is lower than in the CNFC samples, but if stiffness changes are driven by interfacial/interphase phenomena, they would be less influential in the NFC samples anyway. Also, the fact that stiffness changes seem to be somewhat reversible when redrying occurs suggests that mechanically, NFC materials should revert back to their pre-treated properties when

dried. This makes them quite attractive as a material for structures where significant drawing is required, so long as they can be processed when wet.

4.4 Summary

This Chapter has studied the mechanical behaviour of natural fibre composites at elevated temperatures, as well as in different conditions of water treatment. Both composites were stretched at a constant rate until failure at different temperatures varying from room temperature to 160˚C. The experimental results show that preheating treatment can help natural fibre composites exhibit an increased elongation-to-failure, as well as a reduced stiffness. Composites were also stretched in different conditions of water treatment, including the untreated, water-treated and redried conditions. Observations suggest that it is very advantageous to process this class of material system in the wet condition, especially since the mechanical properties can be largely returned to the untreated levels after redrying. Based on SEM examinations on the fractured surfaces, the dominating mechanisms behind the variations of mechanical properties have been determined to be softening in fibre-matrix interface (for the CNFC materials) and fibre plasticization (for NFC materials). Preheating is usually required to improve the formability of material in rapid forming, and the chemical treatments performed in this study were far more effective than preheating in terms of improving the mechanical responses of composite materials in simple forming conditions. Chapters 5 and 6 investigate whether such major breakthrough could be translated to a superior formability of this class of material system in more complicated forming situations.

Stretch Forming Tests

5.1 Introduction

This Chapter details the stretch forming experiments conducted, and investigates the failure behaviour of the composites through examining displacement and strain deformation captured by a real-time strain measurement, the ARAMIS™ system. ***The key finding of the current work is that it proposes an innovative failure criterion for woven composites, called a "new FLC", which uses fibre strain and strain ratio as key parameters. This new failure criterion is more effective than the conventional FLC in detecting the failure in woven natural fibre composites as it can successfully eliminate the path dependency effect.*** This innovative method of examining failure can be applied to engineering structural design and analysis of different woven composite systems as long as the failure mechanism is dominated by fibre fracture. The previous Chapter has proved that pure water and C.A produce the greatest improvement on the failure elongation of both composites in the saturation condition than other chemicals and the conventional preheating method. Part of the scope of this investigation is therefore to examine the forming limits of composites in three conditions of water treatment: untreated, water-treated and redried. FEA simulations are an essential tool in engineering structural design and analysis, and the development of the new FLC would be much less useful if this failure criterion could not be implemented in FEA models. Here, FEA models are developed to simulate the stretch forming process of composites in different conditions, and to compare the new FLC with existing failure criteria in predicting the onset of failure in stretch forming tests.

5.2 Experimental observations

When analysing the forming behaviour of composites, the centre of the material (referred to as the pole) is of great interest. This region undergoes the largest displacement during forming, and exhibits a deformation mode that is affected by geometry as well as fibre orientation. The higher state of strain deformation at the pole compared to the other parts of the sample usually results in the onset of failure in this region. This is a major advantage when conducting forming tests as it can help establish the limiting strain conditions of the material in each deformation mode, ranging from biaxial-stretch to pure shear. Figure 5.1 shows strain evolution at the pole, and in this case data is obtained from a UF70 NFC specimen.

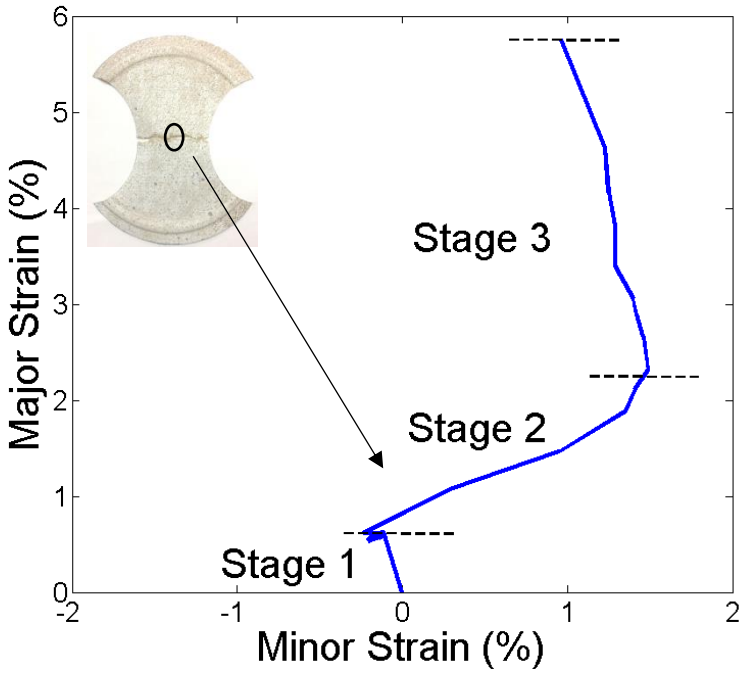

Figure 5.1: Typical strain evolution at the pole in a stretch forming test.

Strain evolution at the pole can be identified as three separate stages including pre-stretch, biaxial-stretch and the major forming path. By analysing the evolution of principal strains at the pole, Sexton [19] found that the change in strain ratio, and therefore the deformation mode, is caused by minor strains, implying that restriction in

the lateral direction is a key factor for changes in strain ratio. Specimens are fixed to the blank-holder through tightening six M12 bolts with a torque of 15 kN.m on the lock ring mounted beneath. This pre-stretch process results in initial strain deformation, the details of which are explained later. A composite exhibits a forming mode of biaxial stretch when it establishes initial contact with the punch. At this stage, only a small region at the pole deforms and the rest of the material surface can be considered as fixed, resulting in the forming mode of biaxial stretch during this period. As soon as the lateral restriction starts to disappear, bi-axial stretch behaviour ends and the third stage starts. At this stage, the composite is allowed to be drawn into the die cavity in the lateral direction due to the lack of restriction in this direction. The strain information at failure can therefore be obtained by the ARAMIS system, and used for constructing Forming Limit Curve, the details of which are described in Sections 5.2.1.4 and 5.2.2.2.

5.2.1 NFC materials

The benefit of conducting stretch forming tests is to find out the forming limits in different deformation modes. To examine the changes in deformation modes during stretch forming tests, the evolution of surface strain ratio is studied at the end of each of the three stages. The relationship between deformation modes and strain ratios is illustrated in Table 2.2 of Chapter 2. The ARAMIS™ system does not have built-in algorithms to provide information on strain ratio, so a Python script is developed to calculate this. To avoid illegal floating point issues, the script deals specifically with the situation when the ARAMIS™ system reports a major strain of 0. In such cases, a strain ratio of 0 is reported, instead of taking the ratio between the principal strains. It is noted that prior to forming, a lock-ring was used to fix specimens completely, avoiding materials at the flange regions from drawing into the die cavity. Too large or too small tightening torque leads to either premature failure when the composite fails during pre-

stretch, or edge movement. None of these two phenomena are identified during experiments.

5.2.1.1 Evolution of surface strain ratios

Seven geometries in total are tested, the evolutions of surface strain ratios of which are described in Figures 5.2-5.5. Figure 5.2 shows the surface strain evolution of the full circle specimen, and Figures 5.3-5.5 compare the effect of fibre orientations on surface strain ratio for hourglass specimens with a width of 100 mm, 70 mm and 25 mm, respectively.

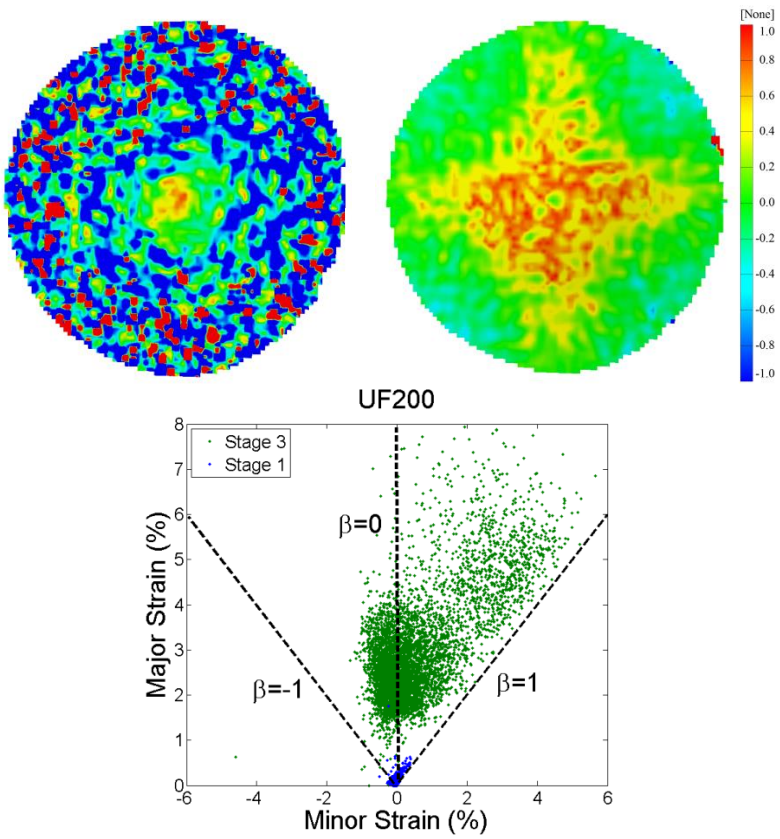

Figure 5.2: Evolution of contours of surface strain ratio (deformation mode) and FLD for UF200 specimen.

Figure 5.2 illustrates the evolution of surface strain ratios and FLD of the UF200 specimen. The UF200 specimen does not exhibit the bi-axial stretch stage (stage 2) as

the major deformation mode remains unchanged during forming. In the pre-stretching stage, only the central region of the specimen is formed in the major deformation mode of biaxial-stretch. The rest part of the material is slightly strained, leading to a random distribution of strain ratios. It needs to be noted that the major deformation mode at the centre of the specimen remains biaxial-stretch during the entire forming process, and this region experience the highest strain deformation prior to failure. The visual examination on formed parts also confirmed that the failure initiates at this area. Based on the surface strain ratio distribution at the stage just prior to failure, the unsupported regions experience a major deformation mode of plane strain with no pure shear. A considerably smaller amount of strain deformation is experienced in stage 1 as compared to other geometries described later, which can be attributed to the fact that the similar amount of pre-stretch force is acting on a larger area (the UF200 specimen is the largest sample).

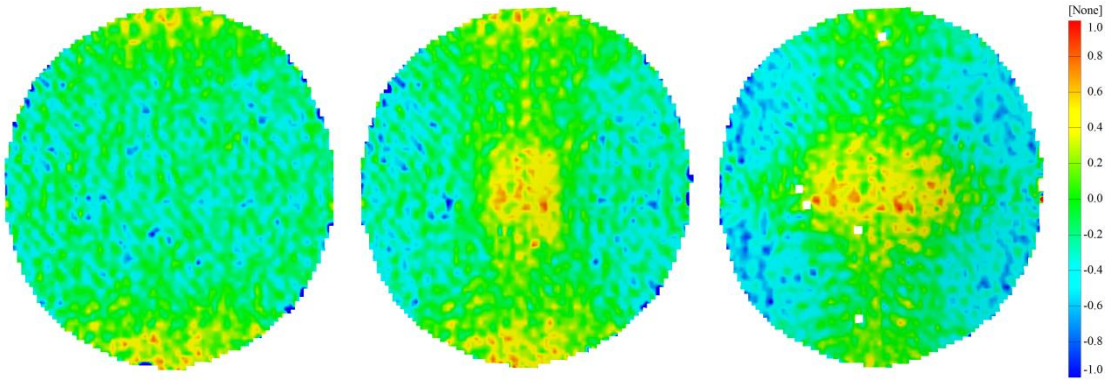

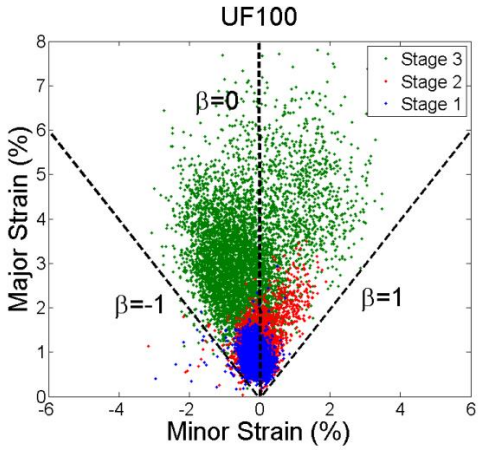

(a)

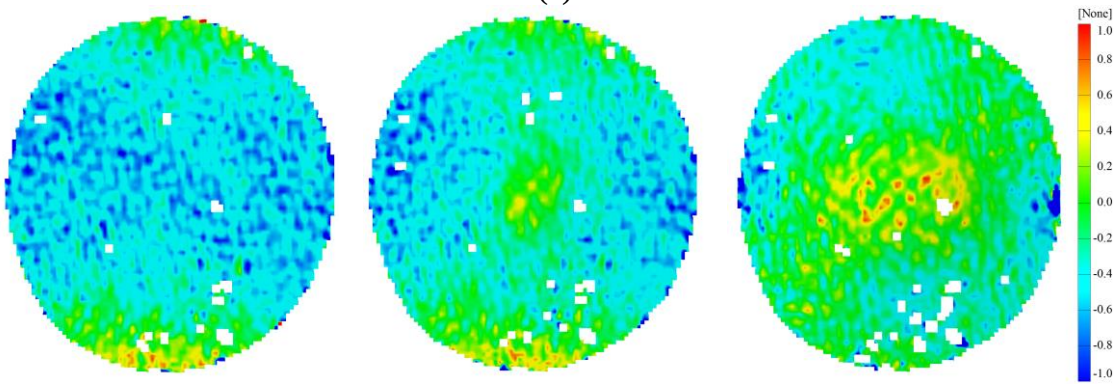

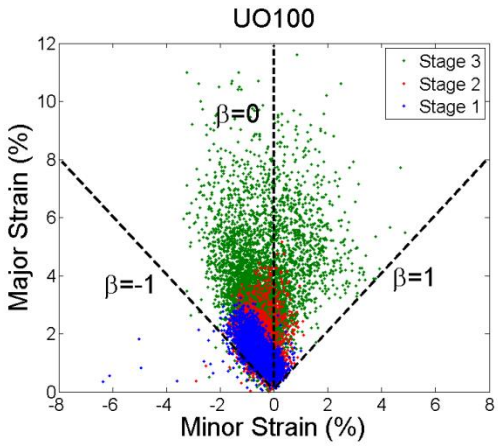

(b)

Figure 5.3: Evolution of contours of surface strain ratio (deformation mode) and FLD,

(a) UF100; (b) UO100.

Figure 5.3 compares the surface strain evolutions of the UF100 and UO100 specimens. It is clear to note that the hourglass samples with a width of 100 mm is able to withstand a much larger strain deformation, from less than 8% to more than 10%, if the stretch direction changes from 0˚/90˚ to 45˚/-45˚ to the fibre directions. This observation is also obtained in other hourglass geometries, which can be attributed to the trellising behaviour of woven composites. The flax fibres tend to rotate over each other under trellising such that they are no longer perpendicular to each other. This leads to the reduction on the amount of strain acting along the fibres, and therefore helps the composite withstand a larger strain deformation. Although the 45˚/-45˚ specimens experience a much larger strain deformation compared to the 0˚/90˚ equivalent composite, the major deformation modes are similar to both samples. In the biaxial-stretch stage, a clear trend of an almost equal increase in major strain and minor strain at the pole is observed. It needs to be recognised that regions other than the pole experience little change in strain deformation at this stage, indicating that the centre of the specimen is deformed to a much greater extent than other areas. This observation is clear and consistent for hourglass samples with a width of 100 mm and 70 mm.

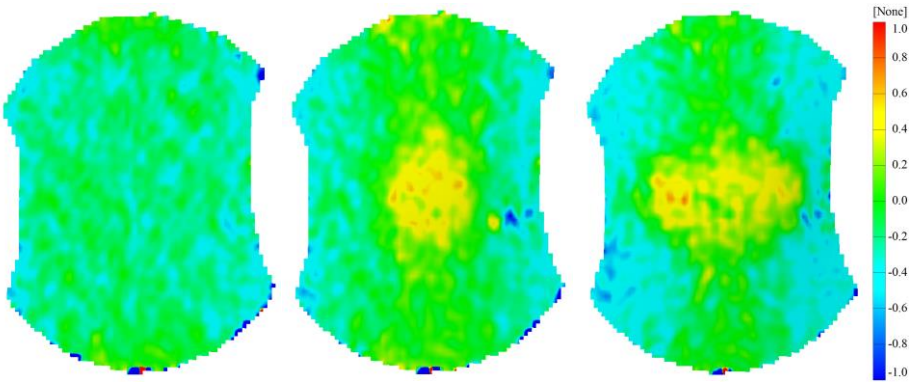

UF70

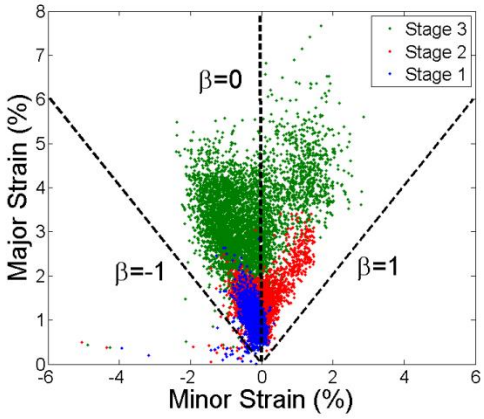

(a)

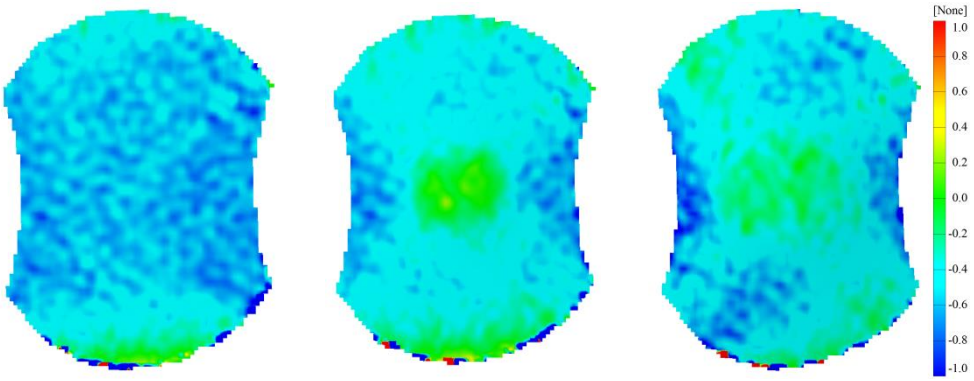

UO70

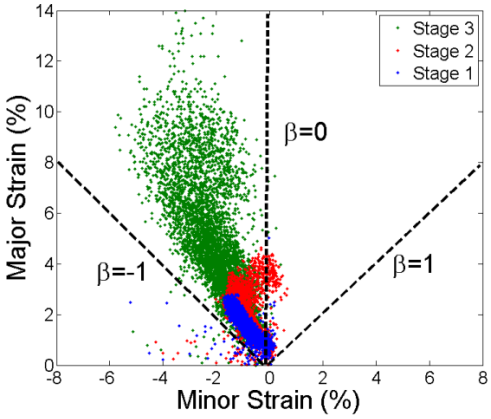

(b)

Figure 5.4: Evolution of contours of surface strain ratio (deformation mode) and FLD,

(a) UF70; (b) UO70.

It is observed that for samples with a width less than 100 mm, the fibre orientation has a dominating effect over sample geometry, as the 45°/-45° samples exhibits a considerably different major deformation mode compared to the 0°/90° equivalent sample. For instance, Figure 5.4 clearly shows that the UO70 specimen experiences smaller (more negative) strain ratio compared to the UF70 specimen, at each forming stage. It seems that sample geometry has a dominating effect over stretch orientation for samples with small widths, due to a small portion of material being fixed at the flange region. Due to the tapered geometry, the pole of the specimens experiences higher major strain than the rest of the areas during forming. In the pre-stretch stage, 45°/-45° specimens experience significantly larger strain deformation compared to 0°/90° equivalent composites. This is expected because a similar amount of force is applied to the sample edges, and the composite exhibits a significantly lower stiffness in off-fibre directions. In addition, given the same fibre orientation, smaller strain deformation is observed in larger samples.

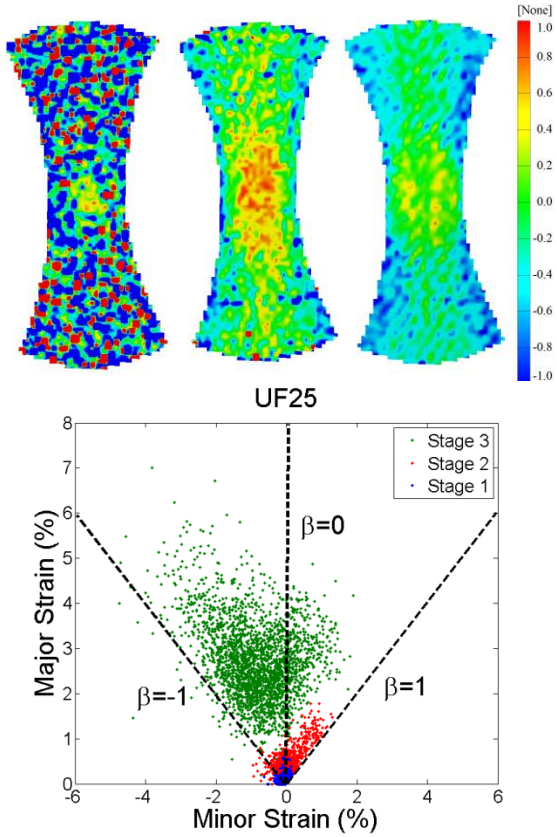

(a)

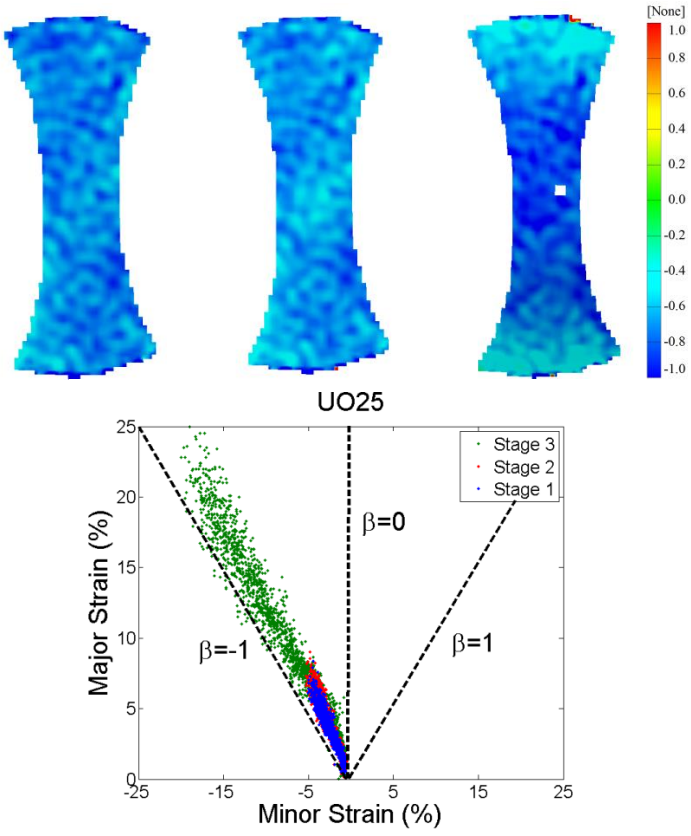

(b)

Figure 5.5: Evolution of contours of surface strain ratio (deformation mode) and FLD,

(a) UF25; (b) UO25.

It is important to notice that the NFC materials exhibit different major deformation modes in 25 mm hourglass samples when the fibre orientation changes from 0˚/90˚ to 45˚/-45˚. The UF25 specimen experiences small deformation in the pre-stretch state, followed by a noticeable amount of biaxial stretch in stage two, and finally fails in the deformation mode close to uniaxial tension. It is observed that the UO25 sample could withstand major strains higher than 20% just prior to failure, which is significantly higher compared to the other samples, especially those formed with the 0°/90° fibre orientation. This specimen also experiences very little variation of the FLD during the bi-axial stretch behaviour. The restriction along the lateral direction vanishes quickly, and as it does in the bi-axial stretch stage.

For 0˚/90˚ hourglass usually experiencing stretching in stretch forming tests, while the dominating deformation mode of 45˚/-45˚ hourglass samples is shear, especially those with smaller widths. The woven structure can help NFC samples exhibit pure shear when off-fibre hourglass samples are formed in which the flax fibres rotate over each other within the ply without being significantly stretched. This trellising behaviour could help this class of material systems to exhibit a significant amount of strain deformation prior to failure. 0˚/90˚ NFC samples, on the contrary, is dominated by stretching during forming, leading to failure caused by fibre fracture at smaller forming depths.

This section has shown that the experimental setup of the stretch forming tests conducted in this work could help woven composite materials experience different deformation mode during forming, and more importantly fail at different forming modes. This is essential when validating the efficiency of failure criterion as an effective one should be able to predict the failure initiated in different forming modes.

5.2.1.2 Fibre strain calculations

For the NFC materials investigated in this study, the major failure mechanism is identified as fibre fracture. This is a consistent observation obtained from both visual observations and microscopic examinations of tested composite samples, and the details of this are described in Section 6.2.1.1 and 6.2.2.1. ***One of the key contributions of the current work is that it proposes an innovative failure criterion for woven composites which are dominated by fibre fractures. This new failure criterion uses fibre strain as the key parameter, and therefore requires tracking the evolution of the flax fibres during forming, especially when composites trellis under shear deformation.*** This section explains the kinematics used to track the evolution of fibre movements as well as to calculate fibre strains, followed by the development of an algorithm used in the ARAMIS system to compute fibre strains.

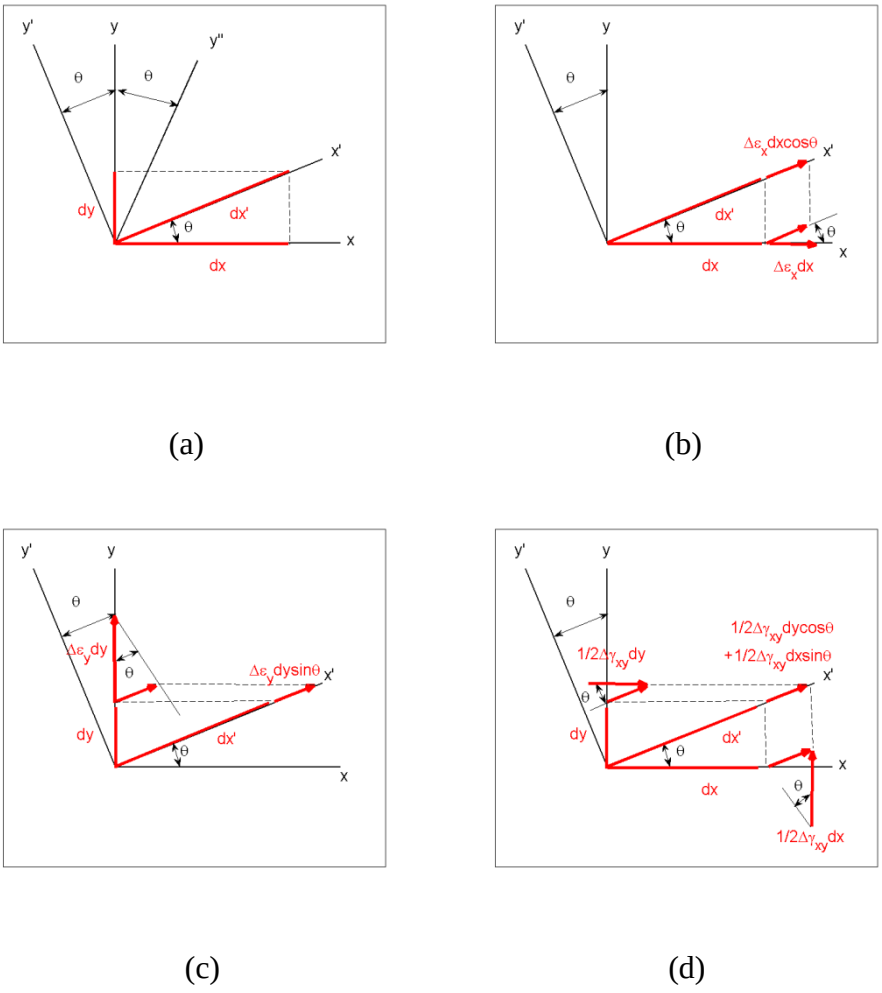

Figure 5.6: Illustration of how to calculate fibre strain (a) overview; (b) normal strain in the x direction; (c) normal strain in the y direction; and (d) shear strain.

Figure 5.6 illustrates how to transform strains in the original X, Y and shear directions to the principal direction after rotation. Figure 5.6a shows that under shear deformation, the flax fibres are aligned with the X' and Y'' directions, and that the Y' direction is perpendicular to the X' direction. According to strain measurements, incremental strains in the global coordinate system can be calculated as:

$$\Delta\boldsymbol{\varepsilon_x}^{\mathbf{i}} = \boldsymbol{\varepsilon_x}^{\mathbf{i}} - \boldsymbol{\varepsilon_x}^{\mathbf{i-1}}, \quad \Delta\boldsymbol{\varepsilon_y}^{\mathbf{i}} = \boldsymbol{\varepsilon_y}^{\mathbf{i}} - \boldsymbol{\varepsilon_y}^{\mathbf{i-1}}, \quad \Delta\boldsymbol{\gamma_{xy}}^{\mathbf{i}} = \boldsymbol{\gamma_{xy}}^{\mathbf{i}} - \boldsymbol{\gamma_{xy}}^{\mathbf{i-1}} \qquad (5.1)$$

where i represents the i[th] increment of the calculation, $\varepsilon_x, \varepsilon_y, \gamma_{xy}$ are the strains in global X, Y and shear directions, and $\Delta\varepsilon_x, \Delta\varepsilon_y, \Delta\gamma_{xy}$ represent the incremental strains in the global X, Y and shear directions.

The elongation along the X' direction is computed first, and its components along the X and Y directions can be calculated as:

$$\boldsymbol{dx'^{,i} = dx/\cos\theta^i}, \quad \boldsymbol{dx'^{,i} = dy/\sin\theta^i} \tag{5.2}$$

where $dx, dy, dx'^{,i}$ correspond to the elongations along the X, Y and X' directions, respectively, and θ^i represents the angle of rotation.

The resultant incremental elongation along the X' direction is the sum of components from the normal strain in the X direction, the normal strain in the Y direction and shear strain (as described in Figures 5.6 b-d).

$$\boldsymbol{\delta x'^{,i} = \Delta\varepsilon_x^i dx\cos\theta^i + \Delta\varepsilon_y^i dy\sin\theta^i}$$

$$\boldsymbol{+1/2 * \Delta\gamma_{xy}{}^i \Delta\varepsilon_y^i \cos\theta^i + 1/2 * \Delta\gamma_{xy}{}^i \Delta\varepsilon_x^i \sin\theta^i} \tag{5.3}$$

$$\boldsymbol{\Delta\varepsilon_x'^{,i} = \delta\varepsilon_x'^{,i}/dx'^{,i}} \tag{5.4}$$

$$\boldsymbol{\Delta\,\varepsilon_x'^{,i} = \Delta\varepsilon_x^i \cos^2\theta^i + \Delta\varepsilon_y{}^i \sin^2\theta^i + \Delta\gamma_{xy}{}^i \sin\theta^i\cos\theta^i} \tag{5.5}$$

where $\delta x'^{,i}$ is the resultant incremental elongation along the X' direction, and $\Delta\,\varepsilon_x'^{,i}$ is the incremental strain along the X' direction.

The incremental strain along the X' direction in Equation 5.5 can be simplified to the expression shown in Equation 5.6 based on trigonometric identities.

$$\boldsymbol{\Delta\,\varepsilon_x'^{,i} = \frac{\Delta\varepsilon_x^i + \Delta\varepsilon_y{}^i}{2} + \frac{\Delta\varepsilon_x^i - \Delta\varepsilon_y{}^i}{2}\cos 2\theta^i + \frac{\Delta\gamma_{xy}{}^i}{2} sin2\theta^i} \tag{5.6}$$

The incremental elongation and incremental strain along the Y' direction can be obtained by substituting ($90+\theta^i$) for θ^i in Equations 5.3 and 5.6.

$$\boldsymbol{\delta y'^{,i} = -\Delta\varepsilon_x^i dx\, sin\,\theta^i + \Delta\varepsilon_y^i dy\cos\theta^i}$$

$$\boldsymbol{-1/2 * \Delta\gamma_{xy}{}^i \Delta\varepsilon_y^i\, sin\,\theta^i + 1/2 * \Delta\gamma_{xy}{}^i \Delta\varepsilon_x^i \cos\theta^i} \tag{5.7}$$

$$\boldsymbol{\Delta\varepsilon_y'^{,i} = \frac{\Delta\varepsilon_x^i + \Delta\varepsilon_y{}^i}{2} - \frac{\Delta\varepsilon_x^i - \Delta\varepsilon_y{}^i}{2}\cos 2\theta^i - \frac{\Delta\gamma_{xy}{}^i}{2} sin2\theta^i} \tag{5.8}$$

where $\delta y'^{,i}$ is the resultant incremental elongation along the Y' direction, and $\Delta\,\varepsilon_y'^{,i}$ is the incremental strain along the Y' direction.

The incremental angle of rotation is then calculated.

$$\Delta\boldsymbol{\gamma_{xy}}'^{,\mathbf{i}} = \boldsymbol{\delta y}'^{,\mathbf{i}}/\mathbf{dx}'^{,\mathbf{i}} + \boldsymbol{\delta x}'^{,\mathbf{i}}/\mathbf{dy}'^{,\mathbf{i}} \tag{5.9}$$

$$\boldsymbol{\delta y}'^{,i}/\boldsymbol{dx}'^{,i} = \left(-\Delta\boldsymbol{\varepsilon}_x^i + \Delta\boldsymbol{\varepsilon}_y{}^i\right)\mathbf{sin}\,\boldsymbol{\theta}^i\,\mathbf{cos}\,\boldsymbol{\theta}^i - \Delta\boldsymbol{\gamma}_{xy}{}^i\,\mathbf{sin}^2\,\boldsymbol{\theta}^i \tag{5.10}$$

$$\boldsymbol{\delta x}'^{,i}/\boldsymbol{dy}'^{,i} = (-\Delta\boldsymbol{\varepsilon}_x^i + -\Delta\boldsymbol{\varepsilon}_y^i)\,\mathbf{sin}\,\boldsymbol{\theta}^i\,\mathbf{cos}\,\boldsymbol{\theta}^i + \Delta\boldsymbol{\gamma}_{xy}{}^i\,\mathbf{cos}^2\,\boldsymbol{\theta}^i \tag{5.11}$$

$$\Delta\boldsymbol{\gamma_{xy}}'^{,\mathbf{i}} = -\left(\Delta\boldsymbol{\varepsilon_x}^{\mathbf{i}} - \Delta\boldsymbol{\varepsilon_y}^{\mathbf{i}}\right)\mathbf{sin2\theta^i} + \Delta\boldsymbol{\gamma_{xy}}^{\mathbf{i}}\mathbf{cos2\theta^i} \tag{5.12}$$

Where $\Delta\gamma_{xy}{}'^{,i}$ is the incremental angle of rotation.

Incremental strain along another fibre direction (the Y'' direction) can be computed by substituting (90-θ^i) for θ^i in Equation 5.8.

$$\Delta\,\boldsymbol{\varepsilon}_{\mathbf{y}}''^{,\mathbf{i}} = \frac{\Delta\boldsymbol{\varepsilon}_{\mathbf{1}}^{\mathbf{i}}+\Delta\boldsymbol{\varepsilon}_{\mathbf{2}}{}^{\mathbf{i}}}{\mathbf{2}} - \frac{\Delta\boldsymbol{\varepsilon}_{\mathbf{1}}^{\mathbf{i}}-\Delta\boldsymbol{\varepsilon}_{\mathbf{2}}{}^{\mathbf{i}}}{\mathbf{2}}\mathbf{cos\,2\theta^i} + \frac{\Delta\boldsymbol{\gamma}_{\mathbf{12}}{}^{\mathbf{i}}}{\mathbf{2}}\mathbf{sin2\theta^i} \tag{5.13}$$

Where $\Delta\,\varepsilon_y''^{,i}$ is the incremental strain along the Y'' direction.

Fibre strains in both directions are then updated accordingly. The maximum of these two strain values is used to represent fibre strain at this point when establishing the new FLC.

$$\boldsymbol{\varepsilon_X}^{\mathbf{i}} = \boldsymbol{\varepsilon_X}^{\mathbf{i-1}} + \Delta\boldsymbol{\varepsilon}_{\mathbf{x}}'^{,\mathbf{i}} \tag{5.14}$$

$$\boldsymbol{\varepsilon_Y}^{\mathbf{i}} = \boldsymbol{\varepsilon_Y}^{\mathbf{i-1}} + \Delta\boldsymbol{\varepsilon}_{\mathbf{y}}''^{,\mathbf{i}} \tag{5.15}$$

$$\boldsymbol{\varepsilon_{fibre}}^{\mathbf{i}} = \mathbf{maximum}(\boldsymbol{\varepsilon_X}^{\mathbf{i}}, \boldsymbol{\varepsilon_Y}^{\mathbf{i}}) \tag{5.16}$$

Where $\varepsilon_X{}^i$ and $\varepsilon_Y{}^i$ represent the strain along the fibre directions, and $\varepsilon_{fibre}{}^i$ is the fibre strain used in the new FLC.

At the end of each increment, the angle of rotation should also be updated and is given by the following expression.

$$\boldsymbol{\theta^{i+1}} = \boldsymbol{\theta^i} + \Delta\boldsymbol{\gamma_{xy}}'^{,\mathbf{i}} \tag{5.17}$$

ARAMIS™ system does not have built-in algorithms to calculate fibre strains, a user-defined Python script is therefore developed to facilitate fibre strain calculations, and this script is incorporated to the ARAMIS™ system. At any given stage, fibre strain is the sum of incremental fibre strains in all the previous stages, which are calculated from the incremental normal strains and shear strains in global axes, and the angle that the fibre axes have rotated with respect to their original coordinates. This value should be used instead of that calculated based on the current state of strain, which is overestimated as the angle between the weft and warp directions is changing all the time. For a given point, the fibre strain in both directions can be determined, and the one with a larger absolute value is used when establishing the new FLC for the composite. Figure 5.7 shows the flow chart of the Python script developed for fibre strain calculations. With this script, the ARAMIS™ system is able to output fibre strains for each mesh point at every time step.

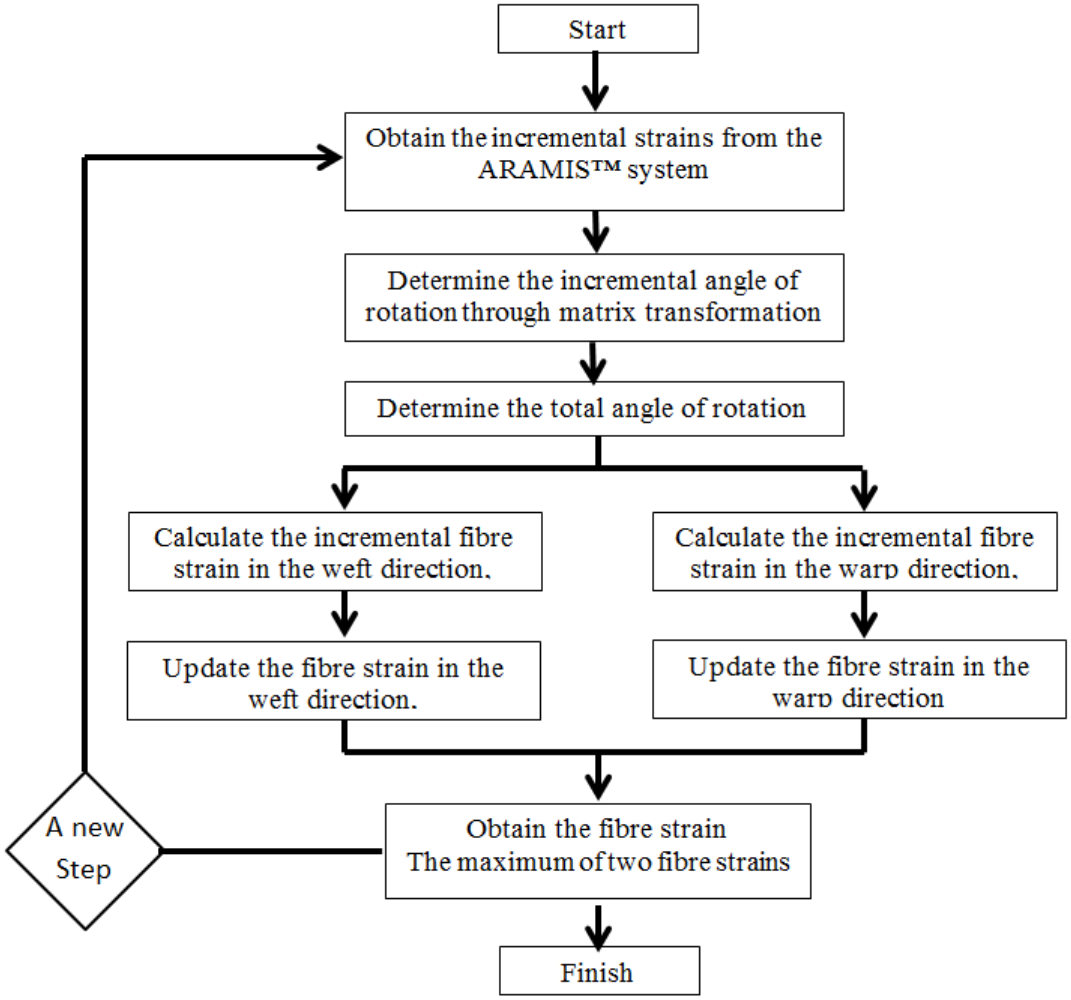

Figure 5.7: Flow chart of the Python script developed for the ARAMIS™ system.

5.2.1.3 Anomalies observed in the conventional FLD

The conventional FLD for the NFC materials is firstly examined. The UF100 and UO100 samples are selected and compared as both specimens exhibit similar forming modes in stretch forming experiments, which is of importance in determining the forming limits of the composite. It is noted that the flax fibres in the UF100 specimen are oriented 0°/90° to the stretching axis, while the UO100 specimen has its flax fibres oriented 45°/-45° to the stretching axis.

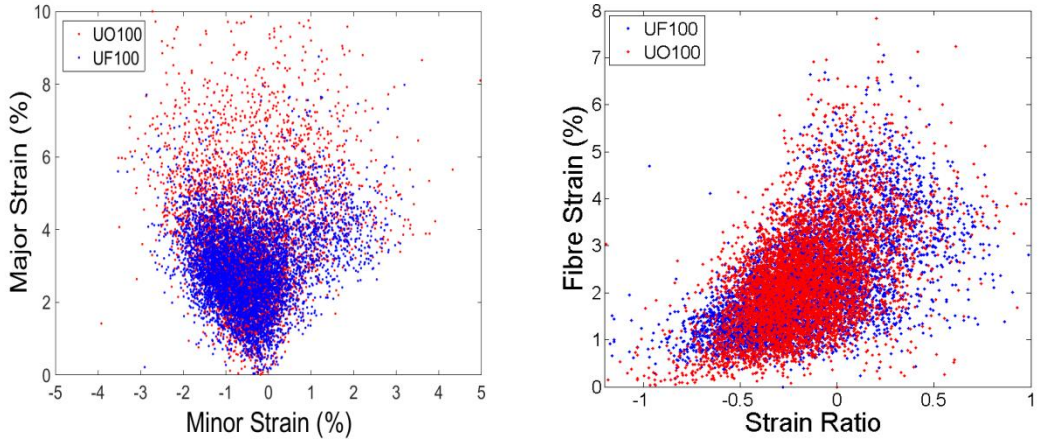

(a) (b)

Figure 5.8: Surface strain distributions of the UF100 and UO100 specimens at the stage of failure (a) the conventional FLD; (b) the new FLD.

Figure 5.8 shows the comparison on surface strain distribution from the same UF100 and UO100 specimens at the stage just before failure, and the only difference is that these two samples are compared in different axes. Figure 5.8a is plotted on the conventional FLD (major strain versus minor strain), while Figure 5.8b is plotted on the new FLD (fibre strain against strain ratio). Each dot in the figure above represents a surface point of the composite specimens, the strain information of which is provided by the ARAMIS™ system. Figure 5.8a shows the surface strain distributions of two specimens using the conventional FLD just before failure, and it suggests that even though the two specimens exhibit similar forming modes, the UO100 sample experiences considerably higher limiting major strain just before failure. Under shear deformation, the trellising behaviour of the woven composite allows the flax fibres in the warp and weft directions to move over each other within the ply such that they are no longer perpendicular to each other. This results in a larger depth to failure (13.3 mm for the UF100 specimen, and 14.7 mm for the UO100 specimen), and therefore increased principal strains. This is combined with the much larger elongation-to-failure

of the polypropylene matrix compared to the flax fibres, as described in the previous section. Based on the strain distributions, the limiting principal strain defined by one of these two specimens is not applicable to the other. This observation would indicate that the composite exhibits varying limiting principal strains at the same forming mode, implying that the conventional FLC is not suitable for describing the failure behaviour of this class of material system.

In metal forming, it is customary to discuss major strain and minor strain. In woven composites, however, the strain acting on the fibres and the matrix should be considered due to the difference in mechanical properties. The current work found that the flax fibre reinforced polypropylene composite exhibits a major failure mechanism of fibre fracture at room temperature. For the composite analysed in the current study, the flax fibres are the limiting factors for elongation of the composite due to the significantly lower elongation-to-failure of the flax fibres compared to that of the polypropylene matrix. Figure 5.8b shows that on the plot of fibre strain against strain ratio, both specimens exhibit a very similar distribution. Even though the UF100 and UO100 specimens are formed to different depths, the flax fibres are strained to a similar extent at failure; the difference observed in principal strains is attributed to the strain acting on the polypropylene matrix which contributes little to the composite failure. This further highlights the possibility of establishing the new FLC for the natural fibre composite using fibre strain and strain ratio. In the work conducted by Zanjani *et al.* [73], a self-reinforced polypropylene composite exhibited a failure behaviour induced by both the fibres and the matrix. The amount of strain acting on the matrix thus contributed to the onset of failure in the composite, validating the application of conventional FLC to the composite in this case.

5.2.1.4 Investigation on the path dependency effect of the conventional FLC

It has been demonstrated that the conventional FLC is not applicable to predict failure initiated in woven composites. Path dependency effect means that the limiting major strain of a surface point is influenced by its historical strain path, and this effect is the mechanism behind the inapplicability of the conventional FLC. This section examines the path dependency effect of the conventional FLC, and investigates whether such issue can be resolved by using the new FLC.

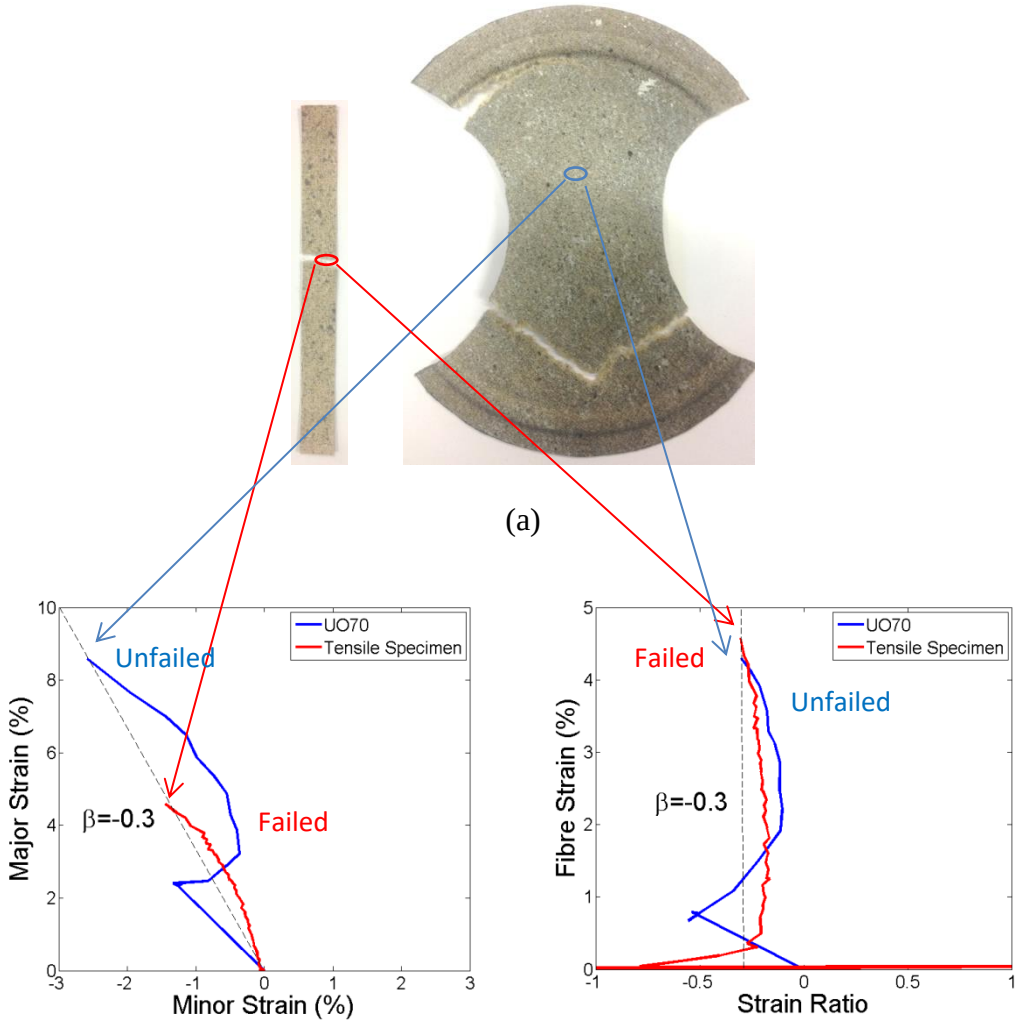

Figure 5.9: Comparison of a tensile specimen (left) with a UO70 specimen (right) (a) tested samples; (b) the evolution of the strain path on the conventional FLD (left) and on the new FLD (right).

To investigate the path dependency effect of the woven composite, two points from the tensile specimen and the UO70 sample are selected and their evolutions of principal strains are compared. The point of interest from the tensile specimen is located along the line of fracture, while that of the UO70 specimen is located slightly above the pole and remains unfailed during the stretch forming test. These two points share a similar deformation mode at the stage of comparison, but experience entirely different historical paths, which is of importance to examine the effect of path dependency on the conventional FLC.

Figure 5.9 compares principal strain evolutions of the pole of the UO70 specimen with that of the tensile specimen on a conventional Forming Limit Diagram (FLD). Strain deformation of the tensile specimen is obtained at the stage of failure, while that of the UO70 specimen is obtained at a forming depth of 14 mm, given that the failure depth is 16.2 mm, this surface point therefore remains unfailed at the last stage of the curve. Forming modes can be represented by different strain ratios in the FLD, ranging from biaxial stretch (1) to pure shear (-1). Even though both specimens experience the same forming mode of uniaxial tension at the stage of selection, it is noted that the unfailed specimen (UO70) could withstand significantly higher limiting principal strains compared to failed specimen (the tensile specimen). Unlike the tensile specimen which experiences a single forming mode (constant strain path), the UO70 specimen experiences changes in strain path due to the nature of stretch forming tests as explained later. This suggests a path dependency phenomenon, such that the limiting principal strains are influenced by the evolution path.

The evolutions of strain path of the same two points of interest are now compared on a plot of fibre strain against strain ratio. Evidently, although principal strains are

significantly higher, the maximum fibre strain of the unfailed points (from the UO70 specimen) does not exceed the limiting fibre strains defined by the failed point (from the tensile specimen). This demonstrates that using fibre strain can help eliminate the path dependency effect, which can be attributed to the fact that fibre strain calculations require tracking of the evolution of fibre movements. Experimental observations also highlight the possibility of establishing a new FLC using fibre strain and strain ratio, and the new FLC is expected to be more effective than the conventional one.

To further investigate the mechanism behind path dependency effects, the evolution of strain deformation at the point of interest in both specimens is studied, as shown in figure 5.10. In uniaxial tension tests, the sample experiences a single deformation mode, resulting in a constant strain path. This linear strain path is different to the strain path history observed in stretch forming test, details of which is explained in Section 5.2.

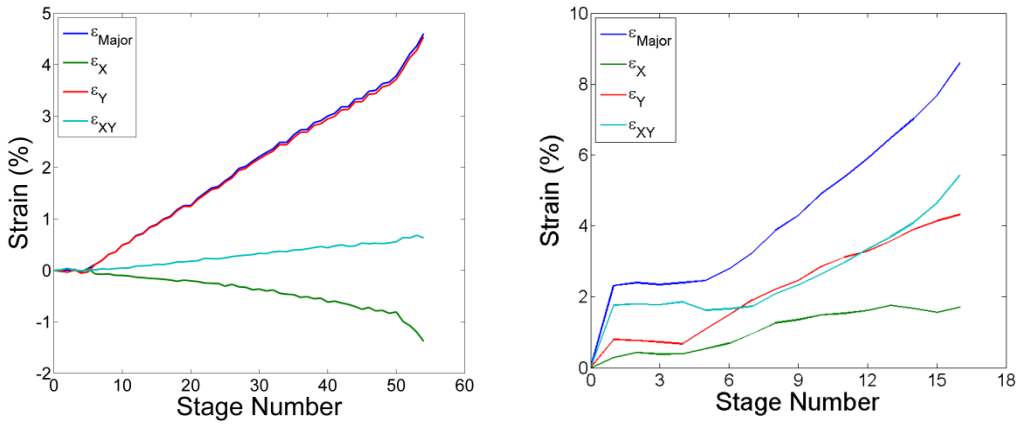

(a) (b)

Figure 5.10: Strain evolutions (a) the UO70 specimen; (b) the tensile specimen.

Figure 5.10 shows the evolutions of major strain and its constituents at the same surface points used in Figure 5.9. In uniaxial tension tests, the major strain is dominated by the strain along the stretching direction, and the perpendicular direction experiences a

negative strain deformation due to the Poisson's effect. The shear component is insignificant in tensile specimen, whereas the UO70 specimen is dominated by its shear strain component which is larger than the strains in the longitudinal direction and transverse directions. As found earlier, the flax fibre reinforced polypropylene composite exhibits a major failure mode of fibre fracture [126]. Therefore, the flax fibres should be the limiting factor for the elongation of the composite due to a much lower elongation-to-failure of the flax fibres compared to the polypropylene matrix. It is therefore hypothesised that the amount of strain acting on the flax fibres is influential in composite failure whereas shear strain has little effect. In addition to this, large shear strains are suggested as the cause of the path dependency phenomenon observed in the conventional FLC. Again, this is because shear strains can lead to higher principal strains, but not necessarily the onset of failure in this class of material system.

5.2.1.5 Establishing the new FLC for the composite

In metal forming, there can be a clear progress from the onset of localised necking to catastrophic failure. It is, therefore, feasible to identify the safe, marginal and failed regions of the FLC for metals. The composite analysed in this study exhibits a low resistance to crack propagation, and failure propagates very quickly during forming. Therefore, for this class of material system there is no marginal region. The new FLC, as shown in Figure 5.11, represents the limiting fibre strain of the composite in all forming modes ranging from pure shear (strain ratio of -1) to biaxial stretch (strain ratio of 1).

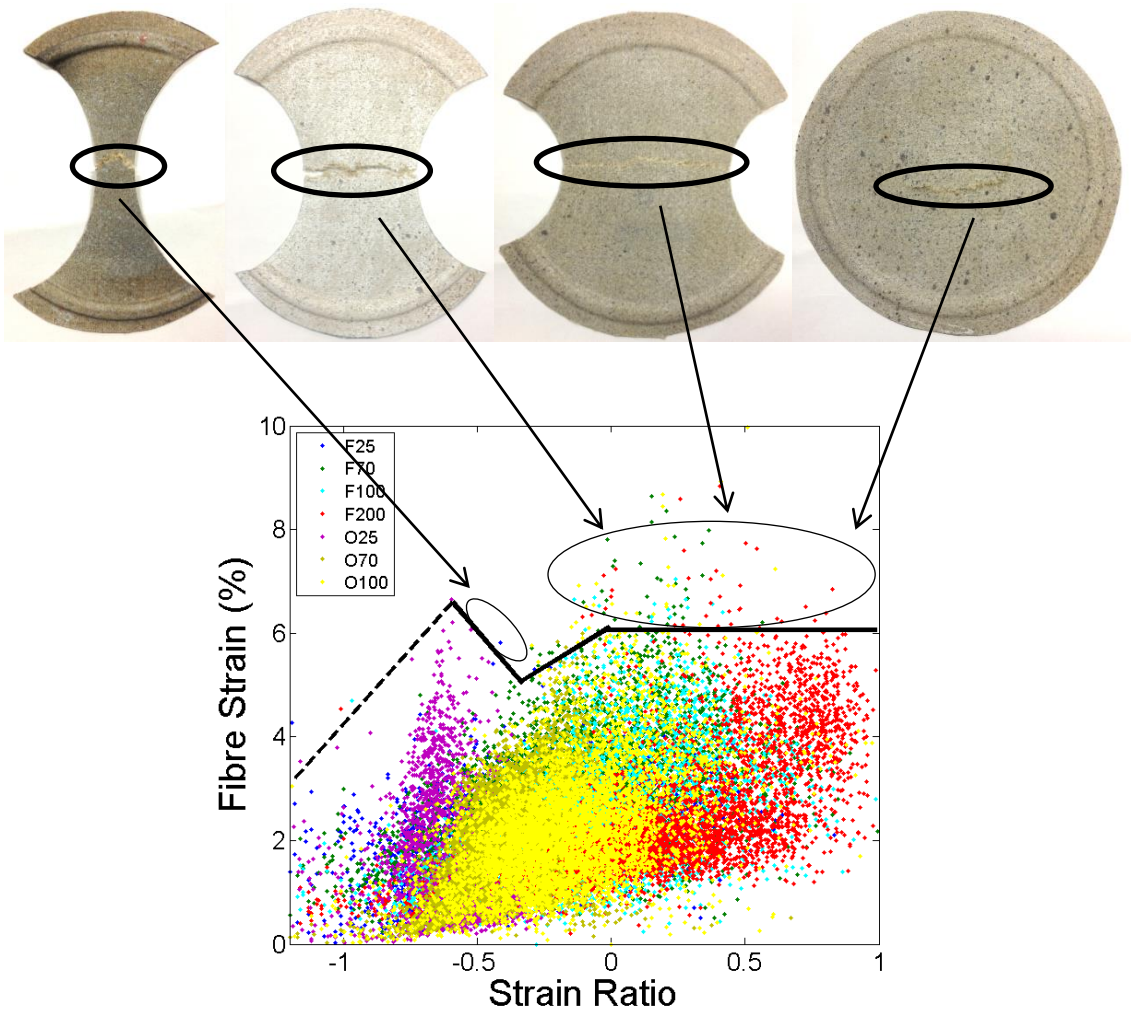

Figure 5.11: Formation of the new FLC for the untreated composite. From left to right at top: formed specimens are F25, F70, F100 and F200.

In this study, the limiting fibre strain in certain strain ratios cannot be observed from the failure regions. For the O25 and O70 specimens which exhibit a major forming mode of pure shear, the failure initiates at the flange region which during forming is blocked from the cameras by the tools. However, safe regions are established based on unfailed points, and it is expected that the limiting fibre strain is higher than that suggested by the safe regions.

Figure 5.11 shows the new FLC over the surface strain distributions of all specimens at the stage of failure, over a wide range of forming modes. Most points above the

proposed failure envelope are located along line fractures in formed specimens, which are expected to be regions where failure initiates. Small localised imperfections cannot be eliminated from consolidated composites, resulting in an increase of principal strains over allowable limits in some regions without failure being experienced. Since the new FLC considers fibre strain, it must be emphasised that this method can only predict failures for composites where the failure mechanism is dominated by fibres. Compared to the conventional FLC, which requires only major strain and minor strain, the new FLC needs more information on surface strains, and more importantly the evolutions of these strains. Clearly, successfully tracking the evolution of fibre movements is fundamental in determining the forming limit of this class of material system, which highlights the need of surface strain measurement equipment such as the ARAMIS™ system.

A similar approach is used to establish the new FLC for the composite in water-treated and redried conditions, and Figure 5.12 compares the new FLCs in different conditions of water treatment. A significantly expanded forming envelope is observed in the water-treated specimen. Such observations can be expected from the improvement in elongation-to-failure, and again indicate an exceptional formability of the water-treated composite. ***This class of material system is therefore very attractive and can be easily used to form parts of a high level of complexity if they can be processed wet in advance.***

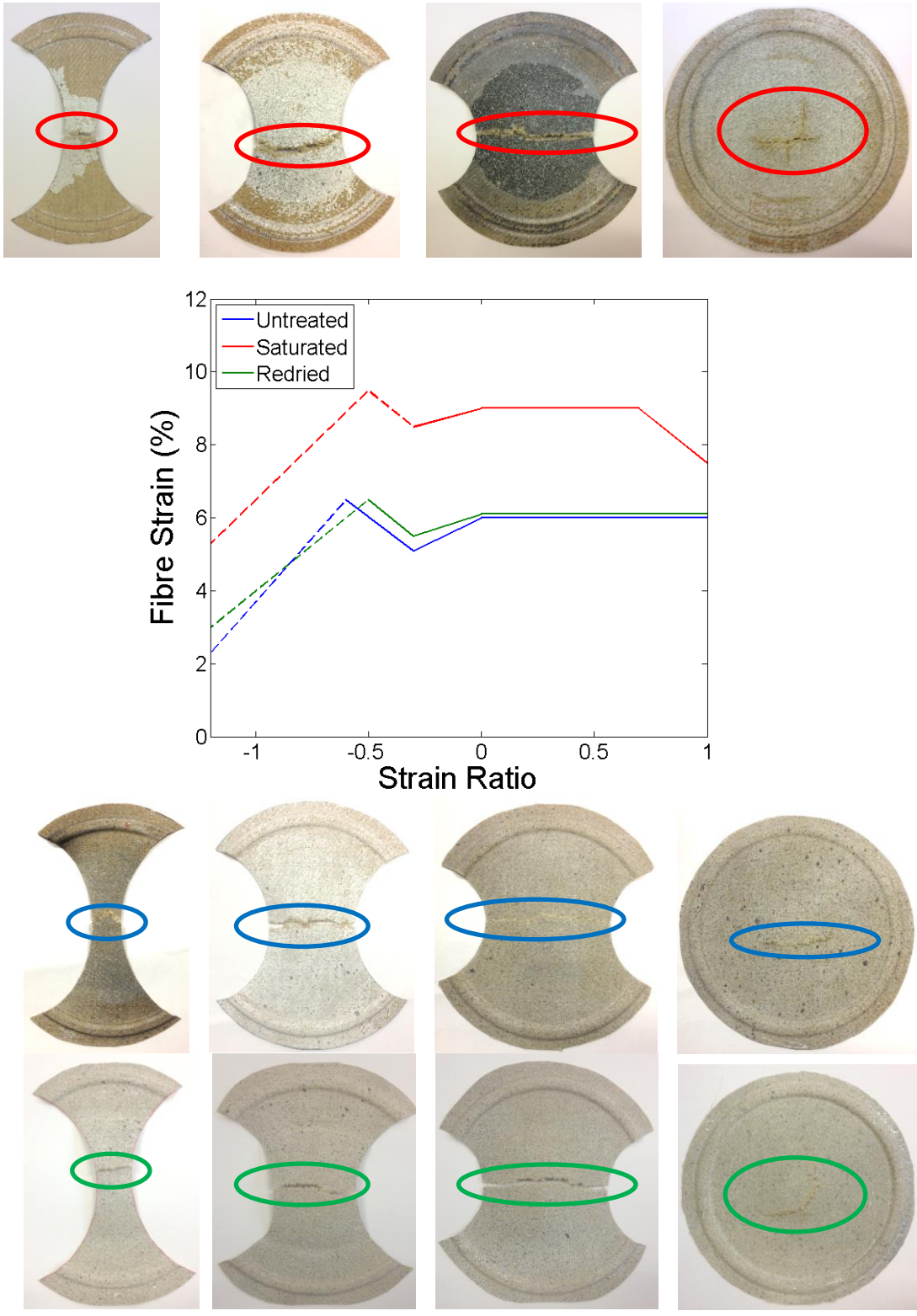

Figure 5.12: The new FLCs for the composite in different conditions of water treatment. The tested samples are F25, F70, F100, and F200 (water-treated, redried, and untreated from top to bottom, respectively).

The new FLCs for the composite in different conditions are expressed in Equations 5.18 to 5.20. It is important to note that the composite exhibits a significantly expanded forming envelope in the water-treated condition, such that the limiting fibre strains of the water-treated composites are increased by 25% in biaxial-stretch, 50% in plane strain, and 70% in uniaxial tension (compared to the untreated composite). This is expected, given the improvement in elongation-to-failure discussed in the previous section, and again indicates good formability of the water-treated composite. This class of material system is therefore very attractive and can be easily used to form the products with complex shapes if they can be processed whilst wet.

For the untreated composite:

$$\boldsymbol{\varepsilon_{Limit}} = \begin{cases} \mathbf{6\%} & \mathbf{0 < \beta < 1} \\ \boldsymbol{\beta} * \mathbf{3.3\%} + \mathbf{6\%} & \mathbf{-0.3 < \beta < 0} \\ -\boldsymbol{\beta} * \mathbf{5\%} + \mathbf{3.5\%} & \mathbf{-0.6 < \beta < -0.3} \\ \boldsymbol{\beta} * \mathbf{5.8\%} + \mathbf{10\%} & \mathbf{-1.2 < \beta < -0.6} \end{cases} \tag{5.18}$$

For the water-treated composite:

$$\boldsymbol{\varepsilon_{Limit}} = \begin{cases} -\boldsymbol{\beta} * \mathbf{5\%} + \mathbf{12.5\%} & \mathbf{0.7 < \beta < 1} \\ \mathbf{9\%} & \mathbf{0 < \beta < 0.7} \\ \boldsymbol{\beta} * \mathbf{1.67\%} + \mathbf{9\%} & \mathbf{-0.3 < \beta < 0} \\ -\boldsymbol{\beta} * \mathbf{5\%} + \mathbf{7\%} & \mathbf{-0.5 < \beta < -0.3} \\ \boldsymbol{\beta} * \mathbf{6\%} + \mathbf{12.5\%} & \mathbf{-1.2 < \beta < -0.5} \end{cases} \tag{5.19}$$

For the redried composite:

$$\boldsymbol{\varepsilon_{Limit}} = \begin{cases} \mathbf{6.1\%} & \mathbf{0 < \beta < 1} \\ \boldsymbol{\beta} * \mathbf{2\%} + \mathbf{6.1\%} & \mathbf{-0.3 < \beta < 0} \\ -\boldsymbol{\beta} * \mathbf{5\%} + \mathbf{4\%} & \mathbf{-0.6 < \beta < -0.3} \\ \boldsymbol{\beta} * \mathbf{5\%} + \mathbf{9\%} & \mathbf{-1.2 < \beta < -0.6} \end{cases} \tag{5.20}$$

where ε_{Limit} is the limiting fibre strain, and β is the strain ratio. Again, it needs to be noticed that the actual limiting fibre strains are greater than the values suggested by the equations above in those regions represented by dashed lines.

5.2.1.6 Comparison with the Maximum Strain failure criterion

The Maximum Strain failure criterion (a strain based failure criterion) is selected to compare with the new FLC proposed in this study. Tensile tests were performed to generate failure strain data for the Maximum Strain criterion. Rectangular specimens of 15 mm by 150 mm were produced, and the composites were cut in such a way that the flax fibres were oriented at 0°/90° and 45°/-45° to the sample axis to obtain normal failure strain and shear failure strain. Tensile tests were conducted through an Instron™ 4505 testing machine, and the specimens were stretched at a constant rate of 5 mm/s with failure being defined as the applied load dropped to 40% of its maximum.

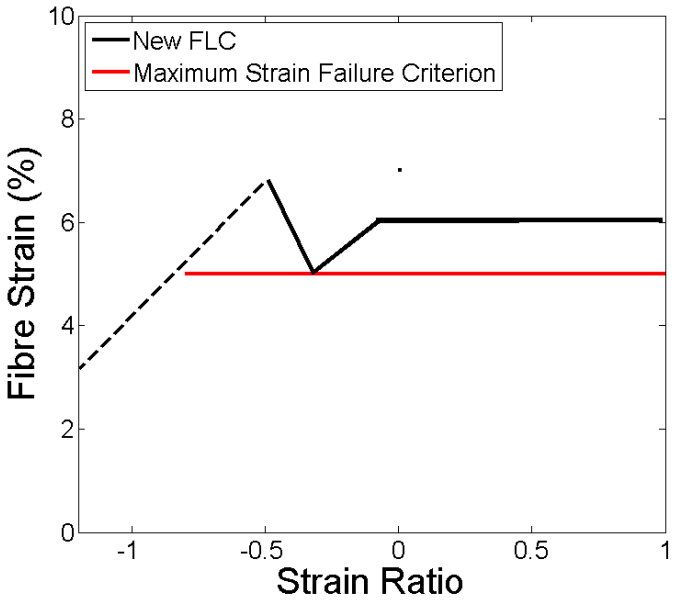

Figure 5.13: Comparison between the new FLC and the Maximum Strain failure criterion.

Through tensile tests, it is observed that the composite has an elongation-to-failure around 5% when it is stretched along fibre orientations. The new FLC suggests a limiting fibre elongation of around 5% at a strain ratio of -0.3, given that the composite has a Poisson's ratio of around 0.3 and is therefore in uniaxial tension. The limiting fibre strain can exceed 5% in several forming modes, and as large as 6% when the strain

ratio is positive or even 6.5% when the strain ratio is -0.5. Evidently, limiting fibre strain is affected by the forming mode experienced by the composite, and can be attributed to the woven structure of the composite in which the interactions between the fibres and the matrix are influential. For the Maximum Strain failure criterion, the failure in the forming mode of pure shear is judged by the limiting shear strain, which is significantly higher than limiting normal strain. In other forming modes, the Maximum Strain failure criterion suggests that the failure strain on fibres is a constant, as shown in Figure 5.13. The assumption that there is no interaction between different constituents seems to be oversimplified for predicting failure in woven composites. For further comparison, the new FLC and the Maximum Strain failure criterion are implemented in FEA simulations in Section 5.3.4.2.

5.2.2 CNFC materials

The major difference between NFC and CNFC materials is that the later composite does not exhibit directionality. It behaves predominantly like isotropic material, meaning that the stiffness and elongation-to-failure are the same in all directions.

5.2.2.1 Evolution of surface strain ratios

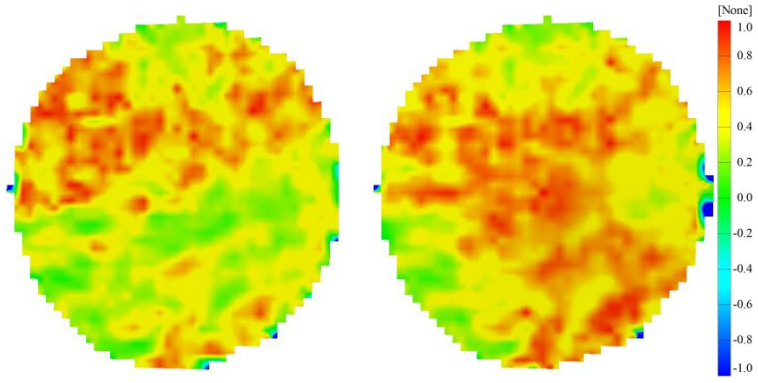

U200

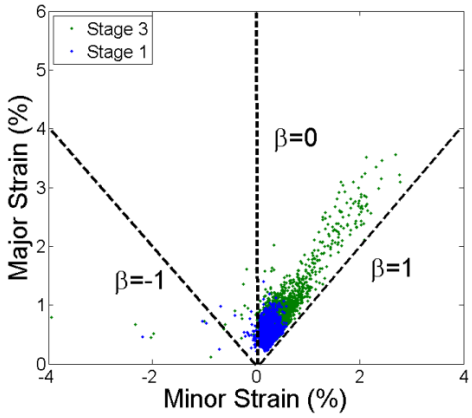

(a)

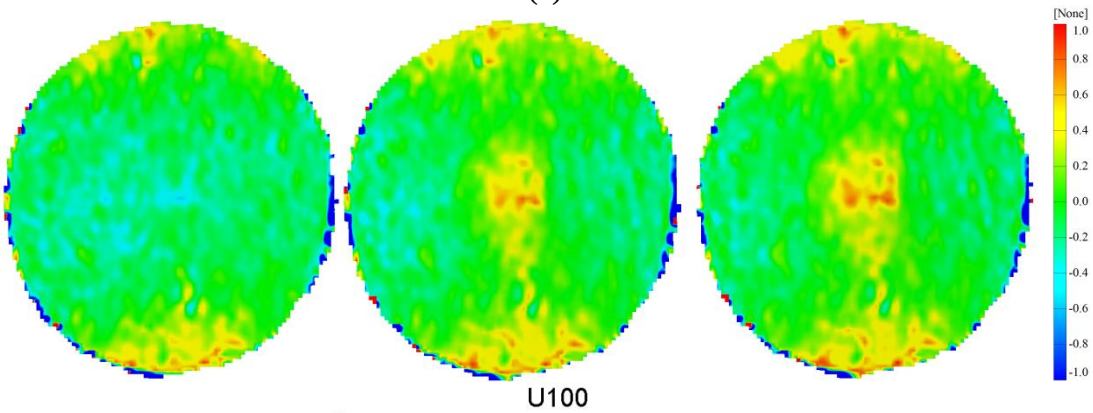

U100

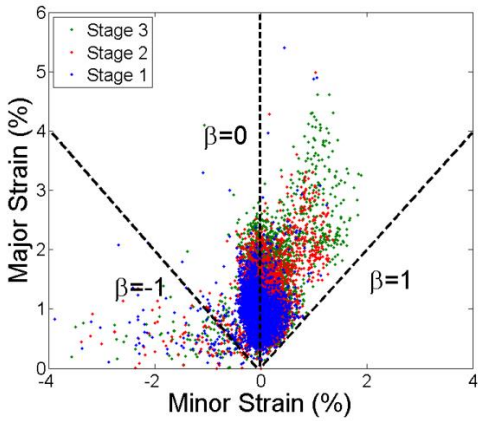

(b)

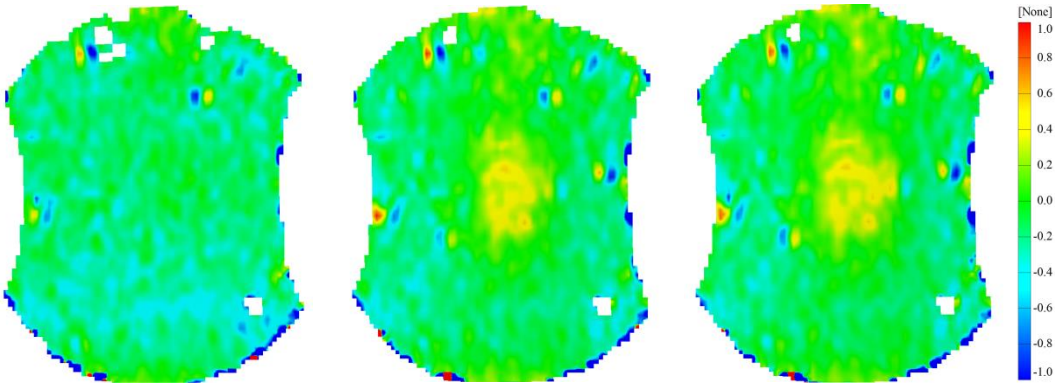

U70

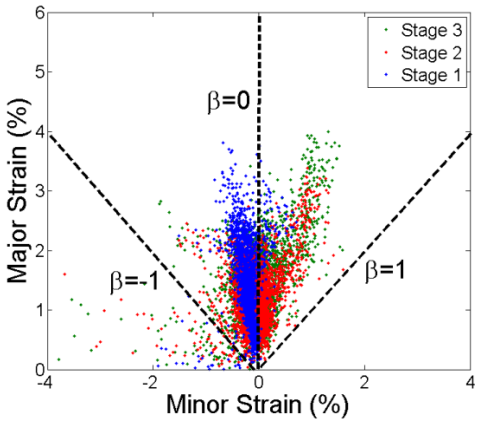

(c)

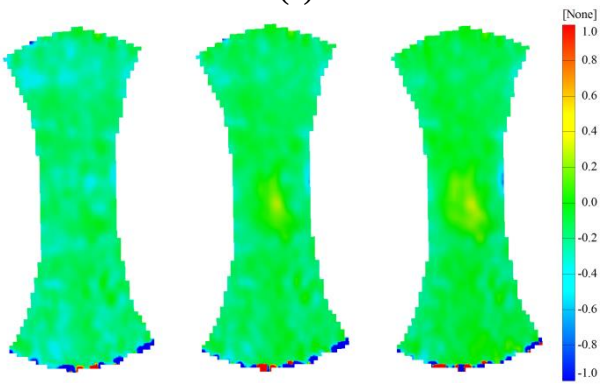

U25

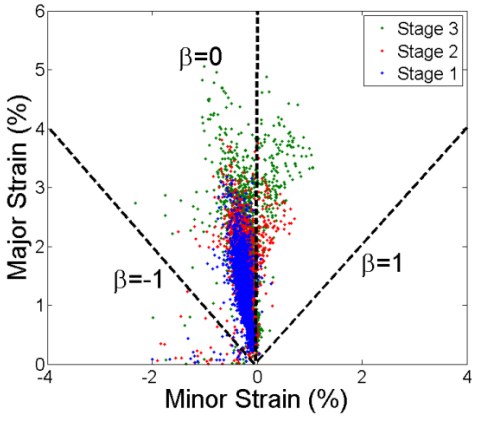

(d)

Figure 5.14: Evolution of contours of surface strain ratio (deformation mode) and FLD.

(a) U200; (b) U100; (c) U70; and (d) U25.

Similar to NFC materials, strain ratio information of CNFC specimens is calculated by the python script created in this work. Figure 5.14 above shows the surface contour of strain ratio for each sample, as well as the FLDs at the end of each stage. The amount of strain deformation is very small at the edges of surface contours, leading to some extremely negative strain ratios. In the pre-stretch stage, all specimens (except the full circle sample which exhibits a major deformation mode of biaxial stretch) experience negligible minor strain, suggesting unequal restriction in the longitudinal and transverse directions. These samples are pulled at both edges in the pre-stretch stage, leading to a deformation mode of in between uniaxial tension and plane strain. As lateral restriction increases with wider samples, the major deformation mode moves towards plane strain (as observed in U70 and U100), suggesting that the lateral direction remains unstrained while both edges are pulling away from each other. Equal amounts of force are applied to the U200 sample from every direction, resulting in a major deformation mode close to biaxial-stretch. In addition, none of the samples exhibits a major deformation mode of pure shear due to the predominantly isotropic nature of CNFC materials. Observations of FLDs at the end of the first stage show a clear trend of lowered maximum strain deformation as sample width increases.

For the full circle sample or the U200 specimen, the composite exhibits a major deformation mode of biaxial stretch during forming, since the entire sample edge is completely fixed during forming. Therefore, unlike other geometries which have three separate stages, the UF200 specimen has only two stages (stage 1 and stage 3). For the U70 and U100 specimens, the pole and its nearby regions shift from the negative minor strain region to the positive minor strain region in the biaxial stretch behaviour. Similar behaviour is not obvious for the U25 sample, which can be attributed to the fact that the biaxial stretch behaviour disappears very quickly due to a small sample width. In the

third stage, specimens exhibit their major deformation mode which is influenced by the sample geometry.

Unlike NFC materials, CNFC materials could not exhibit pure shear behaviour during stretch forming experiments, which is attributed to the fibre reinforcement nature of CNFC samples. The lack of deformation mode of pure shear also results in larger amount of strains acting on the fibres, leading to lower deformation depths. The application of short chopped fibres would help recycle composites at the end of its use-life, and it seems that a trade-off needs to be made between ease for recycling and better formability.

5.2.2.2 Constructing the FLC

The construction of the FLC of the CNFC is based on the principal strain values provided by the ARAMIS™ system. Line fractures in CNFC materials can be narrowed down to short segments where the failure initiates, and this is achieved by setting the frame rate of the ARAMIS™ system to its maximum of 15 images per second. Principal strains of these small segments at the stage just prior to failure are used to construct the FLC, as shown in Figure 5.15. Note that the surface point experiencing strain deformation above the FLC is considered failure. Using FLC to describe failure behaviour provides a quantitative measure for defining the limiting major strains as a function of minor strain, and such mathematical relations can be implemented in FEA models through a user-defined material subroutine.

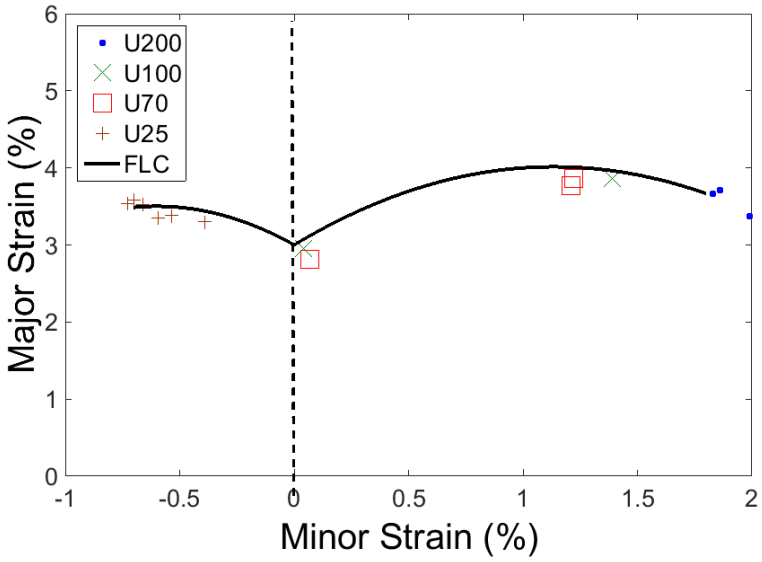

Figure 5.15: FLC of the CNFC materials obtained from stretch forming tests.

Similar to the procedure used to construct the FLC for the untreated specimens, the water-treated as well as the redried samples were cut into hourglass shapes (with varying middle sectional widths) and then formed into a hemispherical dome. Significantly improved elongation-to-failure has been noticed in the water-treated CNFC materials. Figure 5.16 shows that the increased elongation-to-failure can be translated to an increased forming envelope. Numerically, FLCs in different conditions of water treatment can be expressed in the following equations 5.21-5.23. It is not surprising that the redried composite has very similar forming limits to the untreated composite, as ductility has been largely returned to the untreated level when drying from the wet condition. Compared to these two dry conditions, the CNFC exhibits a significantly expanded forming envelope in the water-treated conditions, such that the limiting major strains are increased by 61% in biaxial stretch, and 92.8% in plane strain.

For the untreated composite:

$$\varepsilon_1{}' = \begin{cases} -78.69 * \varepsilon_2{}^2 + 1.79 * \varepsilon_2 + 0.03 & 0\% < \varepsilon_2 < 2\% \\ -139 * \varepsilon_2{}^2 - 1.67 * \varepsilon_2 + 0.03 & -0.6\% < \varepsilon_2 < 0\% \end{cases} \quad (5.21)$$

For the water-treated composite:

$$\varepsilon_1{}' = \begin{cases} 0.0675 & 0\% < \varepsilon_2 < 3\% \\ -183 * \varepsilon_2{}^2 - 2.01 * \varepsilon_2 + 0.0675 & -0.7\% < \varepsilon_2 < 0\% \end{cases} \quad (5.22)$$

For the redried composite:

$$\varepsilon_1{}' = \begin{cases} -25.96 * \varepsilon_{Minor}{}^2 + 0.73 * \varepsilon_{Minor} + 0.035 & 0\% < \varepsilon_{Minor} < 2.1\% \\ -250 * \varepsilon_{Minor}{}^2 - 3.5 * \varepsilon_{Minor} + 0.035 & -0.55\% < \varepsilon_{Minor} < 0\% \end{cases} \quad (5.23)$$

where $\varepsilon_{Major}{}'$ is limiting major strain; and ε_{Minor} is minor strain.

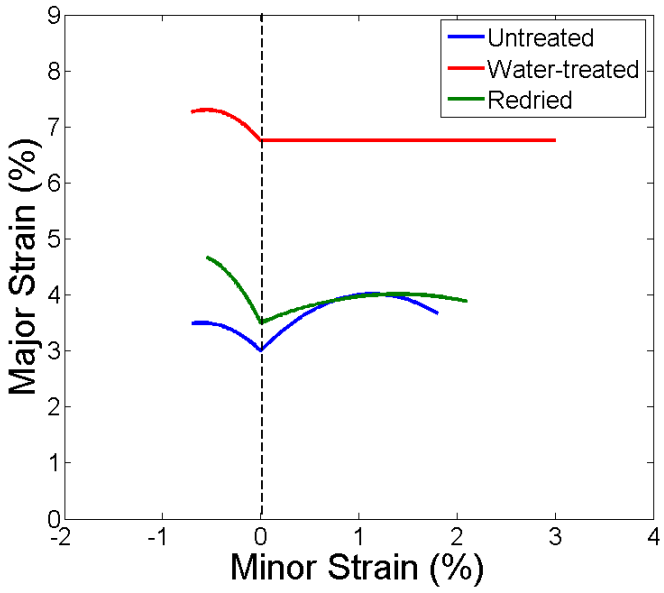

Figure 5.16: Effect of water treatment on FLC for CNFC materials.

5.3 FEA simulations

5.3.1 Material models

Two composite materials, NFC and CNFC, are modelled in FEA simulations. Due to the random distribution of the chopped flax fibres, the CNFC is modelled as quasi-isotropic. The stiffness matrix for the CNFC material is expressed in the following equation.

$$\begin{bmatrix}\sigma_{11}\\ \sigma_{22}\\ \sigma_{33}\\ \tau_{23}\\ \tau_{13}\\ \tau_{12}\end{bmatrix}=\begin{bmatrix}C_{11} & C_{12} & C_{13} & 0 & 0 & 0\\ C_{12} & C_{22} & C_{23} & 0 & 0 & 0\\ C_{13} & C_{23} & C_{33} & 0 & 0 & 0\\ 0 & 0 & 0 & C_{44} & 0 & 0\\ 0 & 0 & 0 & 0 & C_{55} & 0\\ 0 & 0 & 0 & 0 & 0 & C_{66}\end{bmatrix}\times\begin{bmatrix}\varepsilon_{11}\\ \varepsilon_{22}\\ \varepsilon_{33}\\ \gamma_{23}\\ \gamma_{13}\\ \gamma_{12}\end{bmatrix} \quad (5.24)$$

These coefficients are computed using equations for the micromechanical behaviour of a lamina.

$$C_{11}=C_{22}=\frac{E}{1-v^2} \quad (5.25)$$

$$C_{12}=C_{21}=\frac{Ev}{1-v^2} \quad (5.26)$$

$$C_{66}=\frac{E}{2(1+v)} \quad (5.27)$$

$$C_{44}=C_{55}=\frac{5}{6}C_{66} \quad (5.28)$$

where E is the stiffness obtained from the tensile tests stated in Chapter 3; and v is the Poisson ratio. Due to the linear nature, all coefficients in Equations 5.25-5.28 are constants. All other terms are zero, as shell elements do not consider out-of-plane stress. The NFC is characterised as orthotropic, and shares a similar stiffness matrix with CNFCs except that the in-plane shear stiffness C_{66} is determined by the method introduced in the Composites Materials - Design and Applications [134].

The development of constitutive material modeling for both material is the first step of developing FEA simulation of the forming process. The accuracy of the constitutive

material properties is of great importance to the accuracy of the numerical simulation. The constitutive material models of both NFC and CNFC in different conditions of the water-treatment are illustrated in Appendix A and Appendix B, respectively.

5.3.2 Model parameters

Figure 5.17 shows a diagram of the parts modelled in the simulation, including punch, blank-holder, die and full circle flax/PP composite. The full circle specimen is replaced with the corresponding geometry when modelling other geometries. The die stays stationary during forming and the blank holder can only move vertically to allow the action of the blank holder force. The composite was meshed with S4R elements with an approximate size of 2 mm, resulting in more than 5,700 elements in full circle sample and around 2,500 elements in an hourglass sample with a width of 25 mm. The punch is placed just in contact with the blank and it is set to move down at a speed of 20 mm/s. Contact friction has a significant effect on material flow during forming, and penalty contact conditions are assigned to all contact conditions. All the tool geometries are defined as rigid parts and master surfaces, such that the tool is able to penetrate through the sample during forming rather than the other way around. The entire stretch forming simulation is divided into two separate steps, and this analysis procedure follows the experimental procedure. Two steps (Static, General), referred to as Pre-stretch and Forming, are defined in FEA simulations. In the Pre-stretch step, initial boundary conditions are assigned to simulate the lock-ring effect. In the Forming step, the punch is set to move down at a constant speed of 20 mm/s. The initial, minimum, and maximum increment size are defined as 0.1s, 10^{-10}s, and 0.1s, respectively in both steps.

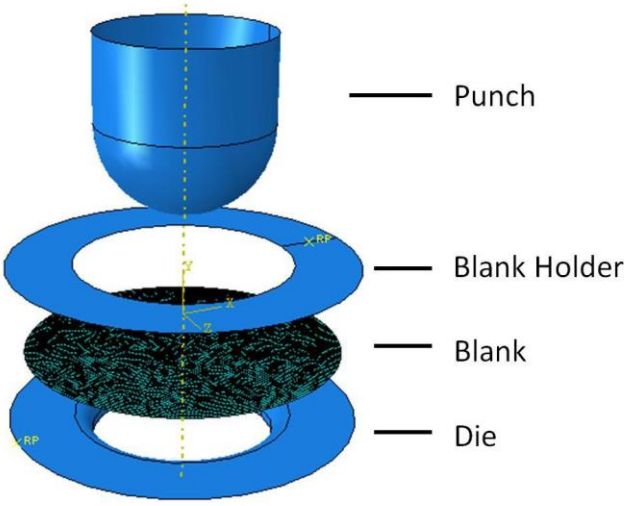

Figure 5.17: Layup of model geometries.

5.3.3 Implementing the failure criterion in FEA simulations

FEA simulations are an essential tool in engineering structural design and analysis, and the development of the new FLC would be much less useful if this failure criterion cannot be implemented in FEA models. One of the key contributions of the current study is to incorporate the FLC and the new FLC in FEA simulations through a user-defined material subroutine. State dependent variable or solution-dependent state variable (SDV) can be calculated from built-in variables in the material subroutine (such as the strains in the global X, Y, and shear directions) through a self-defined relation, and updated at the end of each time increment. In order to implement the failure criteria, SDVs are created to facilitate calculations. In this study, the user-defined material subroutine provides two essential functions to FEA models, including material characterisation as well as failure criterion. For NFCs, eight SDVs are created in total to represent failure indicator, major strain, minor strain, failure flag, strain ratio, fibre strain along the weft direction, fibre strain along the warp direction and fibre strain. Due to the difference in the level of complexity, only the first four SDVs mentioned above are created for CNFCs. For both composites, if the induced fibre strain of a mesh node exceeds the value suggested by the failure criterion, the failure indicator is turned on

and the stiffness in all directions reduces to 0, analogically creating a 'crack' so that the region can withstand applied stress. It is possible in FEA simulations but not reasonable or realistic, for a mesh node to fail and then to become 'unfailed' later during the forming process. To eliminate this unrealistic situation, a SDV named 'flag' is defined to ensure that once failure initiates at a mesh node, this point remains failed regardless of the future strain conditions. Figure 5.18 shows the flow chart of the user-defined material routine developed for NFCs, which is very close to that of CNFCs with a different stiffness matrix and failure criterion.

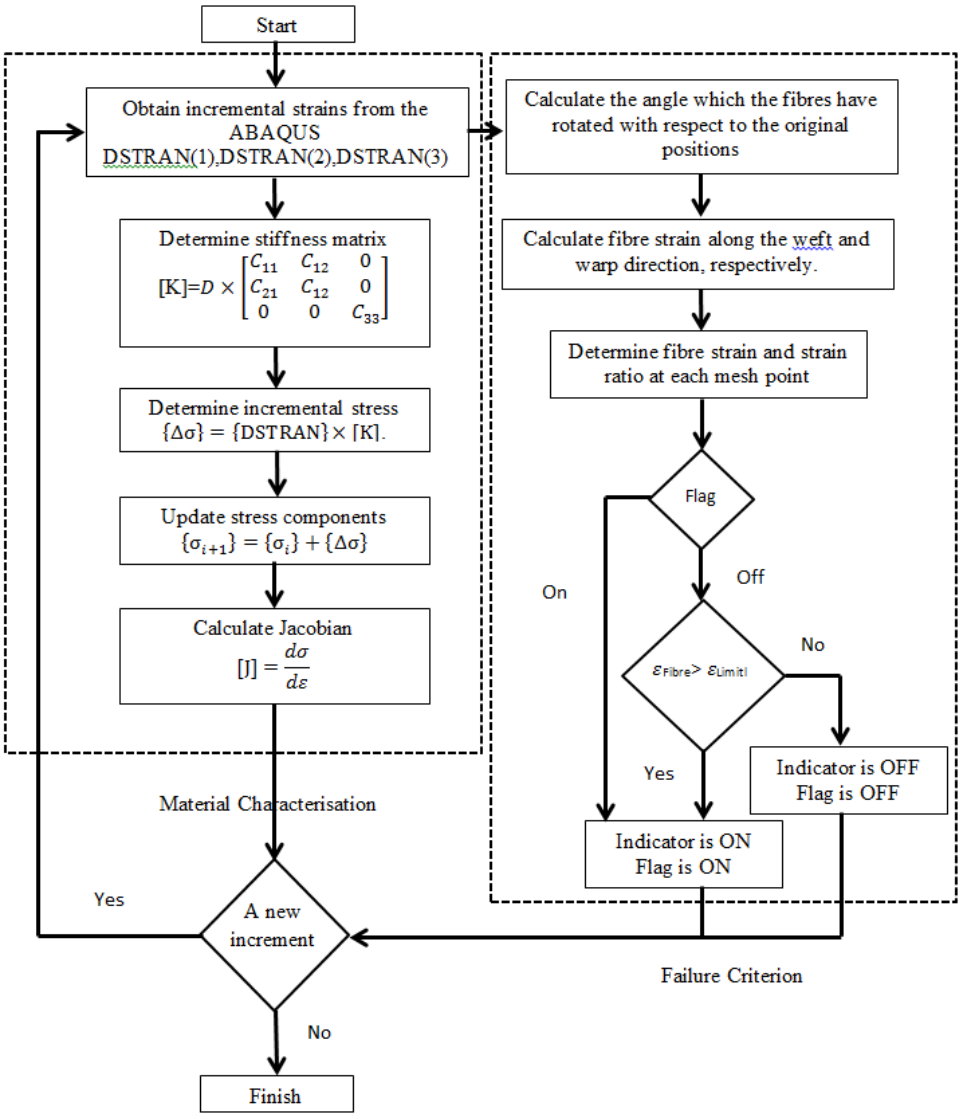

Figure 5.18: Flow chart of the user-defined material routine for NFCs.

5.3.4 NFC materials

5.3.4.1 Evolution of strain path at the pole

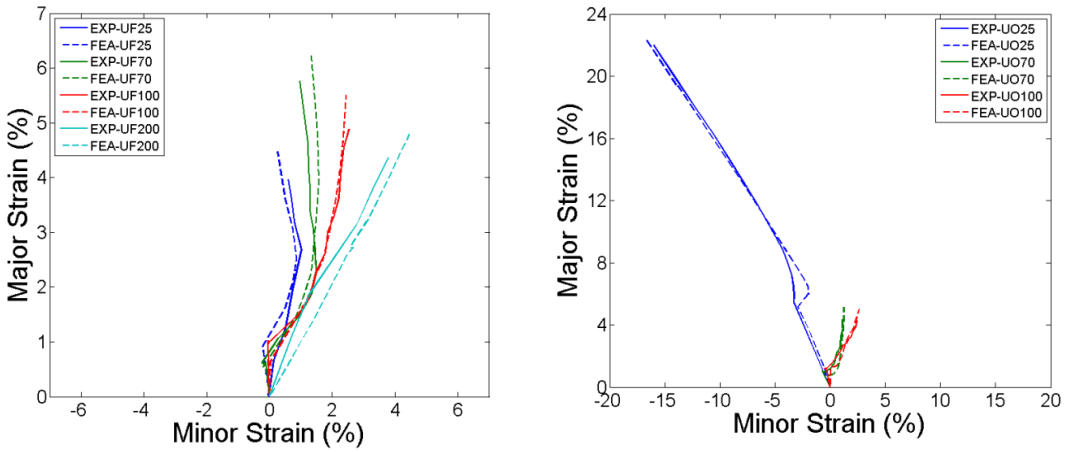

(a) (b)

Figure 5.19: Comparison of strain evolution at the pole between experimental observations and FEA simulations (a) 0°/90° samples; (b) 45°/-45° samples.

The pole is the region of interest for stretch forming tests, and the strain evolution at this point is used to verify the FEA simulation developed in this study. Figure 5.19 shows that the strain evolutions of specimens with different sample widths and fibre orientations can be simulated by FEA simulations, validating the material properties as well as contact conditions. It is noted that the UO25 specimen is able to withstand a major strain of 22% at the stage of failure which is significantly higher than all the other samples. This can be explained by the trellising behaviour of the woven composite. The specimen is much less strained on the flax fibres under such a deformation mode, therefore exhibiting a very high state of principal strains prior to failure. It is observed that for specimens with large widths, sample geometry has a larger effect than stretch directions due to the increased restriction exerted from the tools. For example, the UF100 specimen shares a similar strain evolution with the FO100 sample. Larger specimens experience larger restrictions at the flange region, forcing composites to form

in similar major forming modes. The FEA simulations can predict this trend, and again the slight discrepancy can be attributed to the variation of the mechanical properties of flax fibres as well as to geometric unevenness caused by small localised imperfections.

5.3.4.2 Comparison between the new FLC with the Maximum Strain failure criterion

Based on visual observations on the formed specimens, failure can initiate at two different regions: the pole or the flange region. The pole of the specimen is stretched to a great extent during forming, and in 0°/90° specimens the high level of strain there causes failure. The O25 and O70 specimens experience a large shear deformation at the pole, which allows the composite to withstand a larger forming depth and results in failure at unsupported regions near the die edge. It is a statistically consistent observation that line fractures propagate along the fibre directions, regardless of fibre orientation and sample width. Accordingly, the failure regions of the F25 specimen are in the longitudinal and transverse directions, and those of the O25 specimen are at 45° to them as shown in Figure 5.20. This clearly implies that the flax fibres are the limiting factor for the elongation of the composite.

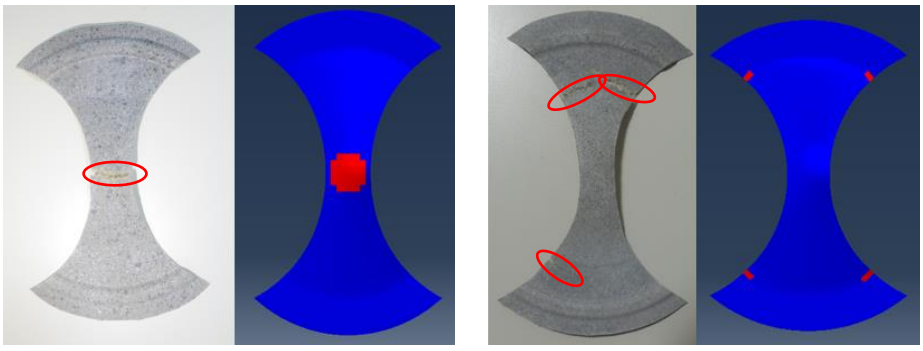

(a) (b)

Figure 5.20: Typical failure regions observed in the formed specimens (circled) and as predicted by the new FLC in FEA simulations (red patches) (a) F25; and (b) O25.

Specimens	Experiment	New FLC	Maximum Strain failure criterion
F25	Pole	Pole	Pole
F70	Pole	Pole	Pole
F100	Pole	Pole	Pole
F200	Pole	Pole	Pole
O25	Flange region	Flange region	Flange region
O70	Flange region	Flange region	Flange region
O100	Pole, flange region	Flange region	Flange region

Table 5.1: Comparison of regions where failure initiates

Both the new FLC and the Maximum Strain failure criterion have been successfully implemented in FEA simulations through a user-defined material routine. FEA models check each mesh element for failure at every stage of the forming simulation. If failure is deemed to have occurred in an element, the stiffness of the element in all directions is reduced to zero. The simulation can recalculate the behaviour of the material under the assumption that failed regions of the sample can no longer withstand applied stress. Table 5.1 summarises the failure regions observed in experiments and predicted by FEA simulations. It is noticed that both criteria can accurately predict the failure regions exhibited in the specimens. It is also observed that in the O100 specimens, the failure can initiate either at the pole or the flange region, suggesting that variations in strain distributions can result in a change in where failure occurs. This agrees with the findings obtained by Davey *et al.* [86].

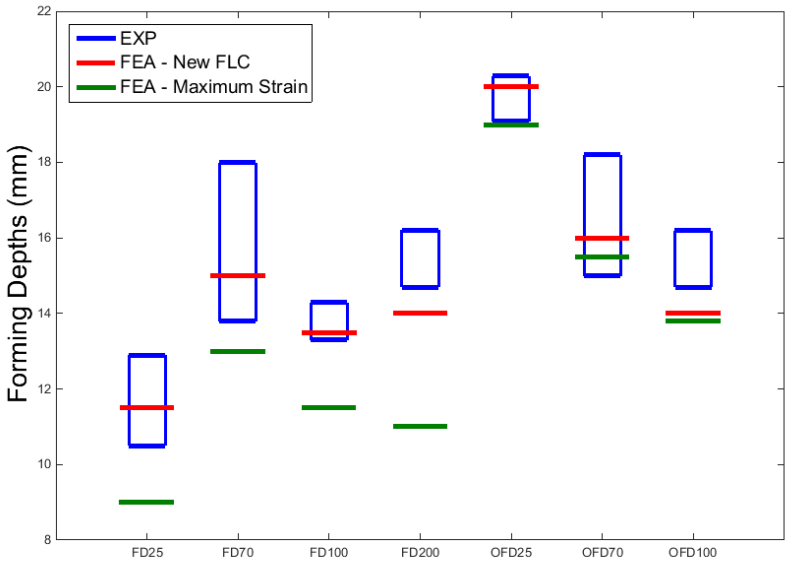

Figure 5.21: Comparison of the forming depths for NFC materials.

Figure 5.21 compares the experimental observations with FEA simulations of failure depths, defined as the vertical displacement of the pole at failure. Even though both criteria use fibre strain as the limiting factor for detecting failure, it seems that the new FLC can significantly improve the accuracy of the predicted failure depths compared to the Maximum Strain failure criteria. A large variation is noticed in the 0°/90° specimens where the Maximum Strain failure criteria consistently underestimates failure depths. The failure in 0°/90° specimens starts at the pole where the strain ratio is positive, and the Maximum Strain failure criterion suggests a constant failure strain (of 5%) which is obtained through tensile tests, and is considerably lower than the actual limiting fibre strain. Again, non-interactive failure criteria seem less accurate for pre-consolidated woven composites where interactions between the fibres and the matrix are considerable. This in turn highlights the need to consider forming modes when expressing the forming limits of this class of material system. It is notable that the new FLC is able to predict failure depths much more precisely than the Maximum Strain failure criterion, which

verifies the accuracy of the new failure criterion to predict failure in composites dominated by fibre fracture.

It is also observed that 45°/-45° specimens generally exhibit a larger failure depth compared to 0°/90° equivalent specimens, which agrees with the finding of Wang *et al.* [126] that large shear deformation can aid in superior formability of composite materials. Both failure criteria can predict failure depths precisely in 45°/-45° specimens, and the difference between the two criteria is insignificant. Failure initiates at the flange region of 45°/-45° specimens, and Figure 5.22 suggests that these regions experience a strain ratio near -0.3, therefore in uniaxial tension where two criteria predict similar limiting fibre strains. It is therefore expected that both criteria predict similar forming depths of the composite when the failure initiates in the forming mode of uniaxial tension.

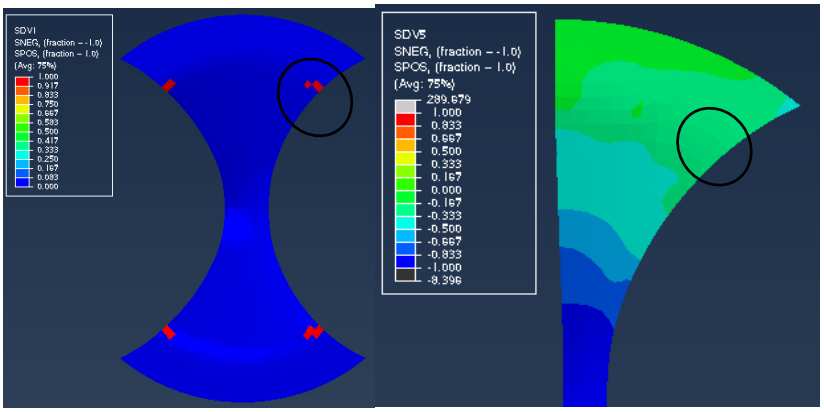

(a) O25

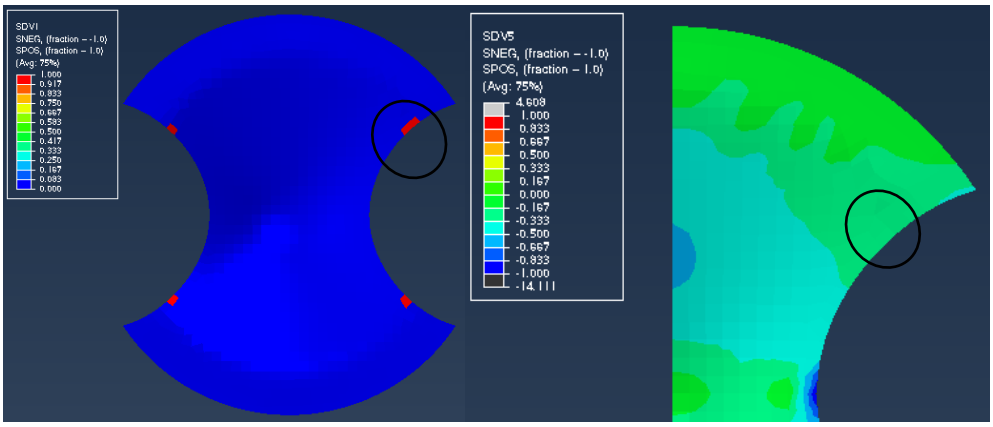

(b) O70

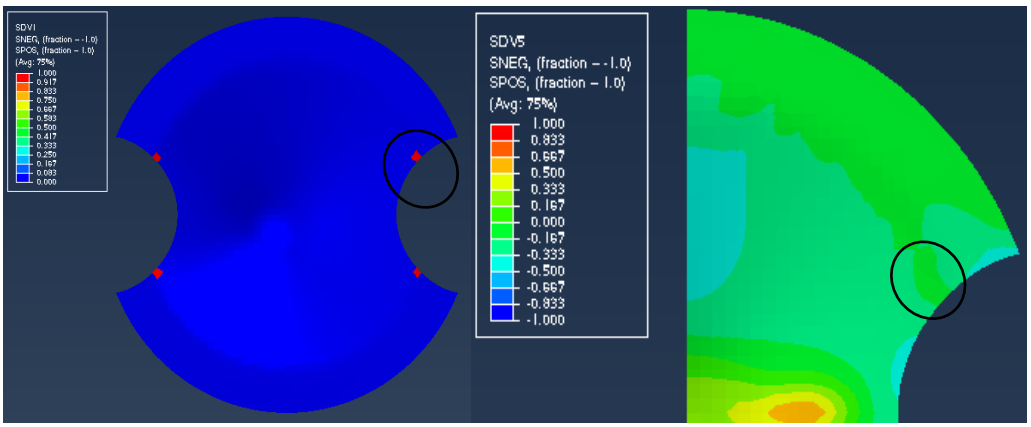

(C) O100

Figure 5.22: Strain ratio of the failure regions in 45°/-45° specimens. Left: regions of failure predicted by FEA simulations (coloured in red); right: Strain ratio distribution of the top-right quarter of the specimen.

5.3.4.3 Predicting failure in different conditions of water treatment

The new FLCs of the NFC in different conditions of the water treatment are implemented in FEA simulations through user-defined material subroutines. Similar to the observations in the formed untreated composites, failure initiates around the pole for 0°/90° samples and at the free edges for 45°/-45° samples (the only exception being the 45°/-45° specimen with a width of 100 mm, where the failure could initiate at either the pole or the flange region). The new FLC can precisely predict the regions of failure. It is statistically consistent that the failure regions propagate along the fibre directions, regardless of treatment.

In addition to the locations where the failure initiates, the new FLC has been verified in terms of failure depths. Up to three repeats are tested for experimental geometries, and the specimen data are used to construct the range of forming depths observed in experiments. These observations are then compared to the forming depth predicted by the new FLC criterion in FEA simulations, as shown in Figure 5.23. Larger failure depths are observed in water-treated composites compared to dry equivalent samples, which is expected given the larger forming envelope of the composite in the wet condition. The composite also exhibits very similar failure depths in the untreated and redried conditions, since the tensile properties have been largely returned back to the untreated levels when redrying. Observations confirm that the new FLC proposed in the current study predicts reasonably in stretch forming tests of the failure depths of the composite in different conditions of water treatment, confirming its usefulness for natural fibre composites.

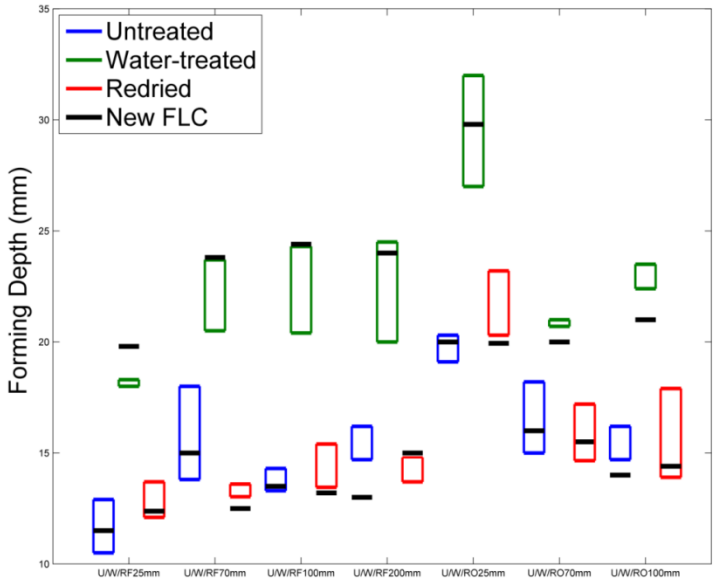

Figure 5.23: Comparison of forming depths observed in experiments, and as predicted by the FEA simulations.

5.3.5 CNFC materials

5.3.5.1 Evolution of strain path at the pole

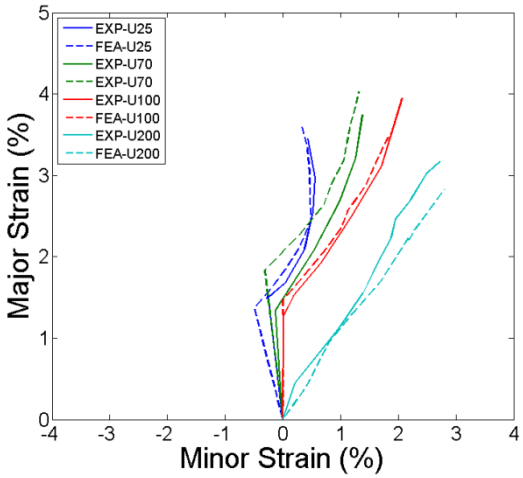

Figure 5.24: Strain evolution of the pole for untreated CNFCs.

Figures 5.24 shows a comparison between experimental observations and FEA simulations of strain evolutions at the pole for untreated specimens with various middle-section widths. It is clear that varying the sample geometry can change the deformation mode of the composite at failure: the composites exhibit a strain ratio of 0.13, 0.19, 0.52

and 0.83 from the thinnest to the widest sample, respectively. Note that strain evolutions from FEA simulations can correctly predict the progress of the major forming path for CNFCs, especially strain conditions at the transitions between different stages. It seems that the material properties assigned to the blank as well as the friction conditions defined between contacting pairs, appear to be accurate. In FEA simulations, the composite was modelled as a homogeneous material which exhibits the same mechanical properties at every single point of the surface. However, the composite does not behave ideally in a homogeneous way due to the variation of mechanical properties of flax fibres and the existence of voids. This can explain the slight discrepancy between experimental findings and FEA simulations.

5.3.5.2 Validating the FLC

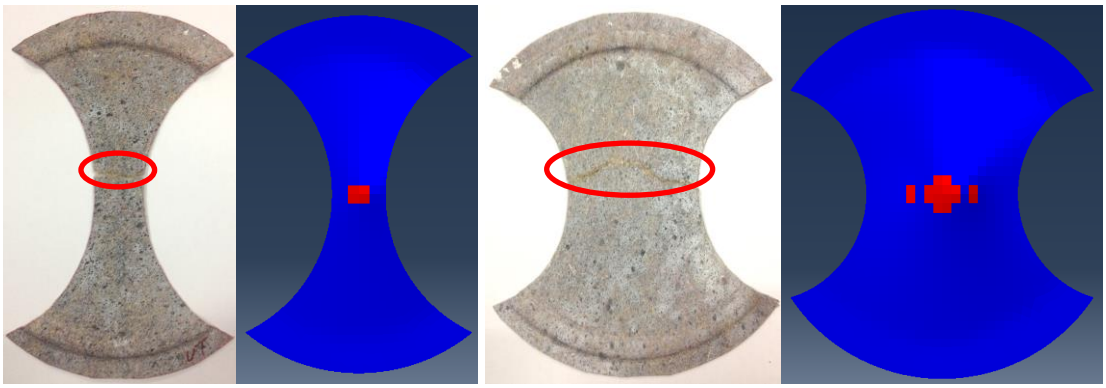

(a) U25 (b) U70

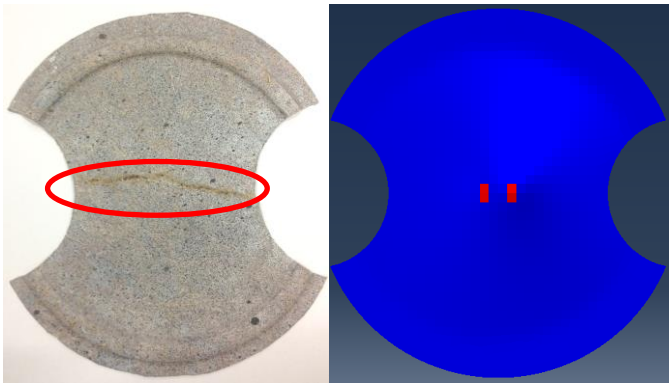

(c) U100

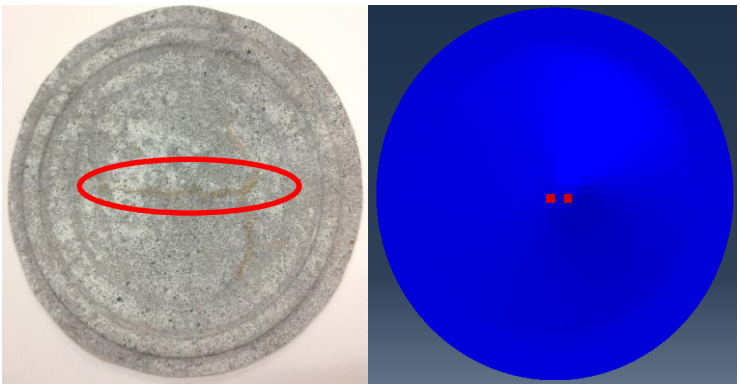

(d) U200

Figure 5.25: The failure regions observed in tested samples (left), and as predicted by FEA simulations (right).

In stretch forming of CNFC materials, all untreated specimens exhibit failure at the region near the pole which remains in contact with the punch during forming and

experiences most strain deformation. Figure 5.25 shows that the FLC constructed in the current study can precisely predict the regions where failure initiates. It is noteworthy that the failure regions observed in the tested samples are much larger than in those predicted by the FLC. In the stretch forming tests conducted in this study, the punch was set to move down at a constant rate of 20 mm/s and then to return to its original position when the load drops by 40% from its maximum. It seems that the CNFC materials can still maintain its strength at the onset of failure, allowing the punch to move a larger displacement and leading to larger failure regions. It should be pointed out that the contour plot of the FEA simulations is taken at the stage when failure first initiates. It does not mean that the composite would exhibit failure regions like the ones coloured in red, instead it suggests that failure is most likely to initiate in those 'flagged' regions. The expansion of the failure region is not within the scope of this study as the material is considered useless as soon as it fails.

In the wet condition, the elongation-to-failure of CNFCs is more than, and such an improvement can be reflected as a larger forming envelope. However, it seems that the improved formability cannot be translated to larger forming depths in stretch forming tests, as shown in Figure 5.26. Forming depth is defined as the punch displacement at the onset of failure. The water-treated composites can withstand larger forming depths compared to dry equivalent samples, with the improvement considerably less than that observed before (elongation-to-failure in uniaxial loading tests and FLC). One explanation is that at large forming depths the major strain at the pole evolves with a much steeper slope, and therefore the improvement in ductility cannot be entirely mirrored to failure depths in stretch forming tests. Observations show that the FLC can predict the failure depth of CNFC materials in stretch forming within a reasonable range, validating the effectiveness of the FLC constructed in this study.

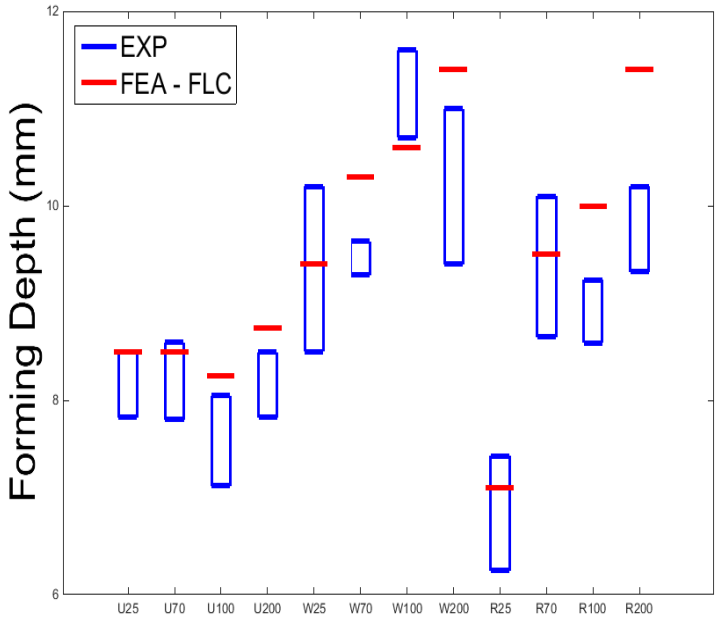

Figure 5.26: Comparison of the failure depths for CNFC materials.

5.4 Summary

This Chapter has studied the forming behaviour of composite materials in stretch forming tests, and determined the forming limits for both NFC and CNFC materials. Composites are cut into hourglass shapes with various middle sectional width as well as fibre orientation to examine different forming modes. The stretch forming process can be identified as three separate stages based on changes in the major deformation mode, including: firstly pre-stretch, secondly bi-axial stretch and finally the major forming path. It is found that the woven structure of the NFC can help exhibit an additional deformation mode of pure shear compared to the CNFC. More importantly, under this deformation mode the NFC specimen is able to withstand much larger strain deformation, which agrees with the findings obtained by Wang *et al.* [126] that shear deformation can aid in superior formability for woven composites. It is also observed that for specimens with large widths, sample width has a dominating effect over stretch directions due to the increased restriction exerted by the tools.

The major reason to conduct stretch forming tests is to determine the forming limits of composite materials. This section has shown that the conventional FLC, which has been widely applied to metal forming, is a valid tool to express the forming envelope of CNFC materials. This is because CNFCs behave predominantly like an isotropic material. Based on the principal strain deformation provided by the ARAMIS system at the surface points where failure initiates, FLCs are constructed for CNFC materials in different conditions of water treatment. However, due to the path dependency effect, this conventional method is found incapable of accurately describing the forming limits of NFC materials. As a result, unfailed surface points are found to exhibit higher principal strains compared to failed ones when both points experience an identical deformation mode. A consistent observation is that the major failure mechanism of NFC materials is fibre fracture. By analysing the evolution of major strain and its Cartesian components, it has found that the path dependency is caused by the effect of strain deformation acting on the polypropylene matrix, which contributes little to composite failure. An innovative failure criterion, named the new FLC, is proposed which uses fibre strain and strain ratio as key parameters, and this new failure criterion can successfully eliminate path dependency as it tracks the evolution of fibre movements. In addition, the new FLC is considered more precise than the Maximum Strain failure criterion, which assumes that there is no interaction between different components of the composite. This assumption is clearly oversimplified for woven composites.

FEA models are developed to simulate the forming process of both composites. From the way strain path evolves at the pole, it seems that the material properties and friction conditions for contact pairs appear to be accurate. One of contributions of the current work is that it creates material subroutines for examining the accuracy of failure criteria in FEA models. To facilitate this process, SDVs have been defined to determine if there

are any surface points experiencing strain deformation higher than the values suggested by the failure criteria. It is observed that the new FLC is much more accurate than the Maximum Strain failure criterion, especially for samples with a fibre orientation of 0°/90°. By comparing FEA simulations with experimental observations, it is shown that the FLC and the new FLC can predict failure regions and failure depths of both composites in different conditions of water treatment. This Chapter has shown that the new FLC is superior to other strain-based failure criteria (the Maximum Strain failure criterion as well the conventional FLC), and this criterion should be applicable to any other woven composite systems as long as the dominating failure mechanism is fibre fracture.

It is important to note that this failure criterion provides a new angle to view the failure theory of composite materials. This Chapter has proved that for composite materials, especially those with inextensible fibres, fibre strain should be focused on when studying the failure behaviour. By doing this, the path dependency issue observed in conventional FLC can be eliminated successfully. Although there are existing failure criteria, such as the Maximum Strain failure criterion, which consider the amount of strain acting on the fibres separately from the total strain deformation. It is confirmed that the limiting fibre strain is influenced by the deformation mode, and therefore should be expressed as a function of strain ratio. The new FLC defines a new method to examine/predict the failure of woven composites, which has the potential to be widely applied in failure study of composite materials.

Dome Forming Tests

6.1 Introduction

When circular samples were formed into a dome structure with the edges not being fixed completely, they will experience a combination of drawing and stretching. This Chapter compares the forming behaviour of composites when different treatments are applied, including preheating, water treatment and tailored blanks. By taking into account the thermal degradation of the composites, the optimal forming temperature windows are determined for this class of material system. Preheating has been widely used to improve the formability of material in rapid forming processes, and the water treatment performed in this study is found to almost double the forming depth of preheated equivalent samples. This important breakthrough in improving the formability of natural fibre composites can aid in rapid forming of this class of material system. Compared to the circular samples used in preheating and those which are given water treatment, tailored blanks suggest an innovative shape of composite in which four portions of material are cut out at the edges of 0°, 90°, 180° and 270° positions. The application of this experimental geometry encourages materials to be drawn into the die cavity during forming, and therefore helps achieve a larger forming depth. Based on strain deformation data provided by the ARAMIS™ system, the major mechanisms behind the improved formability of the treated composites have been determined. The FLC and the new FLC are constructed from stretch forming tests, and this Chapter validates the effectiveness of each of these two failure criteria in dome forming.

6.2 Experimental observations

It is concluded from Chapter 4 that the water treatment can improve the ductility of natural fibre composites more effectively than preheating. The scope of this section is therefore to determine if the improved ductility can be reflected on increased formability in complicated forming conditions such as dome forming where specimens experience a combination of stretching and drawing. In dome forming all samples are cut into a circular shape with a diameter of 180 mm, and formed into a hemispherical dome structure at a punch rate of 20 mm/s. The amount of blank-holder force, ranging from 0 to 14 kN, can be pre-set via the computer connecting to the stamping press machine. A BHF of 7 kN is applied to the samples formed at different temperatures and conditions of water treatment. For the tests performed at elevated temperatures, samples are preheated to 15 ˚C above the forming temperature (to compensate for the temperature drop during transferring samples from the heat press machine to the stamping machine). The required adjustment is verified through temperature observations during the experimental process. In additional to high temperatures, the composites are formed in three different conditions of the water treatment: the untreated, water-treated and redried. The untreated samples are cut and tested as received from the material supplier without additional chemical treatments; the water-treated samples are formed at the maximum saturation level of the water solution; and the redried samples are saturated and then subsequently redried completely before forming. All tailored composites were cut by the mechanical scissor, and then formed at room temperature without the water treatment.

6.2.1 NFC materials

This section investigates the forming behaviour of NFC materials in dome forming tests. NFC materials exhibit a significantly increased formability when specimens are

experiencing various treatments and blank geometry change. From examinations on the formed specimens, fibre fracture is identified as the major failure mode exhibited in this class of material system. This observation on the formed specimens could justify the new FLC proposed in Chapter 5 which uses fibre strain as one of the key parameters. It is also within the scope of the current work to determine if there are mechanisms in addition to the increased ductility (as discussed in Chapter 4) that could help NFC specimens withstand a larger forming depths. The investigation is conducted through comparing the surface strain distributions which provide information on the major deformation of composites.

6.2.1.1 Failure depths in dome forming tests

Failure depth is defined as the punch displacement at the onset of failure in forming, and is also a direct indicator on the formability of forming material. This section compares the effect of two treatments, preheating and the water treatment, as well as that of different blank geometries, full circle and tailored shape.

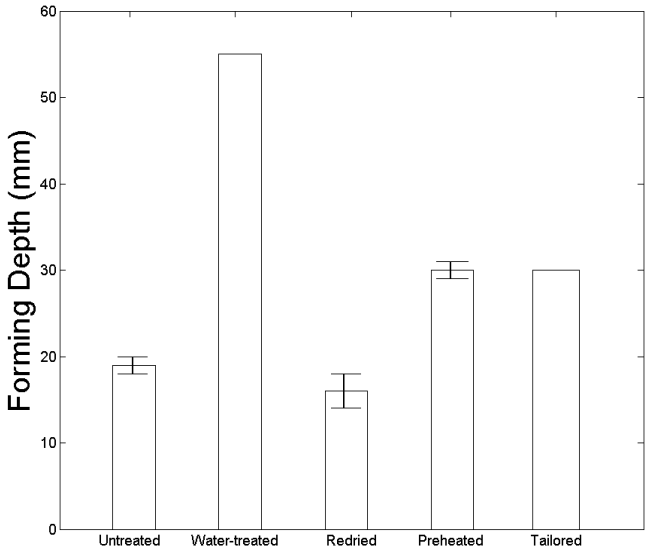

Figure 6.1: Comparison of forming depths.

Figure 6.1 compares the forming depths of the composite in three different conditions of water treatment - untreated, water-treated and redried - as well as that of the composite formed at the optimal forming temperature (T120) and that of the composite formed at the optimal tailored shape (R65). The untreated NFC fails at 18.9 mm, and the water-treated NFC does not fail and reaches a forming depth of 55 mm which is the maximum depth limited by the dimensions of the tools. It is noted that the samples in the dry conditions (untreated and redried) share very similar forming depths, which mirrors the observations on tensile tests. It is noted that preheating can improve the formability of composites to some extent (an average failure depth of 30 mm), but this traditional method is much less effective than water treatment. ***It is found that water-treated composites are able to exhibit an almost doubled forming depth compared to the preheated equivalent sample. This suggests that the water-treatment is superior to preheating when forming natural fibre composites.*** An almost doubled ductility is observed when composite materials are tested in the wet conditions, as stated in Chapter 4. It is worth noting that a significantly larger improvement in forming depth during dome forming (more than 175%) is observed. The mechanisms behind this observation are explained in details in a later section.

A more than 50% increase in failure depth is observed when some materials are cut off along fibre directions. The use of tailored blanks can help NFC materials withstand a greater forming depth by reducing the amount of stretching experienced along the fibre directions, such that optimal tailored shape could withstand a forming depth of 30 mm. ***It is concluded that the application of this novel geometry could lead to similar improvement in forming depth of woven natural fibre composites as compared to the preheating treatment.*** Similarly, the basis of this observation is explained in the following section where surface strain distributions are studied.

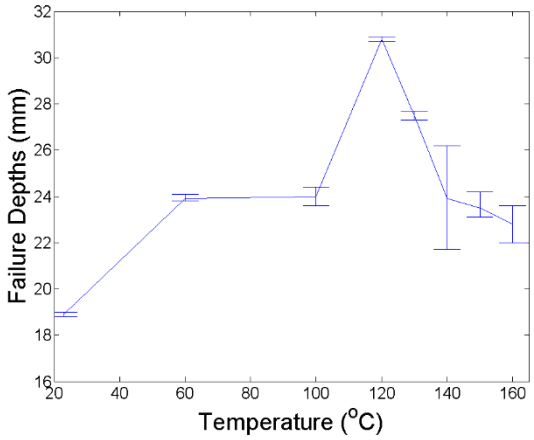

Figure 6.2: Failure depths of NFCs at different temperatures.

The conventional treatment, preheating, can improve the formability of NFC materials. The forming depths of NFC materials in different temperatures are studied, with a particular focus around temperatures where thermal degradation behaviour is observed. According to Figure 6.2, increasing the forming temperature from ambient to 120˚C increases the average failure depths by 55% (from 18.9 to 30.2 mm). Fibre fracture is the dominant failure mechanism for flax/pp composites (this is verified through microscopic examination on fractured surfaces, and detailed in the later section), and the flax fibres are able to withstand larger failure strain at high temperatures. In addition, due to its thermoplastic nature, polypropylene softens as temperature increases. Softening of the matrix helps the stress transfer between fibres which leads to even transformation of load through the specimen. These two effects explain the increase in failure depth from room temperature to 120˚C. After the preheat temperature of 130˚C there is a noticeable drop in failure depth, which is caused by the thermal degradation of the composite. The major mechanism behind the degradation of NFC materials is identified as the melting of the polypropylene matrix, as stated in Chapter 4. The identification of thermal degradation of composite is an important finding of this work

as it identifies the existence of an optimal forming temperature window for this class of material systems.

However, there is no obvious reduction in the elongation-to-failure of the composites in the tensile tests performed at elevated temperatures. There are two reasons for the significant reduction in the forming depths of NFC materials at high temperatures: firstly, stiffness is reduced along fibre directions when the composite is preheated to high temperatures, which leads to more stretching, and in turn, results in larger strains acting on the composite. Secondly, the composite experiences two major deformation mechanisms of drawing and stretching during dome forming tests. According to the findings obtained by Venkatesan [18] who compared the formability of two woven composites with the same matrix material but different fibres in dome forming tests, a woven composite system with a smaller difference between stiffness in the fibre and shear directions experiences larger surface strains, especially along the fibre directions. It is therefore very likely that the composite would behave closer to an isotropic material at high temperatures as the fibre stiffness reduces and becomes closer to that in shear directions. Based on the Python script described in Chapter 5, fibre strains can be determined from the ARAMIS system at every stage of the forming process. Figure 6.3 shows surface fibre strain deformation of 120˚C and 150˚C experimental cases. The comparison is obtained at a forming depth of 23 mm where the latter is just prior to failure, despite that the 120˚C experimental case could form to a larger depth. It is found that the 150 ˚C experimental case experiences much higher fibre strains over the surface, suggesting a possible combination of reduced stiffness and a forming behaviour closer to that of an isotropic material.

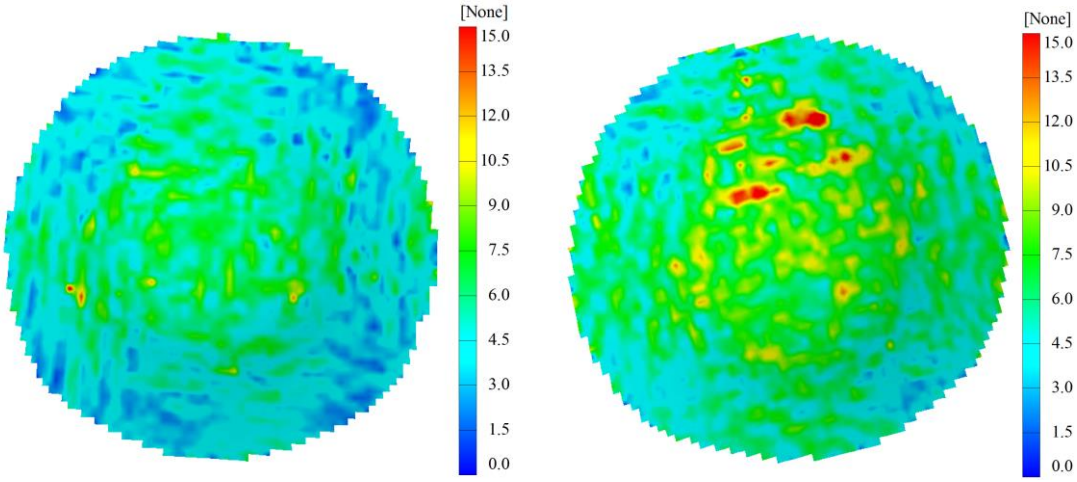

(a) (b)

Figure 6.3: Surface contour plot of fibre strains from (a) the 120˚C experimental case; (b) the 150˚C experimental case.

6.2.1.2 Examination on failure regions

In continuous fibre-reinforced composites, the common failure mechanisms include delamination, longitudinal matrix splitting, intra-laminar matrix cracking, fibre-matrix debonding, fibre pull out and fibre fracture [135]. Under microscopical examinations shown in Figure 6.4, fibre fracture is identified as the major failure mechanism of NFC materials, which rationalises the hypothesis that strain acting on the fibres should be considered when predicting the failure behaviour for this class of material system. It is observed that the most water-treated and tailored composites exhibit similar failure behaviour to that of the untreated and circular composite, which is a single failure region around the pole.

Figure 6.4: Microscopic examination of the fracture.

However, it seems that NFC materials exhibit different failure types at different temperatures, as shown in Figure 6.5: at temperatures less than 100˚C, a single failure region due to fibre fracture (Figure 6.5.a); between 100˚C to 150˚C, multiple failure regions due to fibre fracture (Figure 6.5.b); and around 160˚C, a combination of fibre pull out and fibre fracture (Figure 6.5.c).

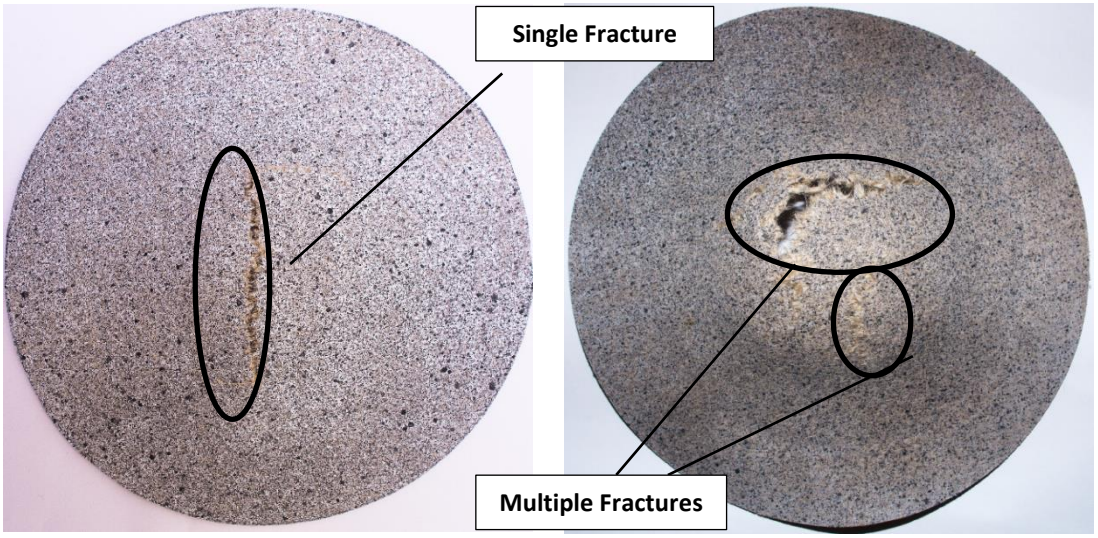

(a) (b)

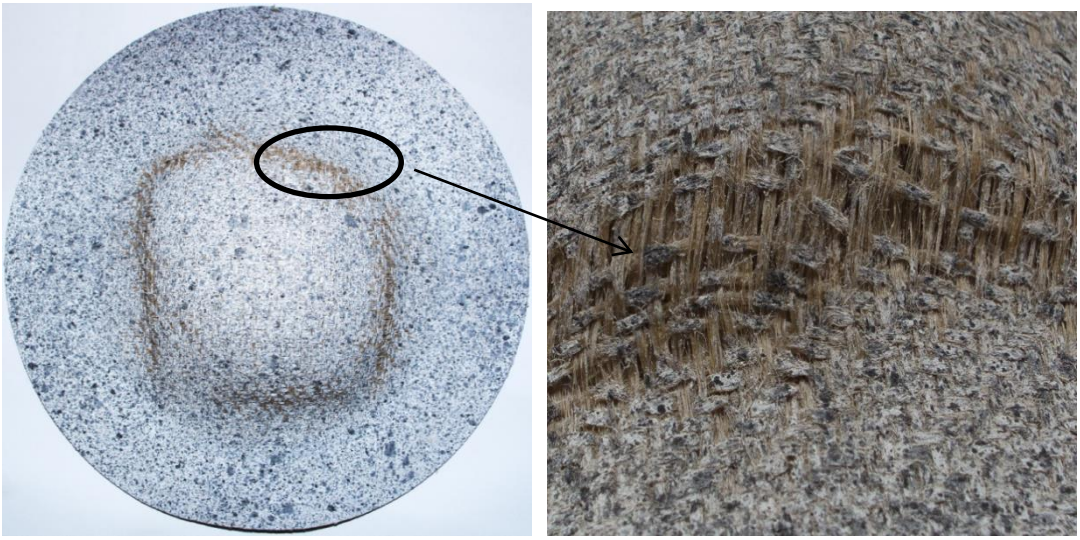

(c) (d)

Figure 6.5: Tested samples formed (a) below 100˚C; (b) between 100˚C and 150˚C; (c) at 160˚C; (d) close-up view of fibre pull out with some fibre breakage in the sample formed at 160˚C.

At low temperatures, there is not much stress transfer between fibres, resulting in fibre breakage around the punch contact region where large strains are experienced. In the experiments, the punch is set to continue to move down an additional displacement beyond the onset of composite failure. Specimens therefore experience additional deformation after the initiation of the fibre fracture, resulting in a line fracture, as

depicted in Figure 6.5a. Similar observations can also be obtained from redried, and most of tailored specimens. Polypropylene softens considerably around 100˚C. This in turn facilitates stress transfer between natural fibres and results in more uniform state of stress in specimens formed between 100 ˚C to 150 ˚C compared to specimens formed at temperatures below 100 ˚C. Forming at temperatures between 100 ˚C to 150 ˚C leads to the initiation of fibre fracture at multiple regions within a short amount of time, as well as a complicated post failure path and post failure shape. The failure mode switches from fibre facture to a combination of fibre fracture and fibre pull-out at 160 ˚C. When the forming temperature approaches the melting temperature of the polypropylene (160 ˚C), composite exhibits a greater molecular mobility and a reduction in molecular orientation. Hence the composite experiences a decrease in mechanical properties and a loss in anisotropy [61]. The degradation of the matrix around 160 ˚C leads to pull out of fibres from the matrix as the dominant failure mechanism with some fibre breakage.

In addition to fibre fractures, out-of-plane buckling can also be observed in samples formed at 120 ˚C, as shown in Figure 6.6. It is visually observed that samples formed at 120 ˚C generally experience the most severe buckling. It is worth noting that this buckling effect does not expand to the formed dome structure and the buckled regions can be eliminated by the trimming process during manufacturing. Therefore, a buckling effect at the flange region is not considered significant in the forming of NFC materials.

Figure 6.6: Buckling of a flax/pp composite tested at 120˚C.

Among all samples, the water-treated composite and R65 experimental case remain intact at the dome area during the test. However, wrinkles are observed at the flange regions of these two specimens. Unlike the composites formed at 120°C where the wrinkles occur at the flange, some of the wrinkles in the water-treated specimens extend to the dome structure, affecting the overall quality of the formed part. It needs to be noted that the wrinkling issue associated with the water-treated composite can be solved without compromising its superior formability of the composite, as described later. Since wrinkling at the flange region can be trimmed in the manufacturing process, as suggested for the T120 sample, the focus should be paid to the wrinkling on the dome structure. During forming, the die obstructs the flange of specimens from the view of ARAMIS™ cameras, thus it is difficult to predict the onset of wrinkling at the flange. The diameter of the formed specimen is found approximately 12% shorter along the fibre directions than at 45° to them, suggesting that the composite is drawn into the die cavity to a greater extent along the fibre directions. This can be attributed to a larger stiffness in the fibre directions compared to the off-fibre directions. In the fibre directions, the punch pulls fibres away from the tools at the flange, and causes the material to be drawn into the die cavity. For the materials oriented at 45°/-45°, the trellising behaviour allows the composite to withstand a greater amount of deformation,

and lowers its resistance to stretching. The difference in resistance to stretching explains the round-square shape of the formed specimen, as shown in Figure 6.7. When the composite is completely drawn into the die cavity along the 0°/90° directions, while is still being squeezed at the four corners, the material at the flange region tends to be drawn towards the centre of the specimen (in the die cavity) as well as to the sidewalls of the specimen (in the hook region of the die). The later mechanism induces lateral compressive stresses in the middle of each round-square edge, and this produces in the side-wall wrinkles.

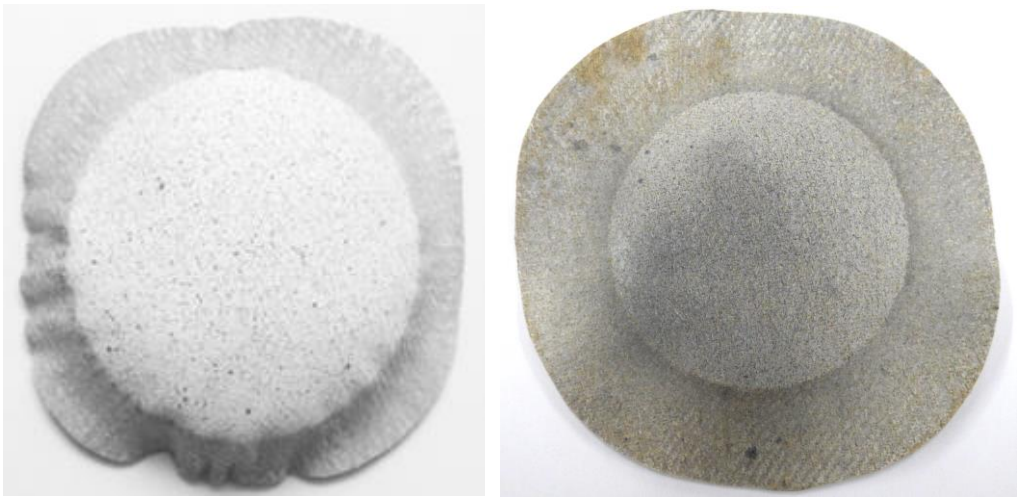

(a) (b)

Figure 6.7: Water-treated natural fibre composites after forming to a depth of 55 mm. (a) diameter of 180 mm; (b) diameter of 200 mm.

In sheet forming, both the initiation and growth of wrinkling depend on many factors including mechanical properties of the sheet, contact conditions, geometry of the workpiece, and etc. [136]. Therefore it is difficult to analyse the wrinkling behaviour, especially its onset simply from the dome forming tests alone. However, a method for minimizing wrinkling observed in formed specimens is investigated. A larger water-treated specimen with a diameter of 200 mm is formed to the same depth of around 55 mm, as shown in Figure 6.7, and it is observed that wrinkling is reduced considerably at

the flange region. More importantly, the dome structure remains free of wrinkles. It is therefore likely that the wrinkling behaviour observed in the water-treated composite (with a diameter of 180 mm) is mainly caused by not enough material at the flange region, which can be removed by using a specimen of the same shape but with a larger diameter (200 mm).

The R65 sample can withstand the maximum failure depth limited by the dimensions of the tools (around 55 mm). However, similar to the water-treated composite, this tailored geometry starts to accumulate materials at sidewalls when the material at the flange region is completely drawn into the die cavity. According to the images taken by the ARAMIS system, wrinkling starts to propagate to the dome structure slightly beyond a forming depth of 30 mm, as shown in Figure 6.8. The composite is therefore considered to have failed at this forming depth.

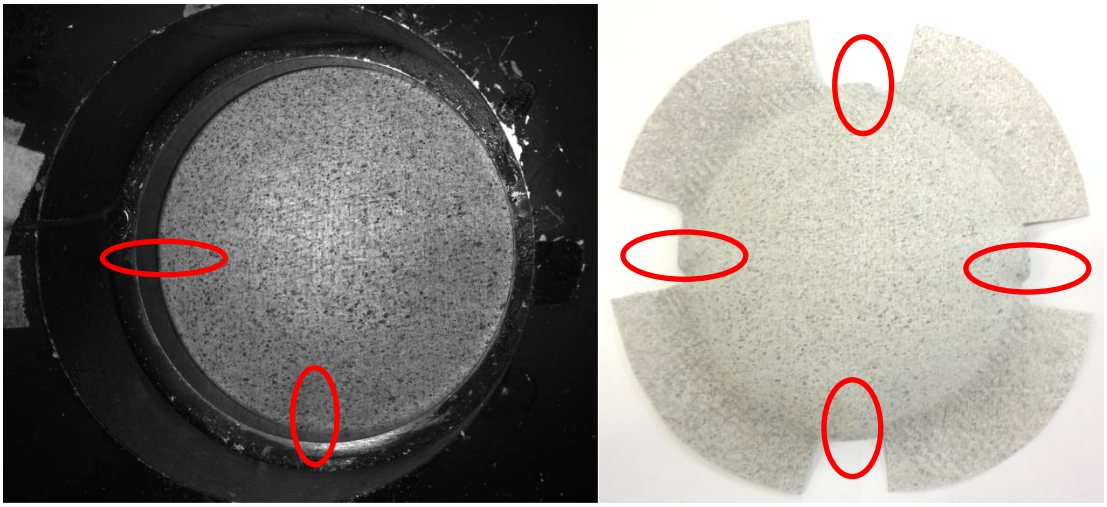

(a) (b)

Figure 6.8: The R65 specimen (a) from the right camera of the ARAMIS system; (b) the tested sample.

It is important to note that fibre fracture is the dominating failure mechanism for this class of material system. Although wrinkling is observed in several samples, the

wrinkling effect is not considered as the major failure mode. Because it can either be removed from trimming process (the T120 sample), or eliminated by using a larger sample geometry (the water-treated sample). For tailored shapes, the failure mode would switch from fibre fracture to wrinkling when the inner radius is reduced to 65 mm, as a result of less amount of material to be stretched at the flange region.

6.2.1.3 Effect of treatments on forming modes

Increased formability of a treated NFC is expected because of the increase in ductility. This section investigates whether there any other mechanisms exist besides the increase in elongation-to-failure. The forming modes experienced by a composite can be illustrated by its FLD. The use of the ARAMIS™ system facilitates surface strain measurements which can provide insights into the forming behaviour of composites at each time step of the forming process. Strain distributions over the entire surface can be compared using FLD. All strain distributions can be enveloped by strain ratios of -1, and 1, which is anticipated in typical dome forming experiments.

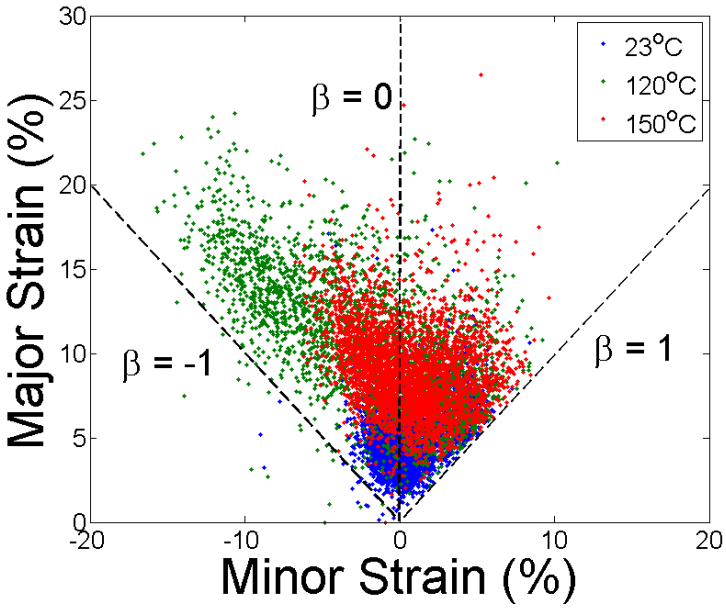

(a)

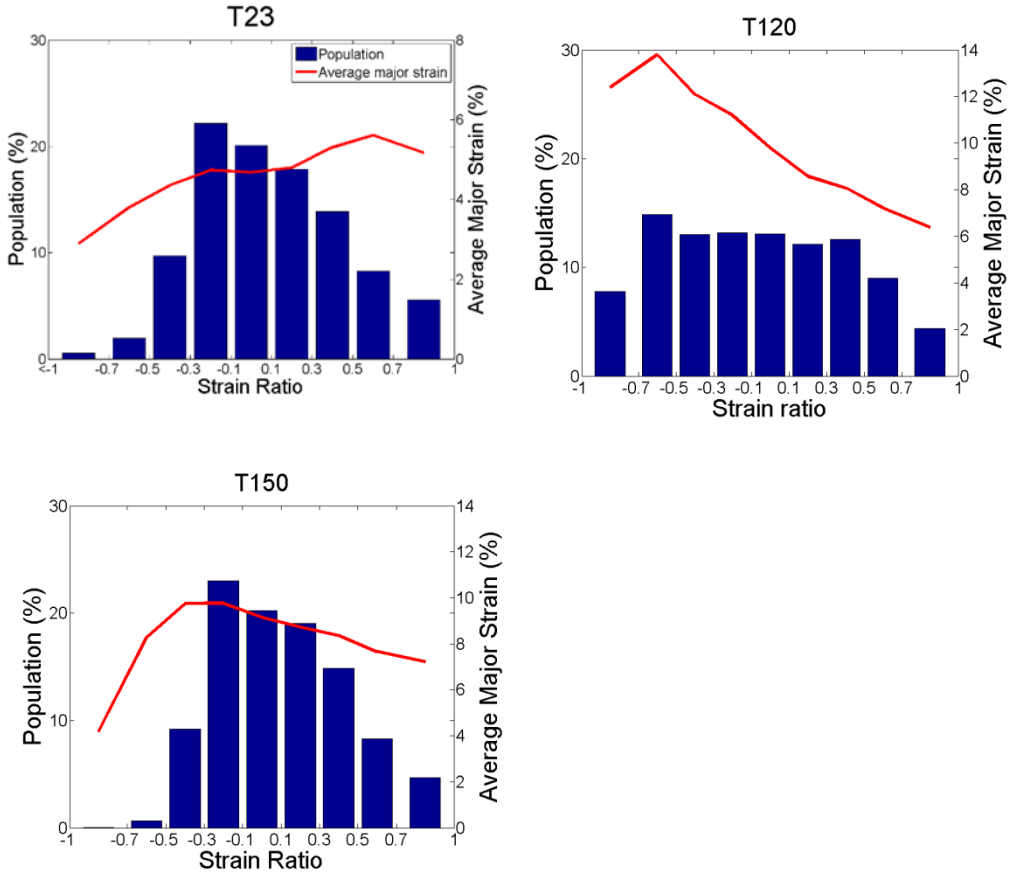

(b)

Figure 6.9: Comparison of surface strain distribution at the stage of failure at different forming temperatures. (a) FLD; (b) Quantitative illustrations.

Figure 6.9 shows the surface strain distributions of samples tested at 23˚C, 120˚C and 150˚C, respectively at the stage just prior to failure. It shows that forming at room temperature results in the least amount of formability in terms of forming depth. Around 120˚C is shown to be the optimal temperature window for forming flax/pp composites. When the forming temperature is increased to 150 ˚C, a significant reduction in shear deformation is observed as a result of the thermal degradation of the composite.

At ambient temperature, surface strain is mainly distributed as biaxial stretch and plain strain. When the polypropylene matrix is not soft, the composite exhibits an insignificant amount of shear deformation. Flax/pp composites have a much higher failure strain in the shear direction than in the fibre direction. Less than 5% of the surface points have a strain ratio less than -0.5, and the strain deformation in the shear direction is also much lower than in other deformation modes. The insignificant shear deformation at low temperature forming can be attributed to the low forming depths. By increasing the forming temperature to 120˚C, there is a significant increase (from less than 5% to approximately 25%) in the number of surface points experiencing the deformation mode of pure shear. In addition, at high temperatures strain deformation in the shear direction is also higher than that in other deformation modes. These observations suggest there is a change in major deformation modes when forming occurs at high temperatures. The effect of temperature is much more substantial in regions not in contact with the punch (regions experiencing forming modes of plane strain and pure shear) than in punch contact regions (regions experiencing biaxial stretch). This phenomenon suggests that at elevated temperatures, greater forming depths are permitted due to additional deformation in unsupported regions.

Compared to T120, there is a significant reduction in shear deformation for the samples formed at 150˚C. This in turn leads to a significant drop in forming depth. The drop in shear deformation can be attributed to the degradation of the composite, leading to the conclusion that by allowing the shear deformation to be the dominant forming mode, the optimal formability can be achieved for this class of composite materials. Even though both the T23 and T150 samples share a very similar population distribution, the latter sample experiences much higher strain values in almost every deformation mode. Again, the reasons are the significantly reduced stiffness and the behaviour closer to isotropic material system.

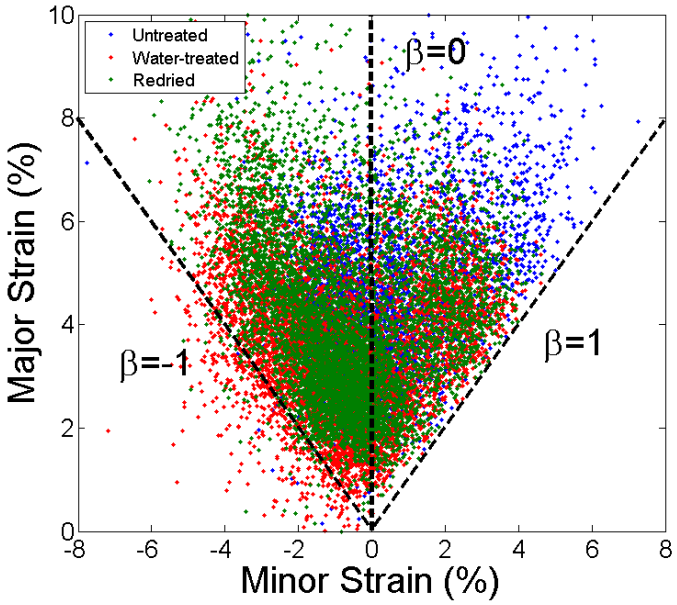

(a)

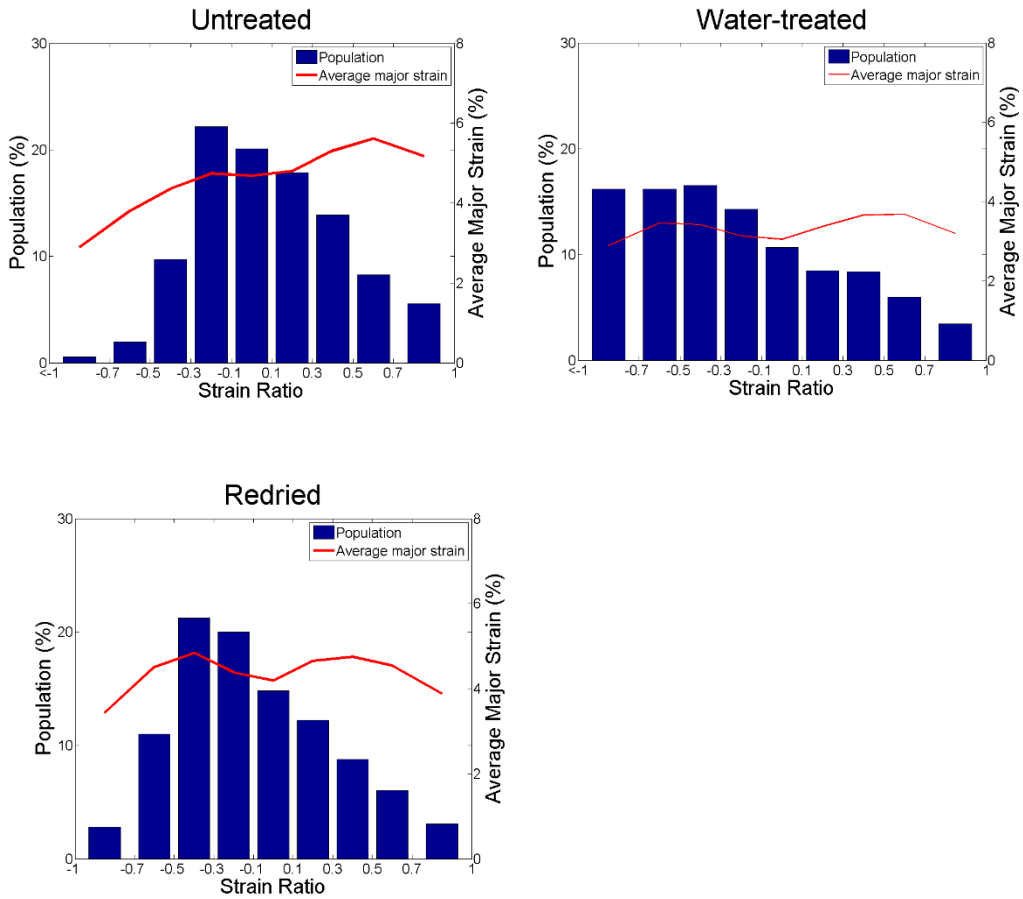

(b)

Figure 6.10: Comparisons of surface strain distribution in different conditions of water treatment. (a) FLD; (b) Quantitative illustrations.

A particular focus is paid on the water treatment, as this treatment is very effective for NFC materials. Although the water-treated specimen could be formed to a greater depth after water treatment, samples are compared at a forming depth of around 19 mm when the untreated and redried samples are just prior to failure. In Figure 6.10, surface points are grouped based on their strain ratio, and expressed in the bar chart. The average major strain is also plotted as a function of strain ratio to determine the change in strain deformation on forming modes. For the untreated and redried composites, approximately 60% of surface points experience a strain ratio in between -0.3 and 0.3, suggesting a major forming mode of plane strain. It is also observed that less than 3% of the dome area experiences pure shear, exhibiting a strain ratio of less than -0.5. ***On the contrary to untreated specimens, observations show that water treatment has altered the major deformation mode exhibited in the composite, such that the water-treated composite exhibits the major forming modes of uniaxial tension and pure shear.*** After the water treatment, there is an apparent increase in the population of surface points (from 3% to 30%) experiencing a forming mode of pure shear. Such a large surface population exhibiting a deformation mode of pure shear is not observed in untreated and redried equivalent samples. Previous studies have shown that large forming depths can be achieved if the material is permitted to undergo large amounts of shear deformation [36]. This can account for the significant increase in the forming depth of the water-treated composite. It seems that the weakened fibre/matrix interface and softened flax fibres of the water-treated specimen help flax fibres in the weft and warp directions move over each other within the ply under shear deformation. Although a reduction in fibre stiffness is also observed in wet condition, it is clear that the composite exhibits a larger difference in stiffness between the fibre and shear orientations after saturation. A similar observation on the major deformation mode of pure shear at small forming

depths was found in a pre-consolidated woven carbon fibre reinforced PEEK composite where the fibres were 15 times stiffer than the polymer matrix [86].

The water-treated composites are formed into a hemispherical dome structure immediately after reaching the maximum moisture ingression level. The surface moisture and the wet paint behave like a layer of lubricant lowering the friction between the specimen and the tools. Less restriction from the tools on material flow helps the composite to be drawn into the die cavity. This would account for the considerable reduction in average major strain deformation over the specimen surface, especially at the pole of the specimen (the reduction in strain deformation is around 40%). A more even distribution of strain deformation is observed in the water-treated sample, which indicates a uniform thickness in the manufactured part. This is important for manufacturing parts of high quality. It is therefore possible for parts to have a more evenly distributed thickness (at a forming depth of 20 mm) when it is saturated prior to forming. It seems that the water treatment can not only improve the formability of NFC materials, but also the quality of the formed parts.

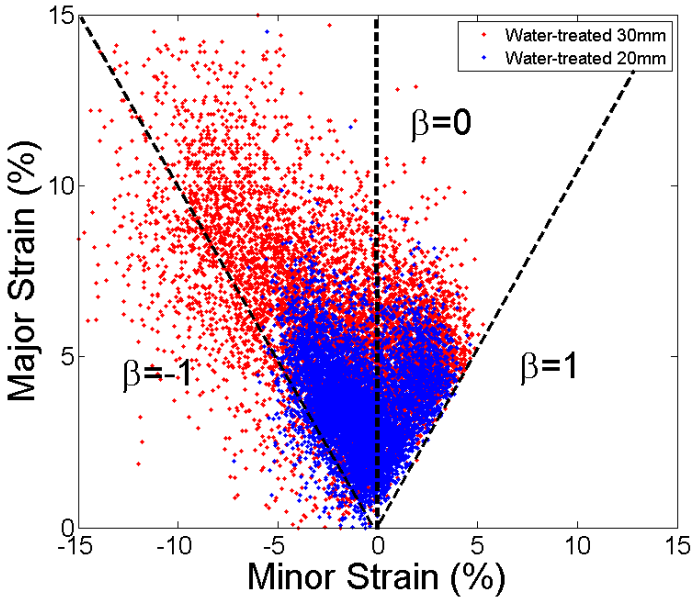

(a)

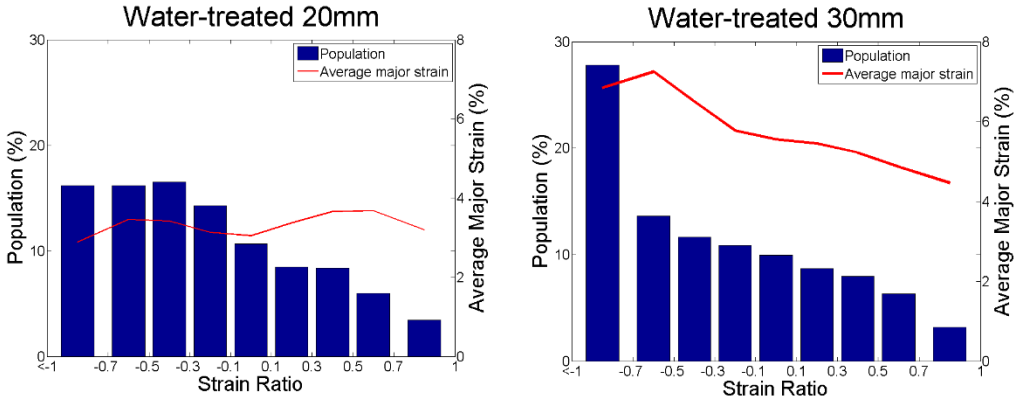

(b)

Figure 6.11: Surface strain evolutions of water-treated specimen at a forming depth of 20 mm, and 30 mm. (a) FLD; (b) Quantitative illustrations.

The following section compares surface strain distributions of the water-treated composites at different forming depths, which provides insights to the change in material behaviour when forming depth increases. Figure 6.11 clearly suggests a change in major forming mode at different forming depths: from a combination of uniaxial tension and pure shear to pure shear. When the forming depth reaches 30 mm, the surface population, which experiences a strain ratio of less than -0.7, increases

remarkably from 16% to 28%. This also explains why the improvement in forming depth is larger than that observed in the elongation-to-failure obtained from tensile tests. The flax fibres are stretched at a constant rate during the entire tensile test. While in dome forming tests the major deformation mode of the composite switches to pure shear at large forming depths, such that the flax fibres are less strained due to the trellising behaviour. An overall increase in strain deformation is anticipated as the specimen is formed to a greater depth. It is noticed that most incremental strain appears in unsupported regions, especially along the shear direction. This means that the increase in average major strain is about 50% at the pole, much less than that at unsupported areas (77% and 123% increase in regions experiencing plane strain and pure shear, respectively). Therefore, the increased failure depth observed in the water-treated composite is a result of higher extensibility of flax fibres as well as the introduction of pure shear. The preheated sample could exhibit a larger forming depth due to similar mechanisms. Compared to preheating, the ductility increases more pronounced and the shear behaviour is more profound in water treatment, resulting in a superior formability observed in this work.

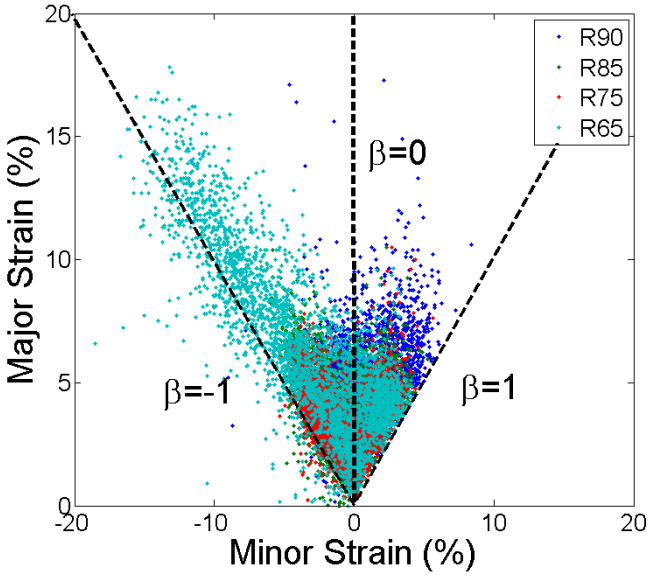

(a)

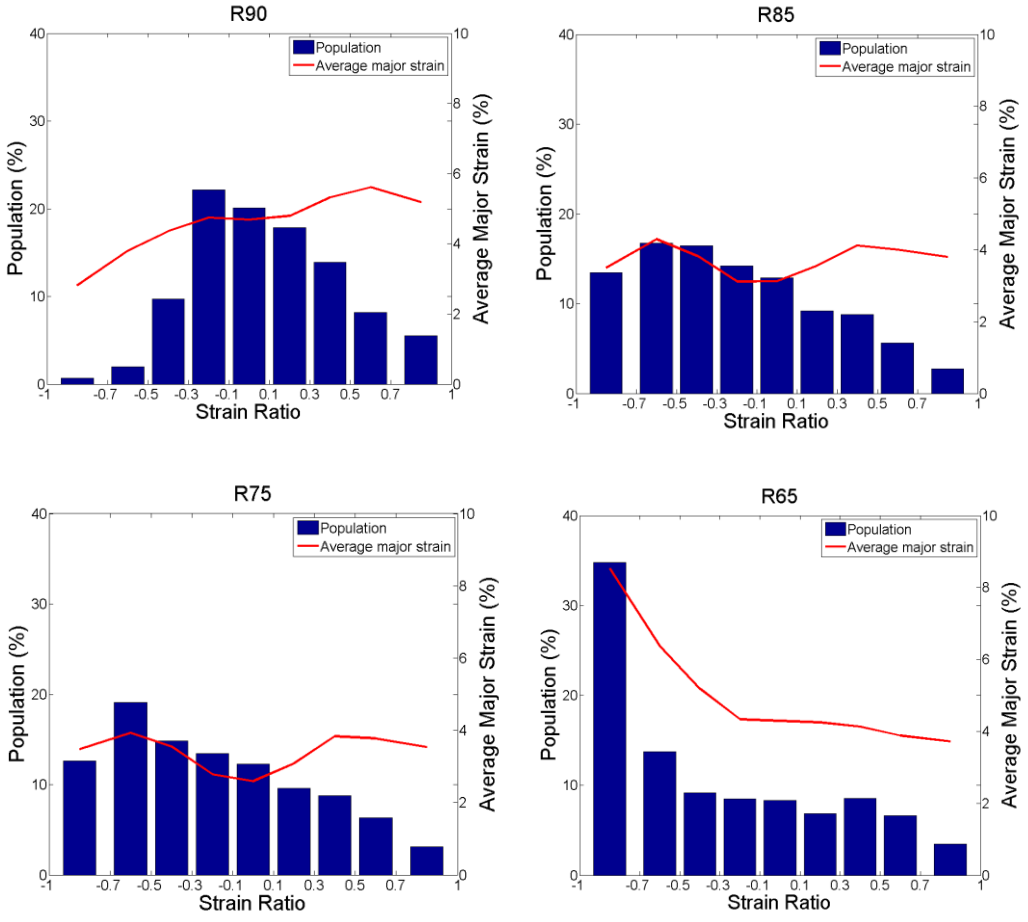

(b)

Figure 6.12: Comparison of surface strain deformation (a) FLD; (b) Quantitative illustrations.

The use of tailored blanks explores the effect of changing blank shapes on untreated specimens. The R90, R85, and R75 specimens exhibit failure at regions around the pole, whereas the R65 sample exhibits wrinkling at the flange regions. From the comparison illustrated in Figure 6.12, in the smaller samples there is a clear increase in the surface population that experiences a deformation mode of pure shear. The number of surface points is increased by more than 35 times (from less than 1% in the R90 sample to more than 35% in the R65 specimen). This is expected because the flax fibres are encouraged to be drawn into the die cavity, which lowers fibre strains and increases shear deformation. Under shear deformation, the flax fibres of the woven composite tend to rotate over each other within the ply in such a way that they are no longer perpendicular to each other. The formability of tailored blanks is improved by allowing matrix shear deformation, which contributes little to composite failure. Similar observations are also observed from preheated and water-treated composites, while unlike treated specimens which exhibit an increased ductility, the elongation-to-failure remains unchanged when a tailored shape is used. Therefore, the major mechanism behind the significantly improved formability of tailored blanks is to shift the strain deformation acting on the flax fibres to the polypropylene matrix.

This section determines the mechanisms behind the improved formability of NFC materials under various treatments and blank shape change. It is concluded that the water treatment is more effective than preheating the samples, and the tailored shape is better than a circular blank. It is arguably that for creating production parts that need to undergo large deformation, a combination of water treatment and tailored blanks could be the optimal way to form this class of material system, as long as there are enough materials at the flange region to avoid wrinkling.

6.2.2 CNFC materials

The previous section has shown the influence of the treatments and tailored blanks on forming behaviour of NFC materials, and this section studies whether such observations can be obtained in CNFC materials.

6.2.2.1 Failure depth in dome forming tests

It is concluded that the significantly improved elongation-to-failure makes it is very advantageous to process CNFC materials in the wet condition. It is therefore important to determine if such an increase in formability can also be achieved in dome forming tests. For CNFC materials, strain concentration is observed prior to catastrophic failure, and the material is considered to fail at the onset of strain concentration. Details of this are described later.

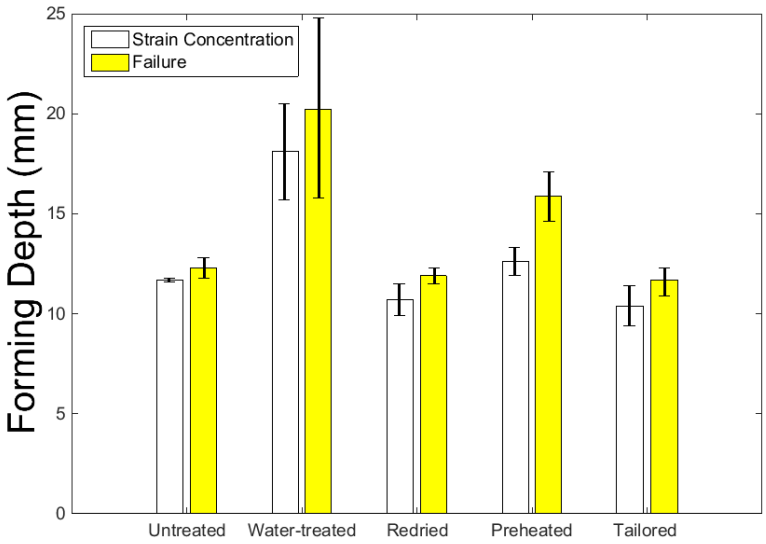

Figure 6.13: Comparison of the forming depths of CNFC materials, at the onset of strain concentration (white bars) and at catastrophic failure (yellow bars).

Figure 6.13 compares the forming depths of the composite in three different conditions of water treatment (untreated, water-treated and redried), as well as that of the

composite formed at the optimal forming temperature (T130) and that of the composite formed at the optimal tailored shape (R75). From tensile tests, it is anticipated samples in the dry conditions (untreated and redried) will exhibit almost identical forming depths in dome forming tests. Water treatment is much more effective than the traditional method in terms of improving formability, as the water-treated composite exhibits a much larger forming depth compared to the preheated equivalent sample. The effect of the traditional treatment, preheating, is very limited for CNFC materials for two reasons. Firstly, even though the composite can be stretched to a greater extent at high temperatures, this improvement is affected in dome forming tests by the reduced stiffness. Secondly, the material starts to degrade when the forming temperature approaches the melting temperature of the polypropylene matrix. The failure depth of the preheated composite (formed at the optimal temperature window of around 130 °C) is compared with the failure depths of the water-treated samples.

After water treatment, dome forming tests show that there is a better correlation between the increase in forming depths during dome forming tests and from the elongation-to-failure obtained in tensile tests, and such increase cannot be achieved using preheated samples. A reduction in stiffness is noticed for both preheated and water-treated composites. The water-treated composites are painted and then formed immediately after reaching the maximum saturation level of the water solution, and the surface moisture at the flange region lowers friction between the specimen and the tools (the blank-holder and the die). Due to this effect, the amount of additional strain caused by reduced stiffness is lowered, resulting in a closer correlation between the increase in failure depths in dome forming tests and the improvement in the elongation-to-failure. It needs to be noted that the amount of improvement in elongation-to-failure still cannot be entirely mirrored in failure depths. Unlike NFC materials, the application of tailored

blanks cannot improve the formability of CNFC materials, such that all tailored blanks experience a forming depth close to that of the circular sample. The mechanisms of this observation are explained in details in a later section when surface strains are studied.

During dome forming of CNFC materials, strain concentration is identified prior to final failure. This can be identified by surface strains as most additional strain deformation is confined in these areas, resulting in significantly higher strain deformation. Figure 6.14 shows the effect of the forming temperature on the failure depths of the CNFC materials, first at the onset of strain concentration, and secondly at catastrophic failure, respectively.

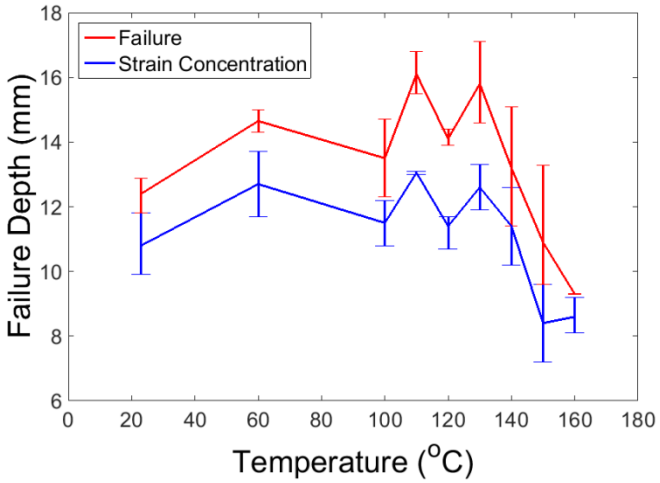

Figure 6.14: Failure depths of CNFCs at different temperatures: at the onset of strain concentration (blue) and catastrophic failure (red).

It can be seen that the composite is able to be formed an additional amount of forming depths beyond the onset of strain concentration. It is noted that the additional depth in forming varies inconstantly with temperature. This could be attributed to the fact that the strain concentration area can either be fibre-rich or matrix-rich, and the composite will be able to withstand additional strain deformation if the strain concentration region

happens to be matrix-rich. On the contrary, at fibre-rich regions the composite would be very likely to exhibit failure almost immediately after the onset of strain concentration. For instance, one of the composites formed at room temperature exhibits failure immediately at the onset of strain concentration.

In this study, to better compare the composite that formed in different conditions, CNFC materials are considered to fail at the onset of strain concentration. Based on Figure 6.15, the tested composite exhibits an insignificant increase in failure depth of, only 16.7%, from an average of 10.8 mm at ambient temperature to 12.6 mm at 130°C. However, a reduction in failure depth is evident when the forming temperature is above 150°C (because an additional 15°C is applied during preheating). This reduction can be attributed to the thermal degradation of the composite, a phenomenon that has been identified in Chapter 4 as due to the melting of the polypropylene matrix. Composites which are formed at temperatures above the thermal degradation temperature exhibit smaller failure depths than those formed at room temperature, suggesting that forming CNFC materials should not be formed at the temperatures beyond the melting point of polypropylene.

It is important to notice that such a reduction is not observed in the elongation-to-failure from the tensile tests performed at high temperatures. To further examine this phenomenon, surface strain contour plots of the composites formed at 23°C, 130°C, and 150°C are selected and compared at the same forming depth. Three temperatures are chosen because there is no temperature effect at the ambient temperature (23°C); the composite exhibits the optimal forming depth at a forming temperature of 130°C and composite starts to degrade at 150°C.

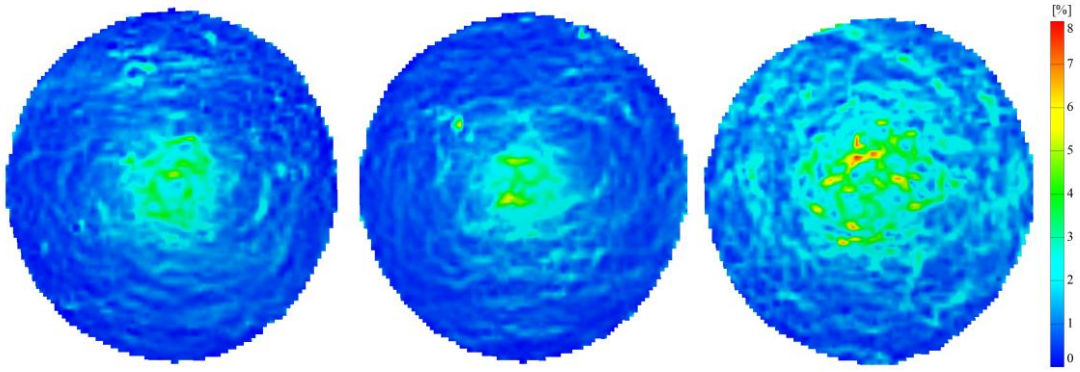

(a) (b) (c)

Figure 6.15: Surface contour plots of composites formed at 23 °C (a); 130 °C (b); and 150 °C (c).

It is clear that, at the same forming depth prior to failure, the composite experiences much higher surface strain when it is formed at 150 °C. In dome forming tests when the amount of blank-holder force remains unchanged the stiffness of the composite is crucial to the amount of stretching and drawing experienced by specimens. A significant reduction in stiffness occurs at elevated temperatures, meaning that composite materials then experiences more stretching, and hence larger strain deformation. Therefore, even though CNFC materials can be stretched to a slightly larger extent at high temperatures, this effect is considerably affected by the additional strain deformation caused by the reduced stiffness. This also explains why the effect of forming temperature on the failure depth of the composite is very limited (only a 7.5% increase), compared to the increase in elongation-to-failure observed in high temperature tensile tests (around 27.3%).

6.2.2.2 Examination on the failure regions

The following section presents the visual examinations on failed CNFC dome structures. It is noted that this class of material system exhibits very similar fracture behaviour of

fibre fractures unless forming above the thermal degradation temperature, leading to fibre pull-offs in addition to fibre fractures.

(a)

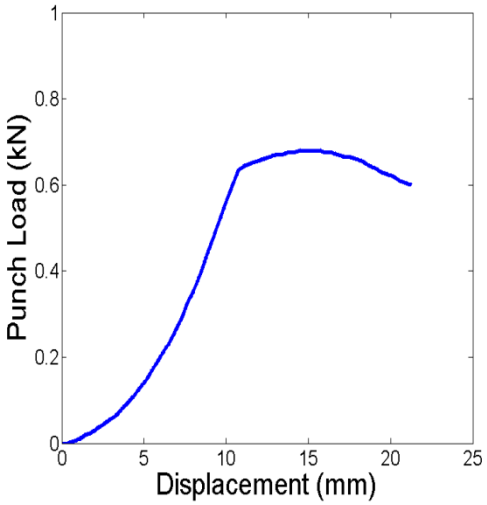

(b)

(c)

Figure 6.16: The CNFC sample. (a) Typical failure regions; (b) Typical punch load versus displacement curve; (c) Sample formed at a temperature of 160°C.

Figure 6.16a shows a typical failure region exhibited in a tested CNFC sample, with a black rectangle emphasizing the area exhibiting fibre pull-off and reorientation. A large number of fractured fibres can be observed in the failure region of the composite. Flax

fibres are short and randomly oriented, and the failure region tends to propagate across rather than along the fibres due to the lower elongation-to-failure of the fibres compared to the polypropylene matrix. As a consequence, irregularly shaped fractured regions are observed in the tested composites. Based on the images taken by the ARAMIS™ system, most failure regions are initiated around the centre of the specimen which is deformed to the largest extent and hence experiences a higher state of strain deformation. During experiments, the punch is set to move down an additional amount of displacement to examine the post-failure behaviour of the composite. Figure 6.16b shows a typical punch load versus displacement curve obtained by the data acquisition system. The area under the curve represents the amount of energy absorbed by a specimen from the tools during forming, and the sudden levelling off in slope at a forming depth of around 10 mm indicates the onset of cracks. The chopped flax/pp composites exhibit a stable and slow drop in punch load after reaching the maximum load, suggesting that the composite exhibits a resistance to the propagation of cracks.

It is worth noting that all CNFC samples, except the one formed at 160°C, share similar failure regions. The polypropylene matrix starts to melt when the forming temperature approaches 160°C, resulting in a dominant failure mechanism in which some fibres are pulled out of the matrix, while some fibre fractures are also observed, as shown in Figure 6.16c. Chopped flax fibres are randomly distributed in the composite, and it is observed that the pulled out fibres tend to reorient towards the centre of the specimen (due to the lack of support and restriction from the polypropylene matrix when it melts). This validates the conclusion that the pull-offs observed at elevated temperatures are caused by the near melt condition of the polypropylene matrix.

6.2.2.3 Effect of treatments on forming modes

As stated in the previous section, failure depths are increased by 16.7% and 87% when CNFC materials are preheated and water-treated, respectively. The amount of improvement is less pronounced than the increase in elongation-to-failure observed in tensile tests (40% in preheated sample and 125% in water-treated sample). It is therefore important to determine the forming behaviour of CNFC materials during dome forming, which could provide insights into the reasons why the improvement in elongation-to-failure cannot be translated to a significantly improved formability in dome forming tests. To determine this, surface strain deformation of the composites formed in different conditions is compared. Strain information of all surface points is provided by the ARAMIS™ system.

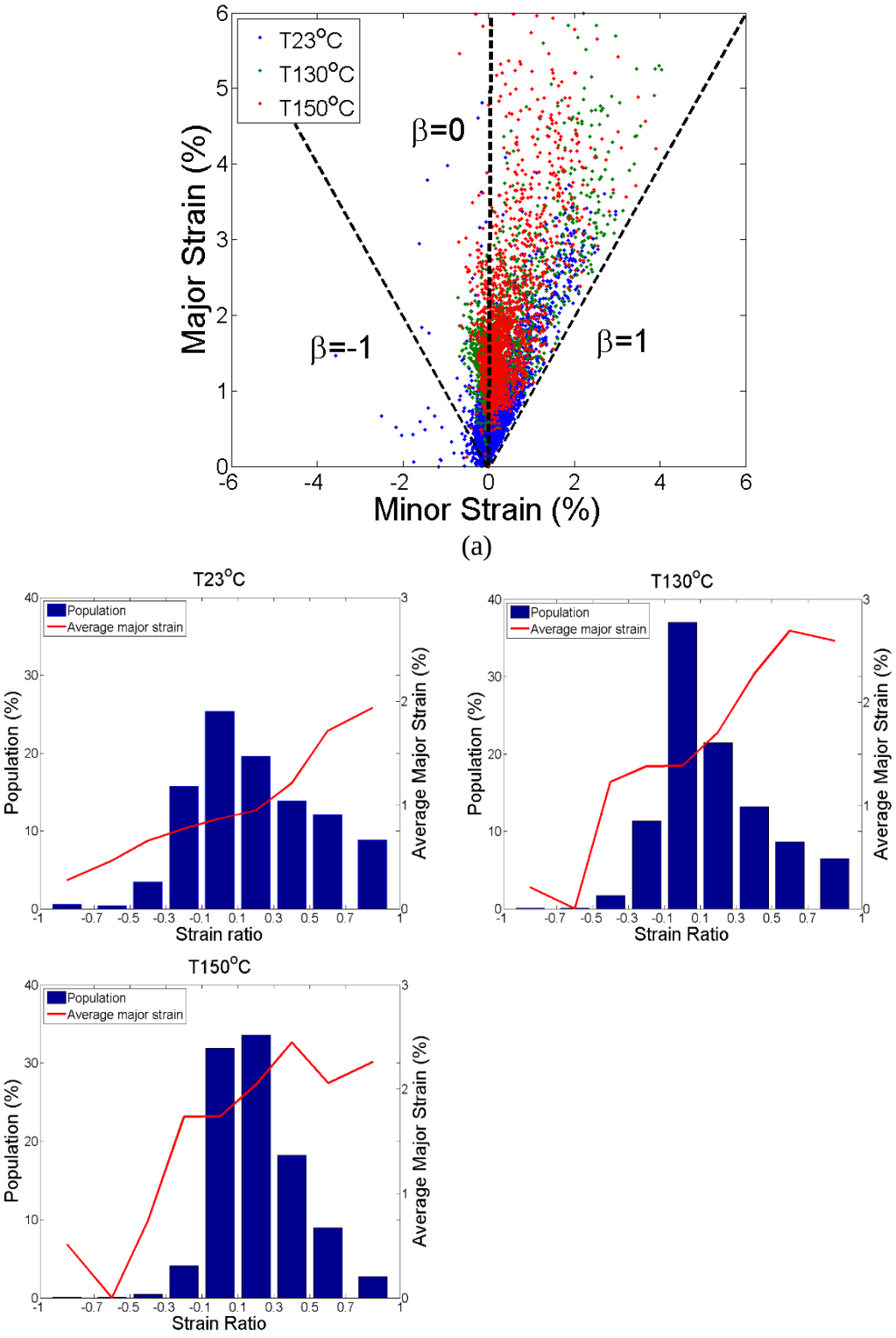

Figure 6.17: Comparison of surface strain distributions of CNFCs at different forming temperatures, (a) FLD; (b) Quantitative illustrations.

Figure 6.17.a shows the surface strain distributions of composite materials formed at 23 ˚C, 130 ˚C, and 150 ˚C at the stage just before failure. The composites experience similar surface principal strains distribution in FLD. Quantitative representations shown in Figure 6.17.b are used to help compare the composites formed in different conditions. All surface points are divided into different groups based on strain ratio. The population is plotted as a bar chart and the average major strain is expressed in a line. Based on this quantitative comparison, despite the fact that the T23 experimental case has a relatively flatter strain distribution, all composites exhibit a major deformation mode of plane strain regardless of the forming temperature. For example, 52%, 69% and 69% of surface points experiencing a strain ratio in between -0.3 and 0.3 for the T23, T130 and T150 sample, respectively. This can be expected from the isotropic nature of the composites, since the chopped flax fibres are randomly distributed. It seems that temperature has insignificant influence on the major deformation mode of the composite, which suggests that the improved formability of the preheated composite is a result of an increased elongation-to-failure at high temperatures. As a result of reduced stiffness at high temperatures, T130 and T150 specimens experience higher average surface strains as well as a very small increase in failure depth (the T23, T130 and T150 samples exhibit strain concentration at forming depths of 11.8 mm, 13.3 mm and 9.6 mm, respectively). The majority of strain deformation is confined to the pole and nearby regions, regardless of the forming temperatures. At the beginning of the dome forming test, most strain is confined to the centre of the specimen, and then shifts to nearby regions at larger forming depths due to the friction between the punch and the specimen.

Surface points in unsupported regions experience plane strain during dome forming tests, and the amount of strain in this area is closely related to the amount of stretching experienced by the composite. When the composite degrades at temperatures

approaching the melting temperature of polypropylene, the stiffness of the composite is significantly reduced. This results in more surface points exhibiting plane strain, and more importantly much higher average major strain in this deformation mode (the average major strain is almost double that of the composite formed at room temperature). Observations clearly suggest that preheating is not very effective in improving the formability of this class of material systems, and that at elevated temperatures (prior to the thermal degradation of the composite) the increase in failure depth is dominated by the increase in elongation-to-failure.

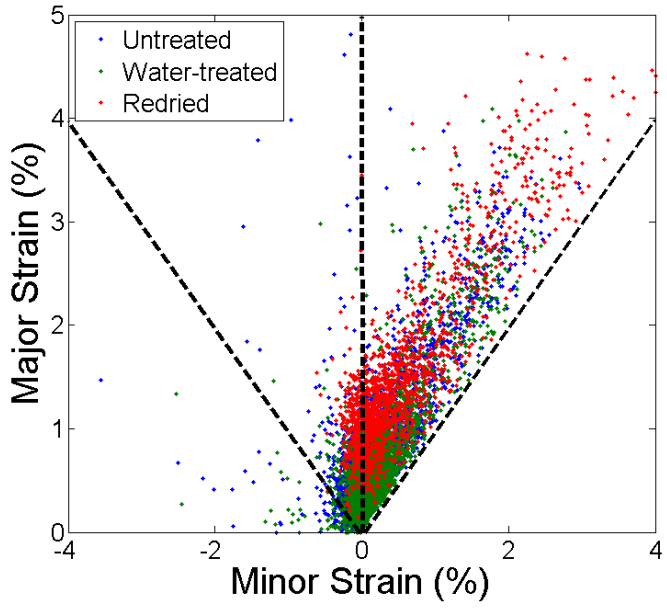

(a)

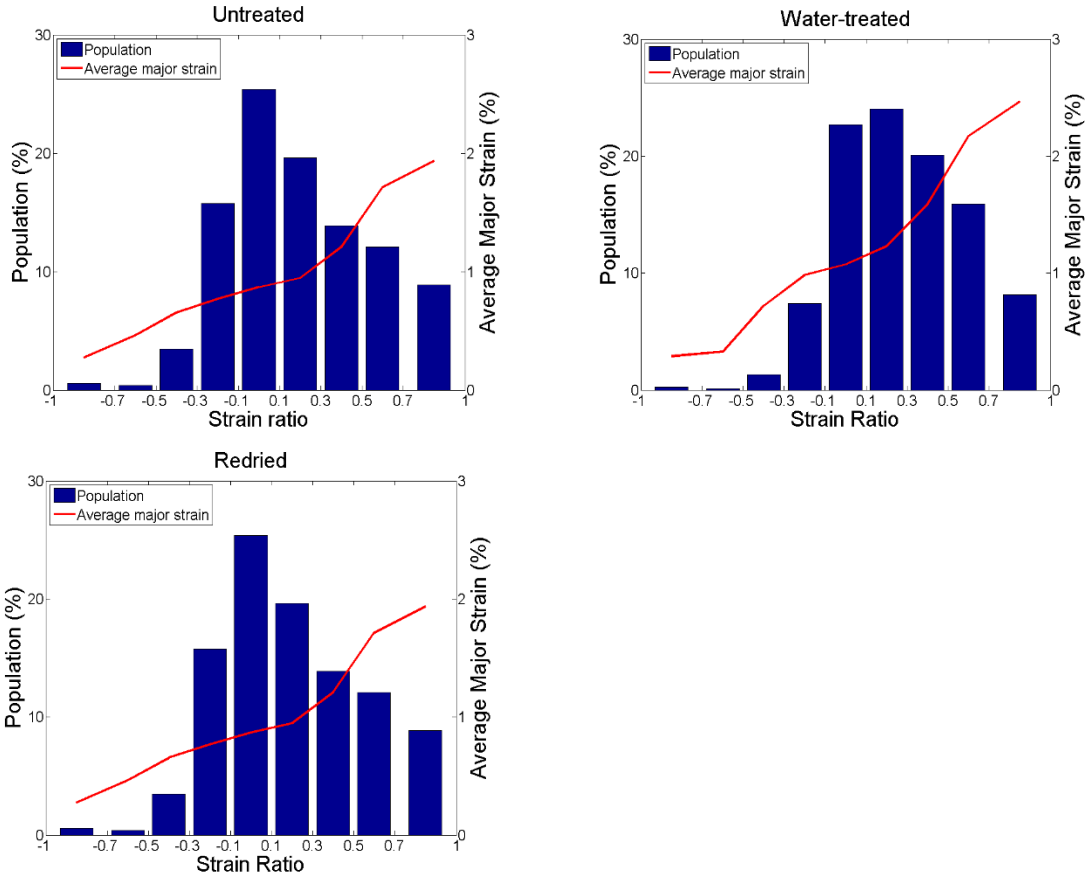

(b)

Figure 6.18: Comparison of surface strain distributions of CNFCs in different conditions of the water treatment. (a) FLD; (b) Quantitative illustrations.

Although the water-treated composite could be formed to a greater depth, the surface strain distributions are compared at a forming depth when the untreated specimen first exhibits strain concentration. Similar to the observations on the preheating treatment, the composites formed in different conditions of water treatment share a similar surface principal strain distribution in FLD shown in Figure 6.18.a. According to the quantitative comparison, all specimens exhibit a major deformation mode of plane strain, such that 52%, 48%, and 54% of surface points exhibit a strain ratio between -0.3 and 0.3 for the untreated, water-treated and redried specimen, respectively. It seems that the water treatment also has an insignificant effect on the major deformation mode. The water-treated composite exhibits a reduced stiffness, which would lead to additional strain deformation as the composite could be stretched to a greater extent at the same forming depth. However, the increase in average surface major strain is not pronounced, and is much less than that observed in the preheated samples. As stated previously, this can be attributed to the reduced friction between the composite and the tools caused by the surface moisture of the water-treated composite.

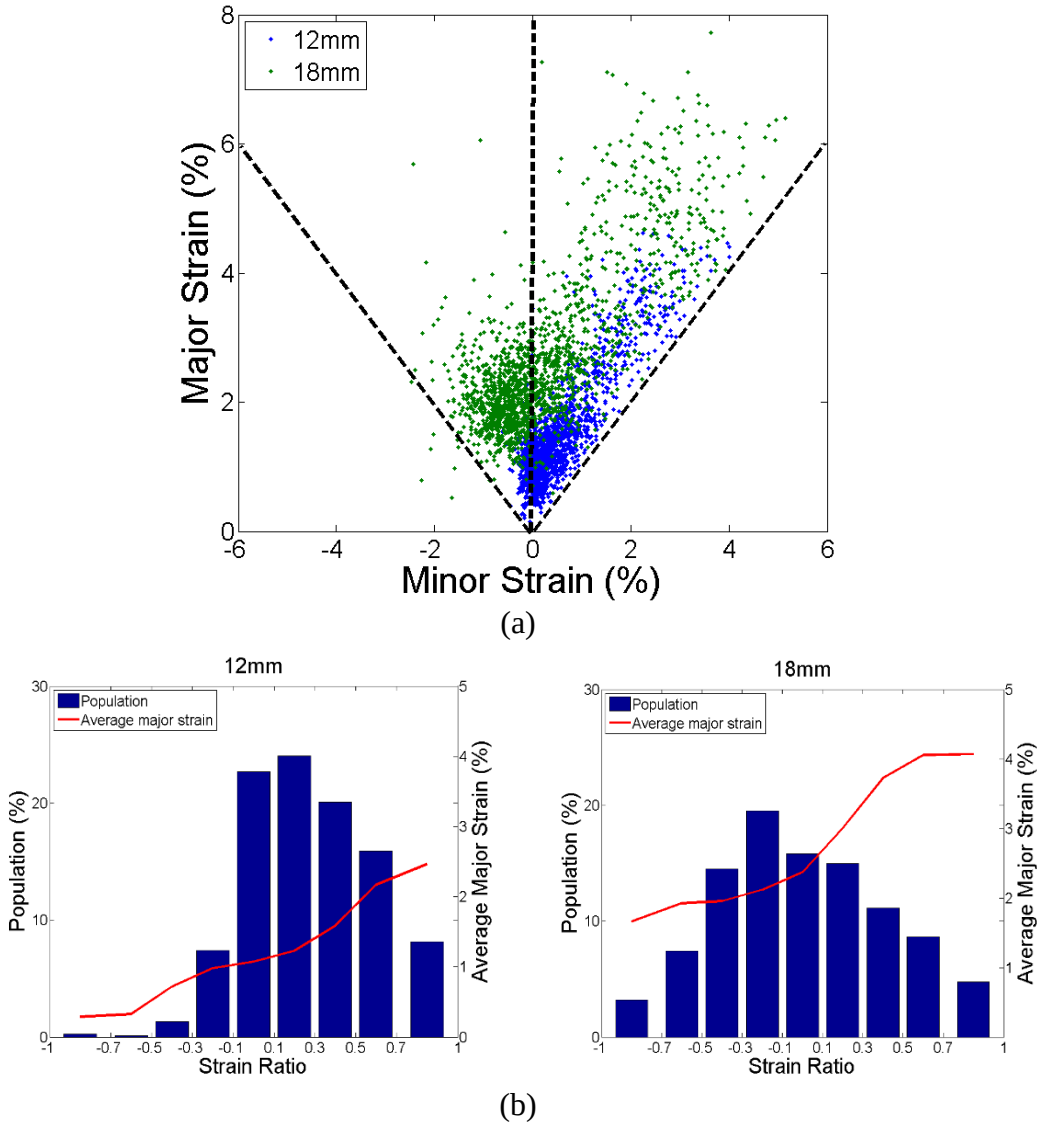

Figure 6.19: Comparison of surface strain distributions at different depths of the water-treated sample. (a) FLD; (b) Quantitative illustrations.

To further examine the effect of water treatment, the surface strain distributions of the water-treated composite are compared at forming depths of 12 mm and 18 mm in Figure 6.19. It can be seen that, although the water-treated sample exhibits a higher state of strain deformation at a larger forming depth, the major deformation mode remains unchanged. Much higher strain at positive strain ratios is observed at a larger forming depth, suggesting that most additional strain deformation is confined to the pole and nearby regions. The improved formability observed in the water-treated composite is

mainly caused by increased failure strain. In dome forming tests, there are two reasons why the water treatment is more effective than the preheating: the major reason is that the water treatment can more effectively improve the elongation-to-failure of the composite; secondly, the surface moisture of the water-treated composite could reduce the friction between the contacting tools and the specimen during forming, thereby lowering strain deformation by encouraging the sample to be drawn into the die cavity.

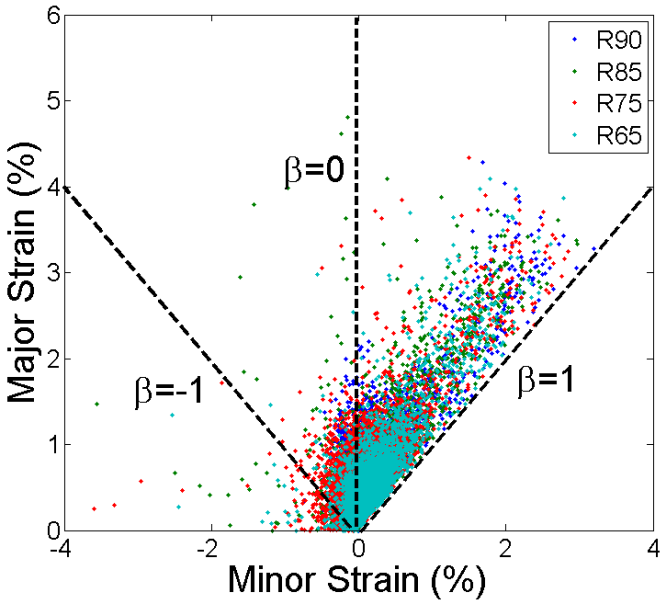

(a)

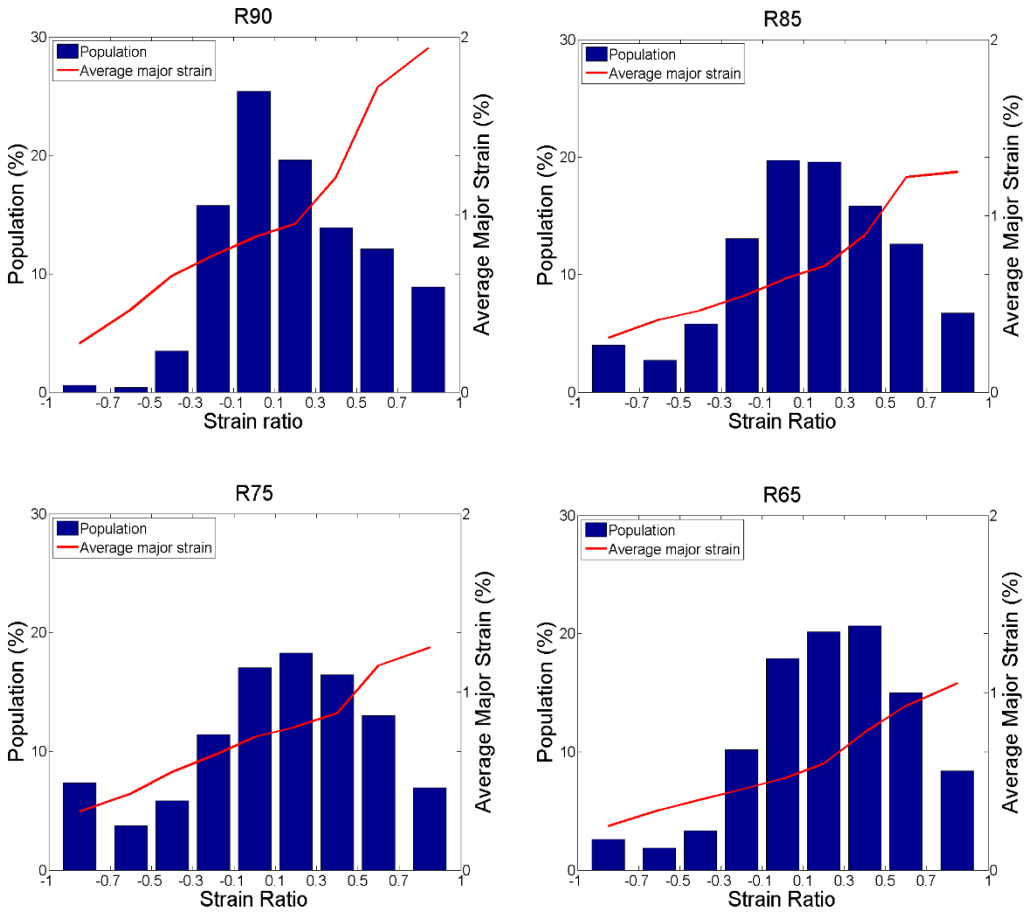

(b)

Figure 6.20: Comparison of surface strain deformation of tailored CNFC samples. (a) FLD; (b) Quantitative illustrations.

This study also uses a tailored geometry in dome forming tests where circular samples are tailored in such a way that four areas are cut at 0°, 90°, 180° and 270° from the sample edge. The application of this geometry is to introduce an imbalance in the way material flow is restricted (with less restriction along the cutting directions). For all tailored CNFC specimens, failure initiates at the pole and nearby regions. Figure 6.20 shows clearly that all tailored CNFC materials exhibit very similar surface strain deformation at the stage of comparison. It is difficult to distinguish one from another from the FLD. Based on the quantitative representations, the major deformation mode of composites remains in plane strain, regardless of the geometry of the tailored blanks. This can be anticipated from the fibre reinforcement nature of CNFC materials. Since the composite predominantly behaves like an isotropic material due to the random distribution of the chopped flax fibres, the reduced areas at the flange region can only contribute a lesser amount of friction along the cutting directions. This effect is limited as flax fibres at other orientations can still be strained and fractured at a similar forming depth. Unlike the preheating and the water treatment which increases the failure strain of the composite, the use of tailored blanks does not alter the limiting strain deformation. Therefore, in tailored blanks there is very little change in failure depths.

It is seen that the treatments used in this study can improve the formability of CNFC materials in dome forming tests to some extent. However, the amount of improvement is less than the increase in failure strain observed in uniaxial loading tests. In addition, the effect of the novel geometry, tailored blanks, is also not pronounced in dome forming tests. Unlike NFC materials which exhibit directionality due to its aligned fibre reinforcement, CNFC behaves predominantly like an isotropic material due to the randomly distributed chopped flax fibres, resulting in incapacity of introducing shear behaviour of materials in dome forming. Short fibres are usually used for the sake of

better recycling at the end of its life cycle, and this study has found that the application of chopped fibres would also affect the formability of composite materials, as well as the effects of additional treatments and blank shape change.

6.3 FEA simulations

The same geometry setup used in stretch forming can be used in dome forming FEA simulations, although boundary conditions are defined differently. Pre-stretch is not included in dome forming tests as the lock-ring tool is not used. Instead a force is applied on the blank-holder to simulate the BHF effect, and just like pre-stretch, this action is simulated in the step prior to the actual forming step. Venkatesan [18] proposed a three points analysis method to study the forming behaviour of woven composites in dome forming tests. This approach is used to validate the FEA simulations. Due to the orthotropic nature of NFC materials, different regions in the composite specimen exhibit different deformation mechanism. Three points are chosen to exemplify three major deformation modes experienced during forming and are illustrated in Figure 6.21. Point A is located at the pole of the sample and exhibits bi-axial stretch behaviour. Point B is located 40 mm from the pole and is aligned in the fibre direction. Point B exhibits plane strain conditions. Point C is located 40 mm away from the pole and is located at angle of 45 $^{\circ}$ to the fibre direction. Point C exhibits pure shear or drawing behaviour. These three deformation mechanisms represent three major forming modes in stamp forming. For CNFC materials, only two points are of interest as point B and C behave identically. It is noted that since the water-treatment is the most effective treatment, this thesis considers only the untreated, water-treated and redried composites in FEA simulations.

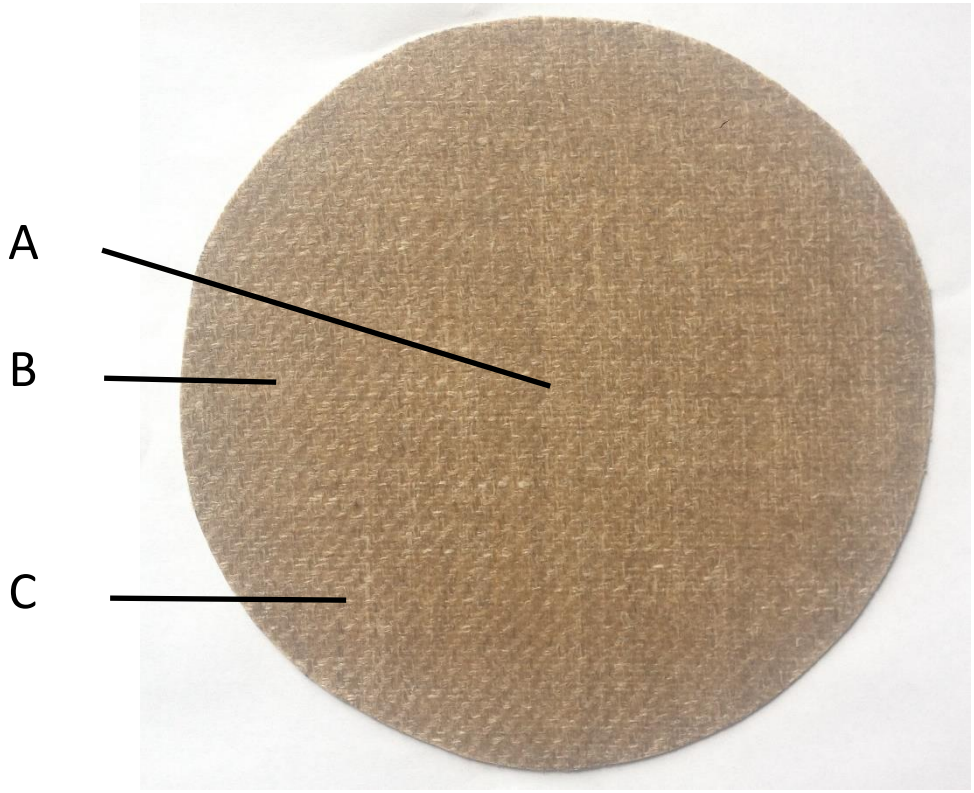

Figure 6.21: Locations of points of interest (A, B and C).

One of the contributions of this thesis is that it determines the forming limits of natural fibre composites from stretch forming tests. This section investigates whether these forming limits can be used to predict failure in forming practice that involves more than one forming mode. FEA models are also able to provide information at the flange region which cannot be observed by ARAMIS™ during experiments. Flange displacement is investigated, which is a direct indicator of the amount of material drawn into the die cavity during dome forming tests.

6.3.1 NFC materials

FEA simulations are developed to simulate the dome forming process of NFC materials, which are validated by comparing with strain evolutions at three points of interest. The efficiency of the new FLC proposed in Chapter 5 is then determined through the

comparison with failure regions and failure depths observed in FEA simulation and experiments.

6.3.1.1 Strain evolution at the points of interest

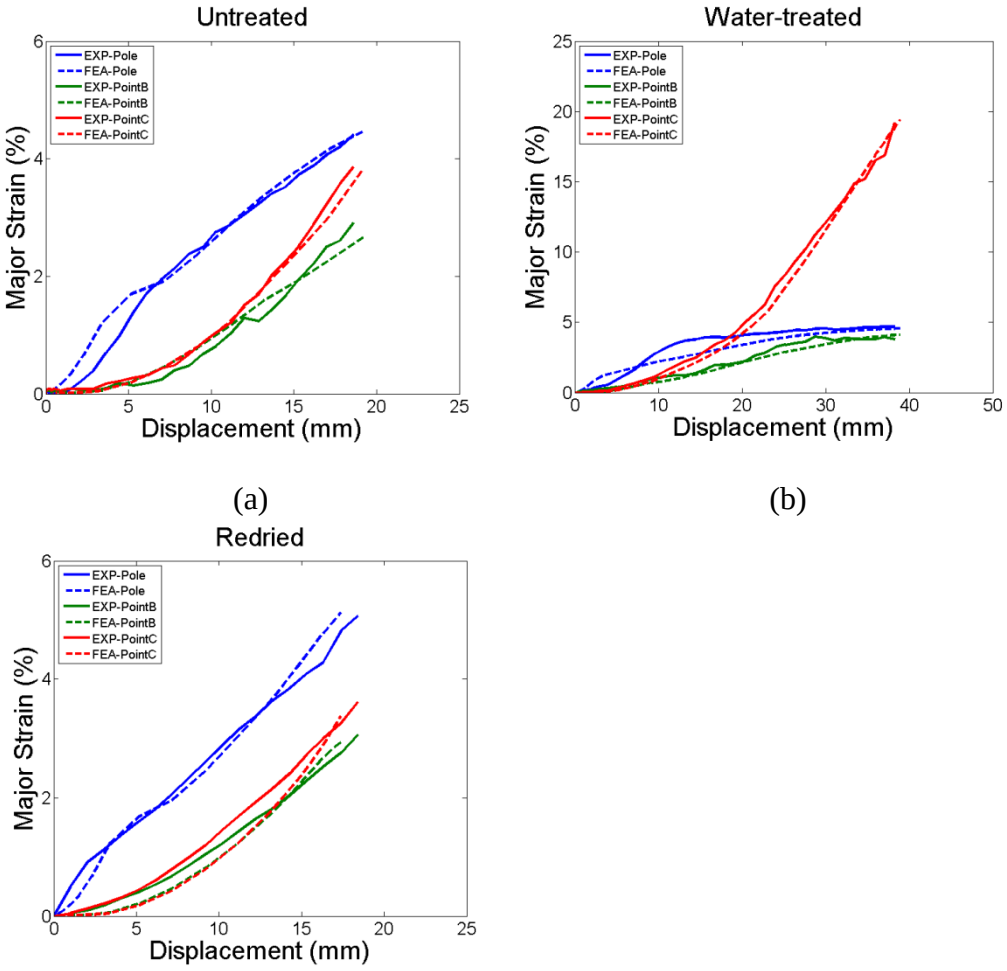

Figure 6.22: Strain evolution at points of interest. (a) Untreated; (b) Water-treated; and (c) Redried.

To obtain an understanding on the forming behaviour of NFC materials in dome forming tests, the evolution of major strain is analysed at points of interest. For this comparative study, the NFC is formed in different conditions of water-treatment at a BHF of 7 kN and a feed rate of 20 mm/s. Figure 6.22 illustrates that greater forming depths are allowed for the water-treated NFC compared to the dry equivalent samples,

which is expected from the significantly increased elongation-to-failure observed in tensile tests. For the untreated composite, the pole experiences larger strain deformation compared to unsupported areas. The redried sample shares similar strain evolutions at the points of interest as the composite exhibits very similar tensile properties. For the water-treated composite, strain deformation at the pole starts to level out at a forming depth of 12 mm, while point B rises linearly during forming. Unlike these two points, point C increases exponentially and then linearly, surpassing point B and A at a forming depth of 10 mm and 20 mm respectively. This suggests a change in major deformation mode of the water-treated composite at larger forming depths. The additional strain deformation shifts from the pole to nearby regions, especially along the 45°/-45° directions. The greater forming depths observed in the water-treated composite are permitted due to a large amount of shear deformation, which agrees with the experimental observations. A reasonable agreement between the experimental outcomes and FEA simulations is seen, meaning that the biaxial-stretch, plane strain, and pure shear behaviour of the composites at different locations can be successfully simulated. Unlike the experiments where the increases and decreases are more rapid, major strain evolves more gradually in FEA models as a result of the homogenised material properties in numerical simulations.

6.3.1.2 Validating the new FLC in different forming conditions

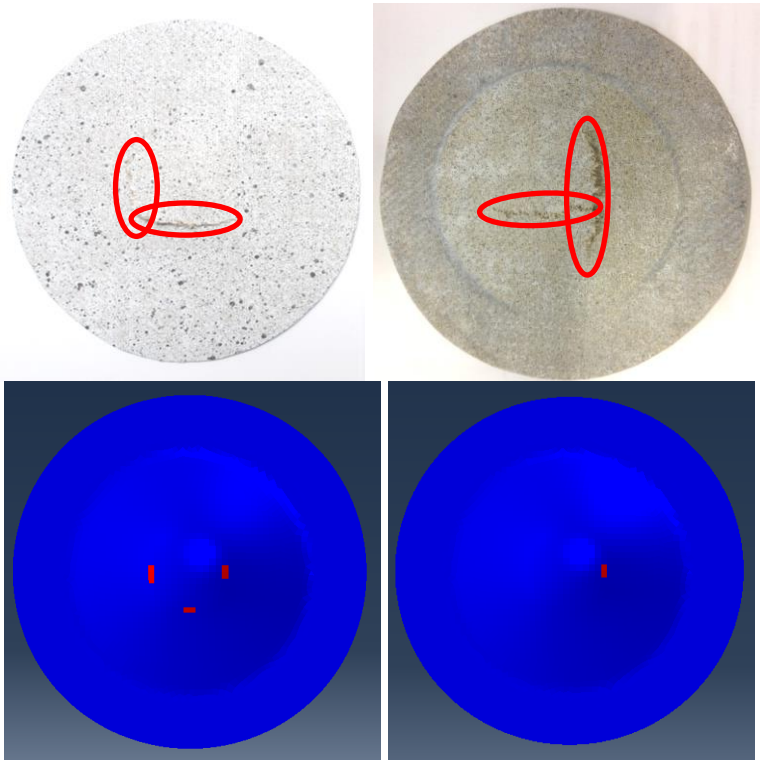

Figure 6.23: Comparison of failure regions observed on the formed samples and those suggested by FEA simulations, left: untreated; right: redried.

The failure for NFC materials in the wet condition cannot be captured by FEA due to the fact that no failure is observed for the largest allowable depth of forming for experiments. The new FLC therefore only applies to the untreated and redried materials. Figure 6.23 shows that FEA simulations can predict the regions where failure initiates during dome forming. In dome forming experiments, the pole experiences biaxial stretch, and the high level of fibre strains causes the onset of failure around this region, regardless of the forming conditions. Due to the woven structure of the composite, NFC materials start to exhibit a major deformation mode of pure shear at large forming depths. More importantly, additional strain deformation generated at large forming depths acts on the polypropylene matrix rather than the flax fibres. Figure 6.24 compares the failure depth of experimental observations and FEA simulations. This

comparison validates the efficiency of the new FLC in predicting the failure behaviour of woven natural fibre composites in dome forming tests.

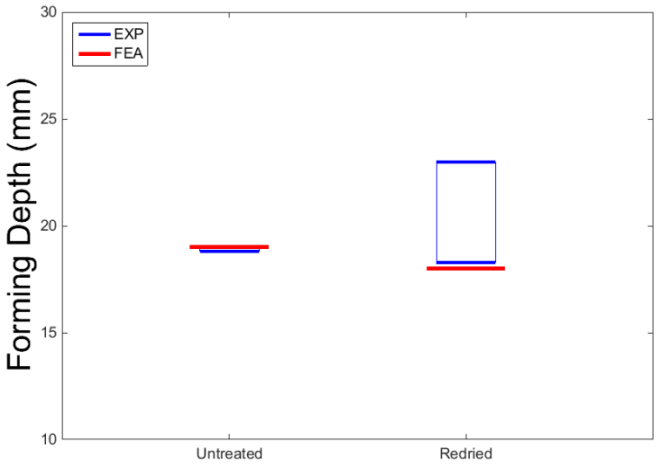

Figure 6.24: Comparison of failure depths observed in experiments (blue) and those suggested by the new FLC (red).

6.3.1.3 In-plane displacement at the flange region

Figure 6.25 shows that flange in-plane displacements are dominated by fibre directions, regardless of water treatment. A larger difference in the amount of flange in-plane displacement is observed in the water-treated composite compared to other equivalent specimens. This agrees with the hypothesis that even though the fibre stiffness is reduced, the composite becomes more anisotropic after water treatment. There is a significant amount of material drawing into the die cavity in the water-treated specimen at large forming depths. In-plane displacements at the flange region increased by more than 12 times (from less than 1 mm at a forming depth of 19 mm to 12 mm at a forming depth of 40 mm). The water-treated composite is stretched and strained along the off-fibre directions, this agrees with the observation that the composite starts to exhibit a major deformation mode of pure shear at large forming depths.

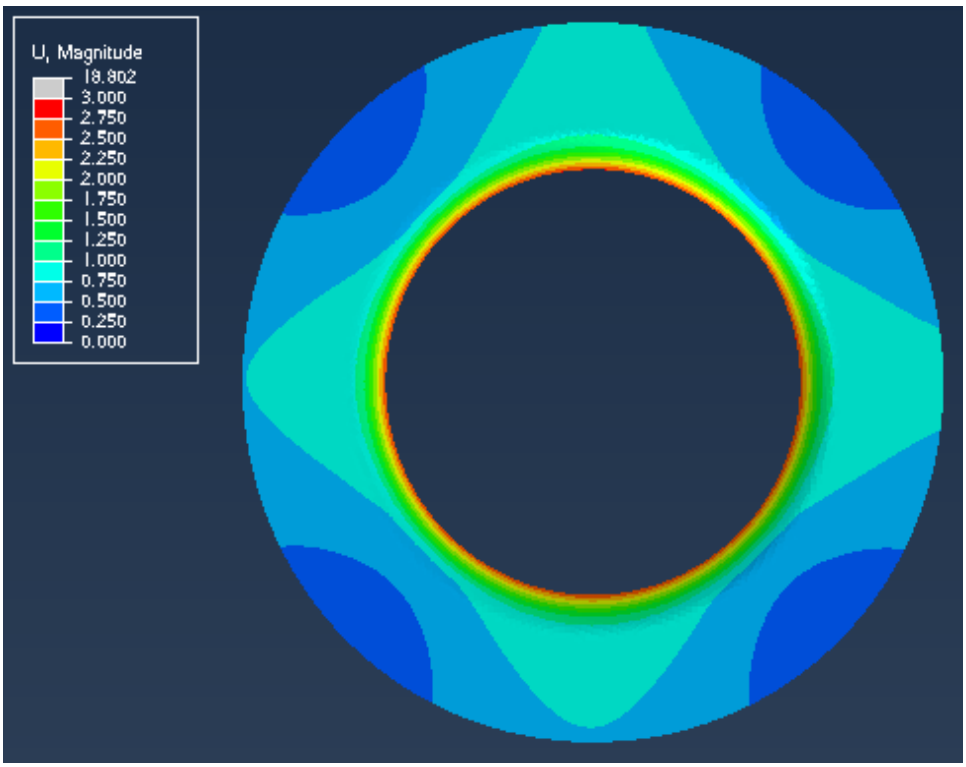
U, Magnitude
18.802
3.000
2.750
2.500
2.250
2.000
1.750
1.500
1.250
1.000
0.750
0.500
0.250
0.000

(a)

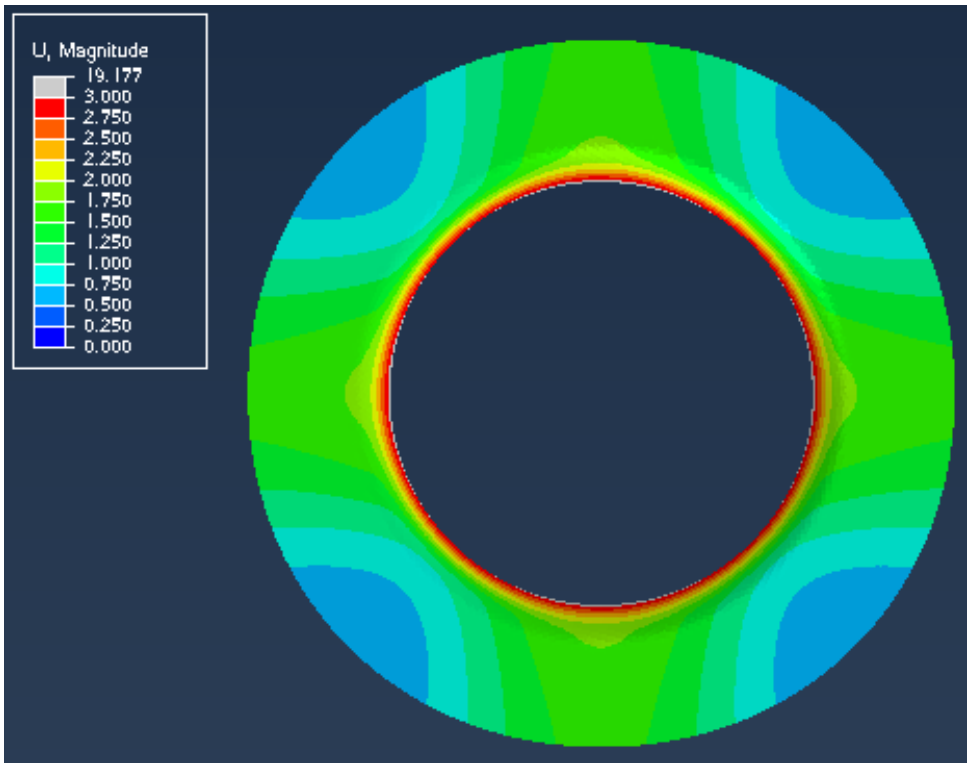
U, Magnitude
19.177
3.000
2.750
2.500
2.250
2.000
1.750
1.500
1.250
1.000
0.750
0.500
0.250
0.000

(b)

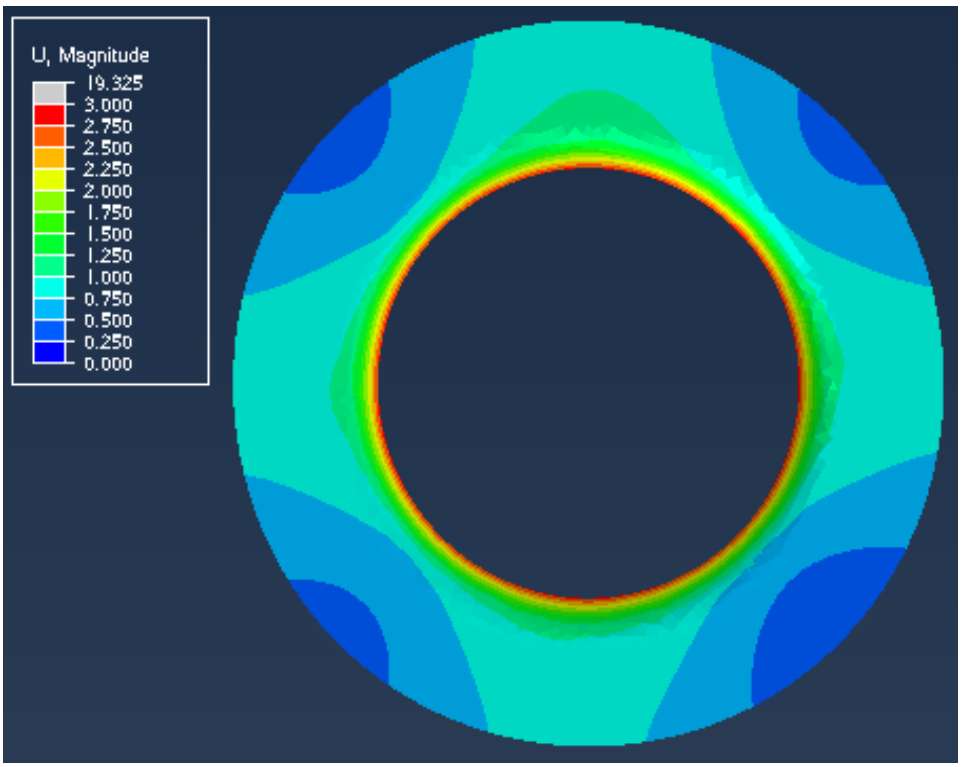

(c)

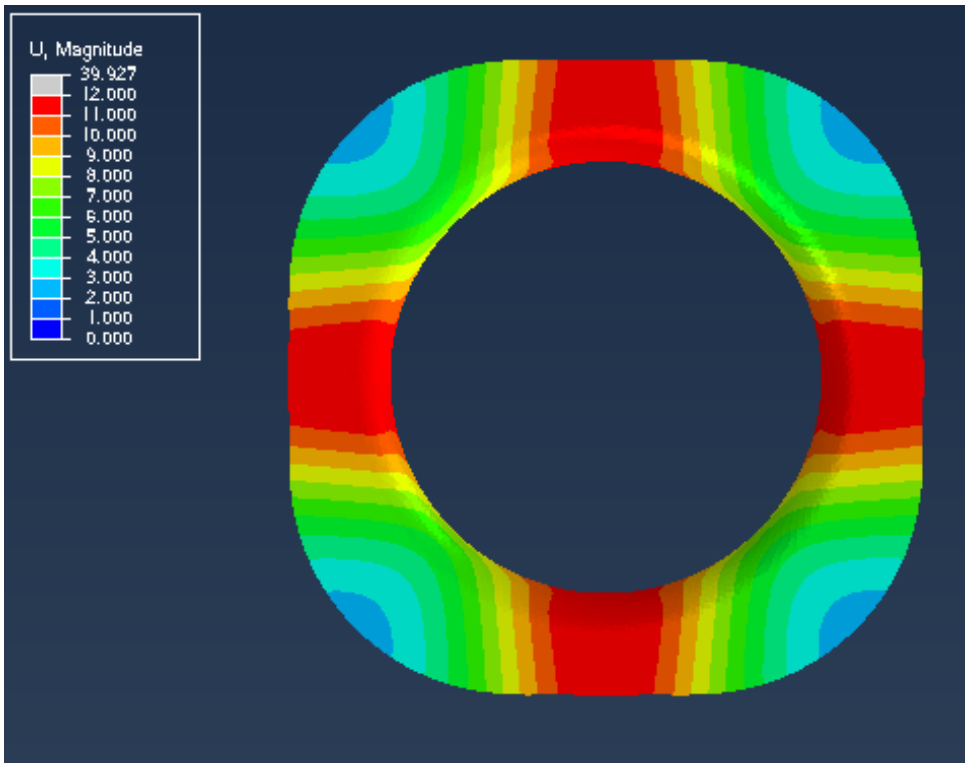

(d)

Figure 6.25: Flange displacement of the composite at a forming depth of 19 mm. (a) untreated; (b) water-treated; (c) redried; and (d) water-treated specimen at a forming depth of 40 mm.

6.3.2 CNFC materials

6.3.2.1 Strain evolution at the points of interest

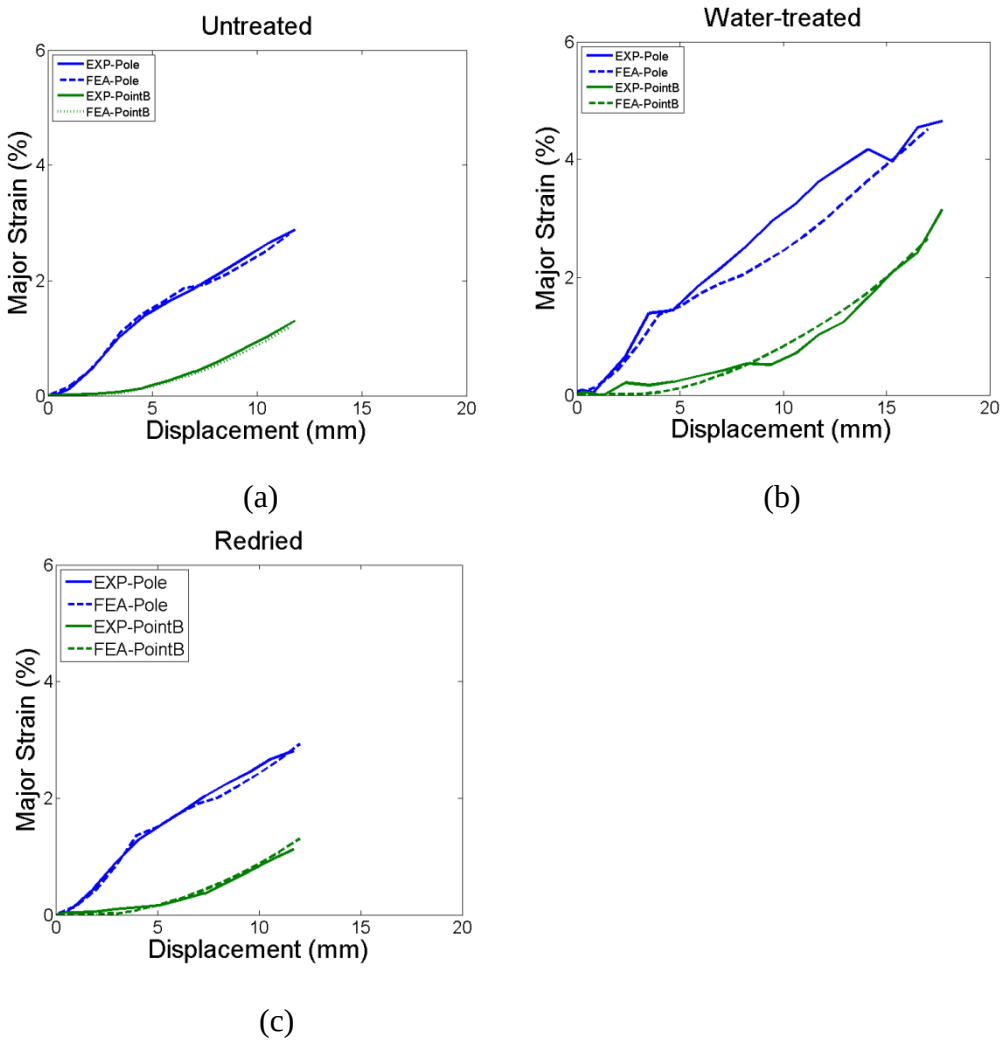

Figure 6.26: Strain evolution at points of interest for (a) Untreated; (b) Water-treated; and (c) Redried samples.

Figure 6.26 shows the evolution of major strain at points of interest. Untreated, water-treated and redried CNFC materials are formed until failure at a BHF of 7 kN and a feed rate of 20 mm/s. Regardless of water treatment, the pole of the composite experiences a larger major strain compared to the unsupported edge during the entire strain evolution, indicating that most strain deformation is confined within the central area of the composite. This correlates well with the finding obtained in the previous sections that major cracks initiate around the pole of the specimen. Fibre fracture is the major failure

mechanism exhibited in the composite, and the flax fibres which are most strained fracture early. Even though the water-treated composite exhibits a greater forming depth compared to dry equivalent specimens, the strain deformation evolves in a similar pattern in different conditions. It is found that the CNFC material exhibits an unchanged major deformation mode, and the improved forming depth is a result of increased failure strain. Water treatment results in an increase in major strain measurement at failure from 2.88% to 4.65% at the pole and 1.18% to 3.15% at point B. The unsupported region starts to be strained beyond a forming depth of 3 mm, resulting in a reduced slope in strain evolution at the pole. This phenomenon can be captured in FEA simulations, and is illustrated in Figure 6.26.

6.3.2.2 Validating the FLC in different forming conditions

Similar to Section 6.3.1.2, the FLC for CNFC is validated in this section through two aspects: the location where the failure initiates, and the punch displacement at the onset of failure.

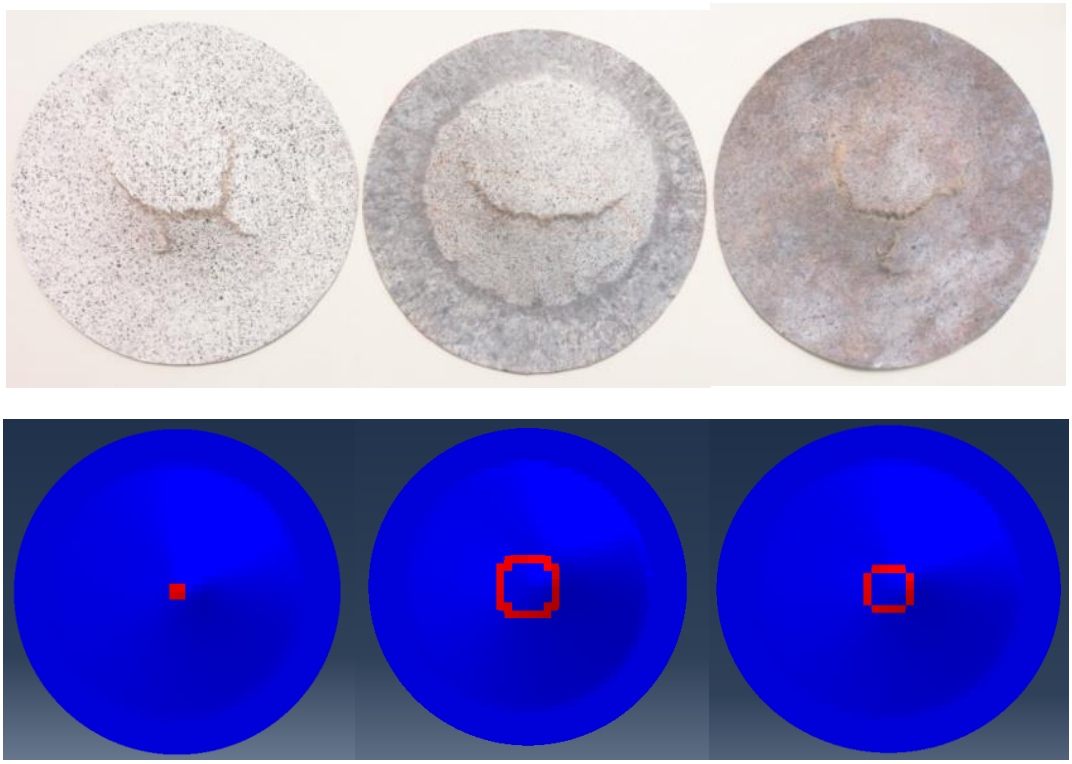

Figure 6.27: Comparison of failure regions observed in formed CNFC samples and that suggested by FEA simulations (red). Left: untreated; Middle: water-treated; Right: redried.

The FLC is constructed for CNFC materials based on experimental observations from stretch forming tests. This section incorporates this failure criterion in FEA simulations through a user-defined material subroutine, and compares them with experimental results. In this UMAT, the indicator is turned on when the FLC is met at this mesh point, otherwise it remains off. The red regions in the contours obtained from FEA simulations suggest the onset of failure. It is noted that the contours in the Figure 6.27 above are obtained at the stage when the failure first initiates. Good agreement on failure regions is observed, with the failure initiating at either the pole or nearby regions, regardless of treatment conditions. As stated previously, the composite is formed to an additional displacement beyond the onset of failure, producing large regions of failure in the formed samples. The aim of this study is to predict the onset of failure, while the shape

of the catastrophic failure is not within the scope of this work. In addition to failure regions, FLC also suggests reasonable forming depths at which the failure initiates. Overall, good agreement is obtained between the failure depths suggested by the FLC and that observed in the tested samples, as shown in Figure 6.28.

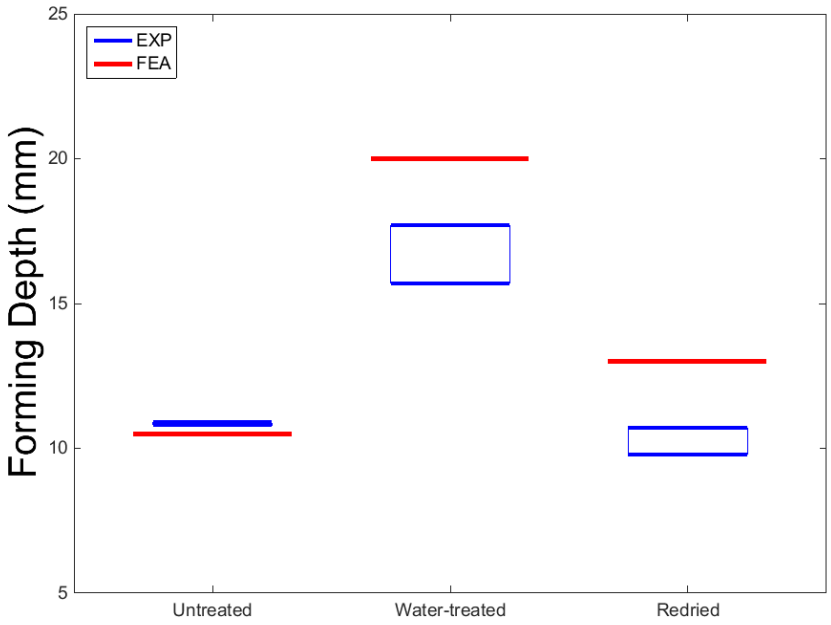

Figure 6.28: Comparison of forming depths observed in experiments (blue) and those suggested by FLC (red) in different forming conditions.

6.3.2.3 In-plane displacement at the flange region

FEA simulations are able to provide information about the flange region which cannot be observed from the ARAMIS™ system during forming, such as the in-plane displacement at the flange region. This information indicates the amount of material drawn into the die cavity, which is closely related to the material stiffness, forming depth, and contact friction.

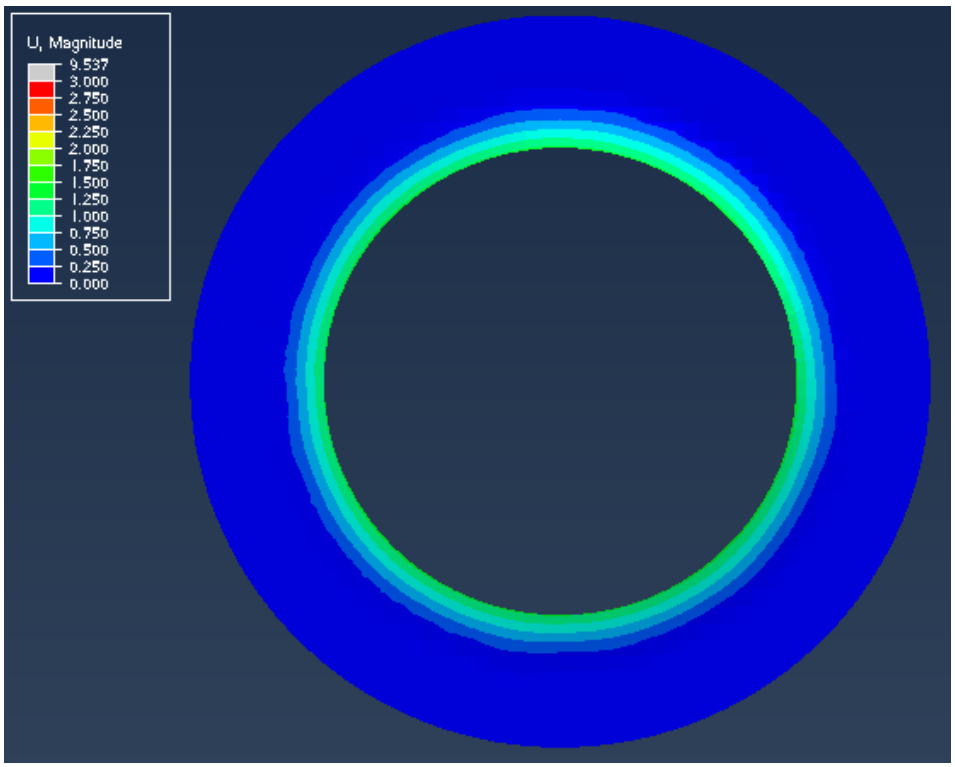
U, Magnitude
9.537
3.000
2.750
2.500
2.250
2.000
1.750
1.500
1.250
1.000
0.750
0.500
0.250
0.000

(a)

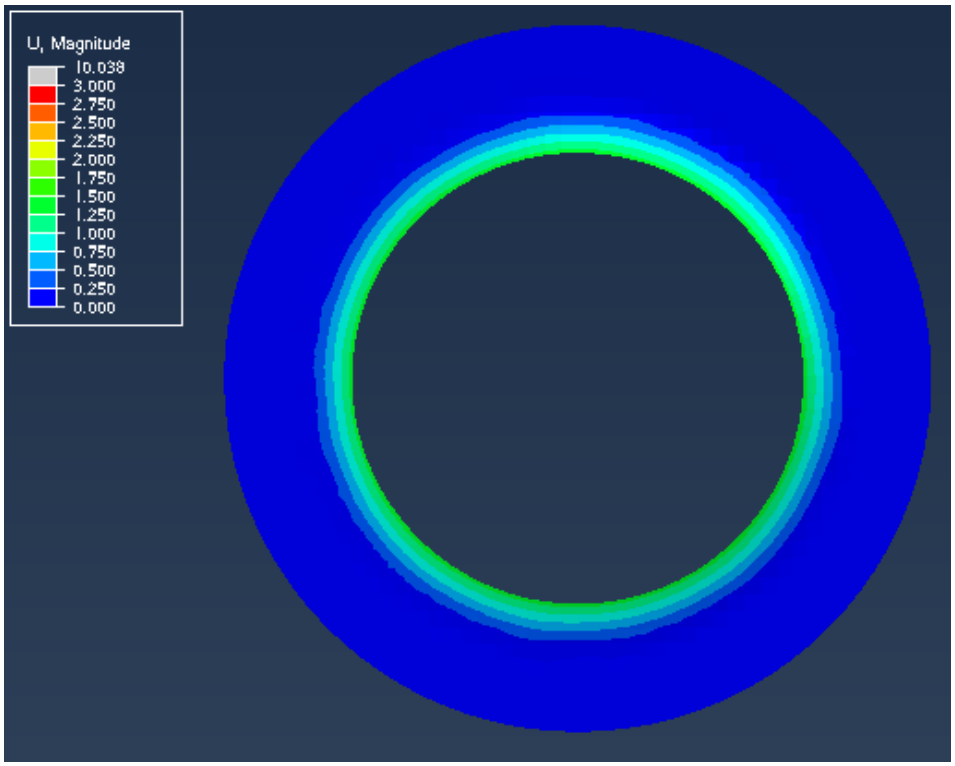
U, Magnitude
10.038
3.000
2.750
2.500
2.250
2.000
1.750
1.500
1.250
1.000
0.750
0.500
0.250
0.000

(b)

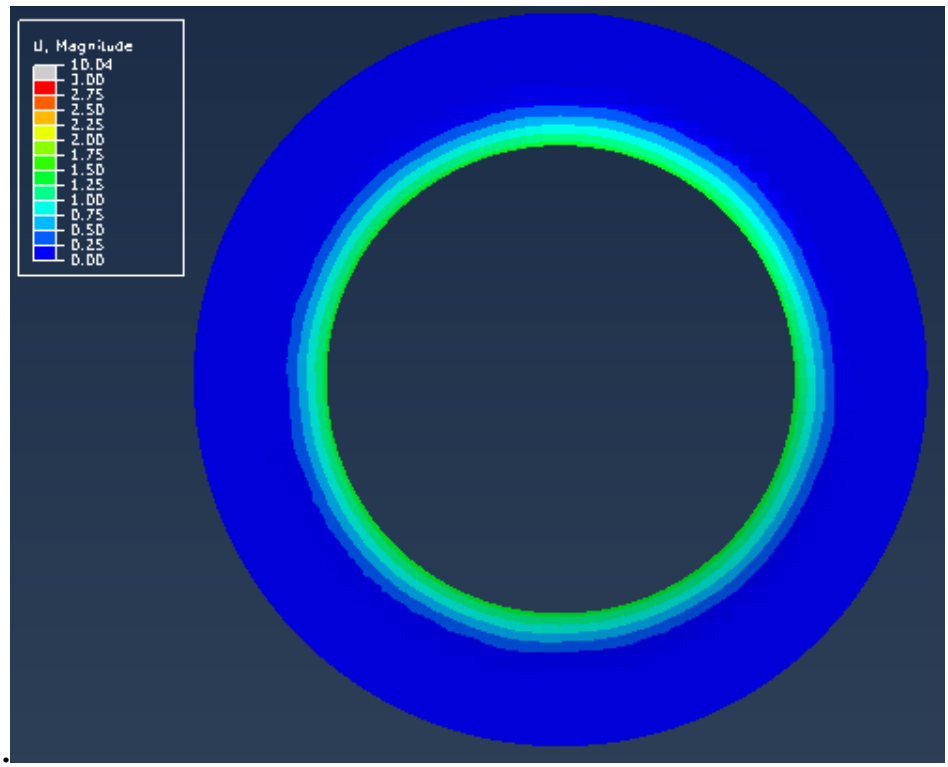

(c)

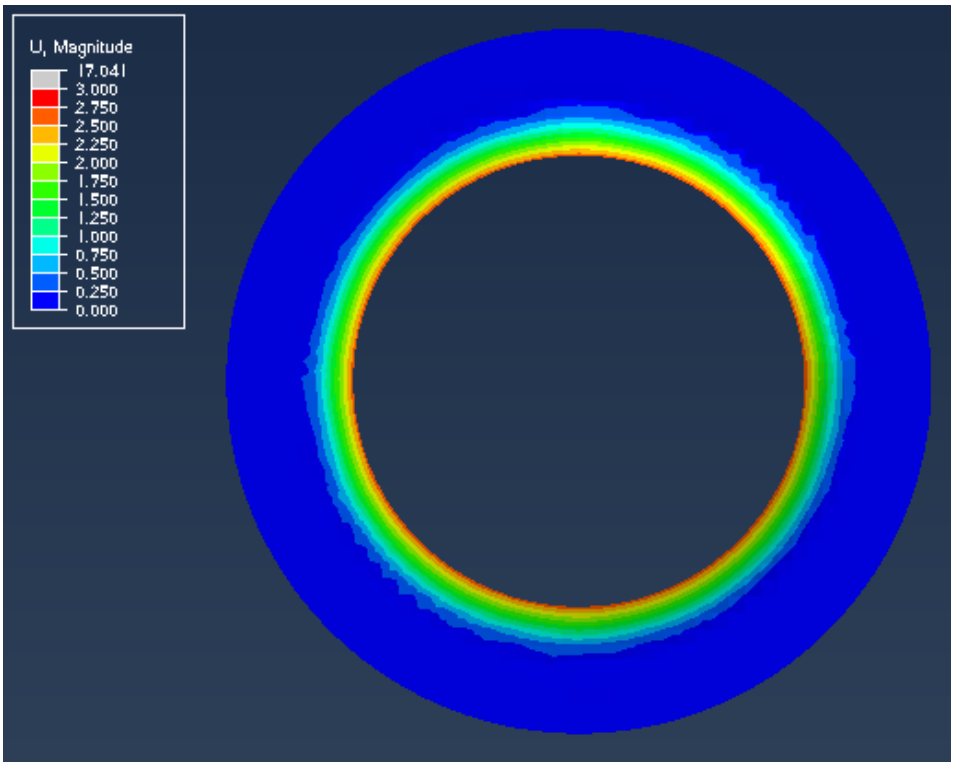

(d)

Figure 6.29: Flange displacement of the CNFC at a forming depth of 10 mm. (a) untreated; (b) saturated; (c) redried specimen; and (d) the saturated specimen at a forming depth of 17 mm.

Figure 6.29 shows that at small forming depths, composites experience a small amount of in-plane displacement deformation at the flange region. It is anticipated that composites formed in dry conditions (untreated and redried) experience a similar amount of flange displacement, while that of the water-treated composite is not much different. This can be attributed to the combination of reduced stiffness (to reduce flange displacements) and lower contact friction caused by surface moisture (to increase flange displacements). When the forming depth increases from 10 mm to 17 mm, a slightly larger in-plane displacement at the flange region is observed. This agrees with the observations obtained earlier that there is no change in major deformation mode of CNFC materials in dome forming tests. It is also important to note that in-plane displacement in the flange region exhibits no directionality, and decreases gradually to the sample edge.

6.4 Summary

This Chapter has investigated the forming behaviour of both NFC and CNFC in dome forming tests, with a particular focus on the mechanisms behind the improved formability of preheated and water-treated composites. Specimens experience two major deformation mechanisms of stretching and drawing. Based on visual observations of the tested samples and microscopic examinations of fractured surfaces, fibre fracture is identified as the dominant failure mechanism for both composites. At a forming temperature of 160 ˚C, fibre pull-out is also observed in addition to fibre fracture. This study has shown that due to the thermal degradation of composites there is an optimal temperature window for forming. For CNFC materials, it is found that the specimen experiences strain concentration prior to catastrophic failure, and the punch displacement between these two levels can vary from sample to sample based on the local fibre loading. To better compare specimens formed in different conditions, the

CNFC is considered to fail at the onset of strain concentration. One of the key finding of this study is that water treatment is superior to preheating treatment, with the water-treated composites withstanding a considerably larger forming depth compared to the preheated equivalents. These observations suggest that it would be very advantageous to process natural fibre composites in the wet condition. By studying surface strain deformation at various forming conditions, it is found that the improved formability of treated CNFC materials is mainly driven by increased elongation-to-failure. In additional to the fact that the strain deformation increases with a steeper slope at larger forming depths, a wider forming envelope of CNFC materials in wet condition could not be translated to a forming depth with similar improvement. Unlike CNFC materials, an improved formability of treated NFC materials is due to a combination of increased ductility as well as the introduction of pure shear. This in turn leads to significantly increased forming depths in dome forming tests. Novel geometries of natural fibre composites, where some areas have four cut-outs at the sample edge (at 0˚, 90˚, 180˚ and 270˚), are used in dome forming tests. The tailored shape encourages materials to draw into the die cavity along the cutting directions. It is found that the effect of tailored blanks is pronounced for NFC materials, but very limited for CNFC materials. This can also be attributed to differences in the nature of the fibre reinforcement. It seems a trade-off needs to be made between better recycling at the end of life cycle (CNFC) and superior formability (NFC) especially under treatments and blank shape change.

In FEA simulations, a force is set up to act on the blank-holder in a way that simulates the effect of BHF. By comparing these results with experimental observations, it is found that the failure criteria obtain in Chapter 5 can predict the region where the failure initiates as well as the punch depth at the onset of failure. These observations could verify the failure criteria to predict the onset of failure of this class of material systems

in different forming practices. In addition to validating the failure criteria, FEA models can also provide information at the flange region which is hidden from view by the die and blank-holder. For NFC materials, the amount of in-plane displacement depends on the directions of the fibres, whereas for CNFC materials it is distributed equally in all directions. Finally, water-treated composites are found to experience significantly more flange displacement at larger forming depths, suggesting that there is a change in the major deformation mode to pure shear. This matches with the observations obtained from ARAMIS™. This Chapter validates the effectiveness of the new FLC for NFC in dome forming tests where samples could experience more complicated forming modes (stretching and drawing) than that experienced in stretch forming. This is concluded that the FLC proposed in this study could be used to effectively predict the failure behaviour of woven composites in rapid forming processes.

Conclusions and Future Work

7.1 Introduction

This work is designed to answer two key questions regarding the forming of natural fibre composites. The first one is when does failure initiate in this class of material systems, and what is the most effective measure for predicting it? To answer this question, hourglass samples are stretched and then formed through the stamping press machine. The ARAMIS™ system beneath the press machine provides displacement and strain deformation which could be used to determine the failure behaviour of the composites. The second relates to how to improve the formability of natural fibre composites. The approach here is to perform dome forming tests in different treatment conditions, namely preheating, water treatment, and tailored blanks.

7.2 Contributions

- Significantly improved ductility is observed when natural fibre composites are saturated with water. Mechanical properties (elongation-to-failure, stiffness, and strength) can almost retain back to pre-treated levels after dried from wet condition. This makes it very advantageous to process natural fibre composites in wet condition. According to the SEM examinations on fractured surfaces, the changes in tensile properties of the chopped and continuous natural fibre composites are caused by different mechanisms.

- Through stretch forming experiments, it is found that the conventional FLC is not suitable for predicting the failure initiated in woven natural fibre composite, as principal strains cannot differentiate the strain on the flax fibres and the

polypropylene matrix. This work has proposed a new FLC for woven composites which expresses limiting fibre strain as a function of forming mode calculated as the ratio of minor strain to major strain. Such a criterion requires tracking the evolution of fibre movements, and this was achieved using a real-time strain measurement system (ARAMIS™). The problem with applying the conventional FLC for predicting the failure behaviour of NFC is that it has path dependency effect. The new FLC is superior to the conventional FLC because it can successfully eliminate this path dependency effect. This work has also demonstrated that the new FLC is more effective than the Maximum Strain failure criterion, highlighting the importance of the interactions between different constituents of woven composites. The new FLC will accommodate different composite material systems as long as the dominating failure mechanism is fibre fracture.

- A key contribution of this study is that it has incorporated failure criteria into FEA simulations through development of a user-defined material routine. This is achieved through the application of SDVs in the UMAT. Based on the FEA models developed in this study, the failure criteria proposed in this study can be used to predict the onset of failure in natural fibre composites in different forming practices (stretch forming, dome forming) as well as in different forming conditions (untreated, water-treated, redried, and tailored blanks).

- Preheating is a traditional treatment method usually used to improve the formability of materials in rapid forming processes. However, it is found that this conventional method is not very effective for natural fibre composites due to thermal degradation at high temperatures. It is found that the water-treated

composites could exhibit an almost doubled forming depth compared to that of the preheated equivalents. As well as requiring less energy, water treatment can be more effective than the conventional method used to form this class of material system. This fundamental breakthrough in improving the formability of natural fibre composites can aid in rapid forming of this class of material system. Due to the directionality of NFCs, improved formability can also be achieved by cutting some areas of a circular sample in the fibre directions. This reduces the amount of strain deformation acting on the flax fibres by encouraging the flax fibres to be drawn into the die cavity in the fibre directions, and hence results in greater forming depths. This treatment can be as effective as preheating in dome forming tests.

7.3 Future work

- This thesis has looked into the effect of improving formability of natural fibre composites through varying chemical solutions, and among which the water solution is found to be the most effective. In the future, it would be valuable to look for any chemical medium that can potentially improve the formability beyond what is observed in this study.

- For production parts, attention needs to be paid to spring back of natural fibre composites. It is expected that such composites would experiences a considerable amount of spring back when an applied load is released, and this is very likely due to the polypropylene matrix. It is crucial to quantify the amount of spring back at the end of rapid forming processes, and more importantly to determine if there are any methods to reduce it.

- Fibre-metal laminate (FML) is a sandwich structure consisting of two outer layers of monolithic metal alloys and a core of composite material. This class of material system can exhibit superior formability compared to monolithic metal alloys. The current work has found that, the water treatment is more effective than other treatments in terms of improving the formability of natural fibre composites. However, FML layers are glued together by melting adhesives, so any water treatment prior to FML manufacturing is therefore likely to be much less effective. In addition, the composite layer of FML can hardly absorb moisture when the entire sandwich structure is merged in water. Therefore, research effort is required to investigate how the formability of natural fibre composites based FMLs might be improved. Tailored blanks may be useful to the FML structure, but again this needs to be verified through experiments.

Bibliography

[1] A. Shalwan and B.F. Yousif, "In State of Art: Mechanical and tribological behaviour of polymeric composites based on natural fibres", *Material and Design* vol. 48, pp. 14-24, 2013.

[2] N. Saba, M. Jawaid, O.Y. Alothman, and M.T. Paridah, "A review on dynamic mechanical properties of natural fibre reinforced polymer composites", *Construction and Building Materials,* vol. 106, pp. 149-159, 2016.

[3] V.K. Thakur, and M.K. Thakur, "Processing and characterization of natural cellulose fibers/thermoset polymer composites", *Carbohydrate Polymers,* vol. 109, pp. 102-117, 2014.

[4] W. Xu, and L. Zhang, "Mechanics of fibre deformation and fracture in vibration-assisted cutting of unidirectional fibre-reinforced polymer composites", *International Journal of Machine Tools and Manufacture,* vol. 103, pp. 40-52, 2016.

[5] M.J.M. Ridzuan, M.S. Abdul Majid, M. Afendi, S.N. Aqmariah Kanafiah, J.M. Zahri, and A.G. Gibson, "Characterisation of natural cellulosic fibre from Pennisetum purpureum stem as potential reinforcement of polymer composites", *Materials & Design,* vol. 89, pp. 839-847, 2016.

[6] Y. Xie, C.A.S. Hill, Z. Xiao, H. Militz and C. Mai, "Silane coupling agents used for natural fiber/polymer composites: A review", *Composites Part A: Applied Science and Manufacturing,* vol. 41, no. 7, pp. 806-819, 2010.

[7] A.C.N. Singletona, C.A. Baillie, P.W.R Beaumonta, and T. Peijs, "On the mechanical properties, deformation and fracture of a natural fibre/recycled polymer composite", *Composites: Part B Engineering* vol. 34, pp. 519-526, 2003.

[8] O. Faruk, A.K. Bledzki, H.-P. Fink, and M. Sain, "Biocomposites reinforced with natural fibers: 2000–2010", *Progress in Polymer Science,* vol. 37, no. 11, pp. 1552-1596, 2012.

[9] Lucintel, "Opportunities in natural fibre composites", *March 2011. Available at: http://www.lucintel.com/lucintelbrief/potentialofnaturalfibercomposites-final.pdf*.

[10] J. Holbery and D. Houston, "Natural-Fiber-Reinforced Polymer Composites in Automotive Applications", *Low-Cost Composites in Vehicle Manufacture*, vol. 58, no. 11, 2006.

[11] A. Belaadi, A. Bezazi, M. Bourchak, F. Scarpa, and C. Zhu, "Thermochemical and statistical mechanical properties of natural sisal fibres", *Composites Part B: Engineering,* vol. 67, pp. 481-489, 2014.

[12] L. Mosse, "Stamp Forming of Fibre-Metal Laminates", 2006. PhD Thesis, The Australian National University.

[13] American Chemistry Council - Plastic Division, "Plastics and Polymer Composites for Automotive Markets" *TECHNOLOGY ROADMAP*, 2014.

[14] E. Ghassemieh, "Materials in Automotive Application, State of the Art and Prospects" Chapter 20, pp. 365-395, 2011.

[15] M. Pervaiz, and M.M. Sain, "Carbon storage potential in natural fiber composites", *Resources, Conservation and Recycling,* vol. 39, no. 4, pp. 325-340, 2003.

[16] M.J. John, and S. Thomas, "Biofibres and biocomposites", *Carbohydrate Polymers,* vol. 71, no. 3, pp. 343-364, 2008.

[17] Z. N. Azwa, B. F. Yousif, A.C. Manalo, and W. Karunasena, "A review on the degradability of polymeric composites based on natural fibres", *Materials & Design,* vol. 47, pp. 424-442, 2013.

[18] S. Venkatesan, "Stamp Forming of Composite Materials: An Experimental and Analytical Study", 2012. PhD Thesis, The Australian National University.

[19] A. Sexton, "Stretch forming of thermo-plastic fibre metal laminates", 2014. PhD Thesis, The Australian National University.

[20] S. Advani and K.T. Hsiao, "Manufacturing Techniques for Polymer Matrix Composites (PMCs)", 2012, Woodhead Publishing.

[21] K. Liu, H. Takagi, R. Osugi, and Z. Yang, "Effect of lumen size on the effective transverse thermal conductivity of unidirectional natural fiber composites", *Composites Science and Technology,* vol. 72, no. 5, pp. 633-639, 2012.

[22] P. Methacanon, U. Weerawatsophon, N. Sumransin, C. Prahsarn, and D.T. Bergado, "Properties and potential application of the selected natural fibers as limited life geotextiles", *Carbohydrate Polymers,* vol. 82, no. 4, pp. 1090-1096, 2010.

[23] M.D.H. Beg, and K.L. Pickering, "Accelerated weathering of unbleached and bleached Kraft wood fibre reinforced polypropylene composites", *Polymer Degradation and Stability,* vol. 93, no. 10, pp. 1939-1946, 2008.

[24] D.B. Dittenber, and H.V.S. GangaRao, "Critical review of recent publications on use of natural composites in infrastructure", *Composites Part A: Applied Science and Manufacturing,* vol. 43, no. 8, pp. 1419-1429, 2012.

[25] C. Baley, "Analysis of the flax fibres tensile behaviour and analysis of the tensile stiffness increase", *Composites Part A: Applied Science and Manufacturing,* vol. 33, no. 7, pp. 939-948, 2002.

[26] A. Le Duigou, L. Pillin, A. Bourmaud, P. Davies, and C. Baley. "Effect of recycling on mechanical behaviour of biocompostable flax/poly(l-lactide) composites." *Composites Part A: Applied Science and Manufacturing,* vol. 39, no. 9, pp. 1471-1478, 2008.

[27] A. Bourmaud, A. Le Duigou, and C. Baley, "What is the technical and environmental interest in reusing a recycled polypropylene–hemp fibre composite?" *Polymer Degradation and Stability*, vol. 96, no. 10, pp. 1732-1739. 2011

[28] A. Bourmaud, and C. Baley. "Rigidity analysis of polypropylene/vegetal fibre composites after recycling". *Polymer Degradation and Stability*, vol. 94, no 3, pp. 297-305. 2009.

[29] V. Srebrenkoska, G.B. Gaceva, and D. Dimeski, "Preparation and recycling of polymer eco-composites I. Comparison of the conventional molding techniques for preparation of polymer eco-composites". *Macedonian Source*, vol. 28, no. 1, pp. 99-109. 2009.

[30] V. Srebrenkoska, G.B. Gaceva, M. Avella, M.E. Ericco, and G. Gentile. "Recycling of polypropylene-based eco-composites". *Polymer International*, vol. 57, no. 11, pp. 1252-1257. 2008.

[31] S.F. Hwang and K.J. Hwang, "Stamp forming of locally heated thermoplastic composites", *Composites Part A: Applied Science and Manufacturing*, vol. 33, no. 5, pp. 669-676, 2002.

[32] F. Yao, Q. Wu, Y. Lei, W. Guo, and Y. Xu. "Thermal decomposition kinetics of natural fibers: Activation energy with dynamic thermogravimetric analysis", *Polymer Degradation and Stability*, vol. 93, no. 1, pp. 90-98, 2008.

[33] P.V. Joseph, K. Joseph, S. Thomas, C.K.S. Pillai, V.S. Prasad, G. Groeninckx, and M. Sarkissova, "The thermal and crystallisation studies of short sisal fibre reinforced polypropylene composites", *Composites Part A: Applied Science and Manufacturing*, vol. 34, no. 3, pp. 253-266, 2003.

[34] L.B. Manfredi, E.S. Rodríguez, M. Wladyka-Przybylak, and A. Vazquez, "Thermal degradation and fire resistance of unsaturated polyester, modified acrylic resins and their composites with natural fibres", *Polymer Degradation and Stability*, vol. 91, no. 2, pp. 255-261, 2006.

[35] A. Athijayamani, M. Thiruchitrambalam, U. Natarajan, and B. Pazhanivel, "Effect of moisture absorption on the mechanical properties of randomly oriented natural fibers/polyester hybrid composite", *Materials Science and Engineering: A*, vol. 517, no. 1–2, pp. 344-353, 2009.

[36] W. Wang, M. Sain, and P.A. Cooper, "Study of moisture absorption in natural fiber plastic composites", *Composites Science and Technology*, vol. 66, no. 3–4, pp. 379-386, 2006.

[37] P.V. Joseph, M.S. Rabello, L.H.C. Mattoso, K. Joseph, and S. Thomas, "Environmental effects on the degradation behaviour of sisal fibre reinforced polypropylene composites", *Composites Science and Technology*, vol. 62, no. 10–11, pp. 1357-1372, 2002.

[38] A. Le Duigou, A. Bourmaud, P. Davies, and C. Baley, "Long term immersion in natural seawater of Flax/PLA biocomposite", *Ocean Engineering,* vol. 90, pp. 140-148, 2014.

[39] C.P.L. Chow, X.S. Xing, and R.K.Y. Li, "Moisture absorption studies of sisal fibre reinforced polypropylene composites", *Composites Science and Technology,* vol. 67, no. 2, pp. 306-313, 2007.

[40] K Goda, M.S. Sreekala, A Gomes, T Kaji, and J Ohgi, "." *Composites Part A: Applied Science and Manufacturing,* vol. 37, no. 12, pp. 2213-2220, 2006.

[41] D. Ray, B. K. Sarkar, A. K. Rana, and N.R. Bose, "The mechanical properties of vinylester resin matrix composites reinforced with alkali-treated jute fibres", *Composites Part A: Applied Science and Manufacturing,* vol. 32, no. 1, pp. 119-127, 2001.

[42] H. Chen, M. Miao, and X. Ding, "Influence of moisture absorption on the interfacial strength of bamboo/vinyl ester composites", *Composites Part A: Applied Science and Manufacturing,* vol. 40, no. 12, pp. 2013-2019, 2009.

[43] A. Espert, F. Vilaplana, and S. Karlsson, "Comparison of water absorption in natural cellulosic fibres from wood and one-year crops in polypropylene composites and its influence on their mechanical properties", *Composites Part A: Applied Science and Manufacturing,* vol. 35, no. 11, pp. 1267-1276, 2004.

[44] Y. Xu, S. Kawata, K. Hosoi, T. Kawai, and S. Kuroda, "Thermomechanical properties of the silanized-kenaf/polystyrene composites", *eXPRESS Polymer Letters* vol. 3, no. 10, pp. 657-664, 2009.

[45] L.A. Pothan, and S. Thomas, "Polarity parameters and dynamic mechanical behaviour of chemically modified banana fiber reinforced polyester composites", *Composites Science and Technology,* vol. 63, no. 9, pp. 1231-1240, 2003.

[46]. P. Kiekens and K.V.D. Velde, "Influence of Fiber Surface Characteristics on the Flax/Polypropylene Interface", *Journal of Thermoplastic Composite Materials,* vol. 14, pp. 244-260, 2001.

[47] N.A. Zanjani and S. Kalyanasundaram, "A Comparison between Forming Behaviours of Two Pre-Consolidated Woven Thermoplastic Composites", *Journal of Materials Science and Chemical Engineering,* vol. 3, no. 7, pp. 180-189, 2015.

[48] N.A. Zanjani and S. Kalyanasundaram, "Stretch Forming Simulation of Woven Composites Based on an Orthotropic Non-Linear Material Model", *Journal of Materials Science and Chemical Engineering,* vol. 3, no. 7, pp. 168-179, 2015.

[49] L. Mosse, P. Compston, W. J. Cantwell, M. Cardew-Hall, and S. Kalyanasyndaram, "The effect of process temperature on the formability of polypropylene based fibre–metal laminates", *Composites Part A: Applied Science and Manufacturing,* vol. 36, no. 8, pp. 1158-1166, 2005.

[50] L. Mosse, P. Compston, W. J. Cantwell, M. Cardew-Hall, and S. Kalyanasundaram, “The development of a finite element model for simulating the stamp forming of fibre–metal laminates”, *Composite Structures*, vol. 75, no. 1–4, pp. 298-304, 2006.

[51] S. Kalyanasundaram, S. DharMalingam, S. Venkatesan, and A. Sexton, “Effect of process parameters during forming of self reinforced – PP based Fiber Metal Laminate”, *Composite Structures*, vol. 97, pp. 332-337, 2013.

[52] J.S. Lee, S.J. Hong, W.R. Yu, and T.J. Kang, “The effect of blank holder force on the stamp forming behavior of non-crimp fabric with a chain stitch”, *Composites Science and Technology*, vol. 67, no. 3–4, pp. 357-366, 2007.

[53] P. Ouagne, D. Soulat, J. Moothoo, E. Capelle, and S. Gueret, “Complex shape forming of a flax woven fabric; analysis of the tow buckling and misalignment defect”, *Composites Part A: Applied Science and Manufacturing*, vol. 51, pp. 1-10, 2013.

[54] J. Cao, R. Akkeman, P. Boisse, J. Chen, H.S. Cheng, E.F. de Graaf, J.L. Gorczyca, P. Harrison, G. Hivet, J. Launay, W. Lee, L. Liu, S.V. Lomov, A. Long, E. de Luycker, F. Morestin, J. Padvoiskis, X.Q Peng, J. Sherwood, Tz. Stoilova, X.M. Tao, I. Verpoest, A. Willems, J. Wiggers, T.X. Yu, and B. Zhu, "Characterization of mechanical behavior of woven fabrics: Experimental methods and benchmark results". *Composites Part A: Applied Science and Manufacturing*, Vol. 39, no. 6, pp. 1037-1053, 2008.

[55] M. Hou, “Stamp forming of continuous glass fibre reinforced polypropylene”, *Composites Part A: Applied Science and Manufacturing*, vol. 28, no. 8, pp. 695-702, 1997.

[56] K. Friedrich, and M. Hou, "On stamp forming of curved and flexible geometry components from continuous glass fibre/polypropylene composites". *Composites: Part A: Applied Science and Manufacturing.* vol. 29, no. 3, pp. 217-226, 1998.

[57] M. Sadighi, E. Rabizadeh, and F. Kermansaravi, "Effects of laminate sequencing on thermoforming of thermoplastic matrix composites", *Journal of Materials Processing Technology*, vol. 201, pp. 725-730, 2008.

[58] M. Hou, L. Ye, and Y.W. Mai, “Review – advances in processing of continuous fibre reinforced composites with thermoplastic matrix”, *Plastics, Rubber Composites Processing Application*, vol. 23, pp. 279-293, 1995.

[59] D. Trudel-Boucher, B. Fisa, J. Denault, and P. Gagnon, “Experimental investigation of stamp forming of unconsolidated commingled E-glass/polypropylene fabrics”, *Composites Science and Technology*, vol. 66, no. 3–4, pp. 555-570, 2006.

[60] M.D. Wakeman, T.A. Cain, C.D. Rudd, R. Brooks and A.C. Long, "Compression moulding of glass and polypropylene composites for optimised macro- and micro- mechanical properties—1 commingled glass and polypropylene", *Composites Science and Technology,* vol. 58, no. 12, pp. 1879-1898, 1998.

[61] N.O. Cabrera, C.T. Reynolds, B. Alcock, and T. Peijs, "Non-isothermal stamp forming of continuous tape reinforced all-polypropylene composite sheet", *Composites Part A: Applied Science and Manufacturing,* vol. 39, no. 9, pp. 1455-1466, 2008.

[62] R. Esmaeilizadeh, K. Khalili, and B. Mohammadsadeghi, "Simulated and experimental investigation of stretch sheet forming of commercial AA1200 aluminum alloy". *Transactions of Nonferrous Metals Society of China,* vol. 24, no. 2, pp. 484-490, 2014.

[63] Y. Dewang, M.S. Hora, and S.K. Panthi, "Influence of Blank Holding Force on Stretch Flange Forming of Aluminum Alloy". *Materials Today: Proceedings*, vol. 2, no. 4, pp. 1934-1941, 2015.

[64] D. He, D. Li, X. Li, and C. Jun. "Optimization on springback reduction in cold stretch forming of titanium-alloy aircraft skin". *Transactions of Nonferrous Metals Society of China,* vol. 20, no. 12, pp. 2350-2357, 2010.

[65] S.K. Panda, and D. Ravi Kumar, "Experimental and numerical studies on the forming behavior of tailor welded steel sheets in biaxial stretch forming". *Materials & Design,* Vol. 31, no. 3, pp. 1365-1383, 2010.

[66] B. Kinsey, Z. Liu, and J. Cao, "A novel forming technology for tailor-welded blanks". *Journal of Materials Processing Technology,* vol. 99, pp. 145-153, 2000.

[67] S.M. Chan, L.C. Chan, and T.C. Lee, "Tailor-welded blanks of different thickness ratios effects on forming limit diagrams". *Journal of Materials Processing Technology,* vol. 132, pp. 95-101, 2003.

[68] A. Sexton, W. Cantwell, and S. Kalyanasundaram, "Stretch forming studies on a fibre metal laminate based on a self-reinforcing polypropylene composite". *Composite Structures,* Vol. 94, pp. 431-437, 2012.

[69] N. Asnafi, G Langstedt, C.H. Andersson, N. Ostergren, and T. Hakansson. "A new lightweight metal-composite-metal panel for applications in the automotive and other industries". *Thin-Walled Structures,* vol. 36, no. 4, pp. 289-310, 2000.

[70] G. Reyes and H. Kang. "Mechanical behavior of lightweight thermoplastic fiber–metal laminates". *Journal of Materials Processing Technology,* vol. 186, no. 1–3, pp. 284-290, 2007.

[71] K.J. Kim, D. Kim, S.H. Choi, K. Chung, K.S. Shin, F. Barlat, K.H. Oh, and J.R. Youn. "Formability of AA5182/polypropylene/AA5182 sandwich sheets". *Journal of Materials Processing Technology,* vol. 139, no. 1–3, pp. 1-7, 2003.

[72] O.A. Sokolova, A. Carradò, and H. Palkowski, "Metal–polymer–metal sandwiches with local metal reinforcements: A study on formability by deep drawing and bending". *Composite Structures,* vol. 94, no. 1, pp. 1-7. 2011.

[73] N.A. Zanjani, A. Sexton, and S. Kalyanasundaram, "Induced forming modes in a pre-consolidated woven polypropylene composite during stretch forming process at room temperature: I. Experimental studies", *Composites Part A: Applied Science and Manufacturing,* vol. 68, pp. 251-263, 2015.

[74] K. Nakazima, T. Kikuma, and K. Asuka, "Study on the formability of steel sheets", Yawata Technical Report, No.264 (1968) September.

[75] K.S. Raghavan, "A simple technique to generate in-plane forming limit curves and selected applications", *Metallurgical and Materials Transactions A,* vol. 26A, pp. 2075-2084, 1995.

[76] L. Gorbatikh, and S.V. Lomov, "3 - Damage accumulation in textile composites, in Modeling Damage, Fatigue and Failure of Composite Materials". Woodhead Publishing. pp. 41-59, 2016.

[77] N. De Greef, L. Gorbatikh, A. Gordara, L. Mezzo, S.V. Lomov, and I. Verpoest, "The effect of carbon nanotubes on the damage development in carbon fibre/epoxy composites". *Carbon,* vol. 49, pp. 4650-4664, 2011.

[78] E. Bogdanovich, M. Karahan, S.V. Lomov, and I. Verpoest, "Quasi-static tensile behaviour and progressive damage in carbon/epoxy composite reinforced with 3D non-crimp orthogonal woven fabric". *Mechanics of Materials,* vol. 62, pp. 14-31, 2013.

[79] M. Kersani, S.V. Lomov, A.W. Van Vuure, A. Bouabdallah, and I. Verpoest, "Damage in flax/epoxy quasi unidirectional woven laminates under quasi-static tension". *Journal of Composite Materials,* vol. 49, pp. 403-413, 2015.

[80] W. Roundi, A.E. Mahi, A.E. Gharad, and J.L. Rebiere, "Experimental and numerical investigation of the effects of stacking sequence and stress ratio on fatigue damage of glass/epoxy composites", *Composites Part B: Engineering,* vol. 109, pp. 64-71, 2017.

[81] Y. Ma, M. Ueda, T. Yokozeki, T. Sugahara, Y. Yang, and H. Hamada, "A comparative study of the mechanical properties and failure behavior of carbon fiber/epoxy and carbon fiber/polyamide 6 unidirectional composites", *Composite Structures,* vol. 160, pp. 89-99, 2017.

[82] J. Mayen, A. Abundez, E. Alcudia, J.A. Arellano, J. Colin, I. Pereyra, and I.P. Lee, "Fractographic relation between progressive failure and strain measurement techniques for recently developed configuration of carbon fiber/epoxy laminate", *Polymer Testing,* vol. 57: pp. 156-164, 2017.

[83] C. Wang, X. Ji, A. Roy, V.V. Silberschmidt, and Z. Chen, "Shear strength and fracture toughness of carbon fibre/epoxy interface: effect of surface treatment", *Materials & Design,* vol. 85, pp. 800-807, 2015.

[84] M. Nourjani Pourmoghadam, R. Shahrokh Esfahani, M. R. Morovvati, and B. Nekooei Rizi, “Bifurcation analysis of plastic wrinkling formation for anisotropic laminated sheets (AA2024–Polyamide–AA2024)”, *Computational Materials Science,* vol. 77, pp. 35-43, 2013.

[85] G. Romhany, T. Barany, T. Czigany, and J. Karger-Kocsis. "Fracture and failure behavior of fabric-reinforced all-poly(propylene) composite". *Polymers for Advanced Technologies*, vol. 18, pp. 90–96, 2007.

[86] S. Davey, R. Das, W. J. Cantwell, and S. Kalyanasundaram. “Forming studies of carbon fibre composite sheets in dome forming processes”, *Composite Structures,* vol. 97, pp. 310-316, 2013.

[87] O.M.L. Asumani, R.G. Reid, and R. Paskaramoorthy, "The effects of alkali–silane treatment on the tensile and flexural properties of short fibre non-woven kenaf reinforced polypropylene composites", *Composites Part A: Applied Science and Manufacturing,* vol. 43, pp. 1431-1440, 2012.

[88] J. Aboudi, S. Arnold, and B. Bednarcyk, "Micromechanics of Composite Materials". pp. 61, Charpter 2, 2013.

[89] L.J. Hart-Smith, “The truncated maximum strain composite failure model”, *Composites,* vol. 24, no. 7, pp. 587-591, 1993.

[90] L.J. Hart-Smith, “Predictions of the original and truncated maximum-strain failure models for certain fibrous composite laminates”, *Composites Science and Technology,* vol. 58, no. 7, pp. 1151-1178, 1998.

[91] S.W. Tsai and E.M. Wu, “A General Theory of Strength for Anisotropic Materials”, *Journal of Composite Materials,* vol. 5, pp. 58-80, 1971.

[92] K. Rohwer, “Predicting fibre composite damage and failure”, *Journal of Composite Materials,* vol. 49, no. 21, pp. 1-11, 2014.

[93] A. Rotem, "Prediction of laminate failure with the Rotem failure criterion", *Composites Science and Technology,* vol. 58, pp. 1083-1094, 1998.

[94] Z. Hashin, and A. Rotem, "A fatigue failure criterion for fibre reinforced materials", *Journal of Composite Materials,* vol. 7, pp. 448-464, 1973.

[95] A. Rotem, and Z. Hashin, "Failure modes of angle ply laminates", *Journal of Composite Materials,* vol. 9, pp. 191-206, 1975.

[96] A. Rotem, and H.G. Nelson, "Fatigue behavior of graphite–epoxy laminate at elevated temperatures", Fatigue of Fibrous Composite Materials. ASTM International, 1981.

[97] A. Rotem, "The Rotem failure criterion: theory and practice", *Composites Science and Technology,* vol. 62, pp. 1663-1671, 2002.

[98] E.C. Edge, "Stress-Based Grant-Sanders Method for Predicting Failure of Composite Laminates", *Composites Science and Technology,* vol. 58, pp. 1033-1041, 1998.

[99] W.E. Wolfe, and T.S. Butalia, "A strain-energy based failure criterion for non-linear analysis of composite laminates subjected to biaxial loading", *Composites Science and Technology,*vol. 58, pp. 1107-1124, 1998.

[100] R.S. Sandhu, "Ultimate Strength Analysis of Symmetric Laminates", No. AFFDL-TR-73-137. AIR FORCE FLIGHT DYNAMICS LAB WRIGHT-PATTERSON AFB OHIO, 1974.

[101] D. Willats, "Advances in the use of high performance continuous fibre reinforced thermoplastics", *SAMPE Journal,* 1984.

[102] B. Madsen and H. Lilholt, "Physical and mechanical properties of unidirectional plant fibre composites—an evaluation of the influence of porosity", *Composites Science and Technology,* vol. 63, no. 9, pp. 1265-1272, 2003.

[103] H.B. Campos, M.C. Butuc, J.J. Grácio, and L.M.F. Duarte, "Theorical and experimental determination of the forming limit diagram for the AISI 304 stainless steel", *Journal of Materials Processing Technology,* vol. 179, no. 1–3, pp. 56-60, 2006.

[104] S.B. Kim, H. Huh, H.H. Bok, and M.B. Moon, "Forming limit diagram of auto-body steel sheets for high-speed sheet metal forming", *Journal of Materials Processing Technology,* vol. 211, no. 5, pp. 851-862, 2011.

[105] V. Uthaisangsuk, U. Prahl, and W. Bleck, "Stress based failure criterion for formability characterisation of metastable steels". *Computational Materials Science,* vol. 39, no. 1, pp. 43-48, 2007.

[106] M.C. Butuc, J.J. Gracio, and A. Barata da Rocha, "An experimental and theoretical analysis on the application of stress-based forming limit criterion". *International Journal of Mechanical Sciences,* vol. 48, no. 4, pp. 414-429. 2006.

[107] B.S. Levy, and C.J. Van Tyne, "An approach to predicting the forming limit stress components from mechanical properties". *Journal of Materials Processing Technology,* vol. 229, pp. 758-768, 2016.

[108] S. Panich, F. Barlat, V. Uthaisangsuk, S. Suranuntchai, and S. Jirathearanat, "Experimental and theoretical formability analysis using strain and stress based forming limit diagram for advanced high strength steels". *Materials & Design,* vol. 51, pp. 756-766, 2013.

[109] W.M. Sing, and K.P. Rao, "Study of sheet metal failure mechanisms based on stress-state conditions". *Journal of Materials Processing Technology,* vol. 67, no. 1, pp. 201-206, 1997.

[110] R. Arrieux, C. Bedrin, and M. Boivin., "Determination of an intrinsic forming limit stress diagram for isotropic sheets". *In: Proceedings of the 12th IDDRG congress, Santa Margherita, Ligure,* pp. 61-71, 1982.

[111] H. Lin, J. Wang, A.C. Long, M.J. Clifford, and P. Harrison, "Predictive modelling for optimization of textile composite forming", *Composites Science and Technology,* vol. 67, no. 15–16, pp. 3242-3252, 2007.

[112] P.F. Liu, Z.P. Gu, Y.H. Yang, and X.Q. Peng, "A nonlocal finite element model for progressive failure analysis of composite laminates", *Composites Part B: Engineering,* vol. 86, pp. 178-196, 2016.

[113] S. Liu, C. Liu, Y. Hu, S. Gao, Y. Wang, and H. Zhang, "Fatigue life assessment of centrifugal compressor impeller based on FEA", *Engineering Failure Analysis,* vol. 60, pp. 383-390, 2016.

[114] M. Penasa, L. Argani, D. Misseroni， F. Dal Corso, M. Cova and A. Piccolroaz, "Computational modelling and experimental validation of industrial forming processes by cold pressing of aluminum silicate powder", *Journal of the European Ceramic Society*. vol. 36, pp. 2351-2362, 2016.

[115] F.J. Harewood, and P.E. McHugh, "Comparison of the implicit and explicit finite element methods using crystal plasticity", *Computational Materials Science,* vol. 39, no. 2, pp. 481-494, 2007.

[116] Obtained from http://mashayekhi.iut.ac.ir/sites/mashayekhi.iut.ac.ir/files//u32/presentation4.pdf, Viewed on the 11th of March, 2015.

[117] Abaqus Theory Manual.

[118] P. Boisse, B. Zouari, and A. Gasser, "A mesoscopic approach for the simulation of woven fibre composite forming", *Composites Science and Technology,* vol. 65, no. 3–4, pp. 429-436, 2005.

[119] K. Vanclooster, S.V. Lomov, and I. Verpoest, "Experimental validation of forming simulations of fabric reinforced polymers using an unsymmetrical mould configuration", *Composites Part A: Applied Science and Manufacturing,* vol. 40, no. 4, pp. 530-539, 2009.

[120] J.H. Lee, J.H. Vogel, and K.Y. Rhee, "An analysis of stretch forming of thermoplastic composites". *Polymer Composites,* Vol. 23, pp. 442-453. 2002.

[121] P. Badel, S. Gauthier, E. Vidal_Salle, and P. Boisse. "Rate constitutive equations for computational analyses of textile composite reinforcement mechanical behaviour during forming". *Composites Part A: Applied Science and Manufacturing,* Vol. 40, no. 8, pp. 997-1007. 2009.

[122] Z. Marciniak, J.L. Duncan, and S.J. Hu, "Mechanics of Sheet Metal Forming", 2002.

[123] P. Harrison, R.H.W.T Thije, R. Akkeman, and A.C Long, "Characterisation and modelling friction at the tool–ply interface for thermoplastic woven composites", In: NATO Advanced Research Workshop: Use of Textile Composites Technology for Safer Vehicles, Kiev, Ukraine, 18-21 May, 2009.

[124] P. Harrison, R. Gomes, and N. Curado-Correia, “Press forming a 0/90 cross-ply advanced thermoplastic composite using the double-dome benchmark geometry”, *Composites Part A: Applied Science and Manufacturing,* vol. 54, pp. 56-69, 2013.

[125] M. Benítez-Guerrero, J. López-Beceiro, P.E. Sánchez-Jiménez, and J. Pascual-Cosp, “Comparison of thermal behavior of natural and hot-washed sisal fibers based on their main components: Cellulose, xylan and lignin. TG-FTIR analysis of volatile products”, *Thermochimica Acta,* vol. 581, pp. 70-86, 2014.

[126] W. Wang, A Lowe, and S Kalyanasundaram, “A study on continuous flax fibre reinforced polypropylene composite in stamp forming process”, *Advanced Composites Letters,* vol. 22, pp. 86-89, 2013.

[127] G. Lebrun, M.N. Bureau and J. Denault, “Thermoforming stamping of continuous glass fiber/polypropylene composites: interlaminar and tool-laminate shear properties”, *Journal of Thermoplastic Composite Materials,* 2004.

[128] J.A.E. Manson, M. Wakeman, and N. Bernet, “Composite processing and manufacturing - An overview”, *Comprehensive Composite Materials,* vol. 2, pp. 577-607, 2000.

[129] M.S. Meon, M.F. Othman, H. Husain, M.F. Remeli, and M.S.M. Syawal. “Improving tensile properties of kenaf fibres treated with sodium hydroxide”. *In Proceedings of the International Symposium on Robotics and Intelligent Sensors 2012 (IRIS 2012), Kuching, Sarawak, Malaysia,* vol. 41, pp/1587–1592, 2012.

[130] C. Schuerch, M.P. Burdick, and M. Mahdalik “Liquid ammonia-solvent combinations in wood plasticization”, *Chemical Treatment,* vol. 5, pp. 101, 1966.

[131] K. Van De Velde and P. Kiekens, “Influence of fibre surface characteristics on the flax/polypropylene interface”, *Journal of Composite Materials,* vol. 14, pp. 244-260, 2001.

[132] A. Arbelaiz, B. Fernández, G. Cantero, R. Llano-Ponte, A. Valea, and I. Mondragon. “Mechanical properties of flax fibre/polypropylene composites. Influence of fibre/matrix modification and glass fibre hybridization”, *Composites Part A: Applied Science and Manufacturing,* vol. 36, no. 12, pp. 1637-1644, 2005.

[133] S. Mishra and M. Sain “Long-term performance of natural fibre composites”, *In Properties and Performance of Natural-Fibre Composites; Pickering, K.L., Ed.; Woodhead Publishing: Cambridge, UK,* pp. 461-502, 2008.

[134] D. Gay, S.W. Tsai and S.V. Hoa “Composites Materials - Design and Applications”, Chapter 18, pp 442, 2003.

[135] W. J. Cantwell, and J. Morton, “The impact resistance of composite materials — a review”, *Composites,* vol. 22, no. 5, pp. 347-362, 1991.

[136] E. Bayraktar, N. Isac, and G. Arnold, “Buckling limit diagrams (BLDs) of interstitial free steels (IFS): Comparison of experimental and finite element analysis”, *Journal of Materials Processing Technology*, vol. 164–165, pp. 1487-1494, 2005.

Stress-strain behaviour of NFC materials in different conditions of the water treatment

Untreated:

$$E_1 = 916 - 8013 * Abs(\varepsilon_1)$$

$$E_2 = 916 - 8013 * Abs(\varepsilon_2)$$

$$G = 30 + 200 * Exp(-10 * Abs(\varepsilon_3))$$

Water-treated:

$$E_1 = 551 + 1112 * Abs(\varepsilon_1)$$

$$E_2 = 551 + 1112 * Abs(\varepsilon_2)$$

$$G = -631 * \left(Abs(\varepsilon_3)\right)^3 + 826 * \left(Abs(\varepsilon_3)\right)^2 - 360 * Abs(\varepsilon_3)$$

Redried:

$$E_1 = 895 - 8674 * Abs(\varepsilon_1)$$

$$E_2 = 895 - 8674 * Abs(\varepsilon_2)$$

$$G = 30 + 200 * Exp(-10 * Abs(\varepsilon_3))$$

Stress-strain behaviour of CNFC materials in different conditions of the water treatment

Untreated:

$$E_1 = 1300\ MPa$$

$$E_2 = 1300\ MPa$$

$$G = 500\ MPa$$

Water-treated:

$$E_1 = 700\ MPa$$

$$E_2 = 700\ MPa$$

$$G = 269\ MPa$$

Redried:

$$E_1 = 900\ MPa$$

$$E_2 = 900\ MPa$$

$$G = 346\ MPa$$